

ISSN number 0971 - 9709



The Journal of Indian Geophysical Union

VOLUME 22, ISSUE 2 | MARCH 2018

AN OPEN ACCESS BIMONTHLY JOURNAL OF IGU



Journal of Indian Geophysical Union Editorial Board	Indian Geophysical Union Executive Council
Chief Editor P.R. Reddy (Geosciences), Hyderabad	President Prof. Shailesh Nayak, Distinguished Scientist, MoES, New Delhi
Associate Editors B.V.S. Murthy (Exploration Geophysics), Hyderabad D. Srinagesh (Seismology), Hyderabad Nandini Nagarajan (Geomagnetism & MT), Hyderabad M.R.K. Prabhakara Rao (Ground Water Geophysics), Hyderabad	Vice-Presidents Dr. Satheesh C. Sheno, Director, INCOIS, Hyderabad Prof. Talat Ahmad, VC, JMI, New Delhi Dr. V.M. Tiwari, Director, CSIR-NGRI, Hyderabad Dr. Sunil K. Singh, Director, CSIR-NIO, Goa
Editorial Team Solid Earth Geosciences: Vineet Gahlaut (Seismology), New Delhi B. Venkateswara Rao (Water resources Management), Hyderabad N.V. Chalapathi Rao (Geology, Geochemistry & Geochronology), Varanasi V.V. Sessa Sai (Geology & Geochemistry), Hyderabad Marine Geosciences: K.S.R. Murthy (Marine Geophysics), Visakhapatnam M.V. Ramana (Marine Geophysics), Goa Rajiv Nigam (Marine Geology), Goa Atmospheric and Space Sciences: Ajit Tyagi (Atmospheric Technology), New Delhi Umesh Kulshrestha (Atmospheric Sciences), New Delhi P. Sanjeeva Rao (Agrometeorology & Climatoplogy), New Delhi U.S. De (Meteorology), Pune Archana Bhattacharya (Space Sciences), Mumbai Editorial Advisory Committee: Walter D Mooney (Seismology & Natural Hazards), USA Manik Talwani (Marine Geosciences), USA T.M. Mahadevan (Deep Continental Studies & Mineral Exploration), Ernakulum D.N. Avasthi (Petroleum Geophysics), New Delhi Larry D Brown (Atmospheric Sciences & Seismology), USA Alfred Kroener (Geochronology & Geology), Germany Irina Artemieva (Lithospheric Structure), Denmark R.N. Singh (Theoretical & Environmental Geophysics), Ahmedabad Rufus D Catchings (Near Surface Geophysics), USA Surjalal Sharma (Atmospheric Sciences), USA H.J. Kumpel (Geosciences, App. Geophysics, Theory of Poroelasticity), Germany Saulwood Lin (Oceanography), Taiwan Jong-Hwa Chun (Petroleum Geosciences), South Korea Xiujuan Wang (Marine Geology & Environment), China Jiro Nagao (Marine Energy and Environment), Japan Information & Communication: B.M. Khanna (Library Sciences), Hyderabad	Hon. Secretary Dr. Kalachand Sain, CSIR-NGRI, Hyderabad
	Joint Secretary Dr. O.P. Mishra, MoES, New Delhi
	Org. Secretary Dr. ASSRS Prasad, CSIR-NGRI, Hyderabad
	Treasurer Md. Rafique Attar, CSIR-NGRI, Hyderabad
	Members Prof. Rima Chatterjee, ISM, Dhanbad Prof. P. Rama Rao, Andhra Univ., Visakhapatnam Prof. S.S. Teotia, Kurukshetra Univ., Kurukshetra Mr. V. Rama Murty, GSI, Hyderabad Prof. B. Madhusudan Rao, Osmania Univ., Hyderabad Prof. R.K. Mall, BHU, Varanasi Dr. A.K. Chaturvedi, AMD, Hyderabad Mr. Sanjay Jha, Omni Info, NOIDA Mr. P.H. Mane, ONGC, Mumbai Dr. Rahul Dasgupta, OIL, NOIDA Dr. M. Ravi Kumar, ISR, Gujarat Prof. Surjalal Sharma, Univ. of Maryland, USA Dr. P. Sanjeeva Rao, Advisor, SERB, DST, New Delhi Dr. N. Satyavani, CSIR-NGRI, Hyderabad Prof. Devesh Walia, North Eastern Hills Univ., Shillong
EDITORIAL OFFICE Indian Geophysical Union, NGRI Campus, Uppal Road, Hyderabad- 500 007 Telephone: +91 -40-27012799; 27012734; Telefax: +91-04-27171564 E. mail: jigu1963@gmail.com, website: www.j-igu.in	
The Open Access Journal with six issues in a year publishes articles covering Solid Earth Geosciences; Marine Geosciences; and Atmospheric, Space and Planetary Sciences.	
Annual Subscription Individual ₹ 1000 per issue and Institutional ₹ 5000 for six issues Payments should be sent by DD drawn in favour of "The Treasurer, Indian Geophysical Union", payable at Hyderabad, Money Transfer/NEFT/RTGS (Inter-Bank Transfer), Treasurer, Indian Geophysical Union, State Bank of India, Habsiguda Branch, Habsiguda, Uppal Road, Hyderabad- 500 007 A/C: 52191021424, IFSC Code: SBIN0020087, MICR Code: 500002318, SWIFT Code: SBININBBHO9. For correspondence, please contact, Hon. Secretary, Indian Geophysical Union, NGRI Campus, Uppal Road, Hyderabad - 500 007, India; Email: igu123@gmail.com; Ph: 040 27012799, 272012734	

CONTENTS

Editorial

S No.	Title	Authors	Pg. No:
1	Critical study on P- and S-waves radiation and computation of earthquake magnitude due to simple crack models	Ajit De	121
2	Stress Orientation from Image log and Estimation of Shear Wave Velocity using Multiple Regression Model: A Case Study from Krishna-Godavari basin, India	Rima Chatterjee and Dip Kumar Singha	128
3	Wavefield decomposition of multi-component OBS data to enhance the seismic signal	N.Satyavani, M. Ravi Kumar and Kalachand Sain	138
4	Fractal Revaluation of Bottom Depth of Magnetic Sources in Bida Basin, Nigeria from High-Resolution Aeromagnetic Data	Levi I. Nwankwo, Peter I. Olasehinde, and Abayomi J. Sunday	143
5	Forecasting Aftershocks of Major Earthquakes	Vinod Kumar and M. Satya kumar	151
6	Hydrogeological and Geophysical Characteristics of Northern Parts of Eastern Chat Khondalitic Aquifers	B.Venkateswara Rao	163
7	Geochemical and Ore-mineralogical Characterization of Beach placer Ilmenite from Srikurmam Deposit, Andhra Pradesh, India	M. Jagannadha Rao, J. VenkataRamana, Aaron A. Jaya Raj, G. Raja Rao and P. Rajesh	171
8	Ferrosyenites - an overview	K. Sai Krishna and R. Mallikarjuna Reddy	178
9	Punugodu Granite Pluton, Nellore Schist Belt, Eastern Dharwar Craton, Se India	Ch. Narshimha, U.V.B. Reddy, V.V. Sessa Sai and K.S.V. Subramanyam	187
10	Long range forecast and development of a Weak southwest monsoon during 2017- pt. I: long range forecast	Onkari Prasad, O. P. Singh and K.Prasad	198
11	Defluoridation of water using Mentha longifolia (Mint) as Bioadsorbent	V.Sunitha and B.Muralidhara Reddy	207
12	Feasible Mitigation Options for Air Pollution and Traffic Congestion in Metro Cities	Kopal Verma and Umesh Kulshrestha	212
13	Probing Chemical Heterogeneity of the Mantle Using Open System Isotopic Models of the Silicate Earth	Seema Kumari and Debajyoti Paul	219
14	Dynamics of drought and present status of drought prediction- an overview.	P.R.Reddy	222
	News at a glance		233
	Book Review: Proterozoic Orogens of India- A critical window to Gondwana by T.R.K. Chetty	P.R.Reddy	237
15	Short-Term Advanced Warning from Some Large Earthquakes- A Research Initiative.	Indra N. Gupta, B.K. Rastogi and Robert A. Wagner	241
	54 th Annual Convention of Indian Geophysical Union (IGU): A Report	K.Sain and ASSSRS.Prasad	247

Quotations on Desertification

Erosion, desertification, and pollution have become our lot. It is a weird form of suicide, for we are bleeding our planet to death.

Gerald Durrell (1925-1995) was a British naturalist, zookeeper, conservationist and author.

We already have the statistics for the future: the growth percentages of pollution, overpopulation, desertification. The future is already in place.

Gunther Grass (1927- 2015) was a German novelist, poet, playwright, sculptor, and recipient of the Nobel Prize in Literature.

Drought does not have to become famine. Too often the international community reacts too late. Too often decisions are taken based on false economies. In the end, we count the cost not just in human lives but in the extra expense of responding to crises that could have been averted for a fraction of the price. The world's drylands are too often an investment desert, seen by governments and the international community as a lost cause.

Ban Ki-moon (1944--) is a South Korean diplomat.

“Increased aridity is making the drylands the most conflict prone region of the world,”

Gnacadjia (1958--) a former environment minister in Benin.

Combating desertification and soil degradation requires better land management, better equipment and new technology to manage water, drought resistant seeds and payment to communities for preserving the soil.

Gnacadjia (1958--) a former environment minister in Benin.

“If not prevented, desertification of the world can one day make the camels as the best and the sole cars of our civilisation!”

Mehmet Murat ildan (1965--) is a Turkish playwright and writer.

There have always been tensions and conflicts between agricultural and pastoral practices but desertification has accentuated them.

Yakubu dalhat of Savanna an environmental defence group.

Editorial

Two year term of present editorial board ends on 31st March, 2018. On the same day present term of office bearers of Indian Geophysical Union also comes to an end. Some of the editorial board members and IGU executive committee members will continue, making the change over reasonably smooth.

As Chief Editor of JIGU for the last 4 years I wanted all our fellow editorial board members (Fellow volunteers) to feel comfortable, listened to, and truly part of the whole process of publication. I have partly succeeded in achieving this. A small group of volunteers succeeded in making the journal structuring a real team effort. I can happily say that support extended in general by majority of editorial board members helped us in introducing various innovative measures, to attract the attention of not only Indian scientists (especially young researchers) but also some from Iran, Nigeria, USA and Canada. My term is ending without causing any disruption to JIGU publication (which at one juncture worried me due to some problems, especially my health). In addition to overall enhancement of quality of the journal we have succeeded in making JIGU a recognised Indian journal by Clarivate Analytics, ICI, NISCAIR and UGC. In spite of some irritants I've had a lot of freedom to implement my ideas. I don't want to anticipate what my successor will propose and implement. I only wish him the success in making JIGU reach higher targets. However, every one of us must maintain our commitment to unequivocally support JIGU and ensure it remains the place to be for the upcoming generations to use happily in publishing their research articles. We cannot ignore environmental and political changes occurring in India and worldwide, and this important topic deserves visibility through articles under the subsection "opinions". I am modestly proud to remain the first retired scientist in charge of JIGU and also the first to be reappointed after my earlier tenure as an editor for about ten years. I am passionate in contributing to the growth of JIGU as a loyal volunteer, something I don't consider exceptional. I have done my duty, like others who contributed to our science in many ways.

I have written unconventional editorials. Some of the readers including highly talented youngsters and experienced seniors have liked them and others criticised them. In bringing out these editorials I acted both as a student and a teacher. Since I have extended voluntary services that kept me busy all the time in shaping up a bi-monthly issue, with limited assistance on a daily basis

I have taken a decision to bring out these unconventional editorials basically to motivate young researchers in developing a liking for our science. With this last editorial from my computer (not from my pen, in literal sense) such unconventional editorials may cease to exist and something better may emerge.

Interested may please read the below and propagate the importance of constantly upgrading our knowledge base by reading many illuminating scientific articles.

***Need to carry out scientific research on natural hazards using frequently updated field data to resolve many issues associated with natural phenomena and anthropogenic interventions**

What Precursors Foretold Greenland's recent 100-Meter Tsunami?

On 17 June 2017, one of the tallest tsunamis in recorded history struck the small fishing village of Nuugaatsiaq in north-western Greenland. The 100-meter wave surprised scientists because earthquakes, which typically drive such waves are not common in that area. Soon after the event, researchers tied the tsunami to a large landslide that had plunged into a nearby fjord, releasing as much energy as a magnitude 4.1 earthquake. Now a new study identifies patterns in seismic data from hours before the slide occurred, which might be helpful in predicting future landslides in glacial regions.

Days or hours before a large earthquake, scientists can often use seismic signals generated by slippage along faults in Earth's crust to predict the size and severity of the coming quake. In the new study, *Poli* analyzed seismic data recorded about 30 kms from where the mass of rocks and dirt fell into the fjord. In the hours before the slide, he found repetitive waves of energy, likely caused by a series of ruptures in the brittle rock, similar to those that happen before earthquakes.

The pattern the author observed fits with a growing body of evidence that the velocity of slippage along weak faults increases exponentially before materials such as Earth's crust or rocks and dirt in a landslide fail. If the physics underlying earthquakes and landslides are indeed similar, as the study suggests, scientists may be able to develop better detection systems for future slides. As the climate warms, causing more landslides in glacial regions, such

predictions could help communities better prepare for disaster. (Source: *Geophysical Research Letters*, <https://doi.org/10.1002/2017GL075039>, 2017).

Future Looks Drier as Drylands Continue to Expand

Drylands currently constitute about 41 per cent of the Earth's land surface and are home to more than 38 per cent of the world's population. Drylands are particularly vulnerable to environmental change. In fact, the areas categorized as dry land have been increasing over recent decades, with further expansion set to continue under the influence of climate change. This will have knock-on effects on communities in regions on almost every continent, their crops and livestock, health and livelihoods. A recent review article in *Reviews of Geophysics* described recent progress in dryland climate change research.

Drylands are areas where the annual potential evapotranspiration greatly exceeds annual precipitation. Over drylands, the air is almost always "thirsty" for water but precipitation is not enough to meet this demand. The locations of drylands are determined mostly by atmospheric circulation and topography. They are primarily found in middle and low latitudes such as northern and southern Africa, Central and East Asia, south-western North America, the west coast of South America, and much of Australia. Both observations and model simulations indicate that global dry lands have expanded over recent decades. For example, the area classified as drylands in the period 1990 to 2004 was 4 per cent larger than that for the period 1948 to 1962.

Each of the subtypes of dryland region: hyper arid, arid, semiarid and dry sub humid has expanded, although the largest expansion has been in semi-arid regions, which now account for more than half of total dryland expansion. Semiarid regions on five continents have all expanded but East Asia accounts for nearly 50 per cent of this global growth. The landscapes of drylands are characterized by low vegetation cover, low nutrition content of soil, and low capacity for water conservation. Dryland expansion means vegetated and fertile land permanently degrading into this state, a process known as "desertification." Climate change model results suggest that under a high emission scenario about 78 per cent of dryland expansion by the end of this century will occur in less developed countries, increasing the dryland coverage rate in these countries to 61 per cent. These areas are already home to disproportionality, more poor and vulnerable people; environmental changes including rising temperatures, water shortages and soil loss will exacerbate poverty and may stimulate large scale migrations.

Recent findings indicate that long-term trends in aridity are mainly attributable to increased greenhouse gas emissions, while anthropogenic aerosols exert small effects but alter its attributions. Meanwhile, human-induced land use or land cover change has likely contributed to aridity trends on regional scales. Research has shown that the greatest atmospheric warming over land during the last 100 years was over drylands, this accounted for more than half of all continental warming. However, the global pattern and inter decadal variability of aridity changes are modulated by oceanic oscillations. The different phases of those oceanic oscillations induce significant changes in land-sea and north-south thermal contrasts, which in turn alter global changes in temperature and precipitation.

So far, we are still not in the position to distinguish quantitatively between increasing aridity caused by natural variability in the climate system and the changes caused by human activities. On the other hand, studies on dryland climates should pay attention not only to long-term trends but also to decadal, multi decadal, and even inter annual variability and their impacts on ecosystems and society. More practically, another pending task is to identify a catastrophic threshold of drylands for developing an early warning system of dry climate related disasters, to take a proactive adaptation, and to mitigate their impacts. The changes occurring in drylands are part of the dynamics of the global climate system so we need "big data" including high-quality ground-based observations and improved satellite retrieval products, as well as climatic proxies from paleoclimate research. Well-developed global and regional climate system models with more reasonable parameterization schemes suitable for dryland areas and so on are particularly required. A special international project comparing dry land climate simulations is planned as part of the current Phase 6 of the World Climate Research Programme's Coupled Model Intercomparison Project (CMIP6) and this will also yield useful information. (Source: Jianping Huang and Congbin Fu; email: hjp@lzu.edu.cn)

The above two research articles emphasize the need to carry out field investigations on a regular basis to collect useful and reliable data, instead of over reliance on extrapolated results based on simulated computer models developed using scanty data; even though models based on quality data can help us arrive at a better solution. No single data set taken on a particular day can yield proper results. Natural hazards continue to occur and repeat at a site or area and as such one has to collect repeat data in a fixed time window to know area specific dynamics of a natural hazard. In the first article scientists have collected useful

data pertaining to a mega tsunami genesis. However, such data can help significantly only when we have repeat data sets to realistically gather unique signals to extrapolate the obtained on surface information on tsunami genesis due to land slide by comparing the unique signals from past earthquakes through real time earthquake models. If we can pick up similar signals before onset of an earthquake we can use these signals as probable precursors. Similarly, unique signals of different type from field data can be used as pre disaster warning to prepare to face onset of different types of natural hazards. In the second article authors have clearly brought out slow spreading temporal changes in drylands that affect both the soil and water (the vital ingredients to help those living in such lands in producing and conserving life saving food and water and safeguarding soil fertility and erosion). Effective prevention of desertification requires both local management and macro policy approaches that promote sustainability of ecosystem services. Since onset and spreading of this disaster is temporally slow compared to earthquakes and tsunamis it is advisable to focus on prevention, because attempts to rehabilitate desertified areas are costly and tend to deliver limited results. Desertification is having major impact in many places on our planet today, and is expected to affect humanity even more in the future as we experience an increase in human population, and as our planet faces scarcity of natural resources such as clean water. The process happens due to a number of reasons, but much of the desertification that is occurring around the world today is caused by human activity on lands that are extremely vulnerable to overexploitation and improper agricultural methods. In arid regions, grass and other vegetation is necessary to keep the soil in place. If the vegetation is overgrazed by livestock, there is nothing that remains to prevent soil from blowing or washing away, and if this process occurs long enough, it can lead to desertification. Desertification makes natural disasters worse. Events such as flooding, dust storms, and pollution, all become stronger in areas with heavily degraded soils. Without any plants stabilizing the soil and slowing down the runoff, rainwater easily accumulates and floods human settlements in the blink of an eye. Except causing damage, flood water also picks up unwanted pollutants while making its progress through urban areas, and that's how pollution spreads over vast areas.

As stated by the authors dryland vulnerability can slowly but steadily lead to desertification if ecosystem health is not improved and area specific evapotranspiration is not controlled. Assessment of future scenarios shows that major interventions and shifts in ecosystem management will be needed to overcome challenges related to desertification.

Such interventions are to be implemented at local to global scales, with the active engagement of stakeholders and local communities. Societal and policy responses vary according to the degree of desertification that a society faces. This intensity of responses needs to be rejected accordingly in National Action Programmes. The new project (CMIP6) under execution (mentioned in the second article) can help if experts from vulnerable regions exchange real field data based models and eliminate the lapses in our preventive measures. Since there are many semi arid tracts in our country we can plan concerted research efforts in these tracts using the expertise (through direct interaction) of scientists fighting desertification in many countries.

All the important observations brought out in these two articles stress the necessity to give due importance to repeatedly acquired real field data as earth system data are intricately intertwined and need to be studied precisely following a viable strategy, instead of coming to conclusions mainly based on statistical data. Such an approach helps us to better understand the role of nature and man in degrading our environment and generating local, regional and global natural hazards. If properly implemented the well conceived strategies can help us to face the ill effects with well articulated resilience attitude.

It is time for us to change our research approaches that are confined to lab / internet based models and concentrate on real time data to address local, regional and global natural hazards assuming every segment of our earth has direct or indirect link with other segments. Such large scale co-operation in data generation, processing and interpretation is vital for us to make our research useful in every sense.

***In This Issue**

In addition to Editorial and News at a Glance this issue contains 15 research articles, Book Review and a report on 54th Annual Convention of IGU. It is heartening to note that 4 of the articles have addressed some of the basic problems faced by the common man. I am happy to publish two articles on forecasting earthquakes adopting entirely different approaches.

One important phase of my life comes to an end on 31st March. I have been inspired and motivated by number of challenges, which helped me to live my life with an amount of satisfaction. Managing JIGU helped me to learn many lessons; both good and not so good; an essential part of LIFE. I thank one and all for their support and help.

P.R.Reddy

Quotations to Inspire Success in Your Life and Profession

"I find that the harder I work the more luck I seem to have."

Thomas Jefferson (1743-1826) was an American statesman, one of the Founding Fathers of the United States.

"Success usually comes to those who are too busy to be looking for it."

Henry David Thoreau (1817 -1862) was an American philosopher and historian.

"It is better to fail in originality than to succeed in imitation."

Herman Melville (1819 -1891) was an American novelist and short story writer.

"Don't be afraid to give up the good to go for the great."

John D. Rockefeller (1839 -1937) was an American oil industry business magnate, industrialist and philanthropist.

"Success is not final; failure is not fatal: It is the courage to continue that counts."

Winston S. Churchill (1874 - 1965) was a former Prime minister of United Kingdom.

"If life were predictable it would cease to be life, and be without flavor."

Eleanor Roosevelt (1884-1962) was an American politician, diplomat and activist.

"You're only here for a short visit. Don't hurry, don't worry. And be sure to smell the flowers along the way."

Walter Hagen (1892 -1969) was an American professional golfer.

"All of life is peaks and valleys. Don't let the peaks get too high and the valleys too low."

John Wooden (1910 -2010) was a head coach of basketball at the University of California.

"The road to success and the road to failure are almost exactly the same."

Colin R. Davis (1927 -2013) was an English conductor.

"There are two types of people who will tell you that you cannot make a difference in this world: those who are afraid to try and those who are afraid you will succeed."

Ray Goforth (1931-1990) was leader of technical staff at Boeing.

"However difficult life may seem, there is always something you can do and succeed at."

Stephen Hawking (1942--) is an English theoretical physicist, cosmologist and author.

Critical study on P- and S-waves radiation and computation of earthquake magnitude due to simple crack models

Ajit De

Department of Mathematics, Siliguri College, Siliguri-734001, India
Email: ajit_math@rediffmail.com

ABSTRACT

The seismic radiation due to a dynamic crack model has been obtained in frequency domain by considering integral transformed displacement field in an infinite medium. The far field seismic spectra of P- and S-wave arrivals have been computed for the model. Study has also been extended in case of static elliptical shear crack model. Constant far-field displacement spectra have been observed at low frequencies and decay as some power of inverse frequency at high frequencies. Earthquake magnitude or Richter magnitude due to the source model has been computed and a comparative study of different magnitude scales has been presented. The special character of the source model has been compared and discussed with spectral scaling law.

Key words: Earthquake, Seismic radiation, Crack, Fourier transform, Richter magnitude.

INTRODUCTION

The radiation due to dislocation or crack models is useful in the study of deformation due to earthquakes. The radiation from simple source model has been obtained here in frequency domain by taking Fourier transformation. The total moment of any seismic source can also be obtained as low frequency limit of transformed time domain displacement field. It has been observed that individual earthquake is different from each other and can be modeled with different spectral scaling law. In the present study, far field seismic spectra at the body wave arrivals have been computed for both static and dynamic crack models with spectral behavior of the source time function. The spectral scaling law for the models has also been represented. An effort has also been made to compute the possible amplitude or earthquake magnitude for the source model and a comparative study of different magnitude scales has also been presented.

Earthquake source theories forecast a constant far-field displacement spectrum at low frequencies and the spectrum is inversely proportional to some power of frequency (ω) at high frequencies (Molnar et al., 1973; Brune, 1970). The near field signals radiated by earthquakes may become quite complex due to scattering, multipathing etc. and hence the actually observed seismogram resembles the source time function only at long periods (Madariaga, 2007). In general, the seismic spectra are of different types. It has been observed that spectra decay approximately as inverse square of the frequency (ω) at high frequencies (Aki, 1967; Brune, 1970) and the sources are described by seismic moment and corner frequency. But the spectrum of a trapezoidal source-time function is proportional to seismic moment (M_0) at low frequencies, a ω^{-1} segment at intermediate frequencies and a ω^{-2} fall off at high frequencies (Shearer,

2009). Earthquake size can be quantified by seismic moment (M_0) as it is directly related to the fundamental physical property of the source and various magnitude scales can be represented as functions of seismic moment. It is to be noted that the different earthquake measurement scales (M_L , m_b and M_S) exhibit large scatter among individual events of same moment and this may be due to variations in stress drop or other source properties or regional variations (Shearer, 2009).

Lancieri et al., (2012) studied the spectral scaling properties of a set of 68 aftershocks of the 2007 November 14 Tocopilla earthquake in north Chile under the assumption that the aftershocks satisfy an inverse omega-square spectral decay model. The aftershocks of Tocopilla earthquake are self-similar and are supported by Aki scaling law of seismic spectrum with the property of invariance of the apparent stress drop with earthquake size and invariance of a non-dimensional constant with the event size. Prieto et al., (2004) studied the scaling relationships of source parameters and self-similarity of earthquake spectra by analyzing 400 small earthquakes and observed that the ratio between radiated seismic energy and seismic moment is nearly constant and the corner frequencies vary inversely as the cube root of seismic moment.

The advantage of the present study is that it can be used to predict a suitable source model of an earthquake event and also the possible spectral amplitude due to some given seismic moment of the event.

FORMULATION AND CALCULATION OF THE SEISMIC SPECTRA

The present study has been extended to tackle two types of source models – Dynamic and Static.

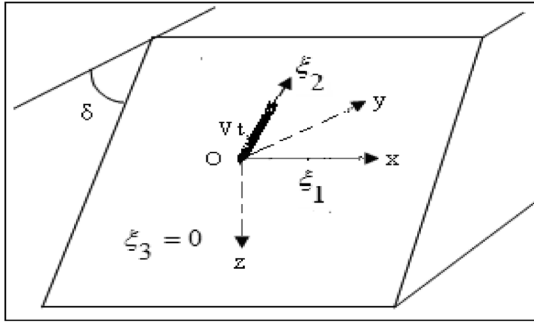


Figure 1. Dynamic Crack model under constant shear traction with two coordinate systems.

Case A: Dynamic Model

Effort has been made to reproduce far-field radiation and predict high frequency radiation by analyzing a two dimensional dynamic shear crack model as was proposed earlier by the author (De, 2014). The shear crack nucleates at a depth below the surface and propagates towards the surface with constant velocity V ($<$ shear wave velocity β) and under the influence of stress drop across the fault plane (De, 2014). The source has been considered as a time dependent dislocation and it acts as trigger for an earthquake with the bounding surface $z = -h$ in the half-space being free. The results in the study have been obtained in an infinite medium and in frequency domain via body force equivalent (De, 2014; Roy, 1979).

The displacement field due to a two dimensional dynamic crack [Figure 1] under constant shear traction acting on an inclined plane of arbitrary dip, can be evaluated following the author's earlier paper (De, (2014)). The displacement field at the outer edge P-wave arrival can be obtained from a similar expression as given in equation (4.13) of the author's paper (De, (2014)), but in an infinite medium by taking limit dimensionless time $\tau \rightarrow \frac{\beta}{\alpha} + 0$. The corresponding spectrum is given by

$$u_r(\omega) \approx \text{Re} \left[-\frac{1}{4\sqrt{2}(1+i)\pi R^*} \left(\frac{V}{\omega}\right)^{3/2} \frac{\mu\pi}{\alpha} A \exp[-i\omega(\beta/\alpha)] \right. \\ \left. \times \exp\left[-\frac{3}{2} \tanh^{-1}\left(\frac{RV}{\beta\omega} \{\cos\delta\eta - i\sin\delta(\eta^2+1)^{1/2}\}\right)\right] \eta \langle \eta e_r + i(\eta^2+1)^{1/2} e_z \rangle \frac{\partial \eta_p}{\partial \tau} \right] (2.1) \\ \left[\left(\frac{RV}{\beta} \{\cos\delta\eta - i\sin\delta(\eta^2+1)^{1/2}\}\right)^2 - \omega^2 \right]^{1/4}$$

where R^* is the epicentral distance, dimensionless time $\tau = \frac{\beta t}{R^*}$ and ω , the angular frequency.

The spectrum corresponding to S-wave arrival as dimensionless time $\tau \rightarrow 1 + 0$ is given by

$$u_s(\omega) \approx \text{Re} \left[-\frac{1}{4\sqrt{2}(1+i)\pi R^*} \left(\frac{V}{\omega}\right)^{3/2} \frac{\mu\pi}{\alpha} A \exp[-i\omega] \right. \\ \left. \times \exp\left[-\frac{3}{2} \tanh^{-1}\left(\frac{RV}{\beta\omega} \{\cos\delta\eta - i\sin\delta(\eta^2 + \frac{\alpha^2}{\beta^2})^{1/2}\}\right)\right] \frac{(2\eta^2 + \frac{\alpha^2}{\beta^2})}{\eta} \langle \eta e_s + i \frac{\eta^2}{(\eta^2 + \frac{\alpha^2}{\beta^2})^{1/2}} e_z \rangle \frac{\partial \eta_s}{\partial \tau} \right] (2.2) \\ \left[\left(\frac{RV}{\beta} \{\cos\delta\eta - i\sin\delta(\eta^2 + \frac{\alpha^2}{\beta^2})^{1/2}\}\right)^2 - \omega^2 \right]^{1/4}$$

The condition at the plane of crack surface $\zeta_3 = 0$:

$$\tau_{32} = \tau_0 + \tau_1 \zeta_2 ; \quad 0 < \zeta_2 < Vt,$$

$$\tau_{33} = 0$$

$$u_1 = u_2 \text{ for } \zeta_2 \notin (0, Vt) \text{ and } \tau_0, \tau_1 = \text{constants.}$$

The spectral behavior of the source time function is of the order $\omega^{-3/2}$, moderate than Brune's inverse omega-squared decay model (Brune, 1970). The corner frequency for the self-similar expanding crack model can be obtained as a spectrum's corner frequency where the high and low frequency trends intersect.

Case B: Static Model

Study has also been extended to a buried elliptic static shear crack model along an inclined fault plane with the bounding surface $z = -h$ in a half-space being free.

The displacement field at the outer edge P-wave arrival due to a static elliptic shear crack model [Figure 2] can be expressed as dimensionless time $\tau \rightarrow \frac{\beta}{\alpha} + 0$ [Appendix -A],

$$\vec{u}_r(\tau) \approx \frac{\alpha}{\beta} abH\left(\tau - \frac{\beta}{\alpha}\right) \text{Re} \left[\frac{\sqrt{2}\beta}{4\pi R_2 \alpha^2 S_2^{1/2}} \frac{8b(1-\nu)P}{\pi} A \frac{\partial K_{p_2}}{\partial \tau} \Big|_{k_{p_2} = \frac{S_2}{R_2}} \right. \\ \left. \left\{ \left(\tau - \frac{\beta}{\alpha}\right)^{3/2} \left(\frac{\alpha}{\beta}\right)^{3/2} \vec{M}_{p_1}\left(i\frac{S_2}{R_2}\right) + 2i\left(\tau - \frac{\beta}{\alpha}\right)^{3/2} \left(\frac{\alpha}{\beta}\right)^{1/2} \vec{M}_{p_2}\left(i\frac{S_2}{R_2}\right) \right\} \right] \chi = \chi^* (2.3)$$

or equivalently, $\vec{u}_r(\tau) \approx M_0 H\left(\tau - \frac{\beta}{\alpha}\right) \text{Re} \left[\frac{\sqrt{2}\beta}{\pi^2 R_2 \alpha^2 S_2^{1/2}} A \frac{\partial K_{p_2}}{\partial \tau} \Big|_{k_{p_2} = \frac{S_2}{R_2}} \right. \\ \left. \left\{ \left(\tau - \frac{\beta}{\alpha}\right)^{5/2} \left(\frac{\alpha}{\beta}\right)^{3/2} \vec{M}_{p_1}\left(i\frac{S_2}{R_2}\right) + 2i\left(\tau - \frac{\beta}{\alpha}\right)^{3/2} \left(\frac{\alpha}{\beta}\right)^{1/2} \vec{M}_{p_2}\left(i\frac{S_2}{R_2}\right) \right\} \right] \chi = \chi^* (2.4)$

where \bar{A} is some constant and ν is the Poisson's ratio.

The substitutions used in the above equation are

$$\xi = K \cos \chi, \quad \eta_p = K \sin \chi \quad \&$$

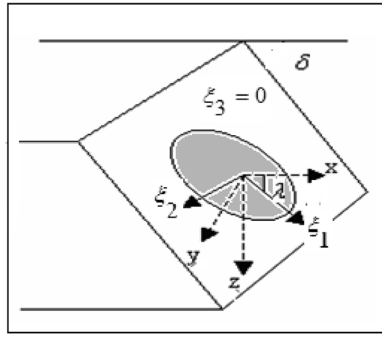
$$x = r \cos \theta, \quad y = r \sin \theta.$$

Thus the corresponding amplitude of the spectrum is given by,

$$u_r(\omega) \approx M_0 \text{Re} \left[-\frac{1}{\omega^{5/2}} \frac{2(1+i)}{\pi^2 R_2 \alpha} \left(\frac{\beta}{S_2 \alpha}\right)^{1/2} \Gamma(5/2) e^{-i\omega(\beta/\alpha)} \right] \chi = \chi^* (2.5)$$

and similarly for S-wave,

$$u_s(\omega) \approx M_0 A'' \text{Re} \left[-\frac{1}{\omega^{5/2}} \frac{2(1+i)}{\pi^2 R_2 \alpha} \left(\frac{\beta}{S_2 \alpha}\right)^{1/2} \Gamma(5/2) e^{-i\omega} \right] \chi = \chi^* (2.6)$$



The constant in-plane shear loading on the crack surface $\xi_3 = 0$

$$\tau_{\xi_1\xi_3} = -PH \left(1 - \sqrt{\frac{\xi_1^2}{a^2} + \frac{\xi_2^2}{b^2}}\right) \delta(t) \delta(\xi_3)$$

$$\tau_{\xi_2\xi_3} = -PH \left(1 - \sqrt{\frac{\xi_1^2}{a^2} + \frac{\xi_2^2}{b^2}}\right) \delta(t) \delta(\xi_3)$$

$$\tau_{\xi_3\xi_3} = 0 \quad \forall (\xi_1, \xi_2, \xi_3) \in S$$

Figure 2. Elliptic Shear Crack model with two coordinate systems

where

$$S_2 = \{r(\cos \chi \cos \theta + \sin \chi \sin \theta \cos \delta) + h \sin \chi \sin \delta - \sqrt{a^2 \cos^2(\chi - \lambda) + b^2 \sin^2(\chi - \lambda)}\}$$

$R_2 = \sqrt{S_2^2 + (h \cos \delta - r \sin \theta \sin \delta)^2}$ is minimum at $\chi = \chi^*$ and M_0 = Scalar Seismic Moment of the crack model (Aki, 1966; Kelis-Borok, 1959)

= μ [Area of the elliptic crack face] [1- ν Maximum final dislocation for 100% stress drop]

= $\mu(\pi ab) \frac{3}{4} \left(\frac{\alpha}{\beta} \frac{2b}{\mu\pi} P\right)$ [Poisson's ratio $\nu = 0.25$, for the present case]

= $\frac{18}{7} ab^2 P$ [where $\frac{\alpha}{\beta} \approx \sqrt{3} \approx \frac{12}{7}$, for the present case] (2.7) where P is the uniform stress drop over the fault zone.

Thus, the Scalar Seismic Moment for the elliptic crack model is proportional to the cube of the linear dimension of the model and it may be predicted that the scalar seismic moment M_0 grows as the cube of the linear size of earthquake. The corresponding spectral behavior of the source time function is of the order $\omega^{-5/2}$, steeper than Brune's (1970) inverse omega-squared decay model.

DISCUSSION

The spectra [Eqns. (2.1) & (2.2)] for the dynamic crack model under constant shear traction decay with frequency at least as fast as $\omega^{-3/2}$ at frequencies higher than the corner frequency (De, (2014)). It is clear from Figure 3 that the corner frequency for P-wave spectra due to a two dimensional dynamic crack model moving with rupture velocity more than the shear wave velocity, decreases with the inclination of the fault plane. Similar phenomenon with slight variation of corner frequency is observed for rupture velocity equal to that of shear velocity (Figure 4). It is clear from the equations (2.1) and (2.2) that the shape of the spectra for the model are determined by the parameters $\frac{VR}{\beta} \{\cos \delta \eta - i \sin \delta (\eta^2 + 1)^{1/2}\}$ and $\frac{VR}{\beta} \{\cos \delta \eta - i \sin \delta (\eta^2 + \frac{\alpha^2}{\beta^2})^{1/2}\}$; respectively for P and S waves and can be used to determine the corner frequencies of the respective spectrum. Figure 5 shows that P-wave corner frequency exceeds S-wave corner frequency for the dynamic crack model and spectra are nearly alike for different rupture velocities. The P- and S-wave corner frequency ratio for the model is very near to

one. Our result resembles with the observation of Savage, (1974) and Molnar et al., (1973).

Seismic moment is a key observable parameter related to an earthquake. It is a static measure of earthquake size and quantitative measure related to the amount of earth movement during the event. It is also independent of rupture time history. The elliptic crack model as discussed in equation (2.3) or (2.4) may fit as a better approximation of seismic rupture process than Haskell's dislocation model (Haskell, 1964; Haskell, 1966) and the seismic spectra as presented in equations (2.5) and (2.6) decay as $\omega^{-5/2}$ at high frequencies (Figure 6).

In previous work referring to the computation of theoretical seismogram model due a two dimensional dynamic crack (De, 2014, Figure 2) shows that maximum dimensionless amplitude is 0.112 at the dimensionless time 1.0. We consider the parameters of the study as

$$r = y = 50 \text{ km}, \beta = 3.5 \text{ km/s}, \rho = 2.8 \text{ gm/cm}^3, \mu = 3.43 \text{ MPa}, \tau_0 = 10 \text{ MPa}, \pi = 3.14.$$

Now taking the approximate empirical formula for the computation of local (Richter) magnitude, M_L (Bullen and Bolt, 1985)

$$M_L = \log_{10} A + 2.56 \log_{10} D - 1.67 \quad (3.1)$$

where A is the measured maximum ground displacement amplitude in micrometers (at the S-wave arrival) and $D = r$ is the distance from the event (in km), the computed local magnitude M_L is 6.0.

[The computed amplitude for the present case

$$A = \frac{3\tau_0}{\mu\pi^2 r} 0.11 = 1949.62]$$

The local (Richter) magnitude scale is used to measure shallow earthquake events of magnitude less than 6.5 and is used complimentary to other magnitude scales like, Body wave Magnitude (m_b) and Surface wave magnitude (M_s). In the present days the moment magnitude scale (M_w) is used for effective computation of large earthquake events and with the respective formula for its computation is (as defined in Aki and Richards, 2002)

$$M_w = \frac{2}{3} [\log_{10} M_0 - 9.1] \quad (3.2)$$

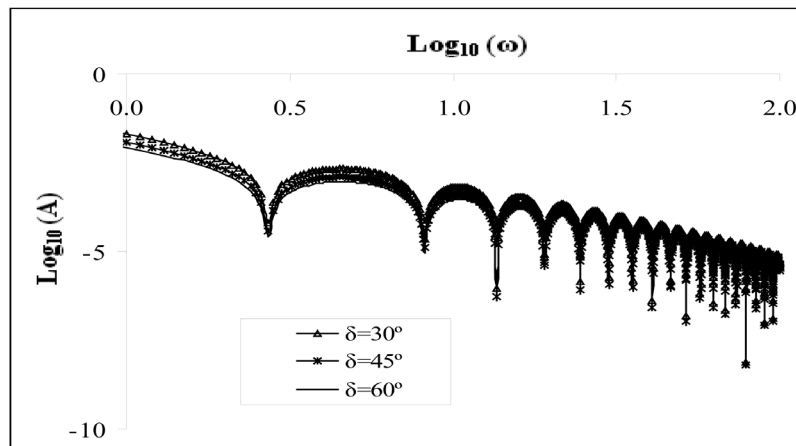


Figure 3. Dimensionless spectra (A) – frequency (ω) graph at an epicentral distance 100 km. (in y-z plane) due to a two dimensional dynamic shear crack model moving with velocity greater than that of shear wave (i.e., $V > \beta$) at the P-wave arrival for different dip angles (δ).

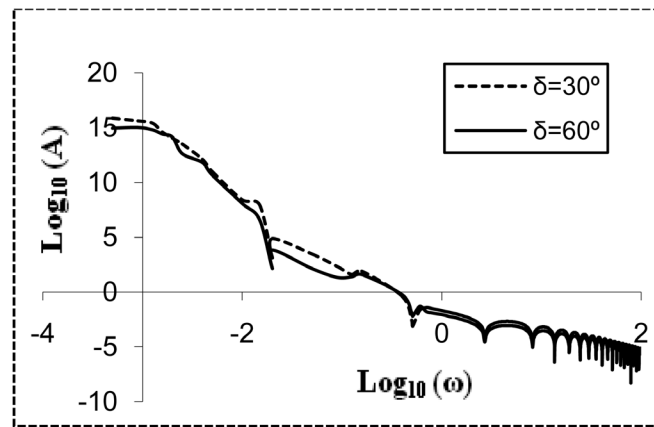


Figure 4. Dimensionless spectra (A) – frequency (ω) graph at an epicentral distance 100 km. (in y-z plane) due to a two dimensional dynamic shear crack model moving with velocity equal to that of shear wave (i.e., $V = \beta$) at the P-wave arrival for different dip angles (δ).

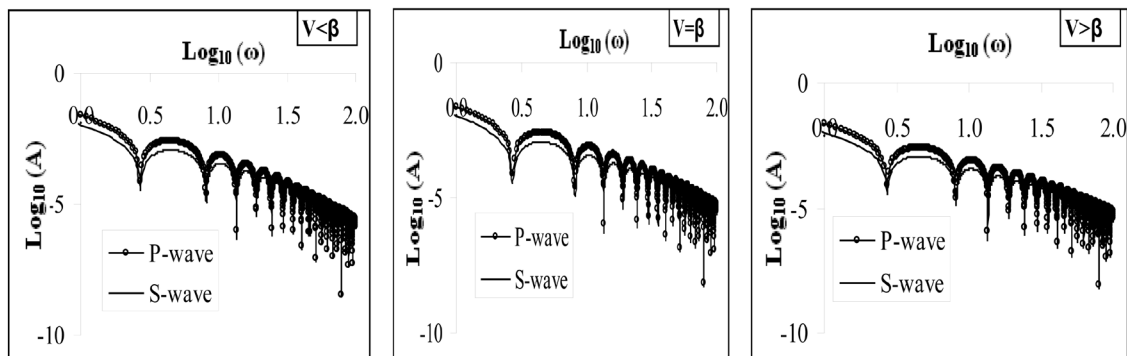


Figure 5. Comparison of dimensionless spectra (A) at the arrivals of P- and S-waves against dimensionless frequency (ω) at an epicentral distance 50 km. (in y-z plane) due to a dynamic two dimensional shear crack model moving with different rupture velocity at the dip angle $\delta = 60^\circ$.

Where, M_0 is the seismic moment in N-m. Local magnitude scale $M_L \approx M_w$ (Prieto et. al., 2004) and the present study establish the fact (Table 1 & 2). The present study also

reveals that the maximum predicted amplitude at a place decreases with the increasing values of dip angle and increase in stress drop increases the predicted amplitude

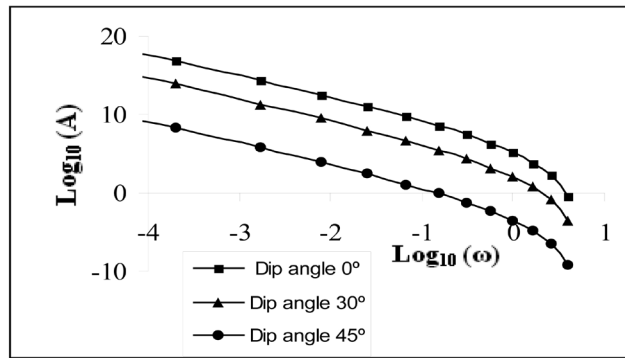


Figure 6. Dimensionless spectra (A) – frequency (ω) graph at an epicentral distance 100 km due to a static elliptic in-plane crack model with semi-axis ratio $a/b = 2$.

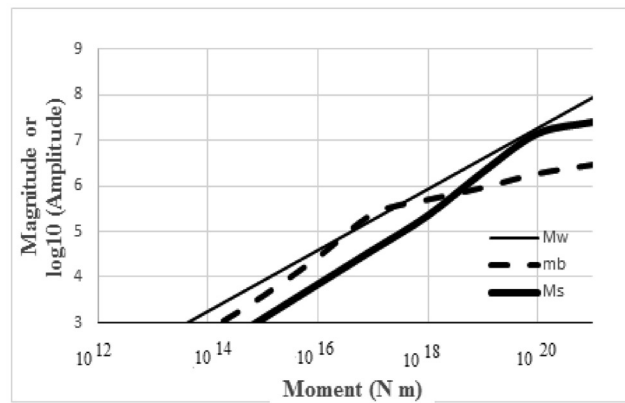


Figure 7. Different magnitude scales (M_w , m_b and M_s) or predicted \log_{10} (Amplitude) for the $\omega^{-3/2}$ shear moving crack model have been presented here as functions of seismic moment (M_0). The crack is moving with a velocity $(9/10)$ times that of shear wave (β) velocity and a constant stress drop of 3 MPa has been assumed. Approximately, the amplitude is proportional to M_0 initially, $M_0^{2/3}$ intermediate stage and finally $M_0^{1/3}$.

Table 1. Comparative study on different magnitude scales at a place (epicentral distance 50 Km.) for different source parameters of the dynamic crack model.

Sl. No.	Rupture velocity (V)	Stress Drop on the fault plane	Dip angle of the fault plane (δ)	Maximum Amplitude (Micrometer)	Seismic Moment (M_0) (N-m)	M_w	M_L
1.	V=0.9 β	3 MPa	30°	595.04	3×10^{17}	5.6	5.4
2.			60°	478.16			5.4
3.		6 MPa	30°	1190.08	6×10^{17}	5.8	5.8
4.			60°	956.32			5.7
5.	V=1.2 β	3 MPa	30°	691.93	4×10^{17}	5.7	5.5

Table 2. Comparative study on different magnitude scales at a place (epicentral distance 50 Km.) For different source parameters of the static crack model with semi-axis ratio $a/b = 2$.

Sl. No.	Stress Drop on the fault plane	Dip angle of the fault plane (δ)	Maximum Amplitude (Micrometer)	Seismic Moment (M_0) (N-m)	M_w	M_L
1.	3 MPa	30°	598.60	4.2×10^{17}	5.7	5.5
2.		60°	528.32			5.4
3.	6 MPa	30°	1265.31	8.4×10^{17}	5.9	5.8
4.		60°	927.10			5.6

and seismic moment at a place considerably (Table 1 & 2). The Table 1 shows a comparative study at different rupture velocities of the dynamic crack model and predicts increasing amplitude and earthquake magnitude at higher rupture velocity. Figure 6 shows that \log_{10} (Dimensionless amplitude) = 14.2 (for $\delta = 30^\circ$) at low frequency (ω) limit (i.e., $\omega \rightarrow 0$) and this can be used to compute the seismic moment of the event. The computation reveals that corresponding \log_{10} (amplitude) = $\log_{10} (M_0) = 17.62$ and $M_W = 5.7$. Again Figure 4 shows that \log_{10} (Dimensionless amplitude) = 15.8 (for $\delta = 30^\circ$) at low frequency limit and the corresponding \log_{10} (amplitude) = $\log_{10} (M_0) = 19.22$ and $M_W = 6.7$. Figure 7 shows the predicted amplitude for given seismic moment in different magnitude scales (M_w , m_b and M_S). The m_b approximates M_w upto the magnitude 5.5 and under predicts M_w above that value. But M_S agrees approximately with M_W between 6.6 to 7.3 and under predicts M_W outside the interval. The present study approximately agrees with the results of an ω^{-2} source model of Madariaga (Shearer, 2009) for an assumed constant stress drop of 3 MPa. If the stress drop be increased to another constant value, say 6 MPa and other conditions be kept fixed then the corresponding moment as well as predicted amplitude will rise comparatively. Similar study with slight variation is observed for the static model.

Appendix-A

Approximate displacement field near outer edge P-wave arrival due to the static shear crack model

The displacement field at the outer edge P-wave arrival can be expressed in an infinite medium as dimensionless time $\tau \rightarrow \frac{\beta}{\alpha} + 0$ (De, (2013); Roy, (1984)),

$$\vec{u}_p \approx \lim_{\varepsilon \rightarrow 0, \tau \rightarrow \frac{\beta}{\alpha} + 0} H\left(\tau - \frac{\beta}{\alpha}\right) \int_{\chi^* - \varepsilon}^{\chi^* + \varepsilon} \frac{2ab}{4i\pi R_2 \alpha^3} \frac{8b(1-\nu)P}{\pi} \frac{d\chi}{\chi^* - \varepsilon} \left[\left(\frac{\beta}{4R_2}\right) \frac{\partial K_{P_2}}{\partial \tau} \left\{ \left(\tau - \frac{\beta}{\alpha}\right)^2 i \left(\frac{\alpha}{\beta}\right)^2 \vec{M}_{P_1}(K_{P_2}) - 2\left(\frac{\alpha}{\beta}\right) \left(\tau - \frac{\beta}{\alpha}\right) \vec{M}_{P_2}(K_{P_2}) \right\} \right] d\chi \quad (A.1)$$

where \bar{A} is some constant.

Now evaluating the integral at $\tau = \frac{\beta}{\alpha}$ and proceeding to the limit $\varepsilon \rightarrow 0$,

$$\vec{u}_p \approx H\left(\tau - \frac{\beta}{\alpha}\right) \lim_{\varepsilon \rightarrow 0} \text{Re} \left[\frac{2\varepsilon\alpha ab}{2i\pi R_2 \alpha^3} \frac{8b(1-\nu)P}{\pi} \frac{\partial K_{P_2}}{\partial \tau} \left\{ \left(\tau - \frac{\beta}{\alpha}\right)^2 i \left(\frac{\alpha}{\beta}\right)^2 \vec{M}_{P_1}\left(i\frac{S_2}{R_2}\right) - 2\left(\frac{\alpha}{\beta}\right) \left(\tau - \frac{\beta}{\alpha}\right) \vec{M}_{P_2}\left(i\frac{S_2}{R_2}\right) \right\} \right] \chi = \chi^* \quad (A.2)$$

Again R_2 is minimum at $\chi = \chi^*$ and $R_1(\chi^* + \varepsilon) = R_1(\chi^*) + \frac{1}{2}\varepsilon^2 \frac{S_1}{R_1}$. Thus ε can be approximated as $\varepsilon = \frac{\sqrt{2R_1}}{S_1^{1/2}} \left(\frac{\alpha}{\beta}\right)^{1/2} \left(\tau - \frac{\beta}{\alpha}\right)^{1/2}$. Hence,

$$\vec{u}_p \approx \frac{\alpha}{\beta} abH\left(\tau - \frac{\beta}{\alpha}\right) \text{Re} \left[-\frac{\sqrt{2}\beta}{4\pi R_2 \alpha^3 S_1^{1/2}} \frac{8b(1-\nu)P}{\pi} \frac{\partial K_{P_2}}{\partial \tau} \right]_{K_{P_2} = \frac{S_2}{R_2}} \left\{ \left(\tau - \frac{\beta}{\alpha}\right)^{3/2} \left(\frac{\alpha}{\beta}\right)^{3/2} \vec{M}_{P_1}\left(i\frac{S_2}{R_2}\right) + 2i \left\{ \left(\tau - \frac{\beta}{\alpha}\right)^{1/2} \left(\frac{\alpha}{\beta}\right)^{1/2} \vec{M}_{P_2}\left(i\frac{S_2}{R_2}\right) \right\} \right\} \chi = \chi^* \quad (A.3)$$

where M_{P_j} (K_{P_j}) $\{j=1,2\}$ are functions of K_{P_j} (De, (2013)) and are given by

$$\vec{M}_{P_1}(K) = A^* \frac{\{2\zeta_s(\xi \hat{e}_x + \eta \hat{e}_y) + i(2\xi^2 + 2\eta^2 + \frac{\alpha^2}{\beta^2})\hat{e}_z\}}{2(K\sqrt{a^2 \cos^2(\chi - \lambda) + b^2 \sin^2(\chi - \lambda)})^3} \frac{(\xi^2 + \eta^2 + 1)^{1/2}}{(K^2 + 1)^{1/2}}$$

$$\vec{M}_{P_2}(K) = A^* \frac{\{2\zeta_s(\xi \hat{e}_x + \eta \hat{e}_y) + i(2\xi^2 + 2\eta^2 + \frac{\alpha^2}{\beta^2})\hat{e}_z\}}{2K^2(a^2 \cos^2(\chi - \lambda) + b^2 \sin^2(\chi - \lambda))} \frac{(\xi^2 + \eta^2 + 1)^{1/2}}{(K^2 + 1)^{1/2}}$$

$F(\xi, \eta)A^* = [(A_1 \cos \lambda - A_2 \sin \lambda)\xi \cos \delta + (A_1 \sin \lambda + A_2 \cos \lambda)\eta] (i-1)(\xi^2 + \eta^2 + 1)^{1/2}$
 $F(\xi, \eta) = (2\xi^2 + 2\eta^2 + (\alpha^2/\beta^2))^2 - 4(\xi^2 + \eta^2)(\xi^2 + \eta^2 + 1)^{1/2}(\xi^2 + \eta^2 + \alpha^2/\beta^2)^{1/2}$
 with the path of steepest descent or Cagniard path as

$$\alpha t = (K^2 + 1)^{1/2} (h \cos \delta - r \sin \theta \sin \delta) - iK [r(\cos \chi \cos \theta + \sin \chi \sin \theta \cos \delta) + h \sin \chi \sin \delta \pm \sqrt{a^2 \cos^2(\chi - \lambda) + b^2 \sin^2(\chi - \lambda)}]$$

ACKNOWLEDGMENT

The work was supported financially by U.G.C., New-Delhi, India under MRP (Sanction No. F PSW-200/15-16 (ERO)). The author is thankful to the referees Dr. Anastasia Kiratzi and Dr. S.N. Bhattacharya for critical evaluation and objective reviewing. Thanks are due to Prof. B.V.S. Murty for final refinement and the Chief Editor, JIGU for valuable suggestions and timely support.

Compliance with Ethical Standards:

The author declares that he has no conflict of interest and adheres to copyright norms.

REFERENCES

- Aki, K., 1967. Scaling law of seismic spectrum, J. Geophys. Res., v.72, pp: 1217-1231.
- Aki, K., 1966. Generation and propagation of G waves from the Niigata earthquake of June 16, 1964. Estimation of earthquake movement, released energy and stress-strain drop from G-wave spectrum, Bul. Earthquake Res. Inst., v.44, pp: 23-88.
- Aki, K. and Richards, P.G., 2002. Quantitative Seismology Second Edition, University Science Books, Sausalito, California.
- Brune, J.N., 1970. Tectonic stress and the spectra of seismic shear waves from Earthquakes, J. Geophys. Res., v.75, pp: 4997-5009.
- Bullen, K.E. and Bolt, B.A., 1985. An introduction to the theory of seismology, 4th ed., Cambridge University Press.

Critical study on P- and S-waves radiation and computation of earthquake magnitude due to simple crack models

- De, A., 2014. Two dimensional self-similar expanding crack problems in elastic half-space, *Wave Motion*, v.51, pp: 852-864.
- De, A., 2013. Computation of synthetic seismogram for a buried elliptic in plane shear dislocation model in an elastic half-space, *J. Indian Math. Soc.*, v.80, pp: 243-263.
- Haskell, N.A., 1966. Total energy spectral density of elastic wave radiation from propagating faults. Part-II. A statistical source model, *Bull. Seismol. Soc. Am.*, v.56, pp: 125-140.
- Haskell, N.A., 1964. Total energy spectral density of elastic wave radiation from propagating faults, *Bull. Seismol. Soc. Am.*, v.54, pp: 1811-1841.
- Keilis-Borok, V.I., 1959. On the estimation of the displacement in an earthquake source and of source dimensions, *Annales de Geophysique*, v.12, pp: 205-214.
- Lancieri, M., Madariaga, R. and Bonilla, F., 2012. Spectral scaling of the aftershocks of the Tocopilla 2007 earthquake in northern Chile, *Geophys.J. Int.*, v.189, no.1, pp: 469-480.
- Madariaga, R., 2007. Seismic source theory, in: Kanamori, H. (Ed.), *Earthquake Seismology*. in: *Treatise of Geophysics*, Academic Press, v.4, no.2, pp: 59-82.
- Molnar, P., Tucker, B.E. and Brune, J.N., 1973. Corner frequencies of P and S waves and models of earthquake sources, *Bull. Seismol. Soc. Am.*, v.63, no.6, pp: 2091-2104.
- Prieto, G.A., Shearer, P.M., Vernon, F.L. and Kilb, D., 2004. Earthquake source scaling and self-similarity estimation from stacking P and S spectra, *J. Geophys. Res.*, v.109, B08310, doi:10.1029/2004JB003084.
- Roy, A., 1984. Diffraction of elastic waves by an elliptic crack, *Int. J. Eng. Sci.*, v.22, pp: 729-735.
- Roy, A., 1979. On dislocations and extended sources in an elastic half-space, *Indian J. Pure Appl. Math.*, v.10. no.1, pp: 100 – 111.
- Savage, J.C., 1974. Relation between P- and S-wave corner frequencies in the seismic spectrum, *Bull. Seismol. Soc. Am.*, v.64, pp: 1621-1627.
- Shearer, Peter M., 2009. *Introduction to seismology*, Cambridge University Press, pp: 241-295.

Received on: 20.6.17; Revised on: 27.8.17; Re revised on: 16.10.17; Accepted on: 30.11.2017

Stress Orientation from Image log and Estimation of Shear Wave Velocity using Multiple Regression Model: A Case Study from Krishna-Godavari basin, India

Rima Chatterjee*¹ and Dip Kumar Singha²

¹Dept. of Applied Geophysics, Indian School of Mines, Dhanbad-826004

²Dept. of Geophysics, Institute of Science, BHU, Varanasi-221005

*Corresponding Author: rima_c_99@yahoo.com.

ABSTRACT

Formation Micro Imager (FMI) logs from four boreholes located in the Krishna-Godavari (K-G) basin, covering an area of about 3760sq km onshore, are analyzed to identify natural fractures and breakouts. These features are used to calculate the in-situ maximum and minimum horizontal stress orientation at different depth intervals in the wells. The orientation of maximum principle horizontal stress (S_H) obtained from orientations of breakouts and drilling induced fractures varies from N14.54°E to N21.84°E for the four wells. The dip of natural fracture varies from 4.83° to 29.31° with a dominating mean azimuth N9°E. The orientation of S_H is in close agreement with the regional NNE trend of the horst-graben, the K-G basin. In addition to stress directions, the mechanical properties of the formations, like Young's modulus (Y), bulk modulus (K), shear modulus (G), Poisson's ratio (σ) and unconfined compressive strength (UCS) are estimated from the density and P-and S-wave velocity (V_p and V_s) log data. Further, correlation between V_p and V_s is examined by multiple regression analyses with squared multiple correlation coefficient (R^2) varying from 0.92 to 0.96. The models developed by multiple regression analysis for V_s can be used to estimate elastic moduli and rock strength for other wells in the K-G basin.

Key words: FMI log, Breakout, Drilling induced fracture, Natural fracture, Stress orientation, Rock mechanical parameters, Shear wave velocity, Krishna-Godavari basin.

INTRODUCTION

Borehole breakouts and drilling induced fractures have long been recognized as stress-induced features because we can use information on their azimuth to determine orientations of in situ principal stresses (Nelson and Hillis, 2005; Nelson et al., 2005; Tingay et al., 2009; Nie et al., 2013). Information of in situ stresses plays an important role in evaluation of seismic risk, and analysis of regional and tectonic activities (Zoback, 1992; Bell, 1996; Trautwein et al., 2010). A thorough understanding of in situ stress conditions and rock properties, such as compressive strength, elastic moduli and anisotropy are required to optimize the wellbore design (Das and Chatterjee, 2017). In any sedimentary basin, these rock properties can be derived from the P- and S- wave velocities. Determination of mechanical properties of rocks is important for a variety of reservoir engineering purposes like hydraulic fracturing, estimation of removable reserves, prediction of wellbore stability and subsidence. No core sample and seismic data are, however, available; only image log, velocity log and conventional logs are available to compute in-situ stress and rock properties. Therefore, in this paper, we focus on (a) identification of breakout, drilling induced fractures and natural fractures from image log, (b) determination of in-situ stress orientation, (c) estimation of rock mechanical

parameters and (d) regression models for prediction of S-wave velocity. The S-wave velocity is important in the study of seismic inversion and petrophysical evaluation, particularly for estimation of geomechanical properties. The P-wave and S wave velocities and density values are used to estimate the shear modulus (G), Young's modulus (Y), bulk modulus (K), Poisson's ratio (σ) and unconfined compressive strength (UCS) of rocks in Krishna-Godavari (K-G) basin.

STUDY AREA

The K-G basin developed at the confluence of the Krishna and Godavari rivers at the east coast of India form the largest basin under the eastern Continental Margin of India (ECMI) (Figure 1). It occupies an area of about 20,000 km² onland and another 13,000 km² offshore (Gupta, 2006). K-G basin encompasses large areas both onland and off shore including those located in deep waters. The basin itself came into existence following rifting along ECMI craton during early Mesozoic (Sastri et al., 1973). Both the onland part of the basin and its off shore host a large number of structural traps that have been mapped and a large number of them established through drilling (Rao, 2001). Enhanced activity for hydrocarbon exploration in the K-G basin within the past decades has emphasized the need for a better understanding

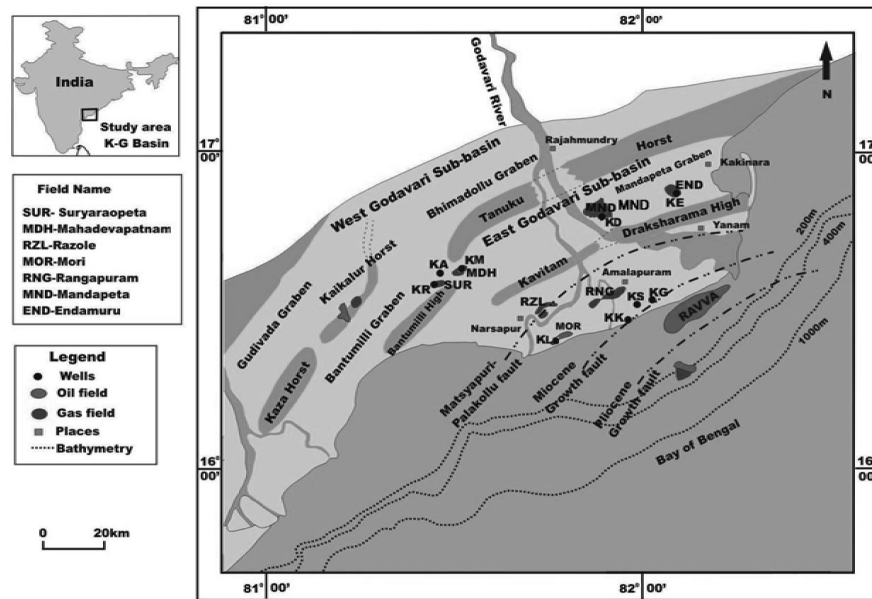


Figure 1. The map illustrates locations of nine wells distributed in the oil/gas fields of Krishna-Godavari basin (after Rao, 2001). Out of these nine wells, data of the four selected wells (KA, KS, KD and KL) are analysed in this study.

of the regional stress regime for the ECMI, in general, and for the K-G basin in particular. Using 4-arm dipmeter caliper log data from 20 wells, a maximum horizontal in situ stress, varying from N54°E to about N-S orientation, was reported by Chatterjee and Mukhopadhyay (2002). In the present study, our aim is to investigate the orientation of horizontal in situ stress from breakout, drilling induced and natural fractures using Formation Micro Imager (FMI) data of four wells; KA, KL, KS and KD drilled by ONGC covering an area of 2005 sq. km in the onshore K-G basin (Figure 1). We also investigate mechanical properties of rocks from five wells; KA, KR, KK, KG and KE distributed in the 3760 sq km area of this basin. The well KA located at the west-Godavari sub-basin encountered the Raghavpuram Shale formation. The wells KS and KL located in the east-Godavari sub-basin have penetrated the Narsapur Claystone, Matsyapuri Sand formation overlying the Vadaparru Shale. The well KD in the same sub-basin encountered the Mandapeta and Gollapalli sandstones overlain by Raghavapuram shale formations. Vertical stress, horizontal stress, pore pressures and fracture pressures were earlier reported for this part of the K-G basin (Singha and Chatterjee, 2014). Knowledge of all these parameters including rock strength is important to understand fracture characteristics of rocks under the stresses induced by hydraulic fracturing for well stimulation (Gray et al., 2012).

Fracture and In-Situ Stress Orientation

Stresses in the Earth can be defined in terms of magnitude and orientation of three principal stresses: maximum, intermediate and minimum. For a vertical well

(as in the present study) and for a normal faulted stress regime, the first principal stress is considered to be vertical (S_v), corresponding to the weight of the overburden, the second principal or intermediate stress as well as the third principal stresses are referred to S_H and S_h indicating the maximum and minimum horizontal principal compressive stresses, respectively. S_H orientation has a significant implication on subsurface fluid flow and fault reactivation (Barton et al., 1988; Tingay et al., 2010a, b) and can be determined from borehole breakouts and drilling induced fractures interpreted from the FMI logs.

Borehole Breakout

Figure 2 shows the typical breakout signatures at several depth intervals of the selected four wells. The well KD in east Godavari sub-basin has penetrated the oldest sediments (Permo-Triassic through Cretaceous sequences) in the K-G basin. The breakouts are observed in this well at depths between 2395m and 2632m, corresponding to a total length of breakout for 114 m. This depth range is characterized by a mean S_H orientation N19.01°E. The well KL has breakouts of 6 m length at a depth interval 1101-1350m characterizing a mean S_H N19.24°E in the Oligocene sediments. The well KS has breakouts at depths between 1300m and 1311m for a length of 8m penetrating the sediments of Oligocene to Miocene with S_H orientation N14.54°E (Singha and Chatterjee, 2014; Singha and Chatterjee, 2015). The deepest well KA, located within 60 km from the well KD in the west-Godavari sub-basin penetrating the early Cretaceous sequences, yields S_H orientation N20.68°E.

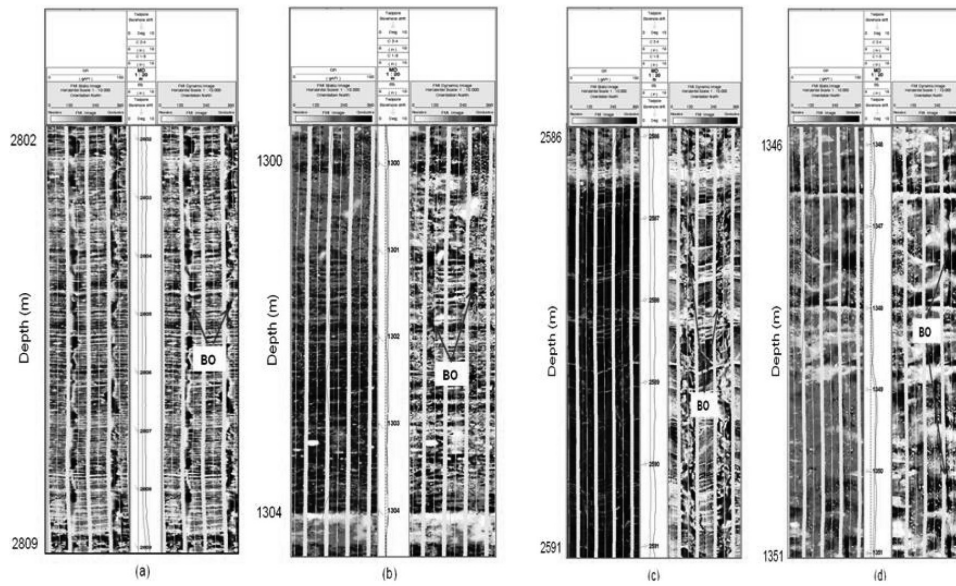


Figure 2: Breakouts observed at selected depth intervals for the wells: (a) KA, (b) KS, (c) (KD) and (d) KL.

Table 1: The orientation of maximum horizontal stress obtained from breakouts and drilling induced fractures observed from FMI logs, Krishna-Godavari basin.

Wells	Depth interval (m)	Length (m)	Orientation from North (degree)		Azimuth of S_H (degree)		Name of Field	Formation	Geological age	
			Azimuth	Mean	Mean	s.d				
Breakout observation										
KA	2800-2807	7	114.14	110.68	N20.68E	±2.76	Mahadevapatnam	Raghavapuram Shale	Early Cretaceous	
	2808-2819	11	110.19							
	2820-2830	10	108.82							
	Total	28								
KL	1101-1104	3	291.11	289.24	N19.24E	±2.64	Mori	Narsapur Claystone	Oligocene	
	1346-1350	3	287.37							
	Total	6								
KS	1300-1303	3	104.65	104.54	N14.54E	±0.12	Rangapuram	Matsyapuri Sandstone	Oligocene to Miocene	
	1306-1311	5	104.48							
	Total	8								
KD	2395-2413	28	106.75	109.01	N19.01E	±1.34	Mandapeta	Gollapalli Sandstone	Jurassic to Early Cretaceous	
	2421-2448	27	109.86							
	2451-2467	16	108.86							
	2476-2482	6	108.33							
	2521-2537	16	110.82					Mandapeta Sandstone	Permo Triassic	
	2581-2592	11	109.75							
	2622-2632	10	110.00							
	Total	114								
Drilling Induced Fracture observation										
KL	1101-1105	4	23.53	21.84	N21.84E	±5.52	Mori	Narsapur Claystone	Oligocene	
	1349-1350	1	209.07							
	1351-1352	1	31.84							
	1445-1448	3	200.43					Matsyapur Sandstone		Oligocene to Miocene
	1558-1565	7	199.03							
	Total	16								

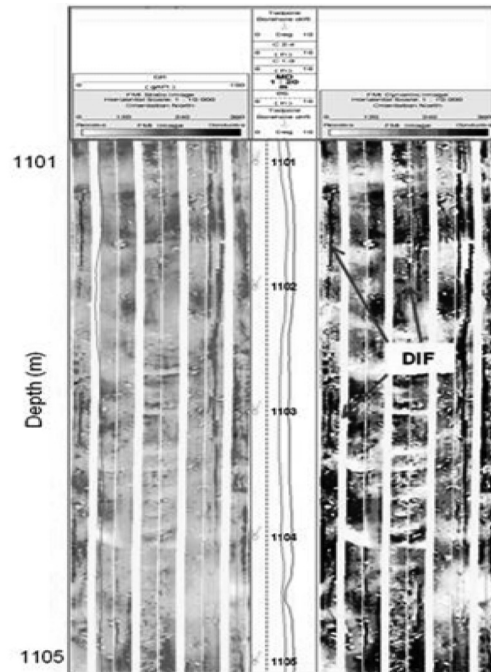


Figure 3: Drilling induced fractures in the selected depth interval are shown.

Drilling Induced Fracture (DIF)

Drilling induced fractures (DIFs) are created when the stresses concentrated around a borehole exceed that required to cause tensile failure of the wellbore wall (Aadnoy, 1990). DIFs typically develop as narrow sharply defined features that are sub-parallel or slightly inclined to the borehole axis in vertical wells and are generally not associated with significant borehole enlargement in the fracture direction (Bell, 1996). The DIFs are only observed for a length of 14m at depth interval 1101-11565m in the well KL (Figure 3). The S_H orientation is $N21.84^\circ E$ in sediments of Oligocene to Miocene. The mean orientation of S_H of the selected four wells is sub-parallel to the NNE regional horst-graben trend.

An average or mean breakout/DIF orientation is calculated as a 'length weighted average breakout/DIF orientation'. Table 1 lists the well identification, depth interval, length, azimuth, mean breakout/ DIF orientation for the given depth interval, and the mean azimuth of S_H for the individual well with standard deviation (s.d), name of oilfield, formation with geologic age. Figure 4 displays the breakout and DIF orientations with depth including the rose diagram indicating the mean S_H direction for the four wells. The S_H orientation obtained from the breakout in well KL differs by 2.6° from that obtained by the DIF.

3.3. Natural Fracture

A fracture is a surface along which a loss of cohesion in the rock texture has taken place. Minerals may fill the entire fracture, converting an open fracture to a healed

or sealed fracture. In this study natural fractures are subdivided into open fracture, partially open fracture and resistive fracture (Rajabi et al., 2010). The fractures are observed on image logs in each wells excepting the well KA. The fluid loss during drilling suggests existence of natural fractures and open or partially open fractures are permeable in-situ. Three types of natural fractures are generally observed; these are: (i) open fracture (OF), which is a resistive fracture, free from fluid and yields white image, (ii) closed fracture (CF), which is low resistive, fluid filled and yields black image, and (iii) partially open fracture (POF), which is moderate resistive, partially fluid filled and yields black-white image. The typical fractures obtained from image logs at the three selected wells (Figure 5) are counted to be 44, 24 and 50 in the KL, KS and KD wells, respectively. Fractures are mostly observed in Narsapur claystone in KL, in Matsyapuri sandstone in KS and in Mandapeta and Gollapalli sandstones in KD, respectively.

The orientations of natural fractures with dips are plotted in stereonet for the wells KL, KS and KD (Figure 6a, b and c). These plots show the distribution of CF, OF and POF in these wells. The dip of the OF and POF varies from 7.8° to 29.31° in well KL, 4.83° to 26.91° in well KS and 6.03° to 22.62° in well KD, respectively. The azimuths of open fractures in well KL, KS and KD vary from $N6^\circ W$ to $N16.62^\circ E$, $N45.69^\circ W$ to NS and $N7^\circ W$ to $N31.85^\circ E$, respectively. Mean azimuth of OF is orientated $N5.31^\circ E$ in well KL, $N22.85^\circ W$ in well KS and $N12.85^\circ E$ in well KD, respectively. The OF as well as POF for the three wells are oriented dominantly in NNE with a few in NNW. Majority

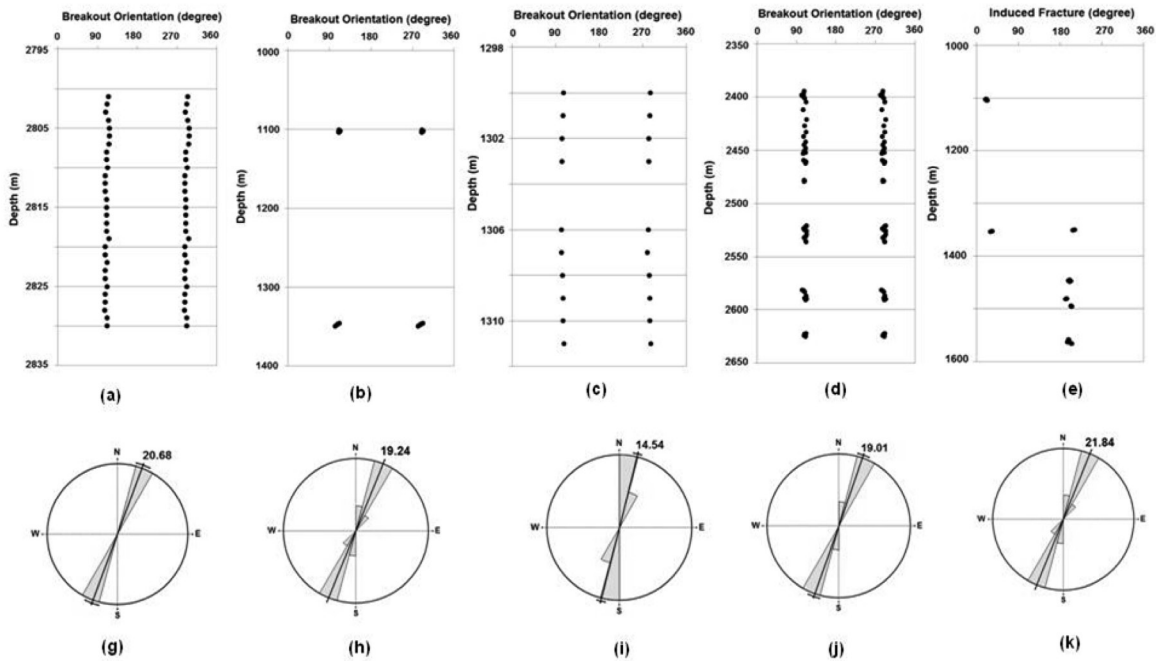


Figure 4: Breakout orientations at the available depth intervals for the wells (a) KA, (b) KL, (c) KS and (d) KD, and (e) orientations of DIF at depths for the well KL are shown. The rose diagrams depict mean breakout horizontal stress (S_H) for the wells: (g) KA, (h) KL, (i) KS, (j) KD, and (k) DIF S_H orientation for the well KL.

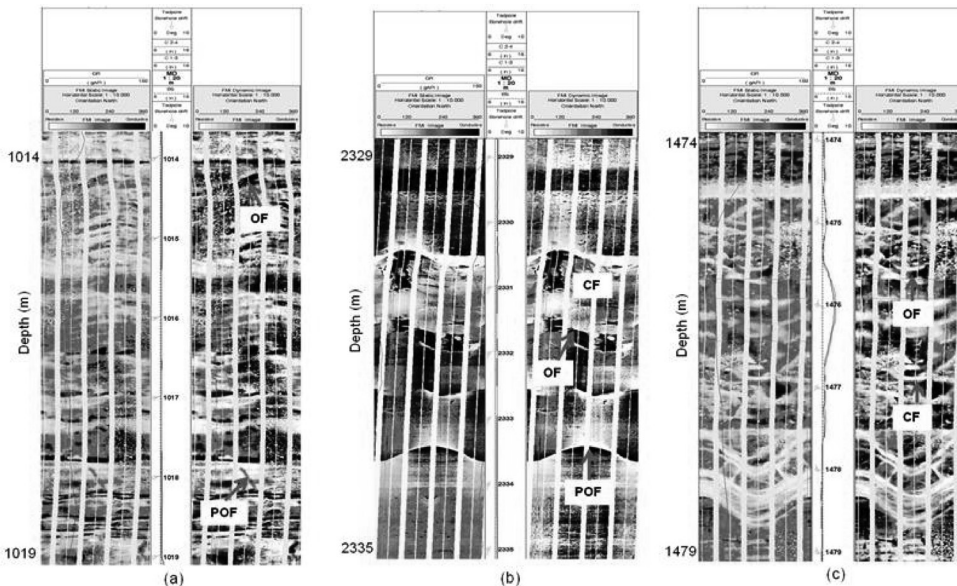


Figure 5: The natural observed fractures CF (closed fracture), OF (open fracture) and POF (partially open fracture) in image logs at selected depth intervals in wells (a) KS, (b) KD and (c) KL.

of the OF follow the mean S_H orientation with a maximum deviation of about 10° .

Azimuths of the natural fractures interpreted from the FMI are dominantly in NNE-SSW with a few in NNW-SSE, and they more or less follow the trend of the faults in the area. The faults and natural fractures are genetically related and are developed under the same stress conditions (Gupta, 2006).

COMPUTATION OF ROCK MECHANICAL PARAMETERS

The orientation of S_H , knowledge of rock mechanical properties and magnitude of in-situ stress with pore pressure are important parameters for planning both drilling and production strategies. Using well logs to predict formation mechanical properties is an indirect technique.

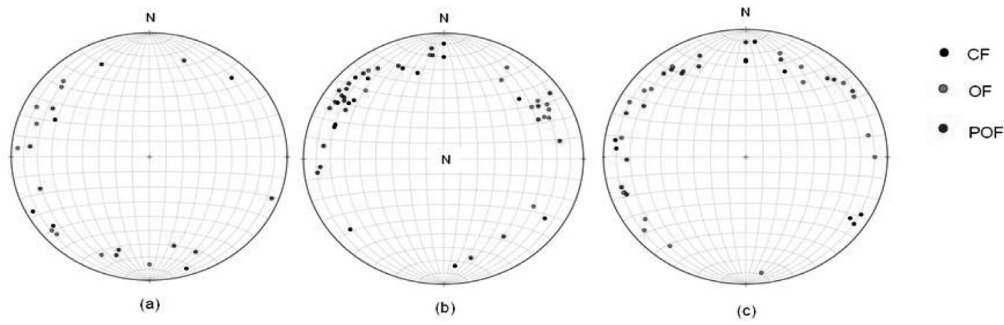


Figure 6: The Stereonet plots show fracture dip and azimuth at the wells (a) KL, (b) KS and (c) KD. CF, Closed Fracture, OF, Open Fracture and POF, Partially Open Fracture.

Table 2. Rock mechanical parameters of geological formations for five wells in K-G basin.

Formation	Depth Ranges in Well		Shear Modulus (GPa)	Young's Modulus (GPa)	Bulk Modulus (GPa)	Poisson's Ratio	UCS (MPa)
	Well	Depth interval (m)	Average	Average	Average	Average	Average
Matsyapuri Sandstone	KK	1988-2380	4.8	12.6	14.4	0.35	37.4
	KG	1095-1400					
Vadaparru Shale	KK	2380-2570	4.9	13.1	23.3	0.34	38.1
Raghavapuram Shale	KR	2023-2424	9.2	23.9	19.0	0.29	62.8
	KA	2800-2830					
	KE	1763-1938					
Gollapalli Sandstone	KE	1938-1980	13.2	31.1	16.5	0.17	75.1
Kommugudem Formation	KE	1980-2116	22.4	56.1	41.8	0.26	74.2

However, the method offers several benefits including cost, continuous estimations of mechanical properties with depths and prevalence of log data. The most commonly used method for deriving elastic mechanical properties from logs is based on relations expressing these properties in terms of acoustic velocities. Due to lack of core samples, we are not able to correlate the static modulus and dynamic modulus. The rock mechanical parameters for five wells: KA, KR, KK, KG and KE have been computed from sonic logs of V_p and V_s (Singha and Chatterjee, 2017). The unconfined compressive strength (UCS), elastic moduli such as: shear modulus (G), Young's modulus (Y), bulk modulus (K) and Poisson's ratio (σ) have been estimated from V_p , V_s and density (ρ) log data using the equations given by Mohammed and Zillur (2001) and by Potter and Foltinek (1997):

$$\text{Poisson's ratio, } \sigma = \frac{1((V_p/V_s)^2 - 2)}{2((V_p/V_s)^2 - 1)}$$

$$\text{Shear modulus, } G = V_s^2 \rho$$

$$\text{Young's modulus, } Y = 2 * G(1 + \sigma)$$

$$\text{Bulk modulus, } K = \rho * \left(V_p^2 - \frac{4}{3} V_s^2 \right)$$

And Cohesive Strength (S_0) as

$$S_0 = 0.025 * 10^{-9} \frac{Y}{K} [0.008 * Vsh + 0.0045(1 - Vsh)],$$

where Vsh is the clay content.

Unconfined Compressive Strength is therefore given by:

$$UCS = \frac{S_0}{0.289}$$

The values G, Y, K, σ and UCS in these five wells vary with depth as well as with lithology as listed in Table 2.

RESULTS AND DISCUSSION

The variations of these parameters are mostly constant for the well KA at a short depth interval 2800-2830m. The breakouts observed for ~28m length indicates shear failure due to relatively low UCS of about 60 MPa with respect to the compressive hoop stress developed at the borehole wall (Barton et al., 1988). Below the breakout, low poisson ratio is observed indicating presence of gas sand. The Raghavapuram Shale at a depth interval 2010-2420m in the well KR is characterized mostly with low G, Y, K values and σ of 0.35. This well has penetrated gas bearing sands with low σ of 0.11 and high resistive value at depth interval 2365 to 2378m. The variation of elastic parameters values at

Table 3. Range of dependent and independent variables for predicting shear wave velocity (Vs) using multiple linear regression analysis.

Wells	Depth interval (m)	P-wave (m/sec)	S-wave (m/sec)	Vsh	Φ
KA	2800-2830	3644-3885	2035-2159	0.51-0.77	0.006-0.05
KR	2023-2429	2529-5242	738-2338	0.002-0.92	0.03-0.56
KM	457-2512	1932-5354	1204-2950	0-0.70	-
KK	1988-2577	2511-2449	1027-2778	0.02-0.63	0.03-0.31
KG	1095-1399	1729-4428	376-2208	0.11-0.46	0.1-0.44
KE	1763-2116	2737-6044	1252-3931	0.02-0.81	0.05-0.54

Vsh, clay content and φ, porosity

Table 4: Summary of multiple regressions for prediction of shear wave velocity (Vs).

Model no.	Independent Variables	Coefficient	Standard Error	t-value	Significance
Model 2 for Vs2	Constant	-559.75	25.47357	-21.9737	5.96E-84
	Vp	0.71	0.008293	85.14415	0
	Vsh	-202.20	33.16041	-6.09775	1.68E-09
Model 3 for Vs3	Constant	-257.709	39.21033	-6.57247	8.97E-11
	Vp	0.677533	0.00837	80.94516	0
	Vsh	-376.223	36.06393	-10.4321	5.81E-24
	φ	-783.87	80.3058	-9.76107	2.49E-21

Vp, P-wave velocity, Vsh, clay content and φ, porosity

depth interval 1980-2570m demonstrates the characteristic signatures of rock mechanical properties in shaly sands in Matsyapuri Sandstone Formation. It is observed that the Vadaparru Shale in this well is characterized by continual increase of elastic moduli and UCS. The least value of G, Y, K and UCS are observed in the well KG at a depth interval 1090-1400m in the Matsyapuri Sandstone Formation. Shale lamina is characterized by high Poisson’s ratio of 0.44 whereas gas producing layers are characterized by low Poisson’s ratio below 0.18. The value of σ varies from 0.32 to 0.47 in the Raghavapuram Shale with lowering of its value down to 0.12 in the Gollapalli Sandstone Formation, and then again-increases in the Kommugudem Formation. Gas producing zone is characterized by low Poisson’s ratio at depth interval 1939m - 1958 m in the Gollapalli Sandstone. The signature of dynamic elastic moduli and UCS suggest the lithofacies changes from shale-dominated to sand-dominated rocks.

S-Wave Velocity Estimate from Regression Model

The information on density, sonic P and S wave velocities are to be known in order to determine the rock mechanical properties from well log data. The P and S wave velocities and density values are used to estimate the elastic moduli for rock strength and geo-mechanical modeling (Singha and Chatterjee, 2015), which are useful for the determination

of maximum and minimum horizontal stresses. However, the absence of the dipole shear sonic logs imposes severe limitations to such applications. We propose regression models for computation of S wave velocity from the four wells KA, KG, KK and KE. Sandstones, shaly sandstones and shales comprise a major component of the K-G basin and are of significant relevance to hydrocarbon reservoir. Many theoretical/experimental models exist considering the effects of porosity (φ), clay content (Vsh), pore shape, fluid, and matrix moduli on the elastic properties of rocks (Gassmann, 1951; Mavko and Nur, 1978; Castagna et al., 1985; Eberhart-Phillips et al., 1989). Therefore, in order to establish predictive models among parameters, simple regression between Vp and Vs has been performed in the first stage of analysis and displayed in Figure 8a. The linear regression relation between Vp and Vs with R² of 0.92 resembles the relation given by Castagna et al. (1985). Multiple regression analyses have been carried out to correlate the Vs with Vp, Vsh as well as with Vp, Vsh and φ for the four wells. The clay content and porosities have been derived from the following equations:

$$Vsh = (GR - GR_{min}) / (GR_{max} - GR_{min})$$

where GR = gamma ray log reading at any depth, GR_{min} = minimum gamma ray reading, GR_{max} = maximum gamma ray reading and porosity (φ) = $\frac{(\rho_{ma} - \rho)}{(\rho_{ma} - \rho_{fluid})}$

Stress Orientation from Image log and Estimation of Shear Wave Velocity using Multiple Regression Model:
A Case Study from Krishna-Godavari basin, India

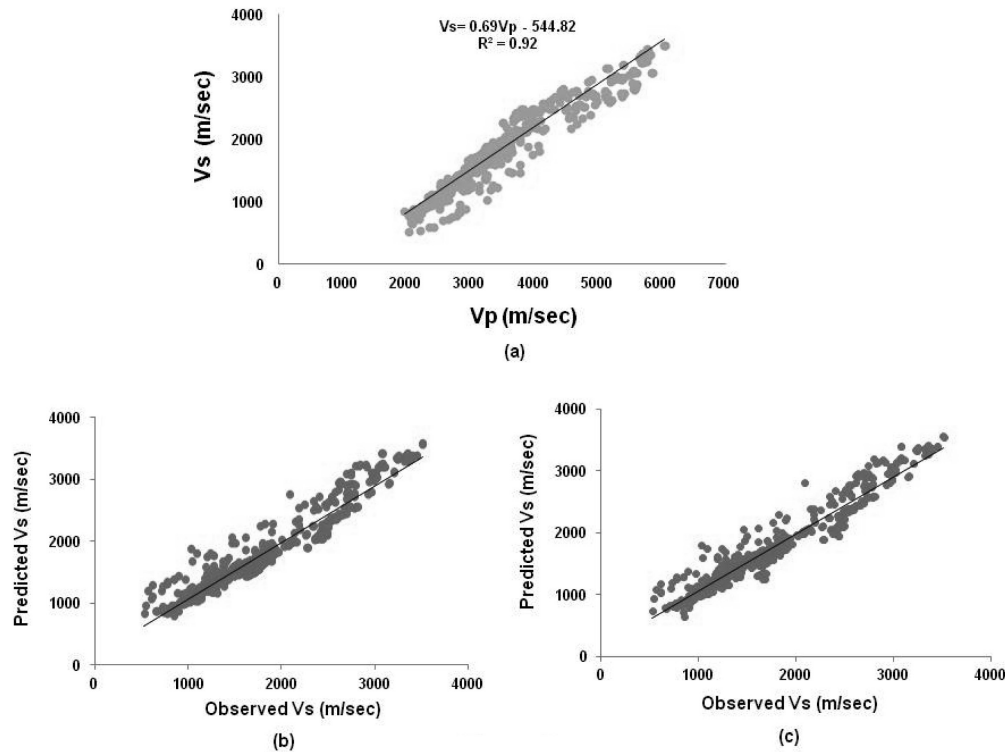


Figure 7: (a) Linear regression relation between Vp and Vs containing 796 observations of the four wells in the K-G basin, (b) correlation between 2nd model predicted Vs and the observed 796 Vs and (c) correlation between 3rd model predicted Vs and the observed 796 Vs.

ρ_{ma} = matrix density point = 2.71 gm/cc, ρ_{fluid} = density of fluid = 1 gm/cc and ρ = density log data of rock in gm/cc

Table 3 shows the well name, depth interval, Vp, Vsh, ϕ and Vs for the multiple regression statistical analysis. The well log data are sampled averaging the log values at depth intervals of 1.8m or less without losing the information for each lithology. Analysis of variance (ANOVA) is a technique that analyzes the relationship between a dependent variable and two/three independent variables using IBM SPSS Statistical Software, version 21.0. The ANOVA model is the simplest linear statistical model with independent variables (Gelman, 2005). The independent variables namely, Vp, Vsh and ϕ are three different groups in this analysis. The squared multiple correlation coefficient (R^2) between the observed and predicted values is a good indicator to check the prediction performance of the model.

The linear regression models for computation of Vs are as follows:

Model 1: $V_s \text{ predicted} = 0.69V_p - 544.82$ with $R^2 = 0.92$

Model 2: $V_s \text{ Predicted} = 0.71V_p - 202.20V_{sh} - 559.75$ with $R^2 = 0.95$

Model 3: $V_s \text{ Predicted} = 0.68V_p - 376.22V_{sh} - 783.87\phi - 257.709$ with $R^2 = 0.96$

All obtained relations are found to be statistically significant according to the Student's t test at 95% confidence level. Table 4 explains the coefficients of

models, standard errors, t-value with significance level. The correlation between observed Vs and predicted Vs for models 2 and 3 are illustrated in (Figures 7b and c).

Validation

The models are validated with the Vs log for the wells KR and KM respectively (Figures 8a, b). The model estimated results match reasonably well with the observed Vs log for these wells. The information on Vs for well KM is not available continuously with depth. Variations between model predicted Vs and observed Vs are observed at depths 2360-2370m in well KR and at shallower depth from 450 to 650m in well KM. Despite little scatter, trends indicate that Vs decrease with increasing clay content and porosity. Model 1 predicts the Vs in clean sand without clay content. In water filled clean sand, model 1 estimates Vs with better precision. In shaly sand, the model 2 estimates better results considering the effect of clay content. Since velocity decreases with increasing porosity, the model 3 reflects the clay and porosity effects.

CONCLUSIONS

The orientation of S_H determined within the four wells in the K-G basin is consistent and is considered to be

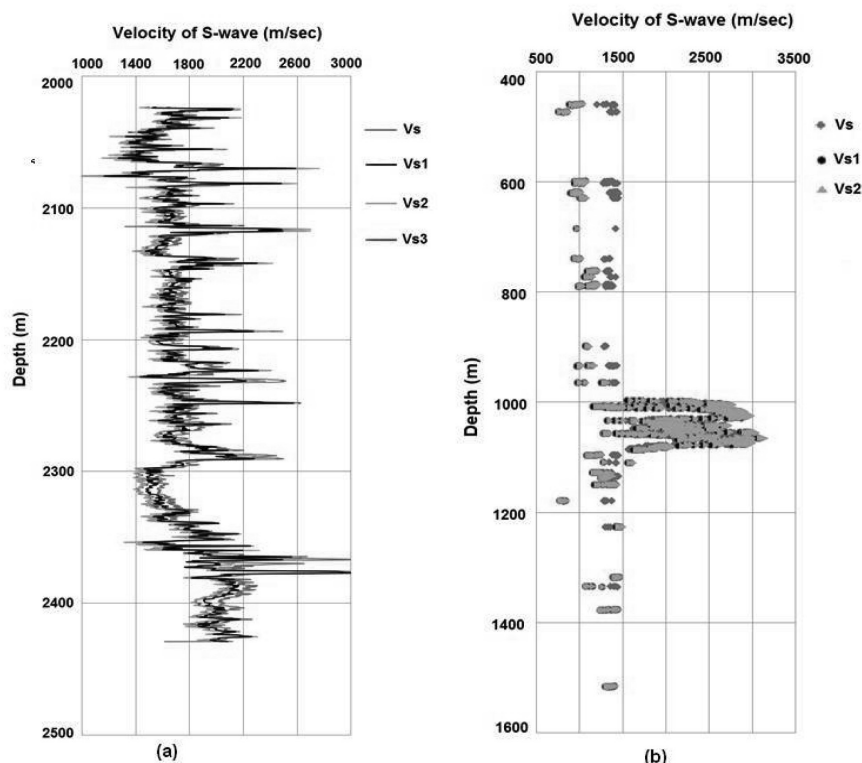


Figure 8: Validation of three models for (a) well KR and (b) well KM. The 3rd model predicted Vs for well KM could not be obtained due to non availability of density logs. Vs: Observed Vs from log, Vs1: predicted Vs from model 1, Vs2: predicted Vs from model 2, and Vs3: predicted Vs from model 3.

more reliable than the existing knowledge. The mean S_H orientation determined at N18.6°E conforms with the known NNE-SSW maximum horizontal stress (Chatterjee and Mukhopadhyay, 2002). The orientations of open fractures at various depth intervals estimated from FMI log are in close agreement with the estimated S_H from the breakouts and DIF with a maximum deviation of 10°. The estimated dynamic elastic moduli and UCS in the selected five wells would be useful in development of geo-mechanical models in this basin. The breakouts are associated with a relatively low strength rock as observed from the well KA. The gas bearing zones are characterized by low Poisson's ratio in the wells KK, KG and KE. Estimation of Vs considering the effect of clay and porosity yields precise dynamic elastic moduli and UCS. This model would be useful in other wells of the basin maintaining mud weight, well casing design, hydro-fracturing and stimulation (Rickman et al., 2008). The models may be further refined with velocity information from offshore wells and incorporating confining pressure and pore pressure corrections.

ACKNOWLEDGEMENTS

Authors are very thankful to ONGC, Dehradun for providing us the well log and geologic information.

Authors also acknowledge the financial support from the Department of Science and Technology (DST-INSPIRE) and Ministry of Earth Science through the R&D project MoES /P.O./Seismo/1(138) 2011 dated 9.11.12. Authors thank Dr.Suman Paul and Dr.J.R.Kayal for objective evaluation and useful suggestions. Thanks are also due to Dr.M.R.K.Prabhakara Rao and Chief Editor for final refinement and apt editing.

Compliance with Ethical Standards

The authors declare that they have no conflict of interest and adhere to copyright norms.

REFERENCES

- Aadnoy, B.S., 1990. Inversion technique to determine the in-situ stress field from fracturing data, *Journal of Petroleum Science and Engineering*, v.4, pp: 127-141.
- Barton, C.A., Zoback, M.D., and Burns, K.L., 1988. In-situ stress orientation and magnitude at the Fenton Geothermal site, New Mexico, determined from wellbore breakout, *Geophysical Research Letters*, v.15, no.5, pp: 467-470.
- Castagna, J.P., Batzle, M.L., and Eastwood, R.L., 1985. Relationships between compressional-wave and shear-wave velocity in clastic silicate rocks, *Geophysics*, v.50, no.4, pp: 571-581.

Stress Orientation from Image log and Estimation of Shear Wave Velocity using Multiple Regression Model:
A Case Study from Krishna-Godavari basin, India

- Chatterjee, R., and Mukhopdhyay, M., 2002. In-situ stress determination using well log data for the oil fields of the Krishna-Godavari basin, *Petrophysics*, v.43, pp: 26-27.
- Das, B., and Chatterjee, R., 2017. Wellbore stability analysis and prediction of minimum mud weight for few wells in Krishna-Godavari Basin, India, *International Journal of Rock Mechanics and Mining Sciences*, v.93, pp: 30-37.
- Eberhart-Phillips, D., Han, D.H., and Zoback, M.D., 1989. Empirical relationships among seismic velocity, effective pressure, porosity, and clay content in sandstone, *Geophysics*, v.54, no.1, pp: 82-89.
- Gassmann, F., 1951. Elastic waves through a packing of spheres. *Geophysics* v.16, no.4, pp: 673-685.
- Geertsma, J., 1961. Velocity log interpretation: the effect of rock bulk compressibility, *Journal of Society of Petroleum Engineers*, v.1, pp: 235-248.
- Gray, D., Abderson, P., Logel, J., Delbecq, F., Schmidt, D., and Schmid, R., 2012. Estimation of stress and geomechanical properties using 3D seismic data, *First Break*, v.30, pp: 59-68.
- Gupta, S.K., 2006. Basin architecture and petroleum system of Krishna Godavari Basin, East coast of India, the Leading Edge, v.25, pp: 830-837.
- Gelman, A., 2005. Analysis of variance-why it is more important than ever, *The Annals of Statistics*, v.33, pp: 1-53.
- Mavko, G.M., and Nur, A.M., 1978. The effect of nonelliptical cracks on the compressibility of rocks, *Journal of Geophysical Research*, v.83, pp: 4459-4468.
- Mohammed, Y.A., and Zillur, R., 2001. A Mathematical Algorithm for Modeling Geomechanical Rock Properties of the Khuff and Pre-Khuff Reservoirs in Ghawar Field, SPE Middle East Oil Show, Bahrain, March, Paper id: SPE 68194, pp: 17-20.
- Nelson, E.J., and Hillis, R.R., 2005. In situ stresses of the West Tuna area, Gippsland Basin, *Australian Journal of Earth Sciences*, v.52, pp: 299-313.
- Nelson, E.J., Meyer, J.J., Hillis, R.R., and Mildreb, S.D., 2005. Transverse drilling-induced tensile fractures in the West Tuna area, Gippsland Basin, Australia: implications for the in situ stress regime, *International Journal of Rock Mechanics & Mining Sciences*, v.42, pp: 361-371.
- Nie, X., Zou, C., Pan, L., Huang, Z., and Liu, D., 2013. Fracture analysis and determination of in-situ stress direction from resistivity and acoustic image logs and core data in the Wenchuan Earthquake fault Scientific Drilling Borehole-2(50-1370m), *Tectonophysics*, v.593, pp: 161-171.
- Potter, C.C., and Foltinek, D.S., 1997. Formation elastic parameters by deriving S-wave velocity Logs, CREWES Report, v.9, pp: 10-23.
- Prasad, M., 2002. Acoustic measurements in unconsolidated sands at low effective pressure and overpressure detection. *Geophysics*. v.67, pp: 405-412.
- Rao, G.N., 2001. Sedimentation, stratigraphy and petroleum potential of Krishna-Godavari basin, East Coast of India, *AAPG Bulletin*, v.85, pp: 1623-1043.
- Rickman, R., Mullen, M., Petre, E., Grieser, B., and Kundert, D., 2008. A Practical Use of Shale Petrophysics for Stimulation Design Optimization: All Shale Plays Are Not Clones of the Barnett Shale, *SPE Annual Technical Conference and Exhibition*, September 21-24, Denver, Colorado, USA, Society of Petroleum Engineers, Paper id: SPE 115258.
- Sastri, V.V., Sinha, R.N., Singh, G., and Murti, K.V.S., 1973. Stratigraphy and tectonics of sedimentary basins on the East coast of penninsular India, *AAPG Bulletin*, v.57, pp: 655-678.
- Singha, D.K., and Chatterjee, R., 2014. Detection of Overpressure zones and a Statistical Model for Pore Pressure Estimation from Well Logs in the Krishna-Godavari Basin, India, *Geochemistry, Geophysics, Geosystems*, v.15, no.4, pp: 1009-1020.
- Singha, D.K and Chatterjee, R., 2015. Geomechanical Modeling using Finite Element Method for Prediction of In-situ Stress in Krishna-Godavari basin, India, *International Journal of Rock Mechanics and Mining Sciences*, v.73, pp: 15-27.
- Singha, D. and Chatterjee, R., 2017. Rock Physics Modeling in Sand Reservoir through Well Log Analysis, Krishna-Godavari basin, India, *Geomechanics and Engineering*, v.13, no.1, pp: 99-117.
- Tingay, M.R.P., Hillis, R.R., Swarbrick, R.E., Morley, C.K. and Damit, A.R., 2009. Origin of overpressure and pore-pressure prediction in the Baram province, Brunei, *AAPG Bulletin*, v.93, pp: 51-74.
- Tingay, M., Reinecker, J., Müller, B., 2008. Borehole breakout and drilling-induced fracture analysis from image logs. *World Stress Map Project Stress Analysis Guidelines*. available online at: www.world-stress-map.org.
- Tingay, M.R.P., Morley, C.K., Hillis, R.R., Meyer, J., 2010a. Present-day stress orientation in Thailand's basins, *Journal of Structural Geology*, v.32, pp: 235-248.
- Tingay, M.R.P., Morley, C.K., King, R.E., Hillis, R.R., Hall, R., Coblenz, D., 2010b. The Southeast Asian Stress Map. *Tectonophysics*, v.482, pp: 92-104.
- Trautwein, B.U., Schulze, K.C., Becker, S., Kukla, P.A., and Urai, J.L., 2010. In situ stress variations at the Variscan deformation front - Results from the deep Aachen geothermal well, *Tectonophysics*, v.493, pp: 196-211.
- Zoback, M.L., 1992. Stress field constraints on intraplate seismicity in eastern North America, *Journal of Geophysical Research*, v.97, pp: 11761-11782.

Received on: 14.09.2017; Revised on: 6.10.2017; Re revised on: 30.10.2017; Accepted on: 13.11.2017

Wavefield decomposition of multi-component OBS data to enhance the seismic signal

N.Satyavani^{1*}, M.Ravi Kumar² and Kalachand Sain¹

¹Gas Hydrate Group, CSIR-NGRI, Hyderabad, Telangana

²Institute of Seismological Research, Gandhi Nagar, Gujarat

*Corresponding Author: satyavani_nittala@yahoo.com

ABSTRACT

The multi-component Ocean Bottom Seismometer (OBS) data captures full wave field by recording on three component geophone and one hydrophone. However, the resultant seismogram includes the free surface multiples that interfere with the recorded wavefield, which has to be removed for further processing. We find that PZ summation, along with the up/down deconvolution is very effective in removing them and renders the multiple-free wavefield. The method is illustrated here, using the OBS data acquired in the Mahanadi basin. In addition to the noise free P wave field, we also obtain the converted (PS) wave field using this approach.

Key words: OBS data, free surface multiples, converted waves, wavefield separation, PP & PS.

INTRODUCTION

Ocean Bottom Seismometer (OBS) instruments are being increasingly used in the hydrocarbon industry and academia so as to maximize the chances of precise identification of resources and in delineation of the crustal structure in most challenging environments. The biggest advantage of using the OBS nodes is that they can record on four components (hydrophone and a three component geophone), which can capture the full wavefield. Each OBS node contains one three (Z,X,Y) component geophone and one hydrophone (P). The geophone records compressional wave on its vertical (Z) component and the converted wave on the two horizontal orthogonal (X,Y) components, while the hydrophone (P) records the pressure pulse data. Conventionally, seismic data is acquired by using surface towed streamers and the P-wave data thus generated is used in imaging the sub surface to a reasonable extent. However, such data has inherent limitations, like, lack of near offsets, no information about the shear waves, imaging problems for the near seafloor geology, acquisition in presence of sea bottom obstructions like pipelines, platforms etc. Multi-component OBS data offers an excellent alternative to handle these issues as the instruments record compressional, converted and pressure wave data that can be used to detect hydrocarbon formations more precisely. The shallow sediments have low rigidity and the vertical resolution available from PS data can be higher than the PP data. It is also noteworthy that the small changes in the rigidity can cause large fractional changes in the shear impedance but only small changes in the compressional impedance, and hence the PS data can contribute greatly in tracing the changes in rigidity, i.e., in detecting the changes that occur due to the changes in saturation, although the

information will not help in establishing the composition of the fluid. However, the main difficulty with the OBS data is that it is contaminated by the surface related multiples to a considerable extent. The data recorded on the OBS includes free surface multiples, in addition to the general multiples that interfere with the recorded wavefield. Removal of the surface related multiples (to have noise-free recorded wavefield) is one of the most important processing steps to be performed before carrying out any processing routines and arriving at a meaningful interpretation. The OBS data collected in Mahanadi basin is presented in this manuscript to demonstrate the efficacy of the wave field decomposition and its utility in suppressing the multiples.

THEORY

The multiples, which are the major contributors to the total recorded wave field can be divided into two components, the receiver side and the source side multiples, shown in Figure 1. As the name itself explains, the receiver side multiples comprises of the receiver ghosts i.e., those events that are reflected from the subsurface, bounce off the seafloor and get recorded at the receiver. The source-side multiples are the reflections that are caused due to the source-ghosts, i.e., the source signal is first reflected off the seafloor and then hits the subsurface, gets reflected and then is recorded at the receiver.

The hydrophone sensors in the OBS are pressure sensitive, while the geophones are displacement sensors, i.e., sensitive to the particle motion and direction. The hydrophone (pressure) data is a scalar measurement and is not dependent on the direction of the particle motion, while the geophone (displacement) data is a vector measurement, and is dependent on the direction of the particle motion.

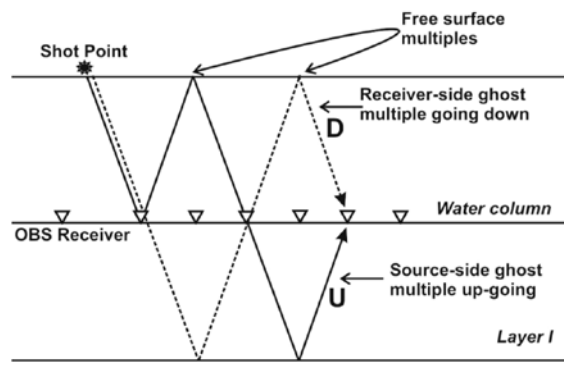


Figure 1. A schematic diagram showing the source-OBS configuration in a marine setting, along with the up-going and down-going waves and their travel paths.

The vertical geophone (Z) and hydrophone (P), present in the same OBS setup, therefore, record the multiple signals with opposite polarity and this can be used to attenuate the noise effectively and hence, a simple addition of the data on vertical (Z) component with the data on hydrophone (P) component can result in elimination of the free surface multiples. Following the approach of Backus et al (2012), and the sensor responses explained therein, the hydrophone response (P) and vertical response can be combined to create upgoing (U) wavefield and downgoing (D) wavefield as shown below, expressed in frequency domain:

$$D = P + Z / \cos(\phi) \quad (1)$$

$$U = P - Z / \cos(\phi) \quad (2)$$

where, ϕ is the angle of incidence.

However, the PZ summation requires that the datasets (P&Z) be calibrated to provide same response to up-travelling wave. This calibration is achieved either by applying a constant gain (Backus et al, 2006) or by using a calibration filter (Haines et al, 2010). This technique is popularly called as PZ summation (Barr and Sanders, 1989; Backus et al, 2006; Haines et al, 2011) and is very effective in attenuating all the “receiver side” multiple energy i.e, the energy which is down-going at the receiver location.

Having removed the receiver-side multiples, we are now left with the “source-side” multiples, which are not down-going at the receiver and are not attenuated by conventional PZ summation. These multiples can be attenuated by deconvolution of the down-going waves from the up-going waves. Fundamentally, the recorded wavefield is a combination (convolution) of the down-going wavefield and the earth’s reflectivity and therefore a simple deconvolution of the down-going wavefield from the up-going wavefield would result in retrieval of earth’s reflectivity. The up-going wavefield in a simple layered medium can be represented as,

$$U = DR \quad (3)$$

From the above equation, it follows that

$$R = U/D + \xi \quad (4)$$

where ξ is the stabilization factor.

Isolation of the PS wavefield can also be attempted using the same technique except that in this case the down-going wavefield has to be deconvolved with the horizontal component that records the maximum converted energy i.e., radial (R) component of the OBS data. Similar to the earlier case the calibration has to be carried out in this case also.

DATA AND METHODOLOGY

The OBS data used in this study was acquired in the Mahanadi offshore region during the year 2010 on board M/V Akademik Fersman. The shot spacing is 25m and the water depth is 2000m. Data up to 6sec with a sampling interval of 4ms is used here. The total shooting length is ~12km, with a maximum offset of 6km either side of the OBS. The data have been rotated from Z,X,Y components to the vertical, radial and transverse (Z,R,T) components and after the rotation, the maximum of the converted energy shifts to the radial, leaving little or no energy on the transverse component (Satyavani et al., 2013). Simple data processing was applied to the data so that the seismic amplitudes are not affected to a large extent. The steps include true amplitude recovery and a band pass filter in the range of 5-15-80-90Hz. The data was then flattened with respect to seafloor, as shown in Figure 2.

Prior to up/down separation, the data was calibrated so that the P and Z components of data have the same frequency response. In the present case, this calibration was achieved by applying a constant gain factor. From the calibrated data, the up-going and down-going fields are obtained using the equation 1 and equation 2. The angle of incidence (ϕ) is computed from the trace offset and OBS deployment depth. The data thus obtained is shown in Figure 3a and 3b. For display purposes, the data have been statically shifted and the seafloor is aligned at near zero

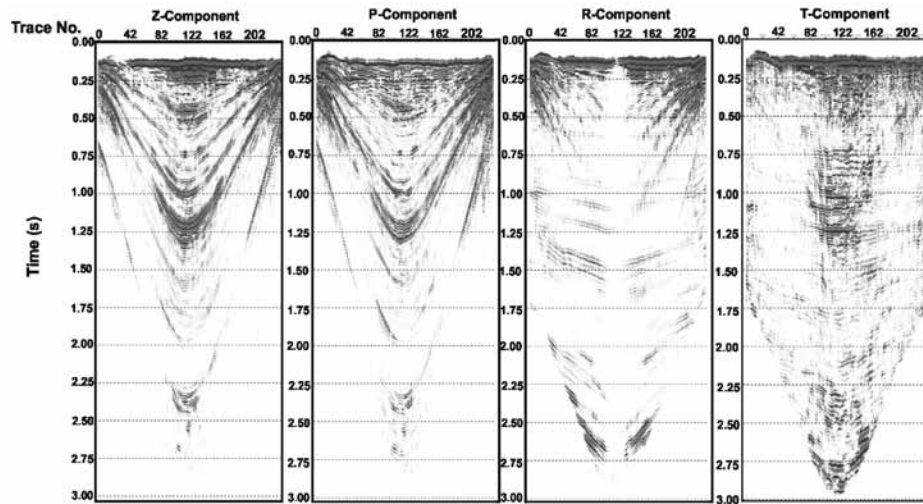


Figure 2. The OBS data acquired in the Mahanadi basin. The vertical (Z) component, the hydrophone (P) component data are retrieved from the instrument and can be treated as field data, while the radial (R) and the transverse (T) component of data are obtained by rotating the two orthogonal (X,Y) components from the field data, in such a way that the energy is maximum on the radial component.

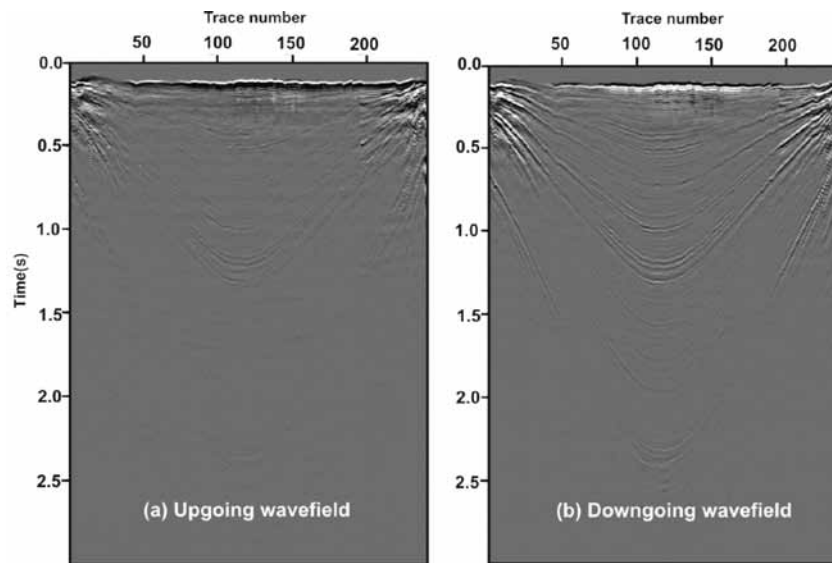


Figure 3. The result of the wave field decomposition. The recorded wavefield is decomposed into the (a) up-going wavefield and (b) down-going wavefield. The up-going wavefield is dominated by the shallow multiples, while the down-going wavefield shows the sharp down-going wavefield, which is later used in the deconvolution.

time. The down-going field shows good amount of multiple energy (seen as lines parallel to offset axis) and a feeble signature of the reflections, while the up-going wavefield shows the dominant reflection energy (seen as distinct hyperbola). The down-going P-wave generally represents the robust wavelet that changes with the receiver location and angle, which is subsequently used in the deconvolution purposes, to extract multiple-free vertical component data and more clear radial data. PZ summation is effective in removing “receiver-side” multiples. However, the “source-side” multiples still exist in the recorded data, which can be removed by up-down deconvolution.

RESULTS

The most reliable and effective way to remove the source-side multiples and extract the noise free P-wave field is to perform the up-down deconvolution. The deconvolution of the vertical component (Z) data with the down going wave field results in the retrieval of the noise-free P-wave field, which is now called as PP reflectivity. A comparison between the recorded P-wavefield and the retrieved PP reflectivity is shown in Figure 4 and the significant improvements in the data quality are highlighted. It is seen that the PP reflectivity (Figure 4a) has much clear,

Wavefield decomposition of multi-component OBS data to enhance the seismic signal

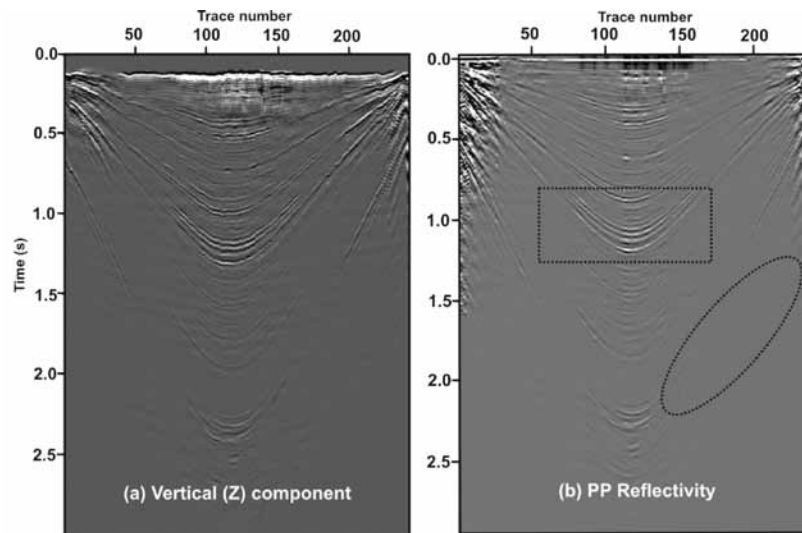


Figure 4. The result of deconvolution of the vertical component data with the downgoing wavefield. (a) shows the recorded vertical (Z) component, while (b) shows the PP reflectivity obtained as a result of deconvolution. Significant improvement in the signal resolution can be noticed in (b) and is highlighted as a dashed rectangle. The dashed oval in (b) shows the attenuation of the multiples and cleaner vision of the marked area compared to (a).

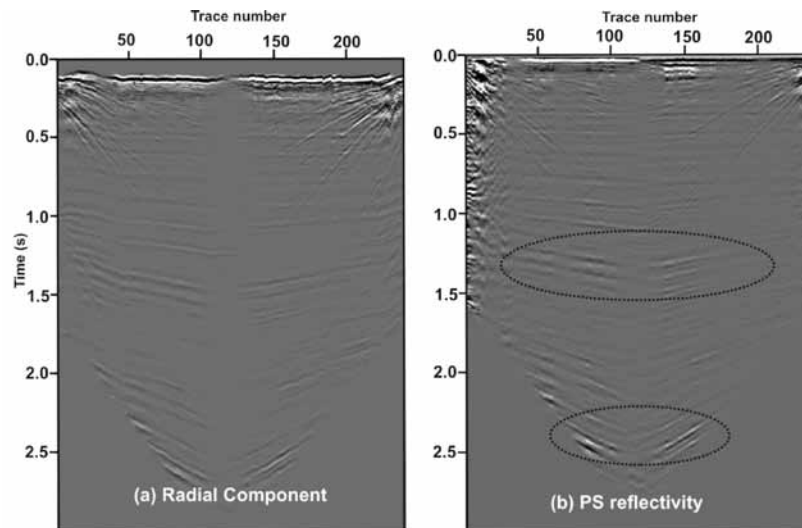


Figure 5. The result of deconvolution of the radial component data with the downgoing wavefield. (a) shows the radial (R) component, while (b) shows the PS reflectivity obtained as a result of deconvolution. Significant improvement in the signal resolution can be noticed in (b) at almost all times and is highlighted as dashed ovals.

highly resolvable PP arrivals compared to the vertical (Z) component (Figure 4b). This comparison proves that the deconvolution could effectively remove the multiple wavefield.

Similarly, the deconvolution of the radial component (R) of the data with the down-going wavefield results in the retrieval of the noise-free PS converted wavefield. Prior to the deconvolution, the radial data are to be calibrated with the down-going field so that they have the same frequency response. The deconvolution process yields the most reliable PS conversions and the deconvolved field is called PS reflectivity. A comparison between the radial

component data and the down-going wave field are shown in Figure 5. The deconvolved wavefield (Figure 5b) shows a marked increase in the spatial and temporal resolution of the converted wavefield compared to the radial (R) component.

CONCLUSIONS

It may therefore, be concluded that the two tier process of PZ summation followed by up-down deconvolution is a significant step to be carried out before the processing of any multi-component dataset, especially the OBS datasets.

These steps provide very reliable, noise-free dataset, which when used in the later stages of processing, leads a consistent interpretation.

ACKNOWLEDGEMENTS

The authors thank the Director, National Geophysical Research Institute (NGRI) for his kind consent to publish this work. The Ministry of Earth Sciences is thanked for funding the project to acquire the seismic data. This is a contribution towards the SHORE-PSC0205 project of 12th Five Year Plan of CSIR-NGRI. Thanks are due to Dr. Kamesh Raju and an anonymous reviewer for useful suggestions. The authors also thank Dr. P. R. Reddy, Chief Editor for inviting the first author to contribute this article and for editing the manuscript.

Compliance with Ethical Standards

The authors declare that they have no conflict of interest and adhere to copyright norms.

REFERENCES

- Backus, M.M., Murray, P.A., Hardage, B.A., Graebner, R.J., 2006. High-resolution multi component seismic imaging of deepwater gas-hydrate systems. *The Leading Edge*, pp: 578-596.
- Barr, F. J., and Sanders, J. I., 1989. Attenuation of water-column reverberations using pressure and velocity detectors in a water-bottom cable. 59th SEG Annual Meeting, pp: 653-655.
- Haines, S.S., Lee, M.W, Murray, P.E., Hardage, B.A., 2010. Ocean-bottom cable seismic data calibration using median filters for waveform separation. Fall Meeting, AGU, San Francisco.
- Haines, S.S., Lee, M.W., Collett, T.S., Hardage, B.A., 2011. Multi component seismic methods for characterizing gas hydrate occurrences and systems in deep water Gulf of Mexico. *Proceedings of 7th International Conference on Gas Hydrates*.
- Satyavani, N., Sen, M.K., Maheswar Ojha, Kalachand Sain., 2013. Azimuthal anisotropy from OBS observations in Mahanadi Offshore, India. *Interpretation*, 2013, v.1, no.2, pp: T187-T198.

Received on: 5.10.2017, Revised on: 1.11.17; Re revised on: 25.11.17; Accepted on: 10.12.17

Quotations on Imaging Ocean Bottom

“My soul is full of longing for the secret of the sea, and the heart of the great ocean sends a thrilling pulse through me.”

Henry Wadsworth (1807-1882) was an American poet and educator.

“There’s nothing wrong with enjoying looking at the surface of the ocean itself, except that when you finally see what goes on underwater you realize that you’ve been missing the whole point of the ocean.”

Dave Barry (1947--) is an American author and columnist.

“At the bottom of the ocean is a layer of water that has never moved...”

Anne Carson (1950--) is a Canadian poet, essayist, translator and professor of Classics.

The Ocean Stirs the heart, inspires the imagination and brings the eternal joy to the soul.

Robert Wyland (1956--) is an American artist.

Being able to breathe underwater would be sweet. There is so much life underneath the water that we don’t know about. I would love to check out the bottom of the ocean to see what’s going on down there.

Cameron Bright (1993--) is a Canadian actor.

Fractal Revaluation of Bottom Depth of Magnetic Sources in Bida Basin, Nigeria from High-Resolution Aeromagnetic Data

Levi I. Nwankwo^{*1,2}, Peter I. Olasehinde¹, and Abayomi J. Sunday³

¹ Department of Geophysics, University of Ilorin, PMB 1515, Ilorin, Nigeria.

² Department of Physical Sciences, Kampala International University, Uganda.

³ Department of Physics, University of Ilorin, PMB 1515, Ilorin, Nigeria.

* Corresponding Author: levinwankwo@yahoo.com

ABSTRACT

The recent high-resolution aeromagnetic (HRAM) data for the whole of Bida Basin in north-central Nigeria has been revaluated for depth to bottom of magnetic sources (DBMS) using the modified centroid method for fractal distribution of sources. Analysis of the HRAM map shows magnetic lineations due to tectonic features that may be connected to regional tectonic framework of West and Central Africa Rift Systems. The HRAM data were also divided into 28 overlapping blocks and each block was evaluated to obtain depths to the top and centroid of magnetic sources. Both depth values were consequently used to calculate the DBMS for each block. The results reveal that the DBMS varies between 5.41 and 19.29 km with an average of 12.01 km. Hence, this study would contribute to further explication of the geo-processes and rheology of Bida Basin in north-central Nigeria.

Key words: Basal depth, magnetic sources, fractals, Bida basin, Nigeria

INTRODUCTION

The revaluation of the depth to the bottom of magnetic sources (DBMS) from recently acquired high-resolution aeromagnetic data of the whole of Bida Basin, north-central Nigeria has been carried out in this study using fractal model. Nonetheless, earlier calculations of DBMS in the Earth's crust were executed through previously established mathematical procedures, namely: spectral peak method (Connard et al., 1983; Blakely, 1995), spectral centroid method (Bhattacharyya and Leu, 1975; 1977; Okubo et al., 1985; Tanaka et al., 1999), scaling spectral or power-law correction method (Maus and Dimri, 1996), and forward modelling of the spectral peak method (Finn and Ravat, 2004; Ravat et al., 2007), among others.

The mathematical scheme for fractal model of aeromagnetic analysis is derived from spectral centroid model (for an extensive description of the spectral centroid model, one may refer to Okubo et al., 1985; and Tanaka et al., 1999). One of the flaws of the spectral centroid model is the assumption of random and uncorrelated distribution of magnetic sources equivalent to white noise distribution because of its mathematical simplicity and non-availability of information about source distribution. However, in reality the source distribution follows correlated fractal distribution, which is referred to as scaling distribution (Maus and Dimri, 1996; Maus et al., 1997; Bansal and Dimri, 2014; Bansal et al., 2011; 2013; 2016; Kumar et al., 2017). Maus et al., (1997) gave an expression of the radial average of power spectrum ($P(k)$) of magnetic

sources expressed in terms of scaling exponent and depth component as:

$$P(k) = C - 2kZ_t - tk - \beta \ln(k) + \ln \left(\int_0^{\infty} [\cos h(tk) - \cos(tw)] \left(1 + \frac{w^2}{k^2}\right)^{-1-\beta/2} dw \right) \quad (1)$$

where k is the wavenumber ($2\pi/\text{km}$), Z_t is the depth to the top, t is the thickness of slab, β is a scaling exponent due to source distribution, and C is a constant.

Following this, a fractal modification of the spectral centroid model (Bhattacharyya and Leu, 1975; Tanaka et al., 1999) was derived by Bansal et al., (2011) for the estimation of DBMS from aeromagnetic data for scaling distribution of sources. The new fractal model, like the spectral centroid model, computes the DBMS in three steps. Primarily, the depth to the top of magnetic sources is computed by correcting power spectrum for scaling distribution of sources as:

$$\ln(k^\beta P(k)) = A_1 - 2kZ_t \quad (2)$$

Next, the centroid depth is computed as:

$$\ln \left(k^\beta \frac{P(k)}{k^2} \right) = A_2 - 2kZ_0 \quad (3)$$

and finally, DBMS Z_b is estimated:

$$Z_b = 2Z_0 - Z_t \quad (4)$$

The scaling component β depends on the geology or fractal distribution of susceptibility. Bouligand et al., (2009) conferred that the spectral peaks in power spectrum could only be found for low values of β , which disappears at higher values and therefore, reasonable values of scaling component should vary from 1.0 – 2.0 for 2D magnetic bodies and 2.5 – 3.5 for 3D distribution of sources. In

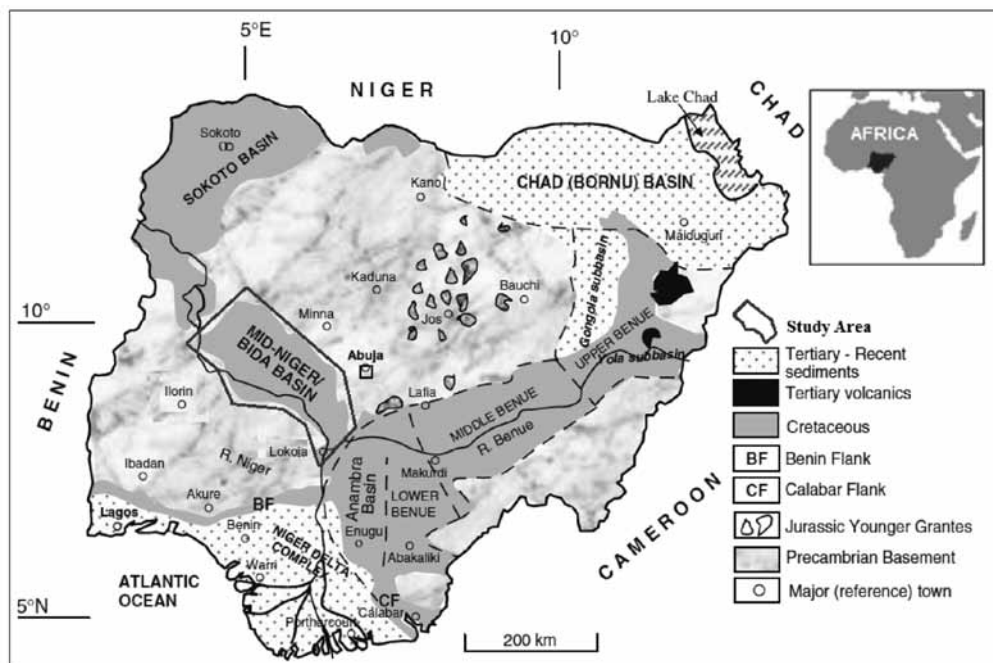


Figure 1. Geological map of Nigeria showing Bida Basin

furtherance, Bansal and Dimri (2014) revealed that scaling components of 2.4 – 4.6 would practically resolve 3D sources while lower scaling components reveal 1D and 2D source distributions. Salem et al., (2014) showed that scaling components ranging from 0 to 1.7 were effectively applied in the Central Red region of Egypt, whereas 0 to 4.0 were used by Kumar et al., (2017) for 2D structures in Central India. The results of Kumar et al., (2017) were however scattered and not correlated with depth and geology signifying complex tectonic nature of the region. Nevertheless, assigning a fixed scaling component value of 1 has been found to be reasonable in previous studies utilizing fractal technique in Austria, Germany, India, and Nigeria (Bansal et al., 2011; 2013; 2016; Gabriel et al., 2011; Bansal and Anand, 2012; Nwankwo, 2015). The value of 1 was used for 2D distribution of sources by assuming that these represent as scaling noise of 1/f type. Recent studies have led to improved DBMS estimations using fractal distribution of sources (Maus et al., 1997; Bouligand et al., 2009; Bansal et al., 2011; Salem et al., 2014). Consequently, it is expected that the application of fractal technique to the newly acquired high-resolution aeromagnetic data of the whole of Bida Basin in north-central Nigeria would yield better DBMS estimates.

Location and Geology of the Study Area

Bida basin (Figure 1) is located in the north-central region of Nigeria. It is bounded by latitudes 8°00'N and 10°30'N and longitudes 4°30'E and 7°30'E and covers an area of approximately 90,750 km².

The geology of Bida Basin has been described extensively by many researchers (Adeleye, 1974, 1976; Osokpor and Okiti, 2013; Jones, 1975; Kogbe et. al., 1983; Obaje, 2009; etc.). The basin is believed to be a gentle down-warped shallow trough filled with Campanian-Maestrichtian marine to fluvial strata. Those with marine affinity, the limestones, often form cappings (under variable thickness of laterites) to the means of the basin. Some form prominent intermediate breaks of slope along the mesa walls (Osokpor and Okiti, 2013). The epeirogenic process responsible for the basin genesis seems closely connected with the Santonian tectonic crustal movements which mainly affected the Benue Basin and south-eastern Nigeria. The buried basement complex probably has a high relief (Jones, 1975) and the sedimentary formations have been shown to be about 2 km thick (Ojo and Ajakaiye, 1976) with a constituted post-tectonic molasse facies and thin marine strata, which are all unfolded.

The stratigraphy of the basin (Figure 2) consists of mainly Patti, Lokoja and Agbaja Formations (Ikumbur et al., 2013). Patti Formation is the only stratigraphic unit containing carbonaceous shale in the basin and is sandwiched between the older Campanian-Maestrichtian Lokoja Formation that contains conglomerates, sandstones and claystones; and younger Agbaja Formation that comprises mostly ironstones (Akande et al., 2005a; 2005b).

Tectonically, rift hypothesis has been proposed as the possible origin and evolution of the basin (Kogbe et. al., 1983; Adeniyi, 1985). Some investigators claim that the rifting in the Bida Basin started in the Upper Cretaceous

Fractal Revaluation of Bottom Depth of Magnetic Sources in Bida Basin, Nigeria from High-Resolution Aeromagnetic Data

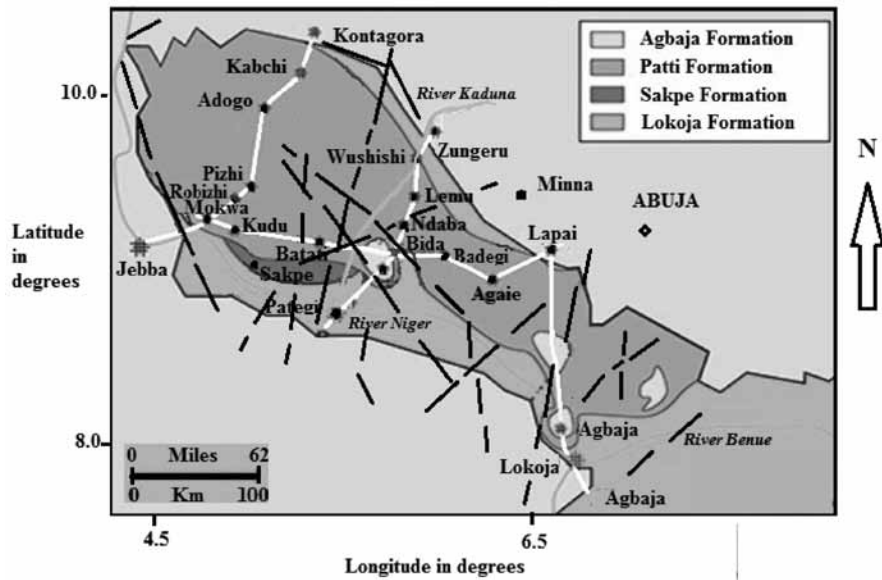


Figure 2. Geologic map of Bida basin showing stratigraphic sequence and lineaments (After NGSA, 1984; Obaje et al., 2015)

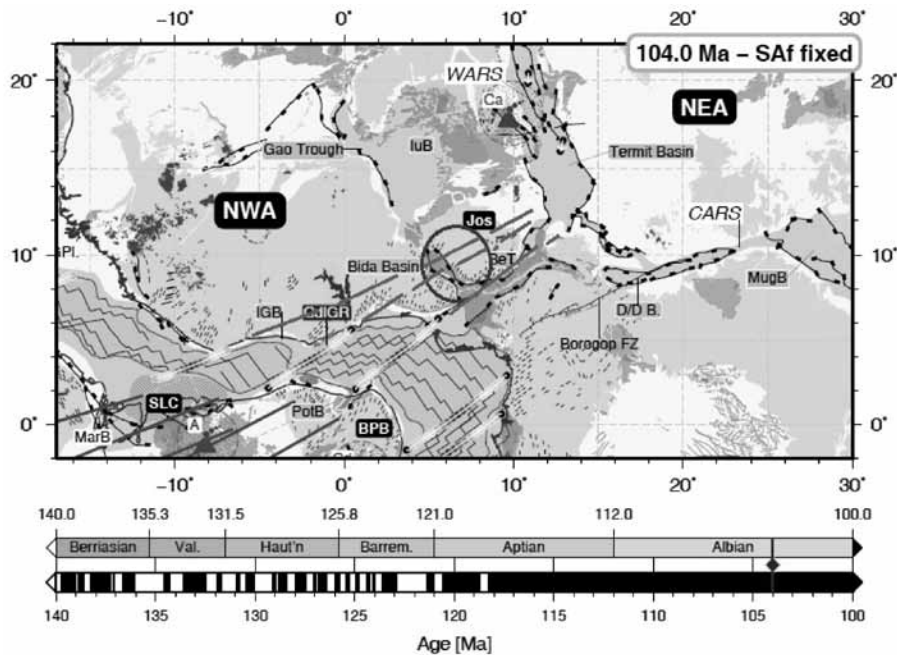


Figure 3. West African Rift System (WARS) and Central African Rift System (CARS) [After Heine et al., 2013]. Gray circle indicates position of Bida basin with extensions of inferred major fracture zones – St. Paul’s, Romanche, and Chain drawn with broken lines. Ajakaiye et al., 1991 had earlier suggested these extensions.

but the entire process began originally from the Benue Trough in the Lower Cretaceous and eventually spread to other rifted basins like Gongola Trough, Yola Trough and Bida Basin (Udensi et al., 2003). The origin of the basin is also said to be closely related to Santonian tectonic crustal movements, which affected the Benue Basin and southeastern Nigeria (Ajakaiye et al., 1991; Ojo, 1990; Kogbe et al., 1983). The inland basins of Nigeria constitute one set of a series of Cretaceous and later rift basins in Central

and West Africa whose origin is related to the opening of the South Atlantic (Figure 3). Ajakaiye et al., (1991) further suggested possible extension of St Paul and Romanche major fracture zones across the basin. Interpretations of Landsat imageries and geophysical data suggest that the basin is bounded by a system of linear faults trending NW-SE (Kogbe et al., 1983). Lineaments map (Figure 2) also reveals varied trends within the basin but dominantly trending NE – SW (NGSA, 1984).

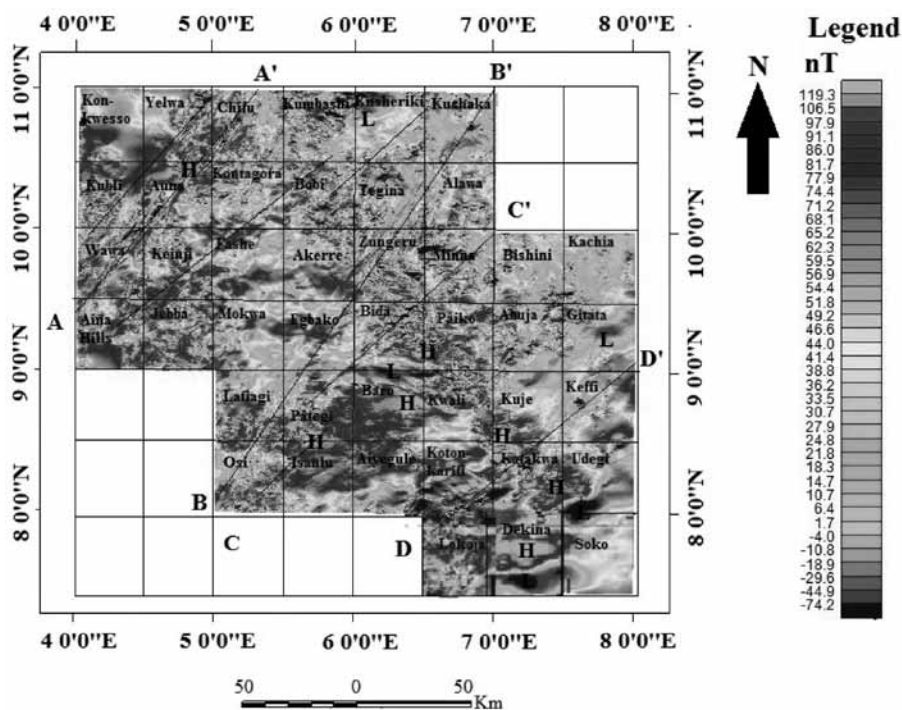


Figure 4. Residual Total Magnetic Intensity Map (RTMI) of entire Bida basin showing inferred lineaments (AA', BB', CC' and DD') – likely paleofracture zones. Magnetic high (H) and low (L) are also shown. A constant 33000 nT was removed as common background field.

Data Acquisition and Analysis

The regional airborne magnetic surveys over the entire Bida Basin and adjoining areas were carried out by the Nigeria Geological Survey Agency (NGSA) between 2004 and 2009. The field surveys were completed using 3 Fixed-wing aircrafts mounted with Scintrex CS3 Cesium vapour magnetometers having data recording interval of 0.1 seconds. The aircrafts were flown at a mean terrain clearance of 80 m with 500 m line spacing and nominal tie-line spacing of 2 km. The flight line and tie-line trends were 135 and 45 degrees respectively. The resulting magnetic data were processed and published as digital half degree high-resolution airborne magnetic (HRAM) intensity digital maps by the NGSA.

Forty three (43) HRAM maps (sheet number 117 - 122, 138 - 143, 159 - 166, 180 - 187, 203 - 208 and 224 - 229) on a scale of 1:100,000, covering a total area of 130,075 square km, were used in this work. The whole data, covering the entire Bida Basin and adjoining areas, were procured from NGSA and assembled into composite total magnetic field intensity (TMI) map (Figure 4). Regional correction, which was based on the International Geomagnetic Reference Field (IGRF-11), was made by the NGSA before the eventual publication as HRAM Maps.

The composite map was then divided into 28 overlapping blocks and each block covering a square area

of 200 km x 200 km was analysed using fractal scheme. A window length (L) of 200 km was found suitable for the reason that magnetic source bodies having bases deeper than $L/2\pi$ may not be properly resolved by spectral method (Shuey et al., 1977). Moreover, a common rule of thumb is that the window size must be about 10 times the expected depth value (Ravat et al., 2007).

RESULTS AND DISCUSSIONS

Examination of the aeromagnetic data from Bida Basin confirms magnetic lineaments and regions, which were deduced as possible tectonic features. Geologic features usually depict magnetic signatures that make them easily recognizable. A major characteristic of magnetic contours is the fact that sudden break in lithology is shown by discontinuity (Ajakaiye et al., 1985; 1991; Udensi et al., 2003). Figure 4 shows series of lineaments and magnetic closures.

A previous study by Ajakaiye et al., (1991) showed that the onshore lineaments in West Africa are the extensions of the St Paul’s, Romanche, Chain and Charcot regional fracture zones (Figure 3), which are believed to be part of major weakness in the crust that predate the opening of the Atlantic ocean and were reactivated in the early stages of continental rifting. Buser (1966) had earlier recognized the existence of paleostructures, which are linked to

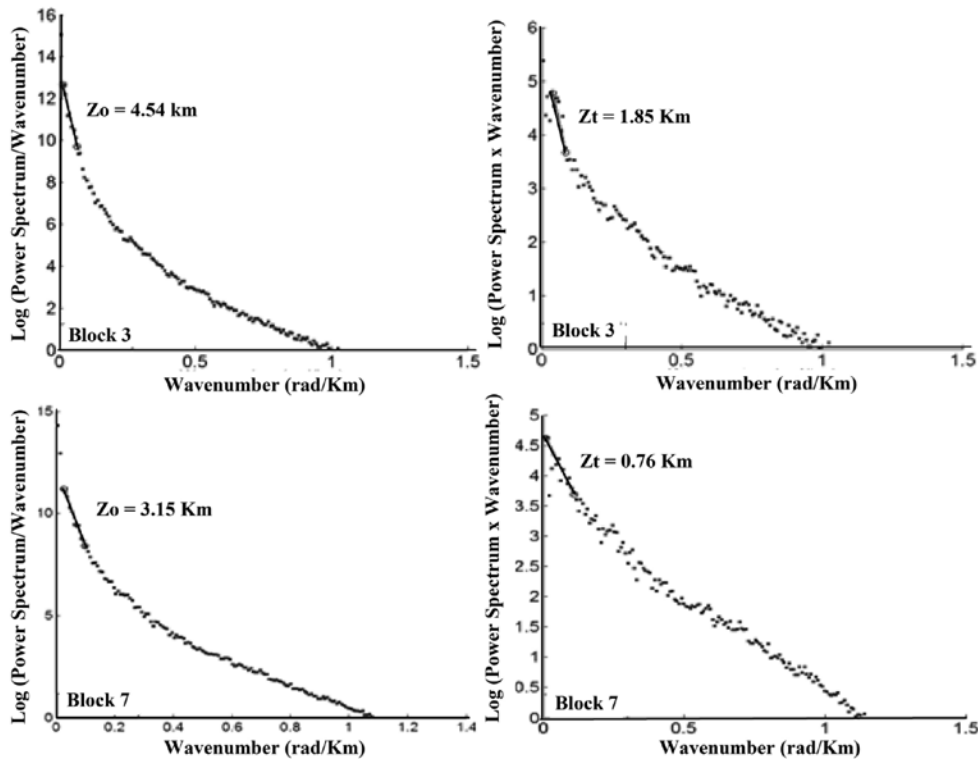


Figure 5. Radial averaged power spectral plots for blocks 3 and 7.

geological events like tectonic movement and intrusions. Consequently, it may not be unlikely that some of the observed major lineaments (BB' and DD'), which trend NE-SW, in Figure 4 could be the St Paul's and Romanche paleostructures. Again, regions of magnetic lows and highs are revealed in the basin. These regions are marked H and L for magnetic high and magnetic low respectively in Figure 4. Conspicuous magnetic highs are located around Dekina, Baro and Pategi; while Bida, Dekina and Udegi have prominent magnetic lows. The low magnetic regions indicate the presence of deep-seated basic igneous intrusions into the basement beneath the basin. Basic igneous rocks are believed to have intruded the Basement Complex beneath the basin (Ojo, 1990). It could thus be inferred that the ancient fracture zones formed weak zones through which the magma that constituted the basic intrusions rose. The presence of large bodies of basic rocks indicated by these results suggests that a deep-seated rift may exist in the crust under the basin. Ojo (1990) further opined that the magnetic low anomalies may have been caused by predominantly basic rocks at depths which vary between 4 and 6 km well below the base of the sediments, which are generally not more than 2 km thick. The high magnetic regions may have resulted from thick sections of sedimentary ironstones. It is important to note that Bida Basin is the only sedimentary basin in Nigeria with abundant ironstones in its formational lithologies (Sakpe ironstone, Batati ironstone, Agbaja ironstone) and its other

formations also contain measurable amounts of ferruginous components (Obaje et al., 2015).

Azimuthally averaged power and wavenumber-scaled power spectra for each of the 28 overlapping blocks were made and used to estimate the depths to bottom of magnetic sources (DBMS). Typical examples for blocks 3 and 7 are shown in Figure 5. The RHS of the figure shows the slope of the lower-wavenumber portion of the spectra, which leads to the estimation of the depth to the top of magnetic sources (Z_t); while the LHS shows the slope of the wavenumber-scaled spectra, which leads to the estimation of centroid depth (Z_o).

The estimated quantitative results are shown in Table 1. The table shows that the DBMS varies from 5.41 to 19.29 km with an average of 12.01 km. This depth information was subsequently used to generate a DBMS isotherm map for the basin as shown in Figure 6.

DBMS varies significantly in the study area. Figure 6 shows that the DBMS values in Bida Basin trend mostly NE – SW with the shallowest portion (less than 8 km) in the north-western part of the basin, and extends eastward while becoming deeper with its deepest depth (about 21 km) at the south-eastern part. In comparison with earlier results (Nwankawo and Sunday, 2017) obtained using conventional centroid method for the whole basin (Figure 7), the derived DBMS values using the modified model are found to be roughly 44% lower, which agrees with the submission of Bansal et al., (2011).

Table 1. Estimated DBMS Values

Blocks	Long (°E)	Lat (°N)	Depth to the top Z_t (km)	Centroid depth Z_o (km)	Depth to bottom Z_b (km)
1	5.00	10.50	0.47	5.3	10.13
2	5.50	10.50	0.39	4.09	7.79
3	6.00	10.50	1.85	4.54	7.23
4	6.50	10.50	0.77	5.33	9.89
5	4.50	10.00	0.85	6.52	12.19
6	5.00	10.00	0.74	5.30	9.86
7	5.50	10.00	0.76	3.15	5.54
8	6.00	10.00	1.24	4.43	7.62
9	6.50	10.00	1.20	4.85	8.50
10	4.50	9.50	1.71	7.10	12.49
11	5.00	9.50	0.55	3.98	7.41
12	5.50	9.50	0.84	5.71	10.58
13	6.00	9.50	0.43	5.65	10.87
14	6.50	9.50	0.66	5.95	11.24
15	7.00	9.50	0.90	7.66	14.42
16	7.50	9.50	0.56	9.09	17.62
17	5.50	9.00	1.05	8.45	15.85
18	6.00	9.00	0.40	7.65	14.90
19	6.50	9.00	1.44	7.13	12.82
20	7.00	9.00	1.35	5.94	10.53
21	7.50	9.00	2.90	6.69	10.48
22	5.50	8.50	0.94	7.05	13.16
23	6.00	8.50	1.07	7.11	13.15
24	6.50	8.50	1.43	8.22	15.01
25	7.00	8.50	0.96	7.25	13.54
26	7.50	8.50	1.78	9.29	16.8
27	7.00	8.00	1.51	10.4	19.29
28	7.50	8.00	2.24	9.78	17.32
Average					12.01

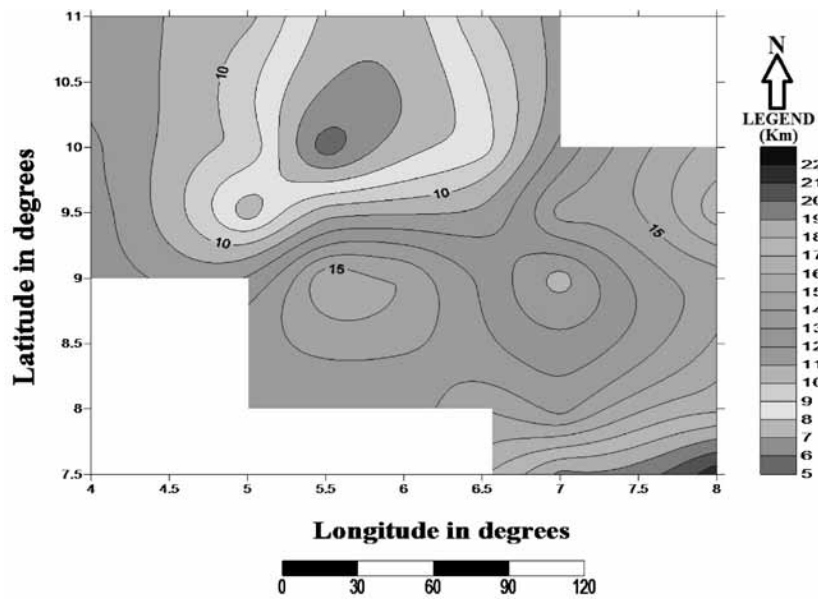


Figure 6. DBMS map of the study area (Contour interval 1 km).

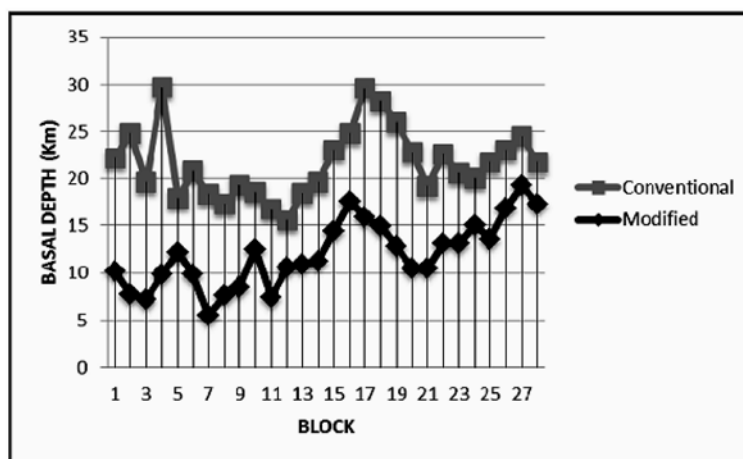


Figure 7. Comparison of DBMS values calculated using modified centroid for fractal distribution of sources with conventional centroid method.

CONCLUSION

The newly acquired high resolution aeromagnetic anomaly data over Bida Basin, north-central Nigeria has been studied using freshly developed fractal model to estimate the depths to bottom of magnetic sources (DBMS). The result shows that the DBMS varies between 5.41 and 19.29 km with an average of 12.01 km. Regions are observed in the basin with shallow DBMS (below 10 km). Further detailed studies are recommended in such regions. More so, the basin is the least studied of all Nigeria's inland basins.

To date, the basin has no information on seismicity, no exploratory wells have penetrated its sequences and subsurface data are limited (Obaje et al., 2009; 2015). Therefore, this study is expected to contribute significantly in the quantitative appraisal of the geo-processes and rheology of Bida Basin in north-central Nigeria.

ACKNOWLEDGMENTS

The authors are grateful to the Nigerian Geological Survey Agency (NGSA) for releasing the HRAM data on a subsidised rate and the University of Ilorin, Nigeria for the facilities made available for the research work. The contribution of Dr. Amada Tijani SHEHU, who untimely passed away recently, is highly acknowledged. Thanks are due to Prof. V.P. Dimri for objective appraisal of the manuscript and useful suggestions to enhance the quality of the manuscript. Also thanks are due to Prof. B.V.S. Murty and Dr. M.R.K. Prabhakara Rao for finer refinement of the revised version. Chief Editor carried out final editing.

Compliance with Ethical Standards

The authors declare that they have no conflict of interest and adhere to copyright norms.

REFERENCES

- Adeniyi, J.O., 1985. Ground total magnetic intensity in part of Nupe basin and the adjacent Basement Complex, Niger State, Nigeria, *Nig. Jour. of Appl. Sciences*, v.3, pp: 67-78.
- Adeleye, D.R., 1974. Sedimentology of the fluvial Bida Sandstones (Cretaceous) Nigeria, *Sedimentary Geology*, v.12, pp: 1-24.
- Adeleye, D., 1976. The geology of the middle Niger Basin. Geology of Nigeria, Elizabethan Publishing Company Limited, Lagos.
- Ajakaiye, D.E., Hall, D.H., and Millar, T.W., 1985. Interpretation of aeromagnetic data across the central crystalline shield of Nigeria, *Geophys. J.R. Astron. Soc.*, v.83, pp: 503-517.
- Ajakaiye, D.E., Hall, D.H., Ashiekaa, J.A., and Udensi, E.E., 1991. Magnetic anomalies in the Nigerian continental mass based on aeromagnetic surveys, *Tectonophysics*, v.192, pp: 211-230.
- Akande, S., Ojo, O., and Ladipo, K., 2005a. Upper Cretaceous Sequences in the Southern Bida Basin, Nigeria. A Field Guidebook: Mosuro Publishers, Ibadan.
- Akande, S.O., Ojo, O.J., Erdtmann, B.D., and Hetenyi, M., 2005b. Paleoenvironments, organic petrology and Rock-Eval studies on source rock facies of the Lower Maastrichtian Patti Formation, southern Bida Basin, Nigeria, *J. Afri. Earth Sci*, v.41, pp: 394-406.
- Bansal, A.R., Gabriel, G., Dimri, V.P., and Krawczyk, C.M., 2011. Estimation of depth to the bottom of magnetic sources by a modified centroid method for fractal distribution of sources: An application to aeromagnetic data in Germany, *Geophysics*, v.76, no.3, pp: L11-L22.
- Bansal, A.R., and Anand, S.P., 2012. Estimation of depth to the bottom of magnetic sources using modified centroid method from aeromagnetic data of Central India, 9th Biennial International Conference & Exposition on Petroleum Geophysics, Hyderabad India.
- Bansal, A.R., Anand, S.P., Rajaram, M., Rao, V.K., and Dimri, V.P., 2013. Depth to the bottom of magnetic sources

- (DBMS) from aeromagnetic data of central India using modified centroid method for fractal distribution of sources, *Tectonophysics*, v.603, pp: 155-161.
- Bansal, A.R., and Dimri, V.P., 2014. Modeling of magnetic data for scaling geology, *Geophysical Prospecting*, v.62, pp: 385–396.
- Bansal, A.R., Dimri, V.P., Kumar, R. and Anand, S.P., 2016. Curie depth estimation from aeromagnetic for fractal distribution of sources. In *Fractal solutions for Understanding complex Systems in earth Sciences* (V. P. Dimri (Ed)). Springer International Publishing, Switzerland.
- Bhattacharyya, B.K., and Leu, L.K., 1977. Spectral analysis of gravity and magnetic anomalies due to rectangular prismatic bodies, *Geophysics*, v.42, pp: 41-50.
- Bhattacharyya, B. K., and Leu, L.K., 1975. Analysis of magnetic anomalies over Yellowstone National Park: mapping of Curie point isothermal surface for geothermal reconnaissance, *Journal of Geophysical Research*, v.8, pp: 4461–4465.
- Blakely, R. J., 1995. *Potential Theory in Gravity and Magnetic Applications*. Cambridge University Press, Cambridge, UK.
- Bouligand, C., Glen, J.M.G., and Blakely, R.J., 2009. Mapping Curie temperature depth in the western United States with a fractal model for crustal magnetization, *J. Geophys. Res*, v.114, no.B, pp: 11104.
- Buser, H., 1966. *Paleostructures of Nigeria and adjacent countries*, Schweizerbart'sche Verlagsbuchhandlung, Stuttgart, Germany
- Connard, G., Couch, R., and Gemperte, M., 1983. Analysis of aeromagnetic measurements from the Cascade Range in Central Oregon, *Geophysics*, v.48, pp: 376-390.
- Finn, C.A. and Ravat, D., 2004. Magnetic depth estimates and their potential for constraining crustal composition and heat flow in Antarctica, *Eos. Trans. AGU* 85 (47) (Fall meeting).
- Gabriel, G., Bansal, A.R., Dressel, I., Dimri, V.P., and Krawczyk, C.M., 2011. Curie depths estimation in Germany: methodological studies for derivation of geothermal proxies using new magnetic anomaly data, *Geophysical Research Abstracts*, v.13, EGU2011-6938.
- Heine, C., Zoethout, J., and Muller, R. D., 2013. Kinematics of the South Atlantic rift, *Solid Earth*, v.4, pp: 215-253.
- Ikumbur, E.B., Onwuemesi, A.G., Anakwuba, E.K., Chinwuko, A.I., Usman, A.O., and Okonkwo, C.C., 2013. Spectral Analysis of Aeromagnetic Data over Part of the Southern Bida basin, West-Central Nigeria, *Int. J. of Fundamental Physical Sci*, v.3, pp: 27-31.
- Jones, H.A., 1975. The Oolitic ironstone of Agbaja Plateau, Kabba Province, *Record of Geological Survey Nigeria*, pp: 20-43.
- Kogbe, C.A., Ajakaiye, D.E., Matheis, G., 1983. Confirmation of rift structure along the middle- Niger Valley, Nigeria, *J. of African Earth Sciences*, v.1, pp: 127-131.
- Kumar, R., Bansal, A.R., Anand, S.P., Rao, V.K., and Singh, U.K., 2017. Mapping of the magnetic basement in the Central India from aeromagnetic data for scaling geology, *Geophys. Prospect.*, doi:10.1111/1365-2478.12541.
- Maus, S., and Dimri, V.P., 1996. Depth estimation from the scaling power spectrum of potential field, *Geophys. J. Int*, v.124, pp: 113–120.
- Maus, S., Gordon, D., Fairhead, D., 1997. Curie temperature depth estimation using a self-similar magnetization model, *Geophys. J. Int*, v.129, pp: 163-168.
- Nigeria Geological Survey Agency (NGSA), 1984. *Lineaments map of Nigeria*.
- Nwankwo, L.I., and Sunday, A.J., 2017. Regional estimation of Curie-point depths and succeeding geothermal parameters from recently acquired high-resolution aeromagnetic data of the entire Bida basin, north-central Nigeria, *Geothermal Energy Science*, v.5, pp: 1-9.
- Nwankwo, L.I., 2015. Estimation of depths to the bottom of magnetic sources and ensuing geothermal parameters from aeromagnetic data of Upper Sokoto Basin, Nigeria, *Geothermics*, v.54, pp: 76-81.
- Obaje, N.G., 2009. *Geology and Mineral Resources of Nigeria*, Lecture Notes in Earth Sciences, Springer, Berlin Heidelberg.
- Obaje, N.G., Idris-Nda. A., Goro, A.I., Dantata, S. H., Okoro, A.U., Akpunonu, E.O., and Jatau, S.B., 2015. New assessment for Central Nigeria's Bida basin highlights geological prospects, *Oil and Gas Journal*, v.113, no.4, pp: 52-59.
- Ojo, S.B., 1990. Origin of a major aeromagnetic anomaly in the Middle Niger basin, Nigeria, *Tectonophysics*, v.185, pp: 153-162.
- Ojo, S.B., and Ajakaiye, D.E., 1976. Preliminary interpretation of gravity measurements in the Middle Niger Basin area, Nigeria, In Kogbe, C.A., (Ed.), *Geology of Nigeria*, 2nd edition, Elizabethan Publishers, Lagos
- Okubo, Y., Graff, R.G., Hansen, R.O., Ogawa, K., and Tsu, H., 1985. Curie point depths of the Island of Kyushu and surrounding areas, *Geophysics*, v.53, pp: 481-494.
- Osokpor, J., and Okiti, J., 2013. Sedimentological and Paleodepositional studies of out cropping sediments in parts of Southern Middle Niger Basin, *Int. J. Sci. and Tech*, v.2, pp: 839-846.
- Ravat, D., Pignatelli, A., Nicolosi, I., and Chiappini, M., 2007. A study of spectral methods of estimating the depth to the bottom of magnetic sources from near-surface magnetic anomaly data, *Geophysical Journal International*, v.169, pp: 421-434.
- Shuey, R.T., Schellinger, D.K., Tripp, A.C., and Alley, L.B., 1977. Curie depth determination from aeromagnetic spectra, *Geophysical Journal of the Royal Astronomical society*, v.50, pp: 75-101.
- Salem, A., Green, C., Ravat, D., Singh, K.H., East, P., Fairhead, J.D., Mogren, S., and Biegert, E.D., 2014. Depth to Curie temperature across the central Red Sea from magnetic data using the de-fractal method, *Tectonophysics*, v.624, pp: 75-86.
- Tanaka, A.Y., Okubo, Y., and Matsubayashi, O., 1999. Curie point depth based on spectrum analysis of the magnetic anomaly data in East and Southeast Asia, *Tectonophysics*, v.306, pp: 461- 470.
- Udensi, E.E., Osazuwa, I.B., and Daniyan, M.A., 2003. The Origin and Tectonic Evolution of the Nupe Basin, Nigeria from Aeromagnetic Study, *ZUMA- Journal of Pure and Applied Sciences*, v.5, no.2, pp: 114-118.

Received on: 2.8.17, Revised on: 28.9.17, Accepted on: 10.10.17

Forecasting aftershocks of major earthquakes

Vinod Kumar* and M. Satya Kumar¹

Shyam Bhawan, Ashok Nagar, Road No. 11, Kankarbagh Colony, Patna-800020

¹ H. No. 6-3-565, Flat No. 301, Akshaya Apartment, Somajiguda, Hyderabad- 500082

*Corresponding Author: vinodmanjusingh@gmail.com

ABSTRACT

Aftershocks of highest magnitude of major earthquakes of magnitude ≥ 7.9 can be forecast on certain lunar days when prominent changes are observed in both values of (Ocean) high tides. If main earthquake occurs on the day when both (Ocean) high tides start decreasing or when both high tides are observed as minimum (continue decreasing) then aftershock of maximum magnitude can be forecast during low tide period. If main earthquake occurs on the day when both high tides start increasing or both high tides are observed as maximum (continue increasing) then aftershock of maximum magnitude can be forecast during high tide period.

Key words: Forecasting; aftershocks; major earthquakes, maximum magnitude; Solar-lunar gravitational force, earth tides, Ocean high tides.

INTRODUCTION

Earthquake, in general, is considered an unpredictable phenomenon. It is caused mainly by the interaction of the tectonic plates as they move. The fault lines or borders between the various plates are where most of the world's earthquakes occur. It is also well known that in areas where the tectonic plates collide, one plate is forced either above or below the other, and produces the high magnitude earthquakes, as well as most obvious geographic phenomenon, major mountain ranges for instance. Ide et al., (2016) investigated three separate earthquake records covering Japan, California and the entire globe. For the 15 days leading up to each quake, they assigned a number representing the relative tidal stress on that day, with 15 representing the highest. They found that large quakes such as those that hit Chile and Tohoku-Oki occurred near the time of maximum tidal strain or during new and full moons when the Sun, Moon and Earth align. For more than 10,000 earthquakes of around magnitude 5.5, the researchers found, an earthquake that began during a time of high tidal stress was more likely to grow and become a significantly high magnitude earthquake, at times to magnitude 8 and above. The aim of the present study is to examine the impact of the different phases of the Moon in forecasting aftershocks of major earthquakes by using tide's tables. Ultimate aim of this study is also to indentify the region where an earthquake is expected.

DATA

Year wise/ month wise earthquakes data, for the period 2009 to 29 September 2017 have been collected from National Earthquake Information Center web site, U.S.A (USGS). Also earthquake data have been collected from

I.M.D. web site from 2007. Shri Venkateshwar Shatabdi Panchangam (hundred years Almanac: 1944 to 2044 AD) has been used to identify lunar day for all earthquakes. Tide's tables from 2009 to 2017 have also been collected from PNP Maritime Service Private Limited, Mumbai, which has been prepared by Survey of India.

PREVIOUS STUDIES

Fredrick and Becker (1976) mentioned that spring tide occurs when the Moon is New or Full, Figure 1. Because the Moon and the Sun are then attracting from the same or opposite directions, lunar and solar tides reinforce each other. The neap tide occurs when the moon is at quarter phase; then the Moon and Sun are at 90° apart in the sky, so that one set of tides is partly neutralized by the other. When the Moon is New or Full also in perigee (nearest point), the difference in level between low and high tides is especially great (Figure 2). When the Moon is at apogee (farthest point) the tidal range shrinks.

Kolvankar et al., (2010) observed that earth tides trigger earthquakes at all depths and up to magnitude 5.0. The lateral stresses applied during earth tides close to Full Moon phase are found to be more effective than those stresses of earth tide during the New Moon phase. Kolvankar (2011) observed that over 98% of world wide earthquakes faithfully follow the straight-line relationship between the Sun position or GMT timings with Earth-Moon distance (EMD) and Sun-Earth-Moon angle (ESM). It is seen that all these earthquakes are triggered by the Earth tides caused by the positions of the Sun and the Moon and this process seems to be the primary triggering mechanism for all worldwide tectonic earthquakes. He has also mentioned that high magnitude earthquake counts from 00 hours (midnight) to 06 hours and shown a pattern

that is inversely proportional to the daily atmospheric variation. The suggested pattern has shown the influence of the temperature. This position again depends upon the Sun's local position (Kolvankar 2010). During Rig Veda era, people/saints were having knowledge about the influence of the Sun and seven planets Moon, Mars, Jupiter, Mercury, Venus, Uranus, and Neptune over each other and on the Earth. They were also having knowledge of the destructive power of the Moon, which is apparent from their prayer to the Moon: "You do not put us in the hands of death, we should see always the movement of the Sun in the sky, we should always remain alive, every day our senility should be beneficial and keep the death of God away from us" (Paramhans Swami Jagdishwaranand Saraswati (2010). This type of fear had not been expressed while praying to any other planet (God). While appreciating the level of understanding the seers had regarding the impact of terrestrial bodies on the Earth, we need to keep in view one basic reality. The Moon is closer to the Earth compared to any other planet and as such perturbations on the Earth and The Moon can affect each other. Apart from the Moon the impact due to the Sun on the Earth is considerable. The Sun being very powerful in every respect compared to any of its planets, can cause instability on every planet including the Earth. Such an impact on the Earth's stability is caused through increase or decrease in the magnitude of solar flares. Apart from the Sun any impact or change in surface manifestations and sub surface structure of the Moon due to different reasons can cause instability on some segments of the Earth, leading to occurrence of earthquakes. These abnormalities can be significant basically due to the Moon's proximity to the Earth. Such impacts from other planets including the biggest planet Jupiter will not affect the Earth unless they are significantly strong and create an amount of instability not only on the Earth and the Moon but also on other planets. Such a possibility happens at times especially on a particular day when the Earth and the Ocean tides increase in magnitude (on certain days including new moon and full moon days).

Tanaka (2010) observed that since tidal forces generate currents in conducting fluids in the Earth's interior, they in turn affect the Earth's magnetic field. Earth tides have also been linked to earthquakes by him. Juan et al., (2000) considered relationship between 21 major earthquakes ($M_s \geq 7.0$) inland and off shore area of Taiwan Island in 20th century and the variance ratio of the lunar-solar tidal force. They observed that the time of these earthquakes is closely related to the variance ratio of the lunar-solar tidal force and therefore that the tidal force plays an important role in triggering earthquakes. Venkatanathan et al., (2005) mentioned that if two or more planets, especially Sun and Moon are aligned more or less in line (0° or 180°) with the Earth, then the Earth would be caught in the middle of a

huge gravity struggle involving the Sun and other planets, including the Moon.

When the speed of rotation of the Earth changes the tectonic plate motion also get affected. Thus the planetary forces act as a triggering mechanism for the accumulated stress to be released abruptly at plate boundaries/ intra-plate faults. It is well known that the gravitational pull of the Moon and the Sun creates tides on the Earth. While tides are most commonly associated with Oceans and large bodies of water, gravity creates tides in the atmosphere and the lithosphere (the surface and interior of the earth extending to sub crustal upper mantle of the Earth). The atmospheric tidal bulge extends far in to the space but the tidal bulge of the lithosphere is limited to 12 inches (30 cm) twice a day (<http://geography.about.com/od/physicalgeography/a/tides.htm>).

Killer tornadoes develop mostly during high tide period (74.1%) under favorable synoptic situations. High tide and low tide periods have been considered from 10th to 3rd and 4th to 9th during each waning and waxing period of the Moon respectively, Kumar et al., 2012.

Bhattacharya (1998) mentioned that the study of Varaha Mihira (Brihat Samhita, 600 AD) gives us a fairly good idea of seismically active areas in India where moderate to large earthquakes occurred. One belt runs north to south along Hazara, Jammu and Kashmir, Punjab, Himachal Pradesh, U.P. hills and western Border areas of U.P., Delhi and Jaipur. Second belt starts at Surat and moves northward to Saurashtra and southern Rajasthan and then runs eastward to Madhya Pradesh, southeast U.P., Bihar, Bengal and Tripura. Third belt is along central Kerala and east coast from Tamil Nadu to southern Orissa through coastal Andhra Pradesh.

It had been mentioned (<http://www.contentwriter.in/articles/others/earthquake.htm>) that most of catastrophic events of earthquakes are associated with any of these two belts:

1. Western Coasts of North and South America, the Aleutian Islands and the Island groups along the eastern Coasts of Asia, such as Japan and the Philippines and thus borders the Pacific Ocean on the east, north and the west.

2. It includes the Mediterranean, the Alps, the Caucasus and the Himalayas and continues into East Indies, where it intersects the first belt. Uttaranchal, Assam and Andaman Nicobar Island chains fall within the 2nd belt and thus face frequent earthquakes of devastating nature.

Variations in Tidal Range on Different Lunar Days

Continuous changes in the values of both high Sea tides (Arabian Sea) during every fortnight have been put under four different categories. Each specific feature is noticed

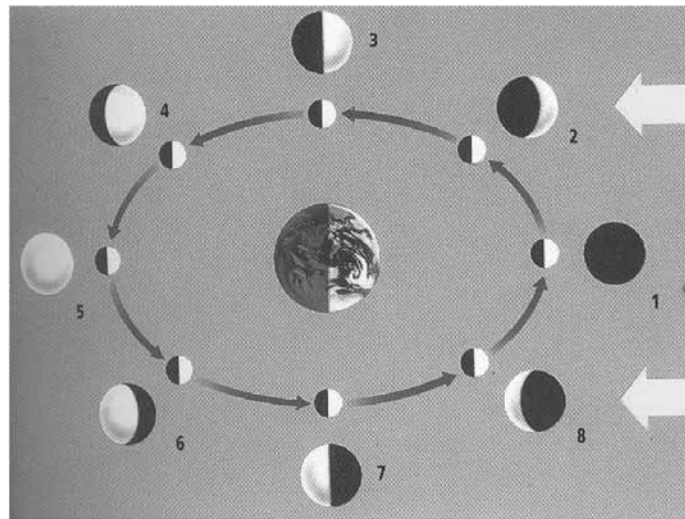


Figure 1. Phases of the Moon.

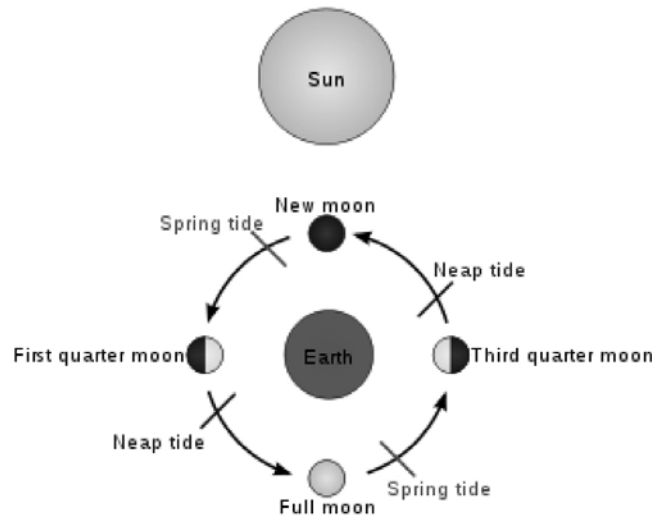


Figure 2. Types of tides.

once in each waning and waxing period in every month and 24 times (normally) in a year. The alphabet 'K' and 'S' denote waning (starts after full moon and up to new moon) and waxing (starts after new moon and up to full moon) period, respectively (Krishna and Shukla Paksha). First day, of the waning and waxing period, has been marked as K-1 and S-1, respectively. It has been observed that when both values of high tides reach maximum on a certain lunar day, then on a certain lunar day both start decreasing. Again both values of high tides go on decreasing daily and on a certain lunar day both values of high tides are observed as minimum. After that on a certain lunar days, both values of high tides start increasing and go on increasing daily. Again on a certain lunar day they reach maximum and the cycle continues. The details of tidal feature, which were found in the tide tables for the years 2009, 2010, 2011, 2012, 2013, 2014, 2015, 2016 and 2017 are as under:

Feature	Lunar days (total number of occurrence)
Both high tides start decreasing (S.D.):	
K-2 (9), K-3 (31), K-4 (50), K-5 (16) and K-6 (1); K (107)	
S-1 (1), S-2 (7), S-3 (34), S-4 (41), S-5 (28) and S-6 (2):	S (113)
Here K-2 (9) denotes, on nine occasions both high tides started decreasing on 2 nd day of the waning period i.e. on Krishana Paksha Dooj. S-1 (1) denotes, on one occasion both high tides started decreasing on 1 st day of the waxing period i.e. on Shukla Paksha pariva. So, out of 220 days [K (107) and S (113)] during 9 years period both tides S.D. on maximum occasions during 4 th lunar day of both fortnights for 84 days [K-4 (50) and S-4 (34): 38%].	
Both tides continue decreasing (C.D.):	
K-7 (1), K-8 (46), K-9 (58) and K-10 (5): K (110)	
S-7 (1), S-8 (43), S-9 (60) and S-10 (1):	S (105)

On these lunar days both high tides reached their minimum heights. So, out of 215 days [K (110) and S (105)] during 9 years period, minimum tides were observed on maximum occasions on 9th lunar day of both fortnights for 118 days [K-9 (58), S-9 (60): 54.8%].

Both tides start increasing (S.I.):

K-9 (2), K-10 (32), K-11 (31), K-12 (34), K-13 (7), K-14 (2), K-15 (1): K (109)

S-9 (1), S-10 (31), S-11 (40), S-12 (25), S-13 (14), S-14 (1), S-15 (1): S (113)

So, out of 222 days [K 109, S 113] during 9 years period, both tides S.I. on maximum number of occasions on 11th lunar day (Aakadashi) of both fortnights for 71 days [K-11 (31), S-11 (40): 31.9%].

Both tides continue increasing (C.I.):

K-1 (21), K-2 (39), K-3 (27), K-4 (3), K-12 (1), K-13 (3), K-14 (3), K-15 (13): K (110)

S-1 (32), S-2 (31), S-3 (31), S-4 (1), S-11 (1), S-13 (2), S-14 (5), and S-15 (12): S (115)

In this case both high tides reached their maximum heights on these lunar days. Out of 225 days during 9 years period, maximum tides were observed on maximum number of occasions during 2nd lunar day in both fortnights of a month for 70 days [K-2 (39) and S-2 (31): 31%].

It is also observed that on 12 and 13 occasions, maximum tides were forecast for full Moon and new Moon's day, respectively during 9 years period. So, out of 225 days [[K (110) and S (115)] during 9 years period maximum tides were observed on only 25 days [K- 15 (13) and S- 15(12)] during new moon's and full moon's day (11%).

METHODOLOGY

Generation and influence of Earth tides have been considered an important triggering mechanism for worldwide occurrence of earthquakes by some seismologists. Researchers in the US have found a link between the position of the Sun and Moon and small tremors deep within the San Andreas Fault - suggesting that the gravitational pull of the astronomical bodies could be causing the Earth's plates to move up and down like the ocean's tides. The San Andreas Fault stretches some 1,287 kilometres (800 miles) through California - is a geological region where the Pacific Plate and the North American Plate meet. To come to that conclusion, the team analysed 81,000 low-frequency earthquakes that occurred between 2008 and 2015 near the Parkfield section of the fault - an area that is constantly jittering with seismic activity. They then compared this data to tidal data from the same timeframe, paying particularly close attention to the two-week 'fortnightly tide', which coincides with the

lunar cycle. When all was said and done, the team found that seismic activity in the region increased when the Moon was in its waxing phase, building up to a full Moon. *Proceedings of the National Academy of Sciences*, 2016 (<https://www.sciencealert.com/the-pull-of-the-sun-and-moon-can-cause-earthquakes-along-the-san-andreas-fault-study-finds>). In a report published by National Geographic News in 2005 it is mentioned that James O. Berkland, California-based geologist in —*An Earthquake Newsletter* believed that the gravitational tugs of the moon, sun, and other planets can influence earthquake activity. He claimed that during the alignment of three celestial objects the Sun, Earth, and Moon that occurs twice a month, at the full and new moons the gravitational forces are at a maximum, especially when the bodies are close together. The Earth and moon are closest together—at perigee—once a month. The Earth and sun are closest together—at perihelion—once a year. Perihelion currently occurs in early January. Maximum gravitation force occurs when perigee occurs on the same day as perihelion. From the seismic data gathered from the Moon, moonquakes occur most frequently at perigee. USGS seismologists negated his theory that influence of celestial bodies on the Earth can lead to seismic activity on the Earth. They opined that though the Earth can trigger quakes on the moon, the moon is too small to trigger any earthquakes. But, the moon is mostly solid and lacks a liquid core like the Earth, which is an active, living planet, and so it is not at all surprising that minor gravitational stresses can trigger earthquakes, Berkland said. Berkland said he accurately predicted several earthquakes, including the October 17, 1989 earthquake in San Francisco, California. At least two major quakes may also support Berkland's theory. The December 26, 2004, magnitude 9.1 in Sumatra, Indonesia, occurred on the day of a full moon. Likewise, the March 27, 1964, magnitude 9.2 earthquake in Alaska occurred on the day of maximum high tide. According to Berkland, such correlations are more than coincidences. They demonstrate a true connection between the moon and earthquake activity (https://news.nationalgeographic.com/news/2005/05/0523_050523_moonquake_2.html).

Ocean tides are linked with earth's tides. Arabian Sea tide's tables from 2009 to 2017 have been studied for forecasting earthquakes aftershocks. An appropriate lunar day has been marked on all day of respective months of the tide's tables. Normally semi- diurnal tides (two high waters and two low waters each day) have been forecast for all the months in the tide's tables. In every month, 3 tides a day have been forecast for three to five days, when two tides were separated by more than 6 hours. In a few cases only two tides were forecast. During 2009, 2010, 2011, 2012, 2013, 2014, 2015, 2016 and 2017, it has been observed that mostly both values of high tides S.D. from 3rd or 4th or 5th day of waning and waxing period and C.D. till

8th or 9th day of both fortnights. Again, mostly both high tides S.I. from 10th or 11th, or 12th and C.I. till 1st or 2nd or 3rd lunar day during waning and waxing period. Although earthquakes are observed daily on global basis, yet it is not possible to locate the earthquakes on the basis of tides trend of any Ocean as impact of earth tides on the Earth surface cannot be located. Once a major earthquake struck (≥ 7.9 magnitude considered), aftershocks can be forecast on the basis of tides trend observed under item "Variations in tidal range on different lunar days". From S.D. trend, K-3, K-4, K-5, S-3, S-4 and S-5; from C.D., K-8, K-9, S-8 and S-9; from S.I., K-10, K-11, K-12, S-10, S-11 and S-12; from C.I., K-1, K-2, K-3, S-1, S-2, and S-3 can be selected for aftershocks forecast as these trends have been observed on maximum number of days. High tides period have been observed from 10th lunar day to 3rd lunar day and low tides mostly from 3rd to 9th lunar day in both the fortnights of the month. 3rd lunar day is observed in both the trends. Lunar days K-3 and S-3, have been observed significantly under trends S.D. (65 days) and C.I. (58 days), as such both have been included for aftershocks forecasting during low and high tide periods. If main earthquake is observed in high tide's period then it would be relevant to consider S.I. and C.I. and for low tide's period S.D. and C.D. trends for forecasting aftershocks. So, for occurrence of aftershocks (≥ 5.0) during high tide's period; K-1, K-2, K-3, K-10, K-11, K-12; and S-1, S-2, S-3, S-10, S-11, S-12 (12 days forecast in a month), and during low tide's period; K-3, K-4, K-5, K-8, K-9; and S-3, S-4, S-5, S-8, S-9 (10 days forecast in a month) can be selected for one month to two months period depending upon the correctness of forecasting and magnitude of earthquake. But if S.D., C.D., S.I. and C.I. trend forecasts are available from the tide's table, these dates should be also included in the forecast if they are not covered by these lunar days. If earthquake occurs on K-3/S-3 lunar day then tide's table has to be consulted to know whether the earthquake has occurred on C.I. or on S.D. If C.I. is observed on K-3/S-3, then forecast for high tide period lunar days should be considered (10th, 11th, 12th, 1st, 2nd and 3rd). If S.D. is observed on K-3/S-3 then forecast for low tide period should be considered. If C.I. has been observed prior to K-3/S-3 and earthquake has been observed on K-3/S-3 then forecast for low tide period should be considered. On the basis of lunar days, forecast can be issued for every 15 days on selected English dates for general public. In Hindu calendar, lunar day starts after Sunrise and continues till Sunrise, whereas English date starts after mid-night. In majority of cases all four trends (S.D., C.D., S.I. and C.I.) observed for Arabian Sea would be observed on the same lunar day for other Seas as spring and neap tides depending upon the position of the Moon. Solar-lunar eclipses are observed on a fixed date for all countries. Any lunar day in U.S.A. will be observed nearly after 12 hours depending upon the difference in

time of the two locations in US and the selected country. Earthquake forecast based on lunar days comes into effect on a lunar day, which starts in India after Sun rise and earthquake forecast based on tide table comes into effect after midnight.

Tide's Tables during Aftershocks

Tide's tables for four important cases of aftershocks of major earthquakes have been given below. Ocean tide's trends for different Seas (S.D., C.D., S.I. and C.I.) may differ in terms of dates but here on the basis of Arabian Sea tide's table examples have been given. These four aftershocks can be successfully forecast:

(1) Earthquake struck Chile (36.12°S/072.9°S) on 27 February 2010 at 0634 UTC (1204 IST: S-14) with magnitude of 8.8 at the focal-depth of 22 km. One of the major aftershocks was observed on the forecast date 11th March 2010 near 34.33°S/071.8°S at 1455 UTC (2025 IST) having magnitude 7.0 and focal-depth as 18 km. All timings in the tide's tables have been given in IST (Hour Minute: HM) and height in Meter (M). Tide tables for 9th, 10th and 11th March are as under:

HM	Height (M)	HM	Height (M)	HM	Height (M)
0239	2.57 (9 th)	0403	2.32 (10 th)	0439	2.05 (11 th)
0609	2.70	0832	2.69	0956	2.95
1237	1.76	1409	1.72	1528	1.53
2115	3.25	2211	3.44	2245	3.65

Earthquake occurred on 11th (S-10) when both high tide values S.I. on 11th. It was observed at 2025 IST and 2nd high tide was observed at 2245 IST. On 11th both high tides show increasing trend (S.I.).

(2) Earthquake struck Honshu Japan on 11th March 2011 at 0546 UTC (1116 IST: S-6) near 38.4°E/144.4°E having magnitude 9.0 at 17 km focal-depth. Aftershock of magnitude of 7.4 at 33 km. depth, was observed at 1432 UTC (2002 IST) on one of the forecast date of 7th (S-4) April 2011 when both high tides S.D. on 7th. Tide tables for 5th, 6th and 7th are as under:

HM	Height (M)	HM	Height (M)	HM	Height (M)
0041	4.02 (5 th)	1007	4.00 (6 th)	0134	3.92 (7 th)
0648	0.57	0713	0.53	0741	0.59
1326	4.28	1358	4.29	1431	4.22
1907	1.39	1939	1.47	2015	1.61

Earthquake was observed at 2002 IST and 2nd high tide was observed at 1431 IST. On 7th both high tides values show decreasing trend (S.D.).

(3) A 7.9 magnitude earthquake of 10 km focal depth struck Nepal on 25th April 2015 (S-7) at 0611 UTC (1141 IST), near 28.1°N/084.6°E. Aftershock of 7.3 magnitude at 10 km focal depth struck on 12th May 2015 (K-9) near 27.7°N/086.0°E at 0705 UTC (1203 IST). This occurred on the forecast date. The tide tables for 11th, 12th and 13th May 2011 are as under:

HM	Height (M)	HM	Height (M)	HM	Height (M)
0443	3.37 (11 th)	0026	1.84 (12 th)	0139	1.63 (13 th)
1049	1.38	0610	3.30	0744	3.42
1746	3.91	1206	1.56	1331	1.62
		1852	3.87	2001	3.92

Aftershock devastated already battered region when both high tides values were minimum on 12th. On 12th both high tides have shown minimum values in comparison to 11th and 13th. Earthquake was observed at 1203 IST, which came in between two high tides.

(4) On 8th Sept 2017, an earthquake occurred (magnitude: 8.1 and depth 56.7 km) over Mexico at 0449 UTC (1019 IST). Aftershock of maximum magnitude (7.1) occurred on 19th September at 1814 UTC (2344 IST: K-2) at the focal-depth of 48.0 Km, 17 minutes prior to forecast date of 20th September. Maximum tide was observed on 20th (C.I.). Tides table for 19th, 20th, and 21st are as under:

HM	Height (M)	HM	Height (M)	HM	Height (M)
0451	0.70 (19 th)	0534	0.68 (20 th)	0024	4.33 (21 st)
1125	4.50	1203	4.54	0612	0.78
1724	0.85	1804	0.71	1236	4.47
2346	4.25			1840	0.65

Maximum magnitude aftershock occurred at 2344 IST, just two minutes before the 2nd highest tide on 19th. On 20th maximum value of high tide was observed at 1203 IST. Only three tides were observed during 24 hours. Lunar days are more marked for major aftershocks than timings of the high tides.

DISCUSSION

Earthquakes and aftershocks occurred during 2009 (2), 2010 (1), 2011 (1), 2012 (1), 2015 (2) and 2017 (1) of major

earthquakes having magnitude ≥ 7.9 . These earthquakes have been considered for forecasting aftershocks. These have been listed under Table 1. In 2013, earthquake having magnitude 8.3 occurred in Sea of Okhotsk at the focal-depth of 598.1 Km. No aftershocks ≥ 5.0 occurred after that day, because the earthquake originated from a depth of nearly 600 Km. Aftershocks of some selected major earthquakes (from the list) continued to occur for a period of one to three months. Aftershocks continued to occur almost daily for quite some time. It is expected that on forecast days, aftershock of magnitude ≥ 5.0 would usually strike. Magnitude of these shocks, on any day, is found to be high. On 3rd January 2009 an earthquake having magnitude 8.0 occurred in Indonesia. It occurred on 7th lunar day (S-7), which comes under low tide period. So, aftershocks having magnitude ≥ 5.0 can be forecast on S-8, S-9, K-3, K-4, K-5, K-8, K-9, S-3, S-4, S-5 and S-8 (11 days) for one month period. Corresponding dates for these lunar days can be found from Hindu almanac/calendar. Aftershocks, which took place on non forecasting days, have been mentioned as other day (O.D.) in the Table 1. Aftershocks have continued for six days i.e. up to 9th January 2009. Aftershock of highest magnitude of 6.0 took place on 6th January on O.D., and aftershocks of magnitude of 5.5/5.7/5.9 have occurred on the forecast day of 4th January. So, difference of just 0.1 has been observed in magnitude of aftershock between forecast day and O.D. On 3rd February 2009, aftershocks occurred nearly 600 km away from the main earthquake epicenter. Also these shocks occurred at relatively deeper focal-depths. Increased distance of epicenters and deeper focal depths suggest that these events are independent of the selected main shock. The above observations helped in discontinuing aftershock forecasting.

Table 1. List of aftershocks from 2009 to 2017.

Date	Time (UTC)	Place	Lat. (Deg.)	Long. (Deg.)	Magnitude (≥ 5.0)/ Depth (km)	Lunar Day	FCST
03.01.2009	1943	Indonesia	0.41S	132.88E	8.0 (7.7 USGS) /17.0	S-7	Main Eq.
	2149		0.32	132.88	5.6/29.0		
04.01.2009	0714		0.40	132.76	5.9/35.0	S-8	True CD
05.01.2009	1924		0.65	133.28	5.2/17.0	S-9	True
06.01.2009	2248		0.66	133.43	6.0/16.0	S-10	Other day: O.D.
07.01.2009	1502		0.41	132.85	5.2/35.0	S-11	O.D.
08.01.2009	1618		0.41	132.93	5.5/18.0	S-12	O.D.
09.01.2009	1435		0.71	133.78	5.2/35.0	S-13	O.D.
11.01.2009	1813		0.55	132.88	5.2/35.0	S-15	O. D.
12.01.2009		No Eq.				K-3	False
14.01.2009	1333		0.51	132.95	5.0/35.0	K-4	True SD
15.01.2009	2352		0.30	132.60	5.0/35.0	K-5	True
19.01.2009	0014		0.47	131.90	5.0/32.0	K-8	True CD
20.01.2009	1046		04.67	129.81	5.5/ 143.0	K-9	True
22.01.2009	0315		0.52	127.43	5.1/132.0	K-12	O.D.
29.01.2009		No Eq.				S-3	False

Forecasting aftershocks of major earthquakes

Date	Time (UTC)	Place	Lat. (Deg.)	Long. (Deg.)	Magnitude (≥ 5.0)/ Depth (km)	Lunar Day	FCST
30.01.2009		No Eq.				S-4	False
31.01.2009	0318		0.70	133.43	5.0/18.0	S-5	True SD
03.02.2009	1357		6.48	130.14	5.1/164.0	S-8	True CD
		FCST discontinued (DIS)					
29.09.2009	1748	Samoa Islands	15.49S	172.10W	8.1/18.0	S-11	Main Eq.
	2345		16.19	172.55	6.0/10.0	S-11	
30.09.2009	0524		15.34	173.29	5.3/10.0	S-12	True
01.10.2009	0613		15.43	173.25	5.8/10.0	S-12	True
02.10.2009	0107		16.33	173.47	6.1/8.0	S-13	O.D.
03.10.2009	0716		16.91	172.96	5.5/10.0	S-14	O.D.
04.10.2009	0910		16.23	173.24	5.5/23.0	S-15	O.D.
05.10.2009	0922		16.44	173.23	5.1/10.0	K-1	True CI
06.10.2009		No Eq.				K-2	False
07.10.2009	2338		16.74	172.40	5.3/10.0	K-3	True
10.10.2009	1941		15.60	173.06	5.9/13.0	K-7	O.D.
11.10.2009	1100		17.59	173.08	5.1/10.0	K-8	O.D.
13.10.2009						K-10	False SI
14.10.2009	1800		14.91	174.82	6.3/10.0	K-11	True
15.10.2009						K-12	False
17.10.2009	0147		14.99	173.75	5.2/10.0	K-14	O.D.
18.10.2009	1202		16.39	173.27	5.4/10.0	K-15	O.D.
19.10.2009	2249		15.36	172.26	6.0/18.0	S-1	True CI
20.10.2009		No Eq.				S-2	False
21.10.2009		No. Eq.				S-3	False
28.10.2009	2356		15.79	173.39	5.5/10.0	S-10	True SI
29.10.2009	1552		15.40	173.21	5.0/10.0	S-11	True
30.10.2009		No Eq.				S-12	False
01.11.2009	2128		15.51	173.75	5.8/105.0	S-14	O.D.
02.11.2009	1706		15.44	173.57	5.5/10.0	S-15	O.D.
03.11.2009		No Eq.				K-1	False
04.11.2009	1835		15.64	171.80	5.2/10.0	K-2	True CI
05.11.2009	0604		17.57	176.89	5.3/35.0	K-3	True
06.11.2009	1735		17.02	173.02	5.1/10.0	K-4	O.D.
11.11.2009						K-10	False
12.11.2009	0213		20.98	178.66	5.8/570.0	K-11	True
13.11.2009	1722		16.07	172.74	5.3/10.0	K-12	True
14.11.2009		No Eq.				K-13	
15.11.2009		FCST DIS				K-14	
27.02.2010	0634	Chile	36.12S	072.90W	8.8/22.0	S-14	Main Eq.
	0801		37.77	075.05	7.4/35.0		
28.02.2010	1125		34.90	071.62	6.2/46.0	S-15	O.D.
01.03.2010	0244		35.04	072.49	5.7/22.0	K-1	True
02.03.2010	0428		36.67	073.30	5.5/35.0	K-2	True CI
03.03.2010	1744		36.61	73.36	6.1/20.0	K-3	True
04.03.2010	0159		33.22	072.12	6.0/24.0	K-4	O.D.
05.03.2010	1142		36.67	073.37	6.6/18.0	K-5	O.D.
07.03.2010	15.59		37.99	073.30	5.9/26.0	K-7	O.D.
10.03.2010	1220		33.56	072.30	5.6/35.0	K-10	True
11.03.2010	1439		34.29	071.89	6.9/11.0	K-11	True SI

Date	Time (UTC)	Place	Lat. (Deg.)	Long. (Deg.)	Magnitude (≥ 5.0)/ Depth (km)	Lunar Day	FCST
	1455		34.33	071.80	7.0/18.0		
	1458		34.61	071.99	5.6/35.0		
	2011		34.38	071.98	5.6/8.0		
12.03.2010	1650		34.23	071.92	5.8/7.0	K-12	True
13..03.2010	1034		37.55	073.46	5.8/35.0	K-13	O.D.
15.03.2010	1108		35.80	073.16	6.2/14.0	K-15	O.D.
16.03.2010	0221		36.22	073.26	6.7/18.0	S-1	True
17.03.2010	1829		35.44	073.04	5.1/22.0	S-2	True CI
18.03.2010	0157		36.57	072.77	5.2/28.0	S-3	True
19.03.2010	0854		35.84	073.47	5.5/14.0	S-4	O.D.
21.03.2010	1831		36.34	073.16	5.5/36.0	S-6	O.D.
26.03.2010		No Eq.				S-11	False
27.03.2010		No Eq.				S-12	False
28.03.2010	2138		35.39	073.39	6.0/29.0	S-13	O.D.
30.03.2010						K-1	False CI
31.03.2010	0710		33.66	071.86	5.3/29.0	K-2	True
01.04.2010	1253		34.65	071.82	5.1/11.0	K-3	True
02.04.2010	2258		36.23	072.88	6.0/24.0	K-4	O.D.
08.04.2010		No Eq.				K-10	False
09.04.2010		No Eq.				K-11	False
10.04.2010	2129		34.64	071.63	5.0/54.0	K-12	True
11.04.2010		FCST DIS					
11.03.2011	0546	Japan	38.3N	142.37E	9.0/29.0	S-6	Main Eq.
11.03.2011	0615		36.28	141.11	7.9/42.0		
	0625		38.06	144.59	7.7/18.0		
	1946		40.48	139.05	6.2/10.0		
12.03.2011	0147		37.59	142.65	6.5/20.0	S-7	O.D.
13.03.2011	0126		35.72	141.64	6.1/8.0	S-8	True CD
14.03.2011	0612		37.78	142.46	6.0/14.0	S-9	True
15.03.2011	1523		40.33	143.29	6.1/19.0	S-10	O.D.
16.03.2011	0352		35.9	140.9	6.0/33.0	S-11	O.D.
17.03.2011	0413		40.13	142.17	6.2/29.0	S-12	O.D.
22.03.2011	0944		39.85	143.44	6.4/7.0	K-3	True SD
	1503		35.8	141.7	6.1/10.0		
23.03.2011	1043		36.67	141.46	5.1/35.0	K-4/ K-5	True
25.03.2011	1136		38.77	141.88	6.2/39.0	K-7	O.D.
26.03.2011	1252		39.39	143.29	5.2/21.0	K-8	True
27.03.2011	2223		38.42	142.01	6.2/19.0	K-9	True CD
29.03.2011	1054		37.40	142.29	6.1/15.0	K-10	O.D.
31.03.2011	0715		38.92	141.82	6.0/42.0	K-12	O.D.
06.04.2011	1354		37.65	141.43	5.3/59.0	S-3	True
07.04.2011	1432		38.28	141.59	7.1/42.0	S-4	True SD
08.04.2011	1842		43.72	147.48	5.3/54.0	S-5	True
11.04.2011	0816		37.00	140.40	6.6/11.0	S-8	True CD
12.04.2011	0507		37.11	140.37	6.1/11.0	S-9	True
13.04.2011	1957		39.58	143.34	6.0/22.0	S-10	O.D.
20.04.2011		No Eq.				K-3	False SD
21.04.2011	1337		35.58	140.30	6.2/43.0	K-4	True
22.04.2011	1525		37.23	140.99	5.2/23.0	K-5	True

Forecasting aftershocks of major earthquakes

Date	Time (UTC)	Place	Lat. (Deg.)	Long. (Deg.)	Magnitude (≥ 5.0)/ Depth (km)	Lunar Day	FCST
05.05.2011	1459		38.18	144.03	6.0/11.0	S-2	O.D.
06.05.2011	1118		38.06	142.20	5.0/11.0	S-3	True SD
07.05.2011	2052		40.24	142.24	5.7/35.0	S-4	True
08.05.2011		No Eq.				S-5	False
11.05.2011	1814		36.1	142.27	5.3/11.0	S-8	True CD
12.05.2011		No Eq.				S-9	False
13.05.2011		Forecast DIS				S-10	
11.04.2012	0838	Indonesia	2.32N	093.06E	8.6/20.0	K-6	Main Eq.
	1043		0.80	092.46	8.2/25.1		
	2356		1.84	089.68	5.8/10.0		
12.04.2012	2021		3.75	092.75	5.3/10.0	K-7	O.D.
13.04.2012	0531		2.65	089.71	5.0/14.0	K-8	True
14.04.2012	1521		0.24	092.14	5.4/22.0	K-9	True
15.04.2012	0557		2.58	090.27	6.2/25.0	K-10	True CD
16.04.2012	1605		0.18	092.24	5.2/10.0	K-11	O.D.
17.04.2012	1944		2.58	092.61	5.0/10.0	K-12	O.D.
18.04.2012	0143		3.33	092.54	5.0/25.0	K-13	O.D.
20.04.2012	2228		3.27	093.82	5.9/21.0	K-14	O.D.
21.04.2012	1104		3.27	093.72	5.2/10.0	K-15	O.D.
22.04.2012	0317		1.38	091.75	5.1/6.0	S-1	O.D.
24.04.2012	1943		1.15	091.72	5.1/10.0	S-3	True SD
25.04.2012		No Eq.				S-4	False
26.04.2012	1921		2.70	094.46	5.6/7.9	S-5	True
29.04.2012	0809		2.70	094.51	5.7/14.0	S-8	True CD
30.04.2012	0800		1.76	089.60	5.7/10.0	S-9	True
04.05.2012	1623		2.00	089.72	5.1/10.0	S-13	O.D.
08.05.2012		No Eq.				K-3	False
09.05.2012		No Eq.				K-4	False
10.05.2012		No Eq.				K-5	False
11.05.2012		Forecast DIS					
24.05.2013	0544	Sea of Okhotsk, No SIG Eq. after this day	54.9N	153.2E	8.3/598.1	S-14	Main Eq.
25.04.2015	0611	Nepal	28.10N	084.60E	7.9/10.0	S-7	Main Eq.
	0645		28.10	084.80	6.6/10.0		
	0917	China-Nepal	28.30	087.30	5.8/5.0		
26.04.2015	0709	Nepal	27.60	085.90	6.9/10.0	S-8	True
	1626		27.60	085.70	5.3/10.0		
27.04.2015	1235	Nepal-India	26.70	088.10	5.1/10.0	S-9	True CD
07.05.2015		No Eq.				K-3	False SD
08.05.2015		No Eq.				K-4	False
09.05.2015		No Eq.				K-5	False
11.05.2015		No Eq.				K-8	False
12.05.2015	0705		27.70	086.00	7.3/10.0	K-9	True CD
	0734		27.60	086.20	5.4/15.0		
	0736		27.60	086.10	6.2/10.0		
15.05.2015	0506		27.80	084.70	5.0/10.0	K-10	O.D.
16.05.2015	1134		27.50	086.00	5.7/10.0	K-13	O.D.
20.05.2015		No Eq.				S-3	False SD
21.05.2015		No Eq.				S-4	False

Date	Time (UTC)	Place	Lat. (Deg.)	Long. (Deg.)	Magnitude (≥ 5.0)/ Depth (km)	Lunar Day	FCST
22.05.2015		No Eq.				S-5	False
26.05.2015		No Eq.				S-8	False
27.05.2015		FCST DIS					
16.09.2015	2254	Chile	31.57S	071.67W	8.3/22.4	S-3	Main EQ
	2318		31.56	071.42	7.0/28.4		
17.09.2015	0355		31.42	071.68	6.5/27.0	S-4	True SD
18.09.2015	0910		32.36	072.22	6.2/8.0	S-5	True
19.09.2015	1252		32.33	072.06	6.2/18.0	S-6	O.D.
20.09.2015	0902		30.23	072.27	5.1/8.6	S-7	O.D.
21.09.2015	1740		31.72	071.37	6.6/35.0	S-8	True
22.09.2015	0713		31.44	071.26	6.0/58.0	S-9	True, CD
23.09.2015	1132		31.61	071.95	5.0/10.0	S-10	O.D.
24.09.2015	1613		30.73	071.37	5.2/41.0	S-11	O.D.
26.09.2015	0221		30.81	071.32	6.3/46.0	S-13	O.D.
27.09.2015	2104		31.66	071.70	5.4/36.9	S-14	O.D.
01.10.2015		No Eq.				S-4	False
02.10.2015		No Eq.				S-5	False
03.10.2017	0626		30.30	071.55	5.9/38.0	K-6	O.D.
04.10.2015	0349		30.31	072.10	5.9/5.5	K-7	O.D.
05.10.2015	1633		30.30	071.53	5.9/34.0	K-8	True
		EQ considered up to 3 weeks					
08.09.2017	0449	Mexico	15.02N	93.89W	8.2/47.4	K-2	Main Eq. C.I.
	0501		15.17	094.29	5.7/36.3		
09.09.2017	0454		15.08	094.06	5.5/29.0	K-3	True
10.09.2017	0722		15.39	094.53	5.8/29.0	K-4	O.D.
11.09.2017	2109		14.90	094.01	5.5/27.0	K-5	O.D.
12.09.2017	0508		15.11	093.97	5.4/42.5	K-6	O.D.
13.09.2017	2130		15.61	095.17	5.1/13.3	K-7	O.D.
15.09.2017		No Eq. ≥ 5.0				K-10	False
16.09.2017	14.18		16.09	095.13	5.6/35.0	K-11	True
17.09.2017	0607		15.77	095.31	5.0/10.0	K-12	True
18.09.2017	1419		15.25	094.56	5.6/10.0	K-13	O.D.
19.09.2017	1814	Eq. observed 17 minutes early, prior to midnight (IST)	18.55	098.48	7.1/48.0	K-14	True, C.I. on 20.09.2017, after midnight of 19 th (IST)
21.09.2017		No Eq.				S-1	False
22.09.2017		No Eq.				S-2	False
23.09.2017	1253		16.62	95.07	6.1/10.0	S-3	True
24.09.2017	1006		15.31	094.17	5.8/47.4	S-4	O.D.
29.09.2017	0400		14.86	094.23	5.4/11.0	S-9	O.D.

Earthquake struck Samoa Islands on 29th September 2009 (S-11). It`s magnitude was 8.1 and focal-depth at 18 km (Table: 1). The earthquake occurred during high tide period, so aftershocks have been forecast for the lunar days: S-12 (two dates), K-1, K-2, K-3, K-10, K-11, K-12, S-1, S-2, S-3, S-10, S-11, S-12, K-1, K-2, K-3, K-10, K-11, K-12 (20 days) for one and half months period. Aftershock of highest magnitude occurred on 14th October (K-11: 6.3, maximum intensity) on the forecast day. The forecast has

been discontinued from 15th November 2009 as failure is getting prominent (aftershocks < 5.0). Earthquake of magnitude 8.8 originating from focal depth of 22 km struck Chile on 27th February 2010 (S-14). It struck during high tide period so aftershocks can be forecast during the following lunar days: K-1, K-2, K-3, K-10, K-11, K-12, S-1, S-2, S-3, S-10, S-11, S-12, K-1, K-2, K-3, K-10, K-11 and K-12. Aftershocks, which occurred on the O.D. having magnitude less than 5.5 have not been included in the

Table 1 to reduce the entries. Relatively high magnitude aftershocks occurred on 11th March (K-11: magnitude: 5.6/ 6.9/ 7.0) and on 16th March (S-1: 6.7), which were forecast days. So, aftershock of highest magnitude, 7.0, occurred on the forecast day. Aftershocks of magnitude ≥ 5.0 continued almost daily till 29th March and extended intermittently till the month of May. Aftershocks forecast have been discontinued after one and half months as more errors (intensity < 5.0) were observed during the last 16 days.

Earthquake of magnitude 9.0 devastated Japan on 11th March 2011 (S-6). It's focal-depth was 29 km. It occurred during low tide period. Aftershocks can be forecast for the lunar days S-8, S-9, K-3, K-4, K-5, K-8, K-9, S-3, S-4, S-5, S-8, S-9, K-3, K-4, K-5, K-8, K-9, S-3, S-4, S-5, S-8 and S-9 (22 days). Aftershocks having magnitude < 6.0 have not been considered in the Table 1, which occurred during non-forecasting days. Significant high magnitude aftershocks occurred correctly on 7th April 2010 (S-4: magnitude: 7.1), 11th April (S-8: magnitude 6.6) and 21st April (K-4: 6.2: ≥ 6.0 magnitude after a break of 7 days) on forecast days. The forecast has been discontinued after 12th May as errors (magnitude < 5.0) were noticed.

Earthquake of magnitude 8.6 a focal-depth of 20 km (0838 UTC) occurred in a vulnerable segment of Indonesia on 11th April 2012 (K-6). Major aftershocks having magnitude 8.2 originated from a depth of 25 km at 1043 UTC on the same day. Earthquake struck during low tide period. Aftershocks can be forecast for K-8, K-9, S-3, S-4, S-5, S-8, S-9, K-3, K-4 and K-5. Aftershock of highest magnitude of 6.2 occurred on 15th, on the day when both tides were observed as minimum on 10th lunar day of waning period (C.D., K-10). Significant aftershocks occurred on 24th (O.D. 5.9), 26th (S-5: magnitude 5.6), 29th (S-8: magnitude 5.7) and 30th (S-9: magnitude 5.7) April 2012. The forecast has been discontinued on 11 May as aftershocks of magnitude less than 5.0 have been observed frequently.

Earthquake of magnitude 7.9 and focal depth of 10 km struck Nepal on 25th April 2015 (S-7), during low tide period. Aftershocks can be forecast for S-8, S-9, K-3, K-4, K-5, K-8, K-9, S-3, S-4, S-5 and S-8 during one month period. A sequence of relatively moderate magnitude aftershocks occurred after a lapse of 14 days; out of them the 7.3 magnitude earthquake was correctly predicted to occur on 12th May 2015 (K-9; magnitude: 7.3). Couple of other aftershocks occurred with magnitudes of 5.4 and 6.2. More casualties occurred in Bihar on 12th May rather than on 25th April. As earthquake magnitude was 7.9, aftershocks having magnitude less than five were very much prominent. The forecast has been discontinued from 27th May 2015 as aftershocks after 16th May were observed frequently with less than 5.0 magnitudes.

Earthquake of magnitude 8.3 occurred in Chile on 16th September 2015 (S-3). On 13th both tides were observed

as maximum (C.I.). So, main earthquake occurred during low tide period. Aftershocks can be forecast for S-4, S-5, S-8, S-9, K-3, K-4, K-5, K-8 and K-9. Aftershock of highest magnitude (6.6) was recorded on 21st September (S-8). The forecast was continued for 21 days.

On 8th September 2017 (K-2) an earthquake of magnitude 8.2 struck Mexico. Both tides were observed as maximum on this day (K-2). So, main earthquake occurred during high tide period. Aftershocks can be forecast for K-3, K-10, K-11, K-12, S-1, S-2 and S-3. As both tides were observed as maximum (C.I.) on 20th September (K-15), this date was also included in the forecast. Aftershock of maximum magnitude (7.1) occurred on 19th September at 1814 UTC (20th date started after 16 minutes -IST). So, earthquake struck 17 minutes early of the predicted forecast period.

Highest magnitude aftershocks have been observed in 7 out of 8 cases during forecast period of major earthquakes from 2009 to 2017 (magnitude ≥ 7.9). It has been also observed that earthquakes having magnitude ≥ 8.0 have not occurred even once on 4th lunar day during either of the two fortnights in 42 cases from 1934, Bihar, India to 2017, Mexico (Table not given).

CONCLUSIONS

(i) Mostly both values of high tides start decreasing (S.D.) from 3rd or 4th or 5th day of waning and waxing period of the Moon and continue to decrease (C.D.) till 8th or 9th day of both the fortnights (minimum value). It is observed that mostly both the high tides start increasing (S.I.) from 10th or 11th, or 12th and continue to increase (C.I.) till 1st or 2nd or 3rd during waning and waxing period (maximum value).

(ii) Heights of Ocean tides will differ from Sea to Sea. In majority of cases all four trends (S.D., C.D., S.I. and C.I.) observed for Arabian Sea would be observed on the same lunar day for other Seas as spring and neap tides depend upon the position of the Moon. This is universally true as lunar day would remain same for all the countries. Solar-lunar eclipses are observed on a fixed date for all the countries.

(iii) In Hindu calendar, lunar day starts after Sunrise and continues till Sunrise, whereas English date starts after mid-night.

(iv) High or low ocean tides, initiated by earth tides, exhibit the intensity of solar-lunar gravitational force on a particular day. Moon's gravitational influence on Ocean tides (including spring and neap) is visible during its different phases.

(v) If an earthquake occurs during low tide period (after CI to 9th lunar day) aftershocks can be forecast for K-3, K-4, K-5, K-8, K-9, S-3, S-4, S-5, S-8 and S-9 during one month period. If CD is observed on 7th or 10th lunar day then this has to be included as an additional day. If it is observed between high tide period, aftershocks can be forecast for K-1,

K-2, K-3, K-10, K-11, K-12 and S-1, S-2, S-3, S-10, S-11, S-12 during one month period. If CI is observed on any other day this has to be included as an additional day.

(vi) Aftershocks (magnitude ≥ 5.0) can be forecast for earthquakes having magnitude ≥ 7.9 for 3 to 8 weeks.

(vii) Aftershocks of highest magnitude earthquakes have occurred as predicted in 7 cases out of 8 cases (87.5%) during forecast period. Lunar days are more marked for major aftershocks than timings of the high tides. Since one could argue that such a correlation is more an accident than a normal activity it is essential to look at various alternative theories, including the proposed in the present study.

(viii) As short term earthquake prediction is not yet achieved unequivocally, in spite of significant efforts by international seismological community, we do believe that the present study would help in introducing a significant input to achieve needed outcome in coordination with other inputs like Spatial and temporal variations of total electron content (TEC) and outgoing long wave radiation (OLR) during the period of greater earthquakes. Before, accepting the present theory as an important one it should be strongly backed up by physical models /processes (with clear quantification). Also in co-ordination with experts, as suggested by one of the learned reviewers some relevant statistical analysis or Wavelet power spectrum using Morlet wavelet analysis needs to be carried out as part of the extension study.

ACKNOWLEDGEMENTS

Authors are thankful to National Earthquake Information Center web site (USGS), USA, IMD web site for using earthquakes data, Survey of India for using their tides tables for the years 2009 to 2017 and PNP Maritime Services Private Limited, Mumbai for publication and providing these tide tables. The authors are thankful for access to "The Definitive Guide, Astronomy" and using the figure-1. They acknowledge with thanks Wikipedia, Google websites for using Figure 2. Authors express their sincere thanks to the reviewer, Dr. Vinayak Kolvankar for his critical comments and useful suggestions. Thanks are also due to Dr. Vineet K Gahalaut for suggesting further work using some important processing methodologies. Authors thank Dr. P.R.Reddy, Chief Editor for proper guidance, suggestions, refined restructuring of the manuscript and apt final editing.

"The great earthquake shall be in the month of May; Saturn, Capricorn, Jupiter, Mercury in Taurus; Venus, also Cancer, Mars in zero."

Nostradamus

Compliance with Ethical Standards

The authors declare that they have no conflict of interest and adhere to copyright norms.

REFERENCES

- Bhattacharya, S.N., 1998. "A perspective of historical earthquakes in India and its neighbourhood up to 1900", *Mausam*, v.49, no.3, p: 375.
- Fredrick, W.L., and Baker, H.R., 1976. "Motion of the Moon", *Astronomy*, p: 124.
- Google search earthquake, (<http://www.contentwriter.in/articles/others/earthquake.htm>)
- Ide, S., Yabe, S., and Tanaka, Y., 2016. *Nature Geoscience*. doi:10.1038/ngeo2796.
- Juan, Z., Yanben, H., and Zhien, Li., 2000. "Variation of lunar-solar tidal force and earthquakes in Taiwan, Islands of China" *Earth, Moon, and planets*, Springer Netherlands, v.83, pp: 123-129.
- Kolvankar, G., Vinayak, Deshpande, S., Shashank, Manjre, S., Abhijeet, Pansare Sandesh, More, Samrudha and Thakur Nisha, 2010. "Lunar periodicities and earthquakes", *New concepts in global tectonics*, News letter, no.56, p: 48.
- Kolvankar, G., Vinayak, More, Samrudha, and Thakur, Nisha, 2010. "Earth tides and earthquakes", *New Concepts in Global Tectonics News letter No. 57*, December 2010, pp: 54-55.
- Kolvankar, G., Vinayak, 2011. "Sun, Moon and Earthquakes", *New Concepts in Global Tectonics*, no.60, September 2011, pp: 50-65.
- Kumar, Vinod, Hosalikar, K.S., Rajeev, V.K., Kamble, D.S., Pareekh, N.I., and Khanun, N., 2013. "Killer tornadoes during High tide period", *Mausam*, v.64, no.2, p: 384.
- National Geographic News, 2005. (https://news.nationalgeographic.com/news/2005/05/0523_050523_moonquake_2.html).
- Proceedings of the National Academy of Sciences, 2016, (<https://www.sciencealert.com/the-pull-of-the-sun-and-moon-can-cause-earthquakes-along-the-san-andreas-fault-study-finds>).
- Saraswati, Paramhansh, Swami Jagdishwaranand, 2010. *Rigvedbhashyama*, Part II, v.7-59, no.4, pp: 1034-1035.
- Tanaka, Sachiko, 2010. *Geophysics, Res. Lett.*, doi: 10.1029/2009G1041581 Venkatanathan, N., Rajeshwara Rao, N., Sharma, K. K. and Periakali, P., 2005. "Planetary configuration: Implications for earthquake prediction and occurrence in Southern Peninsular India" *J. Indian Geophysical Union*, v.9, no.4, pp: 267-276.

Received on: 18.11.2017, Revised on: 1.12.17; Re revised on: 10.12.17; Accepted on: 12.12.17

Hydrogeological and Geophysical Characteristics of Northern Parts of Eastern Ghat Khondalitic Aquifers

B.Venkateswara Rao

Professor, Centre for Water Resources, IST, JNT University Hyderabad
Email: cwr_jntu@yahoo.com

ABSTRACT

In this study various concepts pertaining to khondalitic (Garneti Ferrous Sillimanite gneiss) aquifers and their kaolinisation in the Vijayanagaram district of Andhra Pradesh, India is attempted. The hydrogeological and geophysical studies on these aquifers inferred that the khondalites in this region are sedimentary in origin but later metamorphosed and became hard rocks. These rocks were subjected to intense weathering, faulting, fracturing and folding giving way to accumulation of ground water in two different layers mainly in weathered layer and fractured layer with hydraulic continuity among them. Beneath the streams and low-lying areas most of the khondalite became kaolinised and turned out to be low ground water potential zones. This kaolin, which is essentially clay, is acting as a barrier for the ground water movement towards the stream and forcing it to accumulate in the upland areas between the streams and naturally became groundwater potential zones whenever the formation is fractured and intruded with quartz veins. Lack of resistivity contrast between highly weathered khondalite and fractured khondalite has been noticed in the Vertical Electrical Sounding data at few places. This called for Two-Dimensional (2D) and Three-Dimensional (3D) resistivity imaging surveys to delineate the kaolinised zones to avoid well failures. The extended deeper kaolinisation of the aquifer is responsible for failure of wells in this terrain. At failed wells, kaolinisation is not only deeper but also followed by the basement characteristics either with very thin or no aquifer layer immediately below the kaolinised layer. At successful wells not only kaolinised layer is thinner but also aquifers are thicker resulting in presence of basement characteristics only at deeper depths. Layers having resistivities between 25 - 65 Ohm-m are identified as aquifer layers, which are composed of moderately weathered and fractured khondalitic suite of rocks. Layers with resistivities greater than 65 Ohm-m are interpreted as granite gneissic basement, while the layers with resistivities less than 25 Ohm - m are interpreted as kaolinised layer. The quality of the ground water in this region is generally good and suitable for both drinking and irrigation purposes except at few pockets where Fluoride and Nitrate is present in excess of permissible limits. Similarly, in downstream areas of major streams high salinity is present.

Key words: Khondalite, Aquifer, Kaolinisation, Resistivity, Groundwater potential

INTRODUCTION

Khondalitic suite (garneti ferrous sillimanite gneiss) of hard rocks occurring in Eastern Ghats of India (Figure 1) constitutes nearly one-eighth of the hard rock areas of the country. The Khondalites are named after 'Khonds', the tribesmen living in the mountain jungles of Eastern Ghats (Walker, 1902). Khondalites forming the lower Precambrian group are extensive in the districts of Srikakulam, Vizianagaram, Visakhapatnam and in the upland areas of East Godavari, West Godavari and Krishna districts of Andhra Pradesh, India.

The hydrogeological properties of Khondalitic aquifers in northern parts of Eastern Ghats of Andhra Pradesh are to an extent different from those present in southern parts. For instance the soil and weathered thickness is much higher in the southern parts (about 20m to 30m) compared to the northern parts (about 10 m to 20 m). Similarly, ground water availability in fractured rock of Khondalite is at 50 m in southern parts compared to 30 m in the northern parts. In this region assured surface water supplies are minimal.

The limited surface water facilities are getting depleted slowly as 1/5th out of the average annual rainfall of around 1000 mm goes as recharge to ground water. Since there is no assured surface water supplies, majority of the farmers solely depend on ground water for drinking and irrigation purposes. Since dependence on ground water is increasing systematic ground water exploration and exploitation studies and planned groundwater development have become essential in the region. As a part of such an organized ground water development initiative, natural recharge and modeling studies have been carried out by researchers. Many modeling studies have indicated presence of the natural recharge of 14% to 18% of rainfall in Khondalitic terrain. Since the natural recharge of ground water is not encouraging organized ground water development assumes greater significance in the region, by identifying not only shallower but deeper aquifers. In the present paper, the views of various researches on khondalitic aquifers situated around Vizianagaram and Visakhapatnam are presented in the form a review, covering more than hundred years of research work.

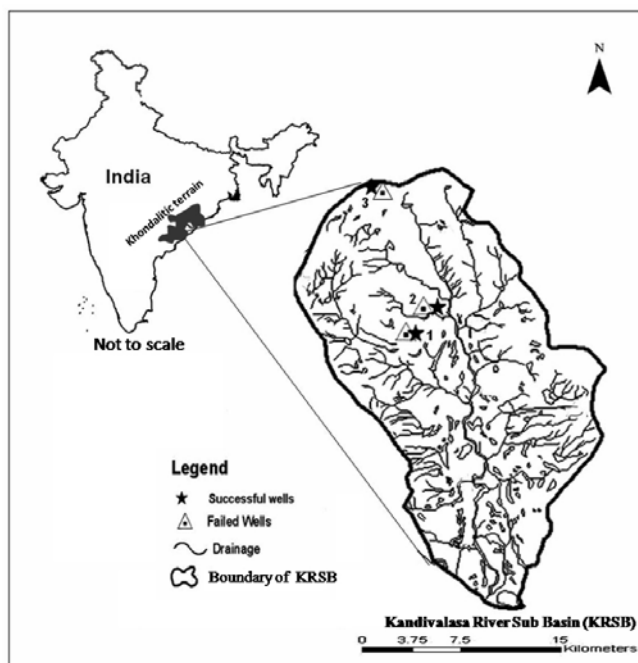


Figure 1. Location map of the study area.

Geology and Tectonics

In view of the presence of Manganese and bauxite ores in the region, most of the early researchers evinced interest on petrological and mineralogical aspects but not on the hydrogeological aspects. Some of the opinions of early workers on the origin of the khondalitic formation are presented here.

Fermor (1909) was probably the first scientist to make an observation that the manganese ores in this area owed their origin to the alteration and concentration of manganese rich igneous rocks. Cross (1914) questioned the validity of the igneous nature of the local rock type and instead suggested a hybrid origin for them. Subsequent works by Fermor (1915) and Prabhakara Rao (1950) have shown that the rocks were indeed hybrid and the manganese ore was sedimentary in origin. Krishna Rao (1952) confirmed the sedimentary origin of khondalites. He stated that they were paragneisses representing metamorphism of original arenaceous, argillaceous and calcareous sediments, the arenaceous constituents giving rise to quartzites, the argillaceous matter to quartz-garnet-sillimanite gneiss and the calcareous sediments to calc granulites. Krishnan (1968) opined that the rocks of Eastern Ghats are the result of high-grade metamorphism of sedimentary rocks.

Later investigations have revealed that the rocks are products of re-crystallisation of a complex series of sediments (Dey, 1968). The typical khondalite is a rock constituting of silimanites, garnets, feldspar and quartz.

The idea that khondalites have been derived from high alumina clays that are fairly high in iron is confirmed by the existence of bauxite and iron deposits (Sarma, 1982). The main khondalitic rocks are associated with charnockites, which is a bluish grey granular granitic rock named after Job Charnock. His tomb was constructed by this rock. These rocks are observed to have an intrusive character in the khondalitic country (Sarma, 1982).

Geological investigations carried out by Rao (1964) and Sriramdas and Rao (1979) have indicated the existence of faulting, folding, cross-folding and domal structures in the region. Narayanaswamy (1975) has explained the structure and tectonics of Eastern Ghats. According to him khondalites and leptinites (garnetiferous quartzofelspathic gneiss) belong to the khondalitic suite of rocks in Eastern Ghats. The charnockitic suite is the basal zone overlain by khondalitic suite. He further pointed out that Eastern Ghats have undergone at least two periods of deformations marked by intense folding, shearing and faulting of khondalites. Kanungo and Murthy (1981) have presented the structural features of khondalites and associated rocks and established a structural superposition of various rock types present, namely, charnockitic gneisses, quartzites, khondalites, calc granulites, granites and granitic veins in that order. Chetty et al., (2002) have studied the shear zones and lineaments in the Eastern Ghat Mobile Belt (EGMB) and found that the lineament patterns are distinct in the contrasting geologic terrains. The presence of shear zone network is strikingly restricted to the EGMB.

Hydrogeology

Probably Mahadevan (1929) was the first scientist to postulate a hydrogeological concept of this region and has pointed out that due to the action of water the khondalites are altered in to two different forms. On the surface the rock changes into a lateritic soil and the subsurface formation when acted upon by water alters itself into kaolin. Sarma (1967) has conceived a four layer system in the khondalitic terrain i.e., the top soil zone underlain by talus zone in foot hill areas, which in turn is underlain by weathered kaolinised portion that merges into a fractured and fissured zone and followed further by basement material. He has further observed that ground water occurs in weathered kaolinised zone and in the fractured and fissured zone. Where the weathered and kaolinised zone consists of sandy clay with sufficiently large permeability, the water table continues into the fractured and fissured zone. But at places where the weathered zone is completely kaolinised and clayey in nature, any well located in it shows water at the bottom of this layer, when it touches the fractured zone the water table eventually rises to some extent offering semi-confined conditions. Venkateswara Rao (1994) also found that weathered and fractured zones have hydraulic continuity. This is proved by the fact that whenever the bore well was drilled near by the open well, the open well yield is considerably reduced and even became dry. Nooka Raju and Jaganmohan Rao (1990) have confirmed the earlier findings that the area is occupied by khondalites intruded by charnockites and quartz veins. The khondalites show a general strike direction of NE-SW and the foliation dips vary from 45° to 75° due SE. Their investigation has revealed that the discharges are higher in khondalites intercalated with quartz veins and fractured quartz feldspathic gneisses, than in feldspathic gneisses and weathered khondalitic suite of rocks.

Later investigation carried out by Venkateswara Rao and Briz-Kishore (1990) in Cheepurupally region of vizianagaram district has shown that flat upland areas are yielding better than low lying areas near the streams. It is found subsequently by Venkateswara Rao (1998b) that at low lying areas, i.e., beneath the streams the khondalite must have transformed itself into kaolin and having more thickness than in the flat uplands. In fact the kaolinisation process is observed from low lands to high lands at a depth of 10 m to 20 m and its thickness is varying from 20 m to 10 m, respectively. This kaolin is acting as a barrier evidently preventing lateral movement of ground water towards the stream. At many places in the khondalitic terrain the kaolinised layer is acting as an aquitard or semi-confining stratum atop the main aquifer of fractured khondalite. The aquitard's contributions to the total well yield in many cases is substantial, a point that underscores the need to seek ways and means of tapping it.

(Venkateswara Rao and Ramadurgaiah, 1996). However, if the kaolinisation is too strong and extends to greater depths of more than 20 m., the yields of the wells are low leading to well failures (Venkateswara Rao et al., 2013). Another important observation is that many successful wells are located in areas of considerable quartzisation hinting at the possibility that the appearance of a quartz vein or quartz pebbles on the ground surface probably related to ground water occurrence (Venkateswara Rao, 1994). Central Ground Water Board (CGWB) investigations have revealed that the depth of weathering ranges from 10 m to as high as 40 m. Higher degree of weathering in Khondalites results in the formation of kaolinite, causing less porosity and permeability (Sudarshan and Rao, 2004).

Hydrogeomorphology

Aerial photo studies by Prudhvi Raju and Vaidhyathan (1981) particularly applicable to khondalitic terrain has shown the existence of fractured zones. Raghavaswamy (1981) described the landforms, land systems and geographical synthesis of the area. According to Sarma (1982), Eastern Ghats have well-developed basins and sub-basins in their watersheds and act as independent ground water basins. This character is responsible for ground water to be available at all levels throughout the Eastern Ghat ranges in spite of their steeply sloping nature. The slopes of the hills vary from 1 in 85 to about 1 in 400. Ramana (1980) has undertaken morphometric analysis of the five river basins in the area, namely, Sarada, Narova, Peddagadda, Gostani and Champavati. The dominating pattern of the tributaries is dendritic. Miller and Miller (1961) have pointed out that homogeneity of formations has given rise to dendritic drainage. The dominance of khondalitic formation in the area has clearly indicated the above point.

The hydrogeomorphological investigations in Kandivalasa River Sub-Basin (KRSB) of Vizianagaram district (Figure 1) by Venkateswara Rao (1998b) revealed that lineaments are fault zones along which stream courses were developed. Ground water potential areas are located on shallow buried pediplains and wash plains in such a way that they are located on gently sloping uplands situated between the lineaments. Non potential areas are those, which are low-lying areas, near the streams and high slope areas near the hillocks.

Geohydrology

The seasonal fluctuation of water table was observed by Subba Rao (1974), Prasad (1980), Narayanaswamy (1980) and Ramana (1980) in different parts of Eastern Ghats. On the average the maximum fluctuation seems to be 3 m. The water table rise is observed to be linearly related to the

amount of rainfall. About a third of the rainfall percolates through the soil surface to recharge the ground water (Sarma, 1982). The average non-capillary porosity of the surface layer is 33%. The water level fluctuations are found to follow the physiography. It is observed that an increase in terrain elevation by one metre results in a fluctuation of 0.5 metre in the ground water level Sarma et.al. (1983). Subba Rao and Krishna Rao (1984) have noted that bore-wells tap ground water in the aquifer while dug wells penetrate only the overlying aquitard. CGWB investigations have revealed that dug wells in these rocks have yields varying from 40 to 12 m³/day in winter months to 10 to 30 m³/day in summer months (Sudarshan and Rao, 2004). The bore well yields in the KRSB is varying from as low as 0.5 m³/hour to high as 27 m³/hour (Venkateswara Rao, 1994).

Venkateswara Rao (2003) has observed the pre monsoon and post monsoon water levels in KRSB of Vizianagaram district and found that ground water potential areas have less fluctuations of water levels than in non-potential areas. This point can be used as a good ground water prospection tool. The groundwater fluctuation studies by Siva Prasad (2017) have indicated that there is 10 m depletion of groundwater levels in the KRSB basin between the years 1993 to 2014. Siva Prasad and Venkateswara Rao (2015) have estimated Transmissivity (T) and Storage Coefficient (S) values of KRSB and found that T values are varying between a minimum of 37.2 m²/day to a maximum of 304.3 m²/day, while S values are varying between a minimum of 2.91x10⁻⁴ to a maximum of 91.5x10⁻⁴. They have also observed that T and S values are minimum at the main stream of the basin where aquifers have been kaolinized to maximum extent. The T and S values are maximum at flat uplands where the aquifers are subjected to minimum kaolinisation. Siva Prasad (2017) has estimated the groundwater recharge in the KRSB and found that about 12 per cent of the total rainfall in the basin goes as groundwater recharge. Groundwater flow model of this basin has indicated that hydraulic conductivity of the weathered layer is varying from 1.6 - 1.9 m/day while that of the fractured layer below it is varying from 1.6 to 2.3 m/day. Groundwater flow modeling studies by Radhika et al., (2000) in Mallavaram basin of East Godavari district covered by khondalitic terrain have shown that the average ground water recharge is of the order of 16% of the total rainfall. Well logging investigations by Venkateswara Rao et al., (2017) have revealed that the aquifer porosity is of the order of 28% in the KRSB. According to the CGWB (2013) report, the stage of development of groundwater for the three mandals of the study area namely Cheepurupalli and Garividi in the Vizianagaram district is nearly 70% which is higher in the Vizianagaram district. The modeling studies in the KRSB by Siva Prasad (2017) have indicated that there is a 100% development of groundwater in the basin and if the present withdrawal continuous, there will

be development of dewatering of aquifers in certain pockets in the next few years. Modelling studies indicated that at least 50% of the groundwater usage has to be curtailed by adopting micro irrigation techniques.

Hydrogeophysical Studies

Sarma (1961) has published the results of the resistivity survey conducted in the neighbourhood of Gostani River. His studies of resistivities of core samples from a bore hole indicated that the resistivities obtained from the surveys served to obtain clearly the resistivity contrasts among different formations though actual correspondence in magnitude was not obtained. Bhaskara Rao and Sarma (1962) have reported the results of geophysical survey carried out near Visakhapatnam Oil Refinery. They observed that the topsoil has resistivity of 200 ohm-m to 500 ohm-m, water saturated rock has 200 ohm-m to 250 ohm-m and unsaturated rock over 500 ohm-m. Sarma (1977) delineated four distinct sub-surface horizons having resistivity ranges of 100 to 160 ohm-m, 12.8 to 68 ohm-m, 360 to 680 ohm-m and 1100 ohm-m, representing the top soil zone, weathered kaolinised khondalite, fissured and fractured zone and hard rock, respectively. The narrow strip of coastal zone between the northern part of Eastern Ghat ranges and Bay of Bengal is also found to be a good source of ground water (Sarma, 1965). Extensive geoelectrical surveys carried out in this area have indicated the possibility of obtaining fresh water at depths extending to 35 m (Prasad, 1980).

Venkateswara Rao and Briz-Kishore (1991) noticed that for a good yield, the thickness of the weathered and fractured layers must not be too high. In fact the higher the weathered depth, the more will the well be susceptible for failure. Further investigations by Venkateswara Rao (1998c) in the KRSB of Vizianagaram district have revealed that there are four distinct subsurface layers: (i) top soil zone with an average thickness of 3 m, (ii) highly weathered khondalite (kaolinised layer) with an average thickness of 16 m, (iii) moderately weathered and fractured khondalite, which is the principal aquifer layer with an average thickness of 20 m and (iv) basement of granite gneiss (Figure 2). Interpretation of geoelectrical data fails to reveal a sharp contrast between the second and third layer at many places as shown in Figure 2. First layer resistivities in the range of 150 ohm-m and more are associated with the occurrence of quartz vein on the ground surface and quartzisation in sub-surface layers leading to good yields from bore wells. The optimum range of resistivity of potential aquifer layer is 25-65 ohm-m. Lower ranges of resistivity are indicative of increasing degree of kaolinisation and higher than 65 ohm-m range represents increasing degree of basement characteristics. There are two ranges of optimum depth to the electrical basement, one is at the 20-30 m range and other is at the 40-45 m range. Depth smaller than 20

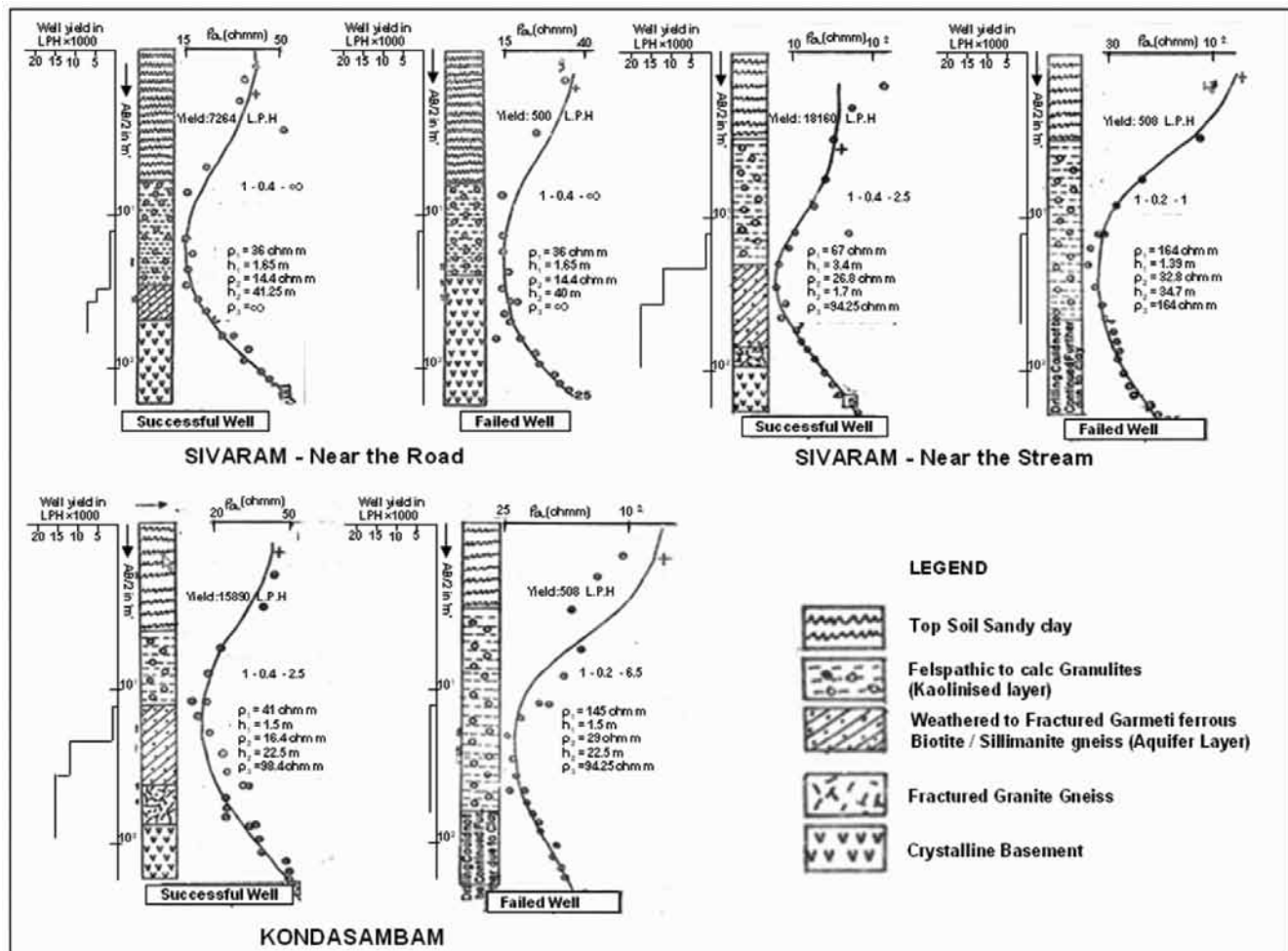


Figure 2. Vertical Electrical Sounding curves, Yield logs and Lithologies of adjacent success and failed wells in KRSB (Venkateswara Rao et al., 2013).

m are inadequate to hold a reasonable quantity of ground water and if the depth is more than 45 m there is likely hood of a deeper and more intensively weathered kaolinised layer to occur in the system. Venkateswara Rao (2002) has further analysed the resistivity data of the KRSB basin with the multivariate statistical analysis. It is inferred that high yielding wells are characterized by an average value of transverse resistance of 1227 ohm-m² and an average value of aquifer resistance of 1093 ohm-m² with the aquifer resistivity ranging between 23-43 ohm-m and its thickness varying in the range of 27- 48m.

Venkateswara Rao et al., (2011) have conducted multi-geophysical techniques at successful and failed wells of KRSB (Figure 1). They found that to produce a good well yield, fracture system must be extended in all the four directions, which is identified with high values of coefficient of anisotropy while the unidirectional fracture system may not produce good well yield, which is identified with less value of coefficient of anisotropy. Shallow seismic refraction method and very low frequency electromagnetic

method could not be of much help to find the fracture zones. Venkateswara Rao et al., (2013) and Venkateswara Rao and Siva Prasad (2015) have conducted 2D and 3D resistivity imaging at successful and failed wells (Figure 1) in the KRSB and found that at failed wells, kaolinization is not only thicker (> 20 m.) but also followed by the basement characteristics either with thin or no aquifer layer immediately below the kaolinised layer. At successful wells, not only the kaolinised layer is thinner (<20 m.) but also aquifers are thicker (> 20 m.). Siva Prasad (2017) has found that kaolinized layers are having low chargeability compared to the other fractured khondalitic formations.

Hydrogeochemistry

Sarma, (1982) has observed that in the Eastern Ghat basins a regular increase in the total dissolved salt content increased with a decrease in elevation. It is also observed that a few pockets of high conductivity zones exist in the area. The highly conductive zones are associated with

areas of the lowest elevation, where, due to absence of movement of ground water, maximum Base Exchange process takes place. Water quality maps of Visakhapatnam basin have been prepared by Sarma et al., (1980) with the help of Piper classification. They observed a general predominance of secondary alkalinity and neutral water with secondary salinity and high dissolved salt content in low elevation areas.

Sarma and Narayana Swamy (1986) have given a hydrogeochemical approach to the interpretation of ground water movement in the unconfined condition of the region. They observed that in general, as the topography sloped down along the hill ranges to the plains, the sequence of bicarbonate-chloride water is followed by chloride-bicarbonate water, again followed by chloride-sulphate water confirming the fact that in general ground water movement follows topography. Subba rao and Krishna Rao (1991) have concluded that in Visakhapatnam basin, wells are undesirable at topographic lows (below 15 m contour line) and desirable at topographic highs (above 15 m contour line) as the former contain water with heavy concentrations of total dissolved solids, total hardness, bicarbonates, chlorides and sulphates associated with corrosion and incrustation of wells, while the latter is free from them.

Hydrogeochemical investigations in the Kandivalasa River Sub Basin by Venkateswara Rao (1998a) have revealed that upland areas of this basin are having neutral quality of water while in the lowland areas, the water is having secondary alkalinity in upstream portion and primary salinity in down stream portion. Studies on Total Dissolved Salts (TDS) and topography across the main stream have shown that the TDS follows the topography i.e., at the flanks the TDS is more and gradually decreases towards the main stream. This may be due to the fact that more salts must have been dissolved in the ground water while it is percolating down greater over burden thickness in reaching water table at the flanks of the basin than that at the main stream where there is less over burden thickness. Along the main stream TDS has gradually increased towards the downstream, a fact that confirms the general belief of identity in the movement of surface and sub surface waters. However, Fluoride is a recent observation by Siva Prasad (2017) who has reported more than 1.5 ppm in some parts of the KRSB. Similarly, he has also observed that Nitrate is another important chemical constituent in groundwater and found to be exceeding the permissible limit of groundwater in more than 50 per cent of the samples collected from KRSB, due to use of more fertilizers in the basin. CGWB has noticed the nitrate values more than 100 mg/L at Vijayanagaram, Cheepurupalli, Payakapadu, Gharbam and Kanimetta stations in the Vizianagaram district. Chemical pollution by way of applying nitrogenous fertilizers in the agriculture sector is the root cause of high nitrate content in the groundwater (CGWB, 2013).

CONCLUSIONS

Northern parts of Eastern Ghat Khondalites are sedimentary in origin but later metamorphosed and became hard rocks. The basement is granitic gneiss. In general charnokites and quartzites have intrusive character in khondalites. These rocks were subjected to intense weathering, faulting, fracturing and folding giving way to accumulation of ground water in two layers mainly in weathered layer and fractured layer with hydraulic continuity among them. Streams followed the fault zones and fractured zones giving rise to dendritic pattern of drainage owing to the homogeneity of khondalitic formation. Beneath the streams and low-lying areas most of the khondalitic formations became kaolonised and turned out to be low potential zones suitable only for open wells. This kaolin, which is essentially clay is acting as a barrier for the ground water movement towards the stream and forcing it to accumulate in the upland areas between the streams and naturally became groundwater potential zones for high yielding borewells whenever the formation is fractured and intruded with quartz veins. Lack of resistivity contrast between highly weathered khondalite and fractured khondalite with Vertical Electrical Sounding data at few places calls for applying 2D and 3D Resistivity Imaging where in more data points and their inversion are revealing the kaolinisation phenomena in the subsurface to avoid well failures. The extended deeper kaolinisation of the aquifer is responsible for failure of wells in this terrain. At failed wells, kaolinisation is not only deeper but also followed by the basement characteristics either with very thin or no aquifer layer immediately below the kaolinised layer. At successful wells not only kaolinised layer is thinner but also aquifers are thicker and basement characteristics are found only at deeper depths. Layers having resistivities between 25-65 Ohm-m are identified as aquifer layers, which are composed of moderately weathered and fractured khondalitic suite of rocks. Layers with resistivities greater than 65 Ohm-m are interpreted to have basement characteristics belonging to the granite gneiss, while the layers with resistivities less than 25 Ohm-m are interpreted as kaolinised. Transmissivity values are varying between a minimum of 37.2 m²/day to a maximum of 304.3 m²/day, while Storage coefficient values are varying between a minimum of 2.91×10^{-4} to a maximum of 91.5×10^{-4} . Groundwater flow model of KRSB basin has indicated that hydraulic conductivity of the weathered layer is varying from 1.6 - 1.9 m/day, while that of the fractured layer below it is varying from 1.6 to 2.3 m/day. The aquifer porosity is of the order of 28% in the KRSB. The quality of the ground water in this region is generally good and suitable for both drinking and irrigation purposes except at few pockets where Fluoride and Nitrate is present in excess of permissible limits. Similarly, in downstream areas of major streams, high salinity is present.

Hydrogeological and Geophysical Characteristics of Northern Parts of Eastern Ghat Khondalitic Aquifers

In view of the increased abstraction of the groundwater, there will be development of dewatering of aquifers in certain pockets in the next few years. Modelling studies have indicated that at least 50% of the groundwater usage has to be curtailed by adopting micro irrigation techniques in the agriculture, enhancing of surface water storage by rainwater harvesting and increasing the groundwater recharge with flood waters.

ACKNOWLEDGEMENTS

Thanks are due to Dr.P.R.Reddy, Chief Editor for his continued support, objective evaluation of the manuscript and apt editing.

Compliance with Ethical Standards:

The author declares that he has no conflict of interest and adheres to copyright norms.

REFERENCES

- Bhaskara Rao, V., and Sarma, V.V.J., 1962. A Case History of Geophysical Prospecting for Water in Visakhapatnam Area, Bulletin of the National Institute of Science, India, no.22, pp: 102-114.
- CGWB (Central Ground Water Board), (2013) Ground Water Yearbook.
- Chetty, T.R.K., Vijay, P., Vijaya kumar, T. and Suresh, B.V.V., 2002. GIS and the Tectonics of the Eastern Ghats, India, GIS Development, v.6, no.12, pp: 21-24.
- Cross Whitman, 1914. The position of the Kodurites in Quantitative Classification, Journal of Geology, v.22, pp: 791-806.
- Dey, A.K., 1968. Geology of India, National Book Trust, New Delhi, India, pp: 178.
- Fermor, L.L., 1909. Manganese Ore Deposits of India, Mem. of G.S.I., v.37, and Rec.35, pp: 1046-1115.
- Fermor, L.L., 1915. Rec. Geological Survey of India, v.XLV, pp: 102.
- Kanungo, D.N. and Murthy, D.S.N., 1981. Structural Features of Khondalites and Associated Rocks Between Vizianagaram-Garividi in Eastern Ghats Belt of India, Geophysical Research Bulletin, v.19, no.1, pp: 35-50.
- Krishnan, M.S., 1968. Geology of India and Burma, Higgin Bothams (P), Madras, India, p: 555
- Krishna Rao, J.S.R., 1952. The Geology of Chipurupalle Area, Visakhapatnam District with Special Reference to the Origin of Manganese Ores, Geological Society of India, v. XXVI, no.1, pp: 36-45.
- Mahadevan, C., 1929. Geology of Vizag Harbour Area, Quar. Jour. Geol.Min. Metal. Soc. India, v.2, no.4.
- Miller C.V., and Miller, C.F., 1961. Photogeology, Mc Graw Hill Book Co., New York, pp: 215.
- Narayanaswamy, A., 1980. Geohydrology of Visakhapatnam Basin, Ph.D. Thesis, Andhra University, India. pp: 192.
- Narayanaswamy, S., 1975. Proposal for Charnockite Khondalite System in the Archean Shield of Peninsular India, In: Precambrian Geology of Peninsular Shield, Geological Survey of India, Miscellaneous Publications, no.23, Part.1, pp: 1-16.
- Nooka Raju, D., and Jaganmohan Rao, D., 1990. Augmentation of Ground Water Yield Through in Well Bores in Hard Rock Terrain in Vizianagaram district – An Appraisal, Procs. Of the Seminar on Ground water Resources Development and Management in Andhra Pradesh S.G.W.D., A.P, pp: 173-174.
- Prabhakar Rao, G., 1950. The Geology of Manganese bearing rocks of Garividi and Garbham, Visakhapatnam District, Quart. Jour. eol.Min.Met.Soc. of India, v.22, no.2, pp: 25-42.
- Prasad, N.V.B.S.S., 1980. Geohydrological and Geophysical Investigations along Visakhapatnam-Bhimilipatnam Coast, Ph.D. Thesis, Andhra University, India, pp: 250.
- Prudhvi Raju, K.N., and Vaidhyanadhan, R., 1981. Fracture Pattern Study from Landsat Imagery and Aerial Photos of a part of the Eastern Ghats in Indian Peninsula, Journal Of The Journal of Geol.Soc. of India, v.22, no.1, pp: 17-21.
- Radhika, K., Venkateswara Rao, B., Gurunadharao, V.V.S., and Dhar, R.L., 2000. Coupled Recharge and Groundwater Flow Model in Mallavaram Watershed in East Godavari District, A.P, Procs. Of the National Seminar on Geophysical Exploration Retrospect and Prospect conducted by Department of Geophysics, Andhra University at Visakhapatnam, pp: 57.
- Raghavaswamy, V., 1981. Landforms and Systems and Geographical Synthesis of Visakhapatnam Tract in the East Coast Plain of India, Ph.D Thesis, Andhra University, India. pp: 285.
- Ramana T.V., 1980. Geohydrological Characteristics of the Ground Water Basins of Khondalitic terrain of Eastern Ghats, Ph.D. thesis, Andhra University, India. pp: 201.
- Rao, G.V., 1964. Structural Control and Origin of the Manganese Ore Deposits in Visakhapatnam Manganese Belt, Andhra Pradesh, International Geological Congress, Part V, pp: 215-227.
- Sarma, V.V.J., 1961. Resistivity Investigations along Gostani River, Bulletin of the National Institute of Science, India, no.22, pp: 77-93.
- Sarma, V.V.J., 1965. Preliminary Investigations on the Occurrence of Fresh Water Wells along Visakhapatnam Beach, Andhra Pradesh, India, Jourl. Ind. Geophy. Uni., v.2, no.4., pp: 197-207.
- Sarma, V.V.J., 1967. Hydrogeology of Visakhapatnam Region of Eastern Ghats, Jour. Ind.Geophy Union, v.4, no.2, pp: 422-431.
- Sarma, V.V.J., 1977. A Case History of the Application of the Geoelectrical Sections of Khondalitic Zones of Eastern Ghats, Geophysical case Histories of India, AEG, Hyderabad, India, v.1, pp: 211-118.
- Sarma, V.V.J., 1982. Ground Water Resources of Northern Eastern Ghats, Procs. Of the Seminar on resources Development and Environment in the Eastern Ghats, Visakhapatnam, pp: 69-75.

- Sarma, V.V.J., and Narayanaswamy, A., 1986. Regional Ground Water Flow Investigations in Visakhapatnam Basin, Andhra Pradesh, *Journal of Geological Society of India*, v.27, pp: 386-391.
- Sarma, V.V.J., Prasad, N.V.B.S.S and Rajendra Prasad, P., 1983. A study of Water Level Fluctuations and Estimation of Recharge and Recession along the Coastal Strip of Visakhapatnam-Bhimilipatnam, *Journal of Association of Exploration Geophysicists*, v.4, pp: 49-65.
- Sarma, V.V.J., Ramana, T.V. and Narayanaswamy, A., 1980. Water Table and Water Quality Studies in Visakhapatnam, *Jour. Of the Institution of Engineers (India)*, v.60, pp: 312-316.
- Siva Prasad, Y., 2017. Geohydrological and Groundwater Modelling Studies of a Khondalitic Aquifer, a Ph.D. thesis, Submitted to JNT University Hyderabad.
- Siva Prasad, Y., Venkateswara Rao, B., 2015. Geohydrological Investigations of a Typical Khondalitic Terrain of Vizianagaram District of Andhra Pradesh, India, *Proceedings of the 32nd & 33rd AHI Annual convention and National Seminar on "Water Resources"*
- Sriramdas, A., and Rao, A.T., 1979. Charnockites of Visakhapatnam A.P., *Jour. Of. Geol. Soc. Of India*, v.20, pp: 512-517.
- Subba Rao, C., 1974. Studies on Some Aspects of Hydrogeology of Chandrampalem Basin, Ph.D. Thesis, Andhra University, India, pp: 220.
- Subba Rao, N. and Krishna Rao, G., 1984. Dug Wells and Bore Wells in Hard Rock Aquifers of Visakhapatnam District, Andhra Pradesh – A Comparative Study, *Journal of Association of Exploration Geophysicists*, v.4, no.4, pp: 11- 18.
- Subba Rao, N., and Krishna Rao, G., 1991. Ground Water Chemistry for Location of Wells in Visakhapatnam area, Andhra Pradesh, *Bhujal News*, v.10, pp: 7-10.
- Sudarshan, G., Rao, P.N., 2004. Ground Water in Andhra Pradesh, unpublished report, CGWB.
- Venkateswara Rao, B., and Briz-Kishore, B.H., 1990. Influence of topography over the Yields of Bore Wells in a Typical Khondalitic Formation, *Procs. Of the Seminar on Ground Water Resources Development and Management in Andhra Pradesh*, Hyderabad, India, pp: 43-50.
- Venkateswara Rao, B., and Briz-Kishore, B.H., 1991. A Methodology for Locating Potential Aquifers in a Typical Semi-Arid Region in India Using resistivity and Hydrogeologic Parameters, *Geoexploration*, v.27, pp: 55-64.
- Venkateswara Rao, B., and Ramadurgaiah, D., 1996. Comparative Analysis of Geoelectric and Lithologic Data in a Typical Khondalitic Terrain, *Procs. of the 2nd International Seminar and Exhibition on Geophysics Beyond 2000* conducted by AEG, Hyderabad. pp: 403-405.
- Venkateswara Rao, B., 1994. Integrated Studies for Evaluation of Ground Water Potential in a Typical Khondalitic Terrain, a Ph.D. thesis in Water Resources submitted to JNT University, pp: 284.
- Venkateswara Rao, B., 1998a. Hydrogeochemical Characteristics of a typical Khondalitic Aquifer". *Procs. of the National Seminar on Conservation of Eastern Ghats*, held at Visakhapatnam by ENVIS centre EPTRI, Hyderabad pp: 154-167
- Venkateswara Rao, B., 1998b. Hydromorphogeological Investigations in a Typical Khondalitic Terrain Using Remote Sensing Data, *Photonirvachak, Journal of the Indian Society of Remote Sensing*, v.26, no.1 & 2, pp: 77-93.
- Venkateswara Rao, B., 1998c. Geoelectrical Characteristics of a Typical Khondalitic Aquifer, *Bhu-jal News* a quarterly journal of CGWB, Ministry of Water Resources, Govt. of India v.13, no.3 & 4 , pp: 21-30.
- Venkateswara Rao, B., Subramanyam, K., Murthy, E.S.R.C., Varalakshmi, V., and Satyanarayana, B., 2011. Problems and Prospects of Geophysical Methods in identifying Ground Water Potential Zones in Typical Hard Rocks of India, *Hydrology Journal*, v.34, no.3 & 4, pp: 85-95.
- Venkateswara Rao, B., Siva Prasad, Y., and Srinivasa Reddy, K., 2013. Hydrogeophysical Investigations in a Typical Khondalitic Terrain to Delineate the Kaolinised Layer using Resistivity Imaging, *the Journal of Geological Society of India*, v.81, pp: 521-530.
- Venkateswara Rao, B., Siva Prasad, Y., 2015. Delineation of Kaolinised Zones by using Three Dimensional Resistivity Imaging in a Typical Khondalitic Terrain to Contain Water Well Failures, *Journal of Geophysics*, v.XXXVI, no.4, pp: 197-209
- Venkateswara Rao, B., Siva Prasad, Y., and Narasaiah, V., 2017. Field work information of SERB sponsored research project, unpublished.

Received on: 15.9.17, Revised on: 27.10.17; Accepted on: 10.11.17

Geochemical and Ore-mineralogical Characterization of Beach placer ilmenite from Srikurmam Deposit, Andhra Pradesh, India

M.Jagannadha Rao^{1*}, J. Venkata Ramana², Aaron A.Jaya Raj³, G.Raja Rao³ and P.Rajesh⁴

¹⁻⁴Department of Geology, Andhra University, Visakhapatnam-530003

¹Department of Geosciences, Dr. B.R.Ambedkar University, Etcherla, Srikakulam

*Corresponding Author: mjrao.geology@gmail.com

ABSTRACT

Ilmenite ores from the Srikurmam placer sand deposit were investigated for their geochemistry and mineralogy. Studies indicated that the ilmenite of Srikurmam placer has TiO₂ content comparable to other placer deposits like Bhimunipatnam in east coast and Ratnagiri in west coast of India. The trace element data indicate that the elements such as Co (315 ppm to 320 ppm), Ni (45 ppm to 49 ppm), Zn (694 ppm to 698 ppm), V (1300 ppm to 1304 ppm) and Cr (648 ppm to 653 ppm) are in higher concentrations. Mn content in the ilmenites of the present study area has significantly low values (0.52 ppm to 0.93 ppm). Ore mineralogical studies indicate that the ilmenite exhibits conspicuous exsolution features. Studies reveal four types of intergrowths; hemo-ilmenite (complex exsolution and lamellar exsolved phase), ilmeno-hematite (Emulsion texture), and irregular exsolved phases exhibiting different grain level textures. Hematite phase in ilmenites incorporates excess iron (average 46.49%) in the structure of ilmenite. Based on the geochemical and ore mineralogical aspects, ilmenites of the Srikurmam placer area is more suitable for pigment-manufacturing. However, the higher concentrations of trace elements may affect the properties of pigment grade oxide. In addition the excess iron may cause environmental problems.

Key words: Beach placer ilmenite, Ore mineralogy, Geochemistry, Srikurmam, Andhra Pradesh.

INTRODUCTION

Ilmenite is a black iron-titanium oxide with a chemical composition of FeTiO₃. Ilmenite is the primary ore of titanium, a metal needed to make a variety of high-performance alloys. Most of the ilmenites mined worldwide is used to manufacture titanium dioxide, TiO₂, an important pigment, whiting, and polishing abrasive (geology.com › Minerals). Ilmenite is the most important ore of the element titanium. It has recently surpassed Rutile as the main ore mineral of that metal. Ilmenite was once used as a minor ore of iron prior to the discovery of titanium as an industrially important metal. (www.minerals.net/mineral/ilmenite.aspx). Ilmenite is named after the Ilmenski Mountains in Russia, where the mineral was first discovered. Ilmenite is slightly magnetic, which means that magnets can be used to separate it from other minerals in mineral sands. It is able to withstand extreme temperatures, and is used in the steel industry to line blast furnaces (www.australianminesatlas.gov.au/education/down_under/minerals.../ilmenite.html).

Placer ilmenite is the major source mineral of the world in the production of titanium metal, which has wide variety of applications. Titanium metal and its alloys are having excellent applications in aero-space industry, gas turbines and in machinery involved in high temperature operations and in defense equipment. Titanium carbide is used in commercial cutting tools.

World reserves of ilmenite are estimated at 740 million tons in terms of TiO₂ content. Major reserves are in China

(27%), Australia (19%), India (11%), South Africa (9%), Brazil and Madagascar (6% each), Norway (5%), Mozambique (2%) and other countries. (Indian Minerals Yearbook 2015).

East coast of India has been known for the occurrence of the economically important ilmenite bearing placer sand deposits. During recent times, demand for ilmenite and its value added products has increased many fold. In this context, India, with an estimated total reserves of 278 million tons (Mukherjee, 1998), including Andhra Pradesh 103.05 million tons (Ravi et al., 2001) is at present placed comfortably. However, ilmenite (FeTiO₂) being the important source for titanium, discovery of new ilmenite resources is essential keeping in view of growing need of titanium based products in various fields.

The present study deals with the study of ilmenite along Srikurmam coast in Andhra Pradesh (Figure 1) where one of the richest beach placer ilmenite deposits exists along the East Coast of India. Srikurmam with an extensive dunal belt system has an average grade of 34% Total Heavy Mineral (THM) concentration with abundant ilmenite and garnet occurrence. Preliminary studies hence indicated ilmenite and garnet to be predominant minerals with a grade ranging from 21.37% to 39.59% and 31.07% to 44.59%, respectively (Yugandhara Rao et al., 2001). However, baseline data pertaining to industrial utility of ilmenite geochemistry are scanty. This research note presents geochemical and ore mineralogical aspects of ilmenite of this deposit and their possible bearing on processing and value-addition.

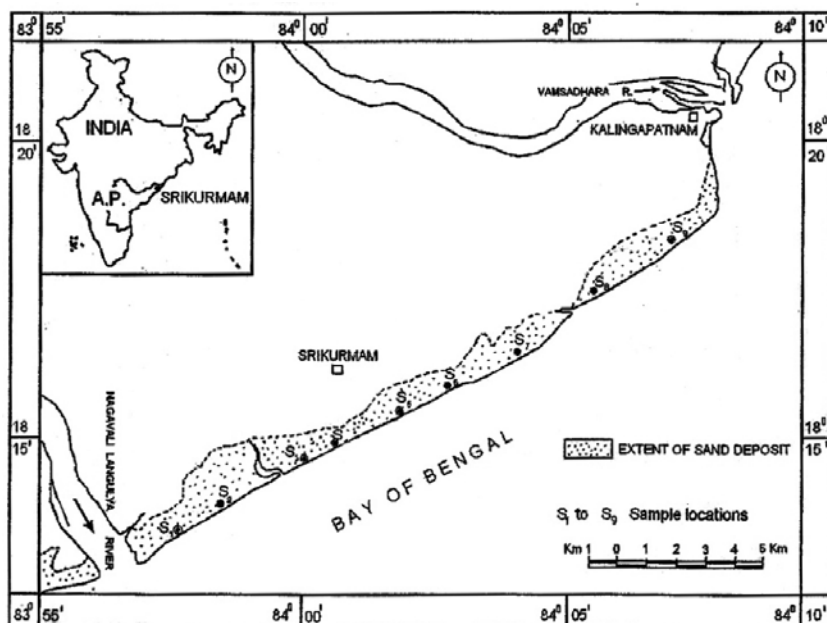


Figure 1. Srikurmam Beach Placer Deposit with Sample Locations.

METHODOLOGY

Keeping in view of the placer sand deposit in an extensive dunal environment, (Figure 2, 3 and 4) representative bulk samples, each of about 30 to 50 kg were collected at 9 locations (Figure 1). Each sample was reduced to required quantity by standard sample reduction techniques. The heavy minerals were concentrated by bromoform (sp. gr 2.89) and the magnetite was separated by hand magnet. The magnetite-free samples were then run through the isodynamic separator, set at ≈ 0.25 amp to separate ilmenite. The separation was repeated 10 to 15 times to ensure high purity of ilmenite (Figure 5.). The purity was checked under a binocular microscope and 99% pure samples were analyzed by Atomic Absorption Spectrophotometer and ICP-MS for major and trace elements. The standards used for the analysis are 100 ppm concentration supplied by Fisher scientific company, USA.

RESULTS

Geochemistry:

The ilmenite samples from the study area were analyzed for their major and trace elemental contents (Table 1.). The results indicate that the TiO_2 content varies from 50.04% to 52.05%. The total iron recorded in the range of 45.41% to 47.53%. Whereas major elemental concentrations such as SiO_2 , Al_2O_3 and MgO recorded lower average values of 0.37%, 0.17% and 0.28% respectively, and had a range between 0.37 and 0.39%, 0.16 and 0.18% and 0.2 and 0.4%, respectively.

The trace elements, namely Cr, Mn, V, Co, Ni, Zn, and Cu are determined in the study. Among the trace elemental concentrations, Vanadium recorded highest concentration around 1300 ppm. Significantly Cr and Zn indicate almost similar concentrations. Cr ranges from 648 to 651 ppm and Zn is found to be in the range of 694 to 698 ppm, but Co is found to be in the range of 315 to 320 ppm, which is almost half that of Cr and Zn. Strikingly, these three elemental concentrations (i.e. Cr, Zn and Co) recorded much lower values than that of V. However, Ni occurs in the range between 45 and 49 ppm with an average abundance of 46.4 ppm, whereas Cu is found to be in the range between 65 and 68 ppm with an average of 66.6 ppm. More significantly Mn content is reported to be very much lower in concentration, ranging between 0.5 ppm and 0.93 ppm. These observations suggest that in the present deposit, the V (Average 1301.80 ppm) and Zn (Average 696.40 ppm) concentrations are comparatively higher than the other deposits, whereas Cr (Average 650.40 ppm) is on par with other deposit and Mn (Average 0.73 ppm) is significantly reported very low concentrations. These observations are pictorially represented in the Figure 6.

Ore Mineralogy:

The detailed ore microscopic examination of the ilmenite grains from the present investigation revealed the wide variety of exsolutions mainly between the minerals hematite-ilmenite, ilmenite-hematite etc. In polished sections ilmenite appears grayish white with a light brownish tinge to pinkish tinge; the reflectivity is moderate. A number of exsolution patterns were observed

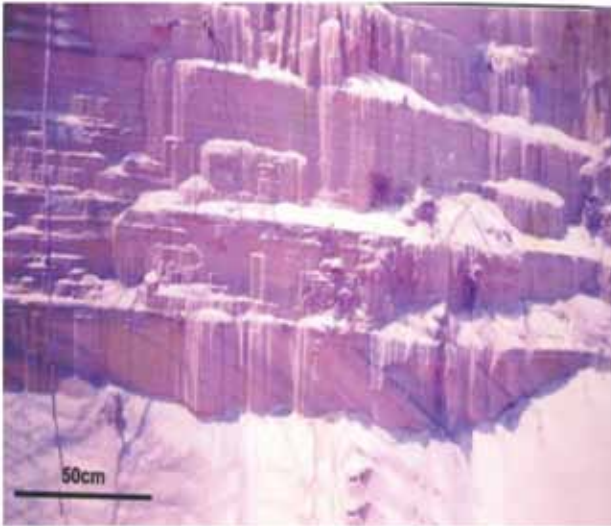


Figure 2. Excellent step and pillar like pattern in a dunal cross section, Srikurmam placer sand Deposit.



Figure 3. Rich ilmenite concentration in the Dune.



Figure 4. Density stratification of black sand with Ilmenite, in the berm cut.

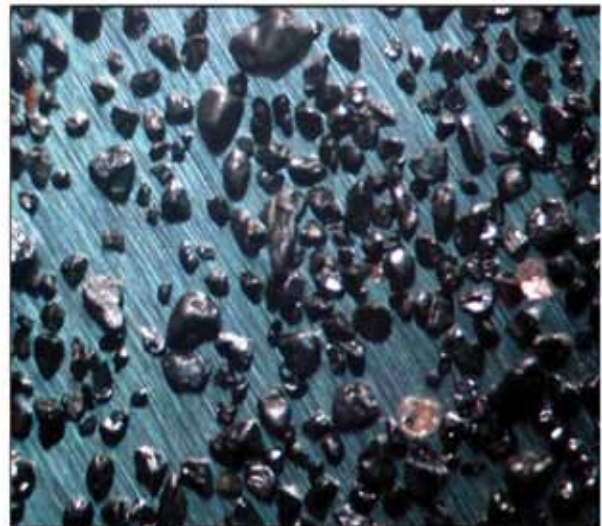


Figure 5. Separated ilmenite grains under binocular Microscope 30X.

in the present study. There are complex exsolved phase grains comprising hematite-ilmenite (Figure 7.a, complex exsolution), (Samsuddin Ahmed et al., 1992). Similarly the formation of ilmenite lamellae within the host hematite indicates the dominant hematite phase (more than 50%). This can be termed as "hemo-ilmenite" (hematite matrix) (Fig.7b, Lamellar exsolved phase) and the hematite exsolved phases within the host ilmenite indicate the dominant ilmenite phase (more than 50%) which can be considered as "ilmeno-hematite" (ilmenite matrix) (Figure 7.c Emulsion texture). This terminology is adopted from earlier reports from literature (Ramdohr, 1969, Samsuddin Ahmed et al., 1992). Similarly, the number of grains showing irregular exsolved phases of ilmenite and hematite can be seen

in Figure 7.d. Some of the grains show pure ilmenite phase. Variations in optical properties such as reflectance, pleochroism, brightness, etc. are significant among the elements of present study. Wide variation in the width of intergrowth lamellae of both ilmenite and hematite phases is identified. The variations in the grain boundaries and micro fractures are very significant, indicating their differences in Ti and Fe contents. Some ilmenites show very fine needle-shaped (hair like) exsolution and are microcrystalline in nature.

The abundance of the lamellae of Hematite within ilmenite makes the grains to be called as Hemo-ilmenites or ilmeno-hematites depending upon the relative percentages of these two phases. The work done by Suzanne et al.,

Table 1. Chemical analysis of ilmenite (major radicals in wt % and trace elements in ppm) from the Srikurmam coastal sand deposit, Andhra Pradesh, compared with other deposits.

S.No	Location	TiO ₂	SiO ₂	Al ₂ O ₃	T-Fe	MgO	Cr	Mn	V	Co	Ni	Zn	Cu
1	S1	51.12	0.38	0.17	46.66	0.2	651	0.74	1302	319	46	697	67
2	S2	51.26	0.37	0.18	45.69	0.4	650	0.53	1301	316	47	695	66
3	S3	52.05	0.37	0.16	45.84	0.3	653	0.52	1304	320	49	694	65
4	S4	51.75	0.38	0.17	45.5	0.2	649	0.64	1302	317	46	696	67
5	S5	50.65	0.39	0.18	47.53	0.2	648	0.93	1303	316	45	698	68
6	S6	50.36	0.36	0.16	47.35	0.3	651	0.81	1300	320	45	697	68
7	S7	50.04	0.38	0.18	45.41	0.4	651	0.69	1300	320	45	695	65
8	S8	51.27	0.37	0.18	47.41	0.22	652	0.90	1304	319	48	698	66
9	S9	51.95	0.37	0.17	47.02	0.3	649	0.81	1300	315	47	698	68
	Average	51.16	0.37	0.17	46.49	0.28	650.4	0.73	1301.8	318	46.4	696.4	66.6
10	B1	47.42	0.22	0.40	49.54	0.42	990	1120	600	90	44	103	8
11	B2	47.36	0.24	0.41	49.95	0.40	1016	1020	720	110	36	188	16
12	B3	50.30	0.29	0.54	46.90	0.30	910	1615	159	160	66	99	9
13	B4	48.18	0.50	0.28	49.29	0.20	416	1724	805	38	90	122	18
14	B5	49.66	0.22	0.50	46.23	0.26	844	1652	201	123	90	101	8
15	B6	50.50	0.80	0.30	46.34	0.32	444	1518	800	57	38	166	8
16	B7	48.12	0.18	0.52	49.26	0.26	1520	8100	512	120	62	124	4
17	B8	51.09	0.50	0.30	46.20	0.25	334	2020	714	88	22	106	12
18	B9	51.09	0.30	0.60	46.10	0.38	1110	1818	188	150	54	112	6
19	B10	52.30	0.44	0.32	44.10	0.18	212	1808	716	10	62	124	4
20	B11	50.05	0.11	0.19	47.28	0.65	504	1520	616	68	41	172	10
	Average	49.71	0.34	0.39	47.38	0.33	754	1628	584	92	55	136	10
21	84/1943-5	51.25	ND	ND	43.79	ND	621	2107	872	194	84	232	ND
22	84/1946-6	56.25	ND	ND	37.50	ND	773	2057	791	178	93	197	ND
23	84/1946-17	50.00	ND	ND	45.08	ND	513	2210	661	93	78	179	ND
24	84/1946-19	53.13	ND	ND	42.55	ND	583	2218	811	153	94	208	ND
25	91/2536-1	51.25	ND	ND	40.64	ND	724	2189	875	153	82	223	ND
26	91/2536-18	53.18	ND	ND	41.47	ND	740	2344	849	123	87	235	ND
27	84/KB/B-1	54.38	ND	ND	40.95	ND	508	2228	738	114	86	207	ND
	Average	52.77	ND	ND	41.71	ND	637	2193	799	144	86	211	ND
28	Q	60.00	0.90	0.10	35.20	0.60	416	3080	420	ND	ND	ND	ND
29	MK	55.00	0.90	0.80	39.80	1.00	256	3080	1232	ND	ND	ND	ND
30	OR	50.20	0.80	0.60	46.90	0.65	160	4235	672	ND	ND	ND	ND
	Average	55.066	0.866	0.833	40.633	0.75	277.33	3465	774.66	ND	ND	ND	ND

S1-S9 Samples of present study, S.No 10-20 Bhimunipatnam, (Jagannadha Rao et al., 2005), S.No 21-27 Ratnagiri (Sukumaran and Nambiar, 1994); S.Nos 28-30 Chatrapur (Mukherjee, 1998), ND-Not determined and T-Fe means total iron content.

(2000) indicated similar exsolved phases in Ilmenites of Skondel, Norway, which are derived from Norite parentage.

The ore mineralogical aspects indicate that the exsolution features of ilmenite under study have resemblance to that from Bhimunipatnam deposit (Jagannadha Rao et al., 2015) and also Cox Bazar ilmenites (Samsuddin Ahmed et al., 1992).The resemblance indicates igneous parentage.

DISCUSSION

The TiO₂ content of ilmenite in the given samples is almost close to the theoretical ilmenite composition reported in literature which is 50.02% (Deer et al., 1965). The average TiO₂ of the present study area (51.16%) is comparable with that of Ratnagiri (52.77%) (Sukumaran and Nambiar, 1994). However, there is comparable variance in the presence of total iron contents of these two deposits

(Table 1). The average total iron content of the ilmenite of the deposit is 46.49%, whereas Ratnagiri ilmenites have an average of 41.71%. The data thus demonstrate that ilmenite of SriKurmam deposit records higher total iron and lower TiO₂ contents as compared to the composition of ilmenites from the published data (Sukumaran and Nambiar, 1994, Mukherjee, 1998). Similarly the Chhtrapur ilmenite has TiO₂ in the range of 50.2% to 60% and total iron in the range of 35.20% to 46.90% (Mukherjee, 1998). However, the TiO₂ and total iron contents of the present study are comparable with those ilmenites reported from Bhimunipatnam where an average TiO₂ and total iron contents are 49.71% and 47.38%, respectively, (Jagannadha Rao et al., 2008). The SiO₂ content (0.36% to 0.39%) is comparable with Bhimunipatnam ilmenites (average 0.34%) and significantly less than that reported for Chhtrapur ilmenites (average 0.86%) (Mukherjee,1998).The Al₂O₃

Geochemical and Ore-mineralogical Characterization of Beach placer ilmenite from Srikurmam Deposit, Andhra Pradesh, India

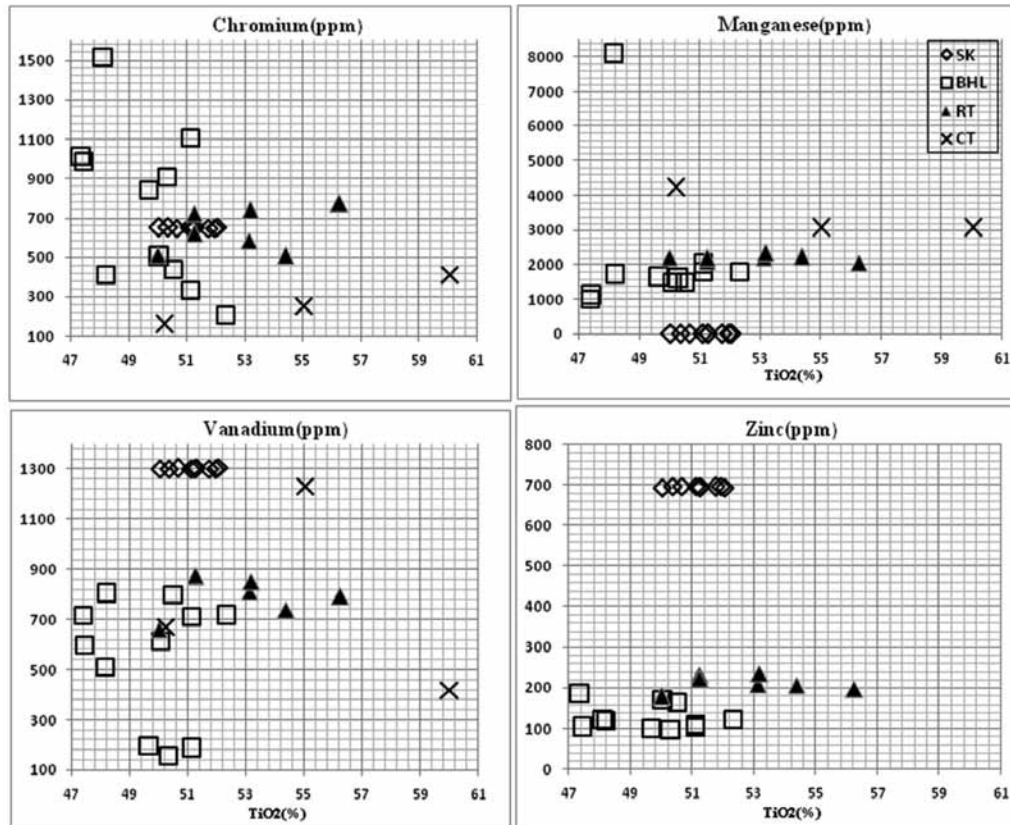


Figure 6. Scatter plots showing variation of Cr, V and Zn vs TiO_2 from different deposits Srikurmam (SK), Bhimuniapatnam (BHL), Ratnagiri (RT) and Chhtrapur (CT).

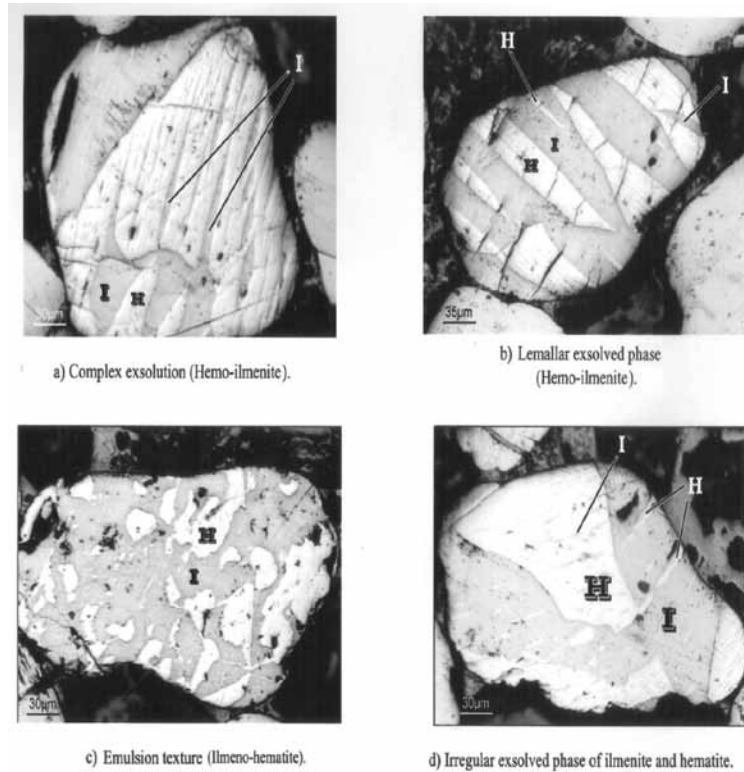


Figure 7. Ilmenite grain morphology with exsolved phases of ore minerals, Ilmenite (I) and Hematite (H).

values are comparatively less than Bhimunipatnam and Chhtrapur ilmenites. Similarly, the MgO% is in the range of 0.2% to 0.4%, significantly lower than that of Chatrapur ilmenites (Mukherjee, 1998) and Bhimunipatnam ilmenites (0.18% to 0.65%) (Jagannadha Rao et al., 2005). The trace elemental concentrations of Cr and V, which are in the range of 648 ppm to 653 ppm and 1300 to 1304 ppm respectively, are higher than that of ilmenites of Chhtrapur (Mukherjee, 1998) and Ratnagiri (Sukumaran and Nambiar, 1994). However, the Cr content of Bhimunipatnam ilmenites (Jagannadha Rao et al., 2005) is comparable with ilmenites of present study, but V concentration is less (average 584 ppm). The other trace elemental concentration, namely Co, Ni, and Cu of the present deposit are higher than the reported data (Table 1). The lower abundance of SiO₂ and higher abundance of Cr, Co, Ni and V suggest that the ilmenites of the present study are showing affinity to a possible basic parentage. Another striking observation is the vast difference in the abundance of the Mn content in the ilmenites of the present study area (0.73 ppm) compared with the other published data from Ratnagiri (2193ppm) (Sukumaran and Nambiar, 1994) and Chhtrapur (3465 ppm) (Mukherjee, 1998) and Bhimunipatnam (1628 ppm) ilmenites (Jagannadha Rao et al., 2005). The low Mn concentration contradicts the theory of the metamorphic parentage of ilmenites from the study area (Ramamohana Rao et al., 1983).

Zn concentration, which is found to be in the range of 694 to 698 ppm is comparatively higher than the other deposits. The report of occurrence of Zincurian ilmenite (Jagannadha Rao et al., 2008) from this area, perhaps explains high Zn concentration.

Earlier studies by (Jagannadha Rao, 1985); (Jagannadha Rao et al., (2005) on the ore mineralogy of Bhimunipatnam deposit indicated that the ilmenite shows high variability in terms of grain size, texture, pattern of exsolutions, composition of exsolved phases etc. In general the ilmenite of Srikurmam deposit is granular or rounded to irregular. Its grain size is around 80 microns.

From the above observations, it is very clear that the ilmenites of the study area recorded marginally less TiO₂ percent and high total iron content than the theoretical formula of the ilmenite. The higher total iron content can be explained due to the fact that these ilmenites are not pure and in fact they can be called as hemo-ilmenites or ilmeno-hematites as per the percentage of exsolved hematite phase. This is also established by the ore mineralogical observations as well. Similarly, the higher abundance of trace elements like V, Zn and Cr is a significant observation. The occurrence of wide variety of exsolutions in ilmenite as mentioned earlier, suggests their derivation from multiple sources or with different paragenesis, especially basic parentage.

(Hegde et al., 2006) have investigated the provenance of Honnavar beach, West coast of India. They have carried out the study with particular reference to ilmenite. They have concluded that the heavy minerals like ilmenite, magnetite and zircon, which are characterizing the Precambrian gneissic, granitic and basic rocks have been derived from the hinterland and subsequently transported by the river Saravathi. However, minerals like garnet, kyanite and staurolite are characteristic minerals of high grade metamorphic source and are derived from reworked paleo beach/off shore sediments. They further established that the high contents of trace elements namely Cobalt, Chromium, Vanadium and Nickel suggest basic source of their derivation.

Mohanty et al., (2003) have undertaken similar studies of geochemical characterization of ilmenite from Chhtrapur beach placer deposit using PIXE and EDXRF methods.

Suzanne et al., (2000) have carried out chemical and petrographic characterization of ilmenite and magnetite from Sokndal region, Norway. Their work emphasized the chemical features and micro textures reflecting the progress of magmatic evolution. They have indicated that the most primitive oxides of the region are ilmenites derived from Norites from Tellnes region.

Babu et al., (2009) carried out studies on recovery of ilmenite and other heavy minerals from Teri sands of Tamilnadu, India. They have established a method using spirals followed by dry high intensity magnetic separator and high tension separator to obtain 99.10% purity of ilmenite. The other minerals like zircon, sillimanite are separated by judicious combination of gravity and floatation process.

Ilmenite of the present study contains nearly 30% of iron as oxides, which is considered to be a polluting agent and consumes more chemicals in the process of manufacturing of TiO₂ or TiCl₄. In addition, ilmenite contains significant quantities of vanadium, chromium, Ni, Co etc., which affect the properties of pigment grade oxide. Chemistry of ilmenite also decides whether the given ilmenite can be processed by the following chloride route or by sulphate route, which will have significant technical and economic implications. The high iron content of ilmenites from the study area (Table 1) may result in excess iron, and as such is environmentally unwanted and consumes more acid in the process. This may have economic and environmental implications (Mukherjee, 1998).

CONCLUSION

The ore mineralogical study established extensive exsolved phases in Srikurmam ilmenite ores. These grain level textures strongly support a magmatic source of ilmenite derivation, rather than metamorphic parentage. The higher abundance of trace element concentration like V,

Geochemical and Ore-mineralogical Characterization of Beach placer ilmenite from Srikurmam Deposit, Andhra Pradesh, India

Zn and Cr further support this observation. As far as the processing of ilmenite is concerned, the high Iron content will have problem of more acid consumption, which has an environmental impact.

ACKNOWLEDGEMENTS:

The authors are thankful to Department of Science and Technology, New Delhi, for the financial assistance in the form of a Research Project entitled "Studies on exsolved phase mineralogy and chemical fingerprinting of East Coast placer elements to establish genetic affinities and to evolve economic implications". The authors gratefully thank Dr.V.V.Sesha Sai for useful suggestions in revising the manuscript. Thanks are due to Dr.P.R.Reddy, Chief Editor for continued support and precise editing of the manuscript.

Compliance with Ethical Standards:

The authors declare that they have no conflict of interest and adhere to copyright norms.

REFERENCES

- Babu, N., Vasumathi, N., and Bhima Rao, R., 2009. Recovery of ilmenite and other heavy minerals from Teri sands (Red sands) of Tamilnadu, India. *Journal of Minerals and materials Characterization & Engineering*. v.8, no.2, pp: 149-159.
- Deer, W.A., Howie, R.A., and Zussman, J., 1965. *An Introduction to Rock-Forming Minerals*, ELBS and Longman. pp: 412-414.
- Hegde, V.S., Shalini, G., and Gosavi Kanchanagouri, D., 2006. Provenance of heavy minerals with special reference to ilmenite of the Honnavar beach, central west coast of India. *Current science*, v.91, no.5, pp: 644-648.
- Indian minerals year book (2015). Part-III (Mineral reviews), 54th Edition, Ilmenite and Rutile, Government of India, Ministry of Mines, Indian Bureau of mines, Nagpur.
- Jagannadha Rao, M., Aaron A Jaya Raj and John Paul, K., 2008. Occurrence of Zincian ilmenite from Srikurmam placer sand deposit, Andhra Pradesh, India. *Current Science*, v.95, no.9, pp: 1124-1126.
- Jagannadha Rao, M., Venkata Ramana, J., Karuna Karudu, T., Ratnakar, P. J., and Sivanatha Reddy, G., 2015. Some Insights into Placer Ilmenites of East Coast of India, with reference to their Occurrence, Variability and Source. *Journal of Economic Geology & Geo Resource management*. Prof. Calamur Mahadevan Commemorative Special v.10, pp: 155-168.
- Jagannadha Rao, M., Venkata Ramana, J., Venugopal, R., and Chandra Rao, M., 2005. Geochemistry and ore mineralogy of Ilmenite from Beach Placers of the Visakhapatnam-Bhimunipatnam Deposit, Andhra Pradesh. *Jour. Geol.Soc. Ind*, v.66, pp: 147-150.
- Jagannadha Rao, M., 1985. Origin of recent sediments along Visakhapatnam-Bhimunipatnam Coast. Unpublished Ph.D. Thesis, Andhra University, Visakhapatnam, pp: 84-85.
- Mohanty, A.K, Vijayan, V., Senugupta, D., Das, S.K., and Saha, S. K., 2003. Geochemical characteristics of ilmenite sands of Chhatrapur beach placer deposit of Orissa, India: A PIXE study. *Int. J. Pixe* 13, 121 (2003).
- Mukherjee, T.K., 1998. *Metals materials and processes*. Meshap Science Publishers, Mumbai, India, pp: 85-98.
- Ramamohana Rao, T., Ranga Rao, N., and Rama Raju, M.V., 1983. Ilmenite of black sand deposits of Visakhapatnam-Bhimunipatnam beach, East Coast of India, India. *J.Mar. Sci.*, v.12, pp: 220-222.
- Ramdohr, P., 1969. *The Ore minerals and their intergrowths*. Pergamon Press, London, UK, pp: 965.
- Ravi, G.S., Gajapathi Rao and Yugandhara Rao, A., 2001. Coastal heavy mineral sand deposits of Andhra Pradesh. *Exploration. Res. At. Min.*, v.13, pp: 53-85.
- Samsuddin Ahmed, Taraknath Pal, and Sachinatah Mitra., 1992. Ilmenites from Cox's Bazaar Beach sands, Bangladesh: their intergrowths. *Jour. Geol. Soc. India*, v.40, pp: 29-41.
- Sukumaran, P.V., and Nambiar, A.R., 1994. Geochemistry of Ilmenites from Ratnagiri Coast, Maharashtra. *Curr. Sci.*, v.67, no.2, pp: 105-106.
- Suzanne A. Mckenroe, Peter Robinson and Peter T. Panish., 2000. Chemical and petrographic characterization of ilmenite and magnetite in oxide-rich cumulates of the Sokndal Region, Rogaland, Norway. *NGU-Bull* 436, 2000, pp: 56.
- Yugandhara Rao, A., Ravi, G.S., Gajapathi Rao, R., Krishana, S., Mir AzamAli and Banerjee, D.C., 2001. Srikurmam – A major Heavy mineral beach and dune sand deposit on the East coast of India. *Hand book of placer mineral deposits, Atomic minerals directorate for Exploration and Research*, v.13, pp: 53-63.
- WEBLINKS (geology.com · Minerals). (www.minerals.net/mineral/ilmenite.aspx). (www.australianminesatlas.gov.au/education/down_under/minerals../ilmenite.html).

Received on: 27.10.17; Revised on: 7.12.17; Accepted on: 23.12.17

Ferrosyenites - an overview

K. Sai Krishna and R. Mallikarjuna Reddy*

Department of Geology, Kakatiya University, Warangal, Telangana-506009

*Corresponding Author: mallikragi@gmail.com

ABSTRACT

Through this paper we present an overview on the ferrosyenites. The ferrosyenites are very rare and geologically interesting rocks that are found in North America, Africa, Antarctica, China, Europe, Ukraine, Greenland and India. Mineralogically ferrosyenites are mainly composed of Fe-rich pyroxenes or Fe-rich olivine (fayalite), alkali feldspar minerals. 90% of ferrosyenites occur in association with gabbros in different alkaline complexes of the world, due to their petrogenetic relation. Chronologically ferrosyenites vary widely in age (9.1 ± 0.4 Ma to 1413 ± 54 Ma). Along with the mineralogical and chronological diversity, the global distribution and nature of occurrence of the ferrosyenites is presented here.

Key words: Ferrosyenite, mineralogy, correlation, global distribution.

INTRODUCTION

Ferrosyenites are rare and geologically interesting rocks that are confined to specific geological setting; associated with the alkaline complexes. Worldwide, the ferrosyenites have restricted occurrence and are recorded at 32 places in North America, Africa, Antarctica, China, Europe, Greenland, India and Ukraine (Figure 1). The ferrosyenites are alkaline and subalkaline in character, which are mainly composed of Fe-rich pyroxenes or Fe-rich olivine (fayalite), alkali feldspars and amphiboles as essential minerals and quartz, biotite, titanite, zircon and calcite as accessory minerals. Globally, in majority of the alkaline complexes, ferrosyenites (~ 90 %) occur along with the gabbro plutons, rare exceptions are Gundlapalle and Sivamalai ferrosyenites of India. In Gundlapalle, the ferrosyenite is found in association with granite, close to the quartzite-limestone sequence of Palnad basin. Further, Gundlapalle ferrosyenite is unique due to the conspicuous presence of nontronite along with ferrohedenbergite. Presence of nontronite is an evidence for extensive hydrothermal alteration of ferrohedenbergite to nontronite, which is formed by the oxidation of Fe^{+2} to Fe^{+3} at the same time with the withdrawal of Ca (Eggleton, 1975). The nontronite is a rare secondary mineral which is identified by Madhavan et al., (1994) for the first time in Gundlapalle ferrosyenite of India. Nevertheless, apart from Gundlapalle other three ferrosyenites consist of ferrohedenbergite (New jersey-USA, Davidki-Ukraine, Klokken-Greenland) but with the absence of nontronite, which is missing due to the absence of hydrothermal fluids to alter the ferrohedenbergite to nontronite. The ferrosyenites vary widely in age (9.1 ± 0.4 Ma to 1413 ± 54 Ma) and exhibit varying mineralogy and petrological characters in different plutons of the world (Table 1).

GLOBAL SCENARIO

On a global perspective, the ferrosyenites sign into proterozoic, as proved by the age determination of Kiglapait intrusion; Western Cripple Creek of North America, Nunarssuit complex from Gardar alkaline province of Greenland and Uppalapadu from peninsular India. Only couple of ferrosyenites represents palaeozoic period from Kambusi (South Africa) and China. The ferrosyenites from Kerguelen Islands of French territories represent Cenozoic period. The oldest ferrosyenite has been recorded at Kiglapait intrusion, which is located in the northern coast of the Labrador Peninsula, here the age of the syenite rocks is 1413 ± 54 Ma old (De Paolo, 1981). The Nunarssuit complex is a very large massif, within the Gardar alkaline province in South Greenland that belong to Proterozoic age, the Rb-Sr age of pyroxene-fayalite syenite is 1154 ± 14 Ma (Blaxland et al., 1978). The fayalite quartz syenite located at West Creek in the eastern part of the Pikes Peak batholith, Colorado has an age of 1085.6 ± 2.5 Ma (Diane et al., 1999).

The ferrosyenite of Palaeozoic age is represented in Mutěnin pluton, which is a part of Bohemian massif (European Variscides, Germany). The pluton consists of "Lower carboniferous" ferrosyenite, which is exposed at north of the village St. Kramolin, (Zulauf et al., 2002). The Kambusi complex in Congo region, Africa is located about 30 km northwest of Bukavu. The complex consists of two intrusions, microgranite and microsyenite which are emplaced during the Cambrian (Ramvegri et al., 1985). The permian age was recorded at Baima igneous complex (BIC) which is located in the central portion of the Panxi rift in China, this complex consists of syenite, fayalite syenite, gabbro, precambrian rocks, granite and magnetite ore. The age of fayalite syenite is 252 ± 2.5 Ma which is

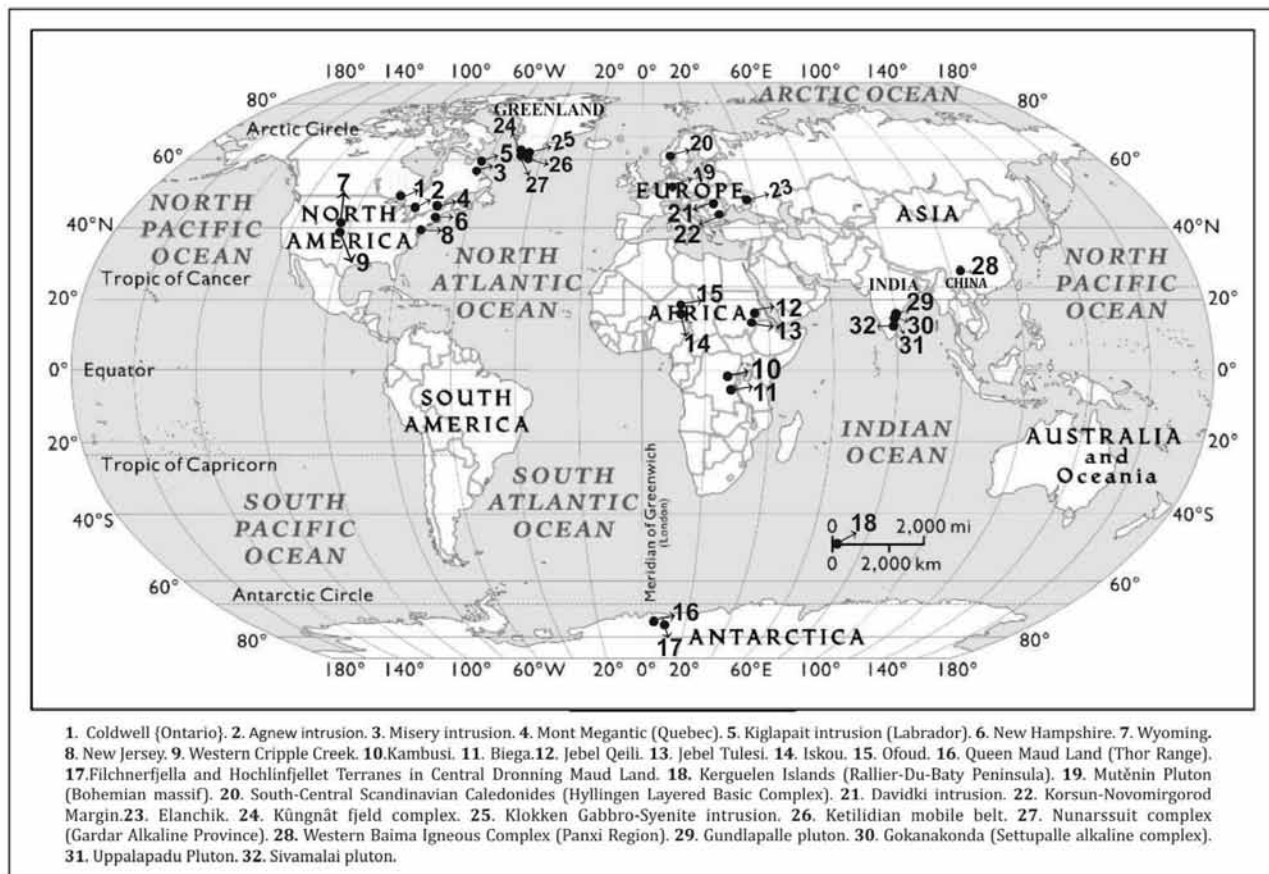


Figure 1. Global distribution of ferrosyenites.

determined by SHRIMP zircon U–Pb technique (Gregory Shellnutt et al., 2008).

The youngest ferrosyenite of the world is located in Rallier du Baty ring complexes (South Centre) of Kerguelen archipelago of the southern Indian Ocean, which occupies an area of 6500 Km². The fayalite syenite here has recorded an age (K–Ar) of 9.1 ± 0.4 Ma (Dosso et al., 1979).

Tectonic Setting of the Ferrosyenites in the World

The ferrosyenites mostly occur in the rift, shear zones, deep fault and orogenic related tectonic setups in the world, which is evident in the famous alkaline plutons and some layered complexes in North America, Africa, Antarctica, China, Europe, Greenland, Ukraine and India Table.1. At present the information on the detailed tectonic settings of the few ferrosyenites of the world is available but the gap in the information with respect to the remaining need to be filled.

Mineralisation in Ferrosyenites

REE Mineralisation is found in only two plutons namely, Misery Syenite intrusion and Devil's Slide ring dike,

New Hampshire. The REE mineralisation in the form of fluorapatite has been reported in the ferrosyenite. The fluorapatite crystals were partly or completely replaced by britholite-(Ce), thereby enriching the rocks in the REEs from the Misery syenite located in north Quebec in Canadian Shield (Petrella, et al., 2014). The genesis of the ferrosyenite has been interpreted due to the process of fractional crystallization in the Misery syenite intrusion (Petrella, et al., 2014). Chevkinite, a titano-silicate of the cerium earths, occur as a well crystallized accessory mineral in fayalite-quartz syenite of the Devil's Slide ring dike just northwest of the village of Stark, New Hampshire (Howard et al., 1956).

Ferrosyenites in India

Proterozoic syenites are widely reported in the Indian sub-continent (eg. Leelanandam, 1989; Madhavan et al., 1994; Madhavan et al., 1995; Srivastava and Chandra, 1995; Sesha Sai, 2013). However, only four ferrosyenite plutons occur in India, viz. Gundlapalle, Gokanakonda and Uppalapadu in the Cuddapah intrusive province of Eastern Dharwar Craton (EDC) and the ferrosyenites of Sivamalai of Tamilnadu. The oldest ferrosyenite has been

recorded with U-Pb Zircon age as 1352 ± 2 Ma, in India from Uppalapadu pluton (Vijaya Kumar et al., 2007). The age of the other two ferrosyenites was not determined yet, but one of the pluton which is intruded into proterozoic Cuddapah basin i.e. Gundlapalle ferrosyenite (3 Km²) is located at a distance of 12 Km from Piduguralla (Lime city) in the Guntur district of Andhra Pradesh. This pluton is situated in the northern part of the Cuddapah intrusive province (CIP). The ferrosyenite pluton has a sharp contact with unique lithological units such as granite (Dharwars), Panyam quartzites and Narji limestones representing Palnad sub-basin of Kurnool group (Madhavan et al., 1994).

The Gokanakonda ferrosyenites are emplaced with in the Settupalle alkaline complex. The subalkaline ferrosyenites (5 Km²) are exposed at the southern marginal portion of the Settupalle alkaline complex. As per mineralogical criteria, the ferrosyenites can be differentiated into two types i) fayalite \pm clinopyroxene syenite and ii) fayalite \pm quartz syenite which are marked by the Gundlakamma River. The contact between fayalite \pm clinopyroxene syenite and gabbro on the eastern side and the contact between fayalite \pm quartz syenite and the gabbro on the western side and in the Northern side with hornblende syenite and in the southern side with granite gneiss are sharp (Leelanandam 1989; Srinivasan and Natarajan 1990). The ferrosyenite hosted in Uppalapadu pluton is mainly associated with nepheline syenite, hornblende syenite, ferrosyenite, anorthosite, olivine

clinopyroxenite and olivine gabbro. The ferrosyenite has sharp contact with olivine gabbro on the eastern side and partly with hornblende syenite and biotite schist on the western side (Krishna Reddy et al., 1997). The Sivamalai pluton of Tamilnadu consists of ferrosyenite, perthite syenite, leuco syenite, biotite nepheline syenite, hornblende syenite. The ferrosyenite has sharp contact with perthite syenite and partly with biotite nepheline syenite on the western side (Holland, 1901; Bose, 1968.1971; Takashi Miyazaki et al., 1999).

Tectonically, the Gundlapalle pluton is very close to a deep seated fault which trends in NE-SW direction (Kaila and Tewari; 1982. Madhavan et al., 1994). Among the four plutons namely Elchuru, Purimetla, Uppalapadu and Settupalle, the presence of ferrosyenites is found only in Uppalapadu and Settupalle. These four plutons are conspicuously confined to an extremely narrow linear belt which is close to the known basement fracture zone, with which the major Bouguer gravity axis runs in close parallelism in a NNE-SSW direction. This belt lies approximately at the junction zone between two contrasting major rock formations and between two fold belts: such as the Dharwar (granite-greenstone) belt towards the west and the Eastern Ghat (gneiss-granulite) mobile belt towards the east (Leelanandam, 1989). The Sivamalai ferrosyenite pluton from Tamilnadu lies within the palghat-Cauvery shear zone (Holland, 1901; Bose, 1968.1971; Takashi Miyazaki et al., 1999).

Table:1. Global distribution of ferrosyenites.

Country	S.No	Location	Rock Type	Mineral Assemblage	Age	Associated Rocks	References
<u>NORTH AMERICA</u>	1	COLDWELL {Ontario} {48° 47'N:86°30'W}	Ferroaugite syenite	Ferroaugite, Fayalite, Ferroedenite-Hastingsite and Ferrichterite.	NA	Gabbro, Nepheline Syenite, Biotite-Gabbro, Granite, Quartz-Syenite, Hybrid Syenite, Granite Gneisses, Ultrabasic Intrusive.	Roger et al.1977 Roger et al.1993
CANADA	2	AGNEW INTRUSION (Southern Province in central Ontario) {81°50'N:46°21'W}	Ferrosyenite	Phenocryst of albite, Alkali feldspar, Hedenbergite, Fayalite.	NA	Leucogabbro.	Vogel et al.1999
	3	MISERY INTRUSION (Northern Quebec)	Ferrosyenite	Fayalite, Hedenbergite, Ferropargasite and Annite.	NA	Coarse grained syenite, Fine grained syenite, Medium grained syenite, Porphyritic quartz syenite	Petrella et al. 2014
	4	MONT MEGANTIC (QUEBEC) 45°27' N:71°07' W	Syenite	Fayalite, Aegirine augite, Perthite and Quartz	NA	Gabbro	Tomas Feininger, 2003 Bedard et al. 1987

Country	S.No	Location	Rock Type	Mineral Assemblage	Age	Associated Rocks	References	
COLORADO	5	KIGLAPAIT INTRUSION (Labrador) {57° 00' N:61°30'W}	Ferrosyenite	Fayalite, Mesoperthite.	1413±54 My	Gabbro, Troctolite	Barmina et al. 2002 De Paolo 1981	
	6	NEW HAMPSHIRE {43°46'N:72°00'W}	Fayalite quartz syenite	Fayalite, Hedenbergite, Quartz, Chevkinite, Hornblende, Plagioclase.	NA	Syenite	Howard et.al 1956	
	7	WYOMING {41°38'N:105°40'W}	Ferrosyenite	Olivine(Fa ₈₇), K-feldspars, Plagioclase, Augite, Ilmenite, Quartz, Titanite.	NA	Anorthosite, Hornblende Syenite, Gneisses, Sedimentary Rock	Kenneth et al., 1987 Dennis et al., 1969	
	8	NEW JERSEY	Clinopyroxene quartz syenite	Ferrohedenbergite, Mesoperthite, Quartz, Fayalite, Plagioclase.	NA	Hornblende Granitic Gneiss	Davis and John C 1972	
	9	WESTERN CREEK Pikes Peak batholith {38°44'N:105°08'W}	Fayalite quartz syenite	Microperthitic Feldspar, Pyroxene, Fayalite, Olivine, Quartz. Magnetite.	1085.6 ± 2.5 Ma	Olivine Gabbro	Diane et al., 1999	
	AFRICA CONGO	10	KAMBUSI {2°15'S:28°38'E}	Microsyenite	Hedenbergite and Fayalite, Fluorite	Cambrian	Microgranite	Ramvegri et al., 1985
		11	BIEGA {2°22'S:28°40'E}	Fayalite syenite	NA	NA	Granites. Syenite	Boutakoff, 1956 Kampunzu et al., 1985 Lubala 1986
		SUDAN	12	JEBEL QEILI {15°31'N:33°47'E}	Fayalite syenite	Fayalite. Ferro-Magnesian Minerals, Ferrohastingsite, Riebeckite, Biotite.	NA	Hastingsite syenite, Gabbro, Riebeckite quartz syenite Microgranophyre Precambrian schist, Rhyolite Lava, Biotite microgranite dykes.
	13		JEBEL TULESI {11°34'N:29°14'E}	Syenite	Fayalite, Biotite, Diopsidic Pyroxene.	NA	Peralkaline granite	Curtits et al., 1985
NIGER	14	ISKOU {18°04'N:8°52'E}	Ferrosyenite	Ferroaugite, Fayalite, Perthite.	NA	Leucogabbro	Daniel et al., 1991	
	15	OFOUD {18° 49'N:8° 43'E}	Ferrosyenite	Sodic amphibole, Ferrohastingsite, Biotite.	NA	Anorthosite	Daniel et al., 1991	
ANTARCTICA	16	QUEEN MAUD LAND (THOR RANGE) {72°55'S :5°20'E}	Fayalite Quartz syenite	Alkali feldspars, Fayalite, Quartz.	NA	Alkali Granites, Charnockite.	Kurt bucher et al., 2006	

Country	S.No	Location	Rock Type	Mineral Assemblage	Age	Associated Rocks	References
EAST AFRICA ANTARCTICA OROGEN	17	FILCHNERFJELLA AND HOCHLINFJELLET TERRANES IN CENTRAL DRONNING MAUD LAND {72°00'S:05°30'E}	Fayalite bearing syenite	Alkali feldspar, Fayalite, Pyroxenes.	NA	Granitic migmatites	Sotaro Baba et al., 2002
FRENCH SOUTHERN ANTARCTIC LANDS	18	KERGUELEN ISLANDS (RALLIER-DU-BATY PENINSULA)	Fayalite syenite	NA	9.1 ± 0.4 My	Syenites, Granites and Micro gabbro	Dosso et al., 1979
EUROPE							
EUROPEAN VARISCIDES, GERMANY.	19	MUTĚNIN PLUTON (BOHEMIAN MASSIF)	Ferrosyenite	K-feldspar, Prismatic Amphibole, Biotite, Plagioclase, Quartz, Orthite, Epidote. Fe-ti oxides.	Lower Carboni- ferous	Diorite, Quartz diorite. Mylonite.	Zulauf et al., 2002
NORWAY	20	SOUTH-CENTRAL SCANDINAVIAN CALEDONIDES (Hyllingen Layered Basic Complex)	Quartz bearing ferrosyenite	Alkali feldspar, Hedenbergite, Olivine Ferroedenite, Albite.	NA	Dunite /Troctolite, Olivine –Rich Unit, Syenitic Differentiates.	Richard et al., 1981 Henning et al., 1995
UKRAINE	21	DAVIDKI intrusion {51°14'N:30°30'E}	syenite	Pyroxenes, Titaniferous Ferrohedenbergite and Hedenbergite.	NA	Gabbro and Plagioclase	Krivdik et al., 1986
	22	KORSUN- NOVOMIRGOROD MARGIN {48°14'N:31°17'E}	Fayalite hedenbergite syenite	Fayalite, Hedenbergite, Ferrohastingsite	NA	Rapakivi Granite, Monozosyenite, Gabbronorite, Labradoritite, Granite.	Krivdik et al., 1988
	23	ELANCHIK {47°28'N:38°12'E}	Fayalite – hedenbergite syenite.	Alkali feldspar Fayalite, Hedenbergite.	NA	Hedenbergite- ferrohastingsite syenite. Leucocratic Granosyenite and Granite	Karamsin, 1979 Krivdik et al., 1986
GREENLAND (South Greenland)	24	KÚNGNÁT FJELD COMPLEX (61°13'N:48°26'W)	Ferrosyenite	NA	NA	Olivine gabbro, Ferrosyenogabbro, Quartz syenite, Granitic rocks	Emeleus and Upton, 1976. Stephenson & Upton et al., 1982
	25	KLOKKEN GABBRO- SYENITE INTRUSION {60°56'N:45°05'W}	Ferrosyenite	Alkali feldspar, Fayalite, Pyroxenes, Ferrohedenbergite.	NA	Late Biotite Syenite Gabbro, Unlaminated Syenite, Layered Syenite,	Blaxland, and Parsons, 1975 Parsons, I., 1979

Country	S.No	Location	Rock Type	Mineral Assemblage	Age	Associated Rocks	References
ASIA CHINA	26	KETILIDIAN MOBILE BELT {60°30'N:45°50'W}	Fayalite- orthopyroxene quartz syenite	Fayalite, Hastingsitic Hornblende, Alkali feldspar, Quartz.	NA	Mozonite, Biotite Granite. Syenite Quartzmonozonite / Quartzmonozonite Gabbro	Thomas Frisch et al., 1976.
	27	NUNARSSUIT COMPLEX (Gardar alkaline province) (60°46'N:48°00'W)	Pyroxene- fayalite syenite	Alkali Feldspar, Ferro- Salite/ Hedenbergite and Fayalite.	1154±14 Ma	Alkali Granite, Augite Syenite	Hodson 1993 Ferguson et al., 1963 Blaxland et al., 1978
	28	WESTERN BAIMA IGNEOUS COMPLEX (PANXI REGION) {102°04'N:27°04'W}	Fayalite syenite	Fayalite, Pyroxenes, Amphiboles, Alkali feldspars. Quartz, Biotite,	252 ± 2.5 Ma	Gabbro, Syenites. Granite,	Gregory Shellnutt et al., 2008
INDIA ANDHRA PRADESH	29	GUNDLAPALLE PLUTON (A.P) {16°24'N :79° 52' E}	Ferrosyenite	Ferrohedenbergite, Alkali feldspars, Hornblende, Nonttronite, Quartz, Biotite, Rutile.	NA	Granites, Quartzite. Limestones	Madhavan et al., 1994
	30	GOKANAKONDA (Settupalle Alkaline Complex A.P) {15°52' N: 79° 52' E}	i) Fayalite ± clinopyroxene syenite)	Alkali feldspars, Fayalite, Titanoaugite/ Fayalite,	NA	Gabbro, Hornblende Syenite, granite gneiss Amphibolite, Quartz Syenites, Nepheline syenite, Mafic Rocks.	Leelanandam et al., 1989 Srinivasan et al., 1990
			ii) Fayalite ± quartz syenite.	Alkali feldspars, Fayalite, Quartz, Biotite.	NA		
TAMILNADU	31	UPPALAPADU PLUTON (A.P) {15035'N :79047'E}	Ferrosyenite	Pyroxenes, Fayalite, Alkali feldspar, Amphiboles, Inverted pigeonite, garnet.	1352+2 Ma	Gabbronorite, Olivine clinopyroxenite, Hornblende Syenites, Nepheline Syenites, Anorthosites, Quartz Syenites, biotite schist.	Krishna Reddy et al., 1997 Vijaya Kumar et al., 2007 Bhattacharyya et al., 2014
	32	SIVAMALAI {77032'E:11002'N}	Ferrosyenite	Ferroaugite, Fayalite Alkali feldspars,	NA	Perthite Syenite, Lueco Syenites, Biotite nepheline syenite, Hornblende syenite	Subba rao et al., 1994 Bose, 1968 Bose, 1971

CONCLUSION

The ferrosyenites are very rare rocks which have distinct mineralogy and petrogenetic significance. Considering the mineralogical criteria, ferrosyenites are plutonic igneous rocks that have fayalite or Fe-rich pyroxenes as essential minerals. However, different authors from around the world used different nomenclature for these rocks. Most of the ferrosyenites from different parts of the world are associated with gabbroic rocks as these rocks have genetic relationship and are derived from gabbroic magma, but in some places the ferrosyenites are also found devoid of gabbroic association i.e. the Gundlapalle and Sivamalai ferrosyenites plutons in India. The age of ferrosyenites in the world is recorded to be from Proterozoic to Cenozoic period. The ferrosyenites of Uppalapadu area in EDC, India, is of Proterozoic age and is the second oldest body in the World after Kiglapait ferrosyenite. Through this work an attempt is made to compile the available data on ferrosyenites in the world with an objective to present an overview and also to indicate the gap. Further research on these rocks in the field of isotope geochemistry and geochronology will contribute to enhance the existing understanding of these rocks.

ACKNOWLEDGEMENTS

The authors are thankful to DST- INSPIRE fellowship programme (IF140406) for providing the required financial assistance. Further, the authors are highly indebted to Department of Geology, Kakatiya University for extending the necessary facilities. Thanks are due to Dr. V.V. Sessa Sai for objective evaluation and useful suggestions. We are grateful to Dr. P.R. Reddy Chief Editor for his support and final editing.

Compliance with Ethical Standards:

The authors declare that they have no conflict of interest and adhere to copyright norms.

REFERENCES

- Ahmed, F., 1975. The geology of J.Qeili igneous complex, Central Sudan. *Geologische Rundschau*, v.64, no.1, pp: 835-846.
- Barmina, G.S., and Ariskin, A.A., 2002. Estimation of chemical and phase characteristics for the initial magma of the Kiglapait troctolite intrusion, Labrador, Canada. *Geochemistry International*, v.40, no.10, pp: 972-983.
- Bédard, J.H.J., Ludden, J.N., and Francis, D.M., 1987. The Mégantic Intrusive Complex, Québec: a Study of the Derivation of Silica-Oversaturated Anorogenic Magmas of Alkaline Affinity. *Journal of Petrology*, v.28, no.2, pp: 355-388.
- Blaxland, A.B., Breemen, O.V., Emeleus, C.H., and Anderson, J.G., 1978. Age and origin of the major syenite centres of the Gardar: Rb Sr studies. *Geol. Soc. Amer. Bull.*, v.78, no.231, p: 44.
- Blaxland, A.B., and Parsons, I., 1975. Age and origin of the Klokken gabbro-syenite intrusion, South Greenland: Rb-Sr study. *Bulletin of the Geological Society of Denmark*, p: 24.
- Bhattacharyya, S., and Sengupta, P., 2014. Modelling of dissolution-precipitation ion-exchange reactions for the development of flame perthite in a suite of sheared alkaline rocks: an example from Chimakurthy, Eastern Ghats, India. *Mineralogical Magazine*, v.78, no.5, pp: 1301-1324.
- Bose, M.K., 1968. Mineralogical study of striped pyroxene in syenitic rocks of Sivamalai South India. *American Mineralogist*, v.53, no.3-4, p: 464.
- Bose, M.K., 1971. Petrology of the alkalic suite of Sivamalai, Coimbatore, Tamil Nadu. *Geological Society of India*, v.12, no.3, pp: 241-261.
- Boutakoff, N., 1956. Les Massifs volcaniques du Kahusi et du Biega (Kivu, Congo belge). *Memories de l'Institut Geologique de l'Universite' de Louvain*. v.9, no.5, pp: 1-41.
- Bucher, K., and Frost, B.R., 2005. Fluid transfer in high-grade metamorphic terrains intruded by anorogenic granites: The Thor Range, Antarctica. *Journal of Petrology*, v.47, no.3, pp: 567-593.
- Curtis, P., and Brinkmann, K., 1986. The Geology of younger intrusive alkali complexes in the-southwestern Nuba Mountains, Sudan.
- Daniel Demaiffe, D., Moreau, C., Brown, W.L., and Weis, D., 1991. Geochemical and isotopic (Sr, Nd and Pb) evidence on the origin of the anorthosite-bearing anorogenic complexes of the Air Province, Niger. *Earth and planetary science letters*, v.105, no.1-3, pp: 28-46.
- Davis, A., Young and Cuthbertson, J., 1994. A new ferrosilite and Fe-pigeonite occurrence in the Reading Prong, New Jersey, USA. *Lithos*, v.31, no.3-4, pp: 163-176.
- De Paolo, D.J., 1981. "Age, source and crystallization-assimilation history of the Kiglapait intrusion as indicated by Nd and Sr isotopes." *Geol Soc Am Ann Meeting, Abstr with Progr*, pp: 437-438.
- Dennis, S., Hodge and Mayewski, P.A., 1969. Gravity Study of a Hypersthene Syenite in the Laramie Anorthosite Complex, Wyoming. *Geological Society of America Bulletin*, v.80, no.4, pp: 705-714.
- Diane, R., Smith, Noblett, J., Wobus, R.A., Unruh, D., and Chamberlain, K.R., 1999. A review of the Pikes Peak batholith, Front Range, central Colorado. *Rocky Mountain Geology*, v.34, no.2, pp: 289-312.

- Dosso, L., Vidal, P., Cantagrel, J.M., Lameyre, J., Marot, A., and Zimine, S., 1979. "Kerguelen: Continental fragment or oceanic island?": Petrology and isotopic geochemistry evidence. *Earth and Planetary Science Letters*, v.43, no.1, pp: 46-60.
- Emeleus, C.H., Upton, B.G.J., 1976. The Gardar period in South Greenland. In: Escher, A., Watt, W.S. (Eds.), *Geology of Greenland. Grønlands Geologiske Undersøgelse*, Copenhagen, pp: 152– 181.
- Feininger, T., and Goodacre, A.K., 2003. The distribution of igneous rocks beneath Mont Mégantic (the easternmost Montereian) as revealed by gravity. *Canadian Journal of Earth Sciences*, v.40, no.5, pp: 765-773.
- Ferguson, J., and Pulvertaft, T.C.R., 1963. Contrasted styles of igneous layering in the Gardar province of South Greenland. *Spec. Pap. Mineral. Soc. Am.*, v.1, pp: 10-21.
- Gregory Shellnutt, J., and Zhou, M.F., 2008. Permian, rifting related fayalite syenite in the Panxi region, SW China. *Lithos*, v.101, no.1, pp: 54-73.
- Henning, S., Sørensen and J., Richard Wilson., 1995. A strontium and neodymium isotopic investigation of the Fongen—Hyllingen layered intrusion, Norway. *Journal of Petrology*, v.36, no.1, pp: 161-187.
- Holland, T.H., 1901. The Sivamalai series of elaeolite-syenites and corundum-syenites in the Coimbatore district, Madras Presidency. *Mem. Geo. Surv. India*, v.30, pt.III, p: 169224.
- Howard, J.H., Evans, H.T., and Chapman, R.W., 1956. Occurrence and age of chevkinite from the Devil's Slide fayalite quartz syenite near Stark, New Hampshire. *American Mineralogist*, v.41, no.5-6, pp: 474-487.
- Hodson, M.E., 1998. The origin of igneous layering in the Nunarssuit syenite, South Greenland. *Mineralogical Magazine*, v.62, no.1, pp: 9-27.
- Karamsin, B.S., 1979. The Azov batholith and its structure. *Geologicheskii Zhurnal*, v.4, pp: 137-43.
- Kampunzu, A.B., Lubala, R.T., Makutu, M.N., Caron, J.P., Rocci, G., and Vellutini, P.J., 1985. Les complexes alcalins de la région interlacustre à l'est du Zaïre et au Burundi: un exemple de massifs anorogéniques de relaxation. *Journal of African Earth Sciences* (1983), v.3, no.1-2, pp: 151-167.
- Kenneth, J.T., Livi, 1987. Geothermometry of exsolved augites from the Laramie Anorthosite Complex, Wyoming. *Contributions to Mineralogy and Petrology*, v.96, no.3, pp: 371-380.
- Krishna Reddy, K., Ratnakar, J., and Leelanandam, C., 1998. A petrochemical study of the Proterozoic alkaline complex of Uppalapadu, Prakasam Province, Andhra Pradesh, India. *Geological Society of India*, v.52, no.1, pp: 41-52.
- Krivdik, S., and Tkachuk, V., 1986. Formational classification of the alkaline rocks of the Ukrainian shield. *Tezisy Dokladov VII Vesesoyuznogo Petrograficheskogo Obshestva*, pp: 85-7.
- Krivdik, S.G., Orsa, V.I., and Bryansky, V.P., 1988. Fayalite hedenbergite syenite of the western part of the korsunovogrod pluton. *Geologicheskii Zhurnal*, v.6, pp: 43-53.
- Leelanandam, C., 1989. The Prakasam Alkaline Province in Andhra Pradesh, India. *Geological Society of India*, v. 34, no.1, pp: 25-45.
- Lubala, R.T., Kampunzu, A.B., and Caron, J.P.H., 1986. Minéralogie, pétrologie et signification géodynamique du complexe alcalin et hyperalcalin du Biega (Kivu-Zaïre). *Annales de la Société géologique de Belgique*.
- Madhavan, V., Rao, J.M., Srinivas, M., Natarajan, R., and Sayeed, A., 1994. Petrology and petrogenesis of syenites from the Cuddapah basin, Andhra Pradesh. *Geological Society of India*, v.43, no.3, pp: 225-237.
- Madhavan, V.V., Rao, J.M., Chalapathi Rao., N.V., Srinivas, M., 1995. The multifaceted manifestations of an intrusive province around the Intracratonic Cuddapah basin, India. *Magmatism in Relation to Diverse Tectonic Settings-A.A. Balkema / Rotterdam*. ISBN 90 5410 275 6 pp: 93-105.
- Parsons, I., 1979. The Klokken Gabbro—Syenite Complex, South Greenland: Cryptic Variation and Origin of Inversely Graded Layering. *Journal of Petrology*, v.20, no.4, pp: 653-694.
- Petrella, L., Williams-Jones, A.E., Goutier, J., and Walsh, J., 2014. The nature and origin of the rare earth element mineralization in the Misery syenitic intrusion, northern Quebec, Canada. *Economic Geology*, v.109, no.6, pp: 1643-1666.
- Richard Wilson, J., Esbensen, K.H., and Thy, P., 1981. Igneous petrology of the synorogenic Fongen-Hyllingen layered basic complex, south-central Scandinavian Caledonides. *Journal of Petrology*, v.22, no.4, pp: 584-627.
- Roger, H Mitchell, and Platt, R.G., 1978. Mafic mineralogy of ferroaugite syenite from the Coldwell alkaline complex, Ontario, Canada. *Journal of Petrology*, v.19, no.4, pp: 627-651.
- Roger, H Mitchell., Platt, R.G., Lukosius-Sanders, J., Artist-Downey, M. and Moogk-Pickard, S., 1993. Petrology of syenites from center III of the Coldwell alkaline complex, northwestern Ontario, Canada. *Canadian Journal of Earth Sciences*, v.30, no.1, pp: 145-158.
- Rumvegeri, B.R., Caron, J.P.H., Kampunzu, A.B., Lubala, R.T., and Vellutini, P.J., 1985. Pétrologie et signification géotectonique des plutonites de Kambusi (sud Kivu, Zaïre). *Canadian Journal of Earth Sciences*, v.22, no.2, pp: 304-311.
- Sesha Sai V.V., 2013. Proterozoic Granite Magmatism along the Terrane Boundary Tectonic Zone to the East of Cuddapah basin, Andhra Pradesh – Petrotectonic Implications for Precambrian Crustal Growth in Nellore Schist Belt of Eastern Dharwar Craton, Geological Society of India, Bangalore, v.81, pp: 167-182.

- Sotaro baba, Horie, K., Hokada, T., Owada, M., Adachi, T., and Shiraishi, K., 2015. Multiple collisions in the East African–Antarctica Orogen: constraints from timing of metamorphism in the Filchnerfjella and Hochlinfjellet Terranes in central Dronning Maud Land. *The Journal of Geology*, v.123, no.1, pp: 55-77.
- Srinivasan, T.P., and Natarajan, R., 1990. Significance of fayalite (+ Quartz) assemblage in Gokanakonda syenite, Prakasam district, Andhra Pradesh. *Geological Society of India*, v.36, no.2, pp: 143-153.
- Srivastava, R.K., and Chandra, R., 1995. Magmatism in relation to diverse tectonic settings. A.A. Balkema / Rotterdam. ISBN 90 5410 275 6.
- Stephenson, D., and Upton, B.G.J., 1982. Ferromagnesian silicates in a differentiated alkaline complex: Kungnat Fjeld. *South Greenland Mineralogical Magazine*. Sep. v.46. pp: 283-300.
- Subba Rao, T., Narayana, B.L., and Gopalan, K., 1994. Rb-Sr age of the Sivamalai alkaline complex, Tamil Nadu. *Proc. Indian Acad. Sci. (Earth Planet Sci.)*, v.103, no.3, pp: 425-437.
- Miyazaki, T., Rajesh, H.M., Mohan, V.R., Rajasekaran, K.C., Kalaiselvan, A., Rao, A.T. and Rao, K.S., 1999. Field study of alkaline plutons in Tamil Nadu and Andhra Pradesh, South India, 1997-1998. *Journal of geosciences*, Osaka City University, v.42, pp: 205-214.
- Thomas Frisch and Bridgwater, D., 1976. Iron-and manganese-rich minor intrusions emplaced under late-orogenic conditions in the proterozoic of South Greenland. *Contributions to Mineralogy and Petrology*, v.57, no.1, pp: 25-48.
- Vijaya Kumar, K., Frost, C.D., Frost, B.R., and Chamberlain, K.R., 2007. The Chimakurti, Errakonda, and Uppalapadu plutons, Eastern Ghats Belt, India: an unusual association of tholeiitic and alkaline magmatism. *Lithos*, v.97, no.1, pp: 30-57.
- Vogel, D.C., Keays, R.R., James, R.S., and Reeves, S.J., 1999. The geochemistry and petrogenesis of the Agnew intrusion, Canada: a product of S-undersaturated, high-Al and low-Ti tholeiitic magmas. *Journal of Petrology*, v.40, no.3, pp: 423-450.
- Zulauf, G., Bues, C., Dörr, W., and Vejnar, Z., 2002. 10 km Minimum throw along the West Bohemian shear zone: Evidence for dramatic crustal thickening and high topography in the Bohemian Massif (European Variscides). *International Journal of Earth Sciences*, v.9 1, no.5, pp: 850-864.

Received on: 8.9.17, Revised on: 10.10.17, Accepted on: 20.10.17

Petrological and Geochemical Characterisation of the Punugodu Granite Pluton Nellore Schist Belt; Implications for Proterozoic Anorogenic Granite Magmatism in the Eastern Dharwar Craton, Southern India

¹Ch. Narshimha, ¹U.V.B. Reddy, ²V.V. Sesha Sai and ³K.S.V. Subramanyam

¹Department of Applied Geochemistry, Osmania University, Hyderabad-500 007, India

²Petrology Division, Geological Survey of India, Southern Region, Hyderabad-500068 – India

³Geochemistry Division, CSIR-NGRI, Hyderabad-500 007, India

*Corresponding Author: narsiou@hotmail.com

ABSTRACT

In this paper we present the in-situ field observations along with petrographic and geochemical results of the Punugodu granite pluton of Nellore schist belt, Eastern Dharwar Craton, South India. Located to the South of Podili alkali granite, the Punugodu granite pluton occupies an area of 7 sq. km. Field studies indicate that the Punugodu granite is deformed along the margins. Enclaves of metavolcanics and quartzite of the Nellore schist belt are observed in the pluton indicating its intrusive nature. Petrographically the rock is mainly composed of K-feldspar, with sub ordinate quartz, amphibole, biotite, pyroxene and hypersolvus in nature. Zircon, titanite, fluorite, apatite and opaques are the accessory phases. Geochemical studies reveal that the Punugodu granite indicates the metaluminous nature and exhibits calc-alkaline trend. Punugodu granite is characterised by high SiO₂ contents ranging from 69.62 % to 72.7 %, high Na₂O + K₂O, relatively low MgO contents ranging from 0.13 % to 0.76 %. The CaO-Na₂O-K₂O contents range from 10.15 % to 11.14 %. Chondrite normalised Rare Earth Elements diagram shows relative enrichment of Light Rare Earth Elements and negative europium anomaly for the Punugodu granite. It is relatively enriched in High Field Strength Elements (HFSE); Zr (85.54 to 311.83 ppm), Y (108.07 to 156.60 ppm), Nb (131.59 to 216.61 ppm) and the (36.38 to 51.62 ppm). In the Y+Nb vs Rb trace element tectonic discrimination diagram Punugodu granite falls in the within plate granite field (WPG). The high SiO₂ and Na₂O + K₂O, relatively low MgO contents along with enriched HFSE and within plate character indicates the anorogenic nature of the fluorite bearing Punugodu granite.

Key words: Punugodu granite, Nellore schist belt, EDC, India

INTRODUCTION

A-type magmatic provinces are widespread in the Earth's crust and have been formed since Archean times as a result of geodynamic processes associated with extensional tectonic environments. The diversity of rock types, with contrasting petrographic and geochemical signatures is a particular feature of A-type magmatism (Whalen et al., 1987; Eby, 1990; Poitrasson et al., 1995; Litvinovsky et al., 2002; Vilalva and Vlach, 2014). Proterozoic A-type granite magmatism was reported along the eastern margin of the Cuddapah basin (Reddy, 1989; 1991). Moeen, (1998), carried out mineralogical studies and P-T estimates of the Nellore schist belt (NSB) litho units. Close to the eastern margin of the Cuddapah basin (Nagaraja Rao et al., 1987; Tripathy and Saha, 2015), a regional curvilinear shear zone defined as Terrain boundary shear zone (TBSZ) was demarcated along the western margin of the Nellore schist belt (Chetty and Murthy, 1994; Chetty, 1999). The TBSZ has been interpreted as a crustal scale

shear zone and a major tectonic feature to the west of the Eastern Ghat Granulite belt (EGMB) of South India (Chetty, 2017). Significant zone of Proterozoic granite magmatism was demarcated in the NSB; close to the eastern margin of the Proterozoic Nallamalai Fold Belt (Sesha Sai, 2013a; Sesha Sai, 2016). Presence of calc silicate bands close to the vicinity of Kanigiri granite and Podili granite is recorded (Prasada Rao and Ahluwalia, 1974). Presence of pyroclastic volcanism in the form of agglomerate was reported by Srinivasan and Roop Kumar (2007). Rare metal mineralisation in the granite around Kanigiri area is reported by Banerjee et al., (1983), while Dharma Rao and Reddy (2007) carried out trace element and geochronological studies on the Kanigiri granite. The Mesoproterozoic Kanigiri granite (Gupta et al., 1984; Sain et al., 2017) is located to the west of Punugodu pluton. Punugodu granite pluton was initially noticed by Reddy and Sesha Sai (2003). Saha et al., (2015), studied the tectono stratigraphic evolution of the Nellore schist belt. We present the in-situ field observations in addition to petrographic

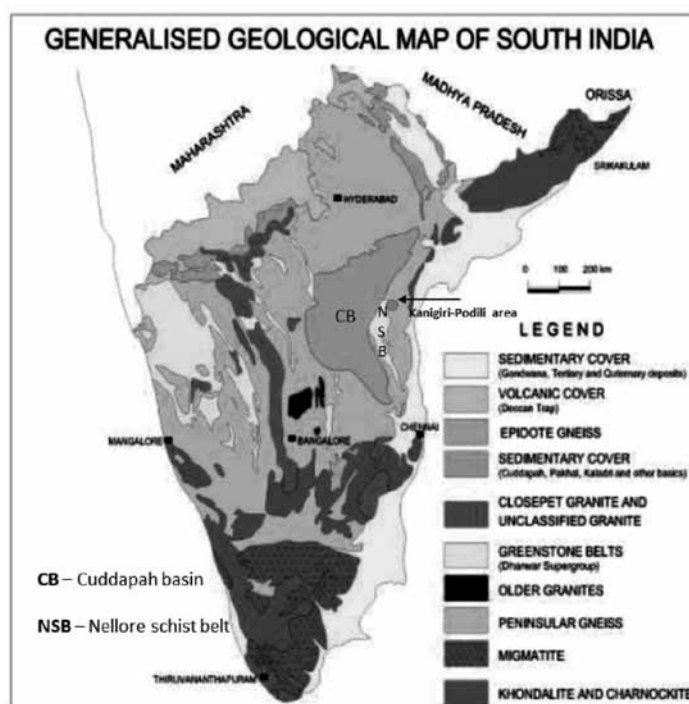


Figure 1. Geological Map of South India showing the location of the Kanigiri-Podili area to the east of Cuddapah basin, Eastern Dharwar Craton, SE India (modified after GSI, 2013).

and geochemical details of the Punugodu granite pluton of Nellore schist belt and explain the spatial relationship of the pluton with adjoining NSB litho units.

GEOLOGY OF PUNUGODU AREA

The Punugodu granite pluton is located in the Northern part of the NSB in Eastern Dharwar Craton (EDC), SE India (Figure 1). The Punugodu pluton is an N-S trending oval body that occupies an area of about 7 sq. km. Field studies indicated two sets of fractures (i) N-S trending vertical fractures and (ii) NNW-SSE trending sub-vertical fractures with steep easterly dips. Geologically the area around Punugodu comprises metavolcanic and metasedimentary sequences of the Neoproterozoic NSB (Ravikant, 2010). The rocks the NSB are intruded by granites (Figure 2) of Proterozoic age (Gupta et al., 1984; Dharma Rao and Reddy, 2007; Sessa Sai, 2013a; Sain et al., 2017) and mafic dykes of dolerite and gabbro composition (Srinivasan and Roop Kumar, 1995). Quartzo-feldspathic veins traverse the granites in N-S and WNW-ESE directions (Sessa Sai, 2006). The Podili alkali granite (Prasad Rao and Ahluwalia, 1974; Sessa Sai, 2004; 2013a) lies to the north of Punugodu pluton, while the Kanigiri granite lies to its west (Figure 2).

To the northeast of the Punugodu granite, highly deformed biotite granite is reported at Andhra Konda (Sessa Sai, 2004). Detailed field, petrographic and petrochemical characterisation of the granitic rocks around Kanigiri –

Podili area is carried out and the comparative studies on field, petrography, mineral chemistry and geochemistry are provided in a tabular form (for details see Sessa Sai, 2013a). Astrophyllite bearing alkali granite was reported along the western margin of the Podili pluton (Sessa Sai, 2013b). An olivine gabbro is noticed in the form of an intrusive dyke to the South of Kanigiri granite and South west of Punugodu pluton (Srinivasan and Roop Kumar, 1995).

Contact thermal effect resulted in the formation of hornfels rocks that are noticed mainly along the margins of the Punugodu pluton with the host NSB lithounits (Figure 2a). Remnants of schistose rocks and quartzites of NSB are noticed in the upper parts the pluton (Narshimha et al., 2016). However, the presence of NSB volcanic enclaves in the pluton indicates its intrusive nature.

Field and Petrography

The Punugodu granite is mesocratic, phaneritic, massive equigranular and coarse grained. It is exposed as a low-lying hillock (Figure 3a) to the south of Podili pluton in northern part of the NSB. Enclaves of metavolcanics and calc-silicate rock of NSB are also found in the Punugodu pluton (Figure 3b). At places clusters of mafic minerals and deep blue fluorite crystals are noticed in the Punugodu granite, when examined with hand lens. Petrographic studies indicate that the rock is hypersolvus in nature.

Petrological and Geochemical Characterisation of the Punugodu Granite Pluton Nellore Schist Belt; Implications for Proterozoic Anorogenic Granite Magmatism in the Eastern Dharwar Craton, Southern India

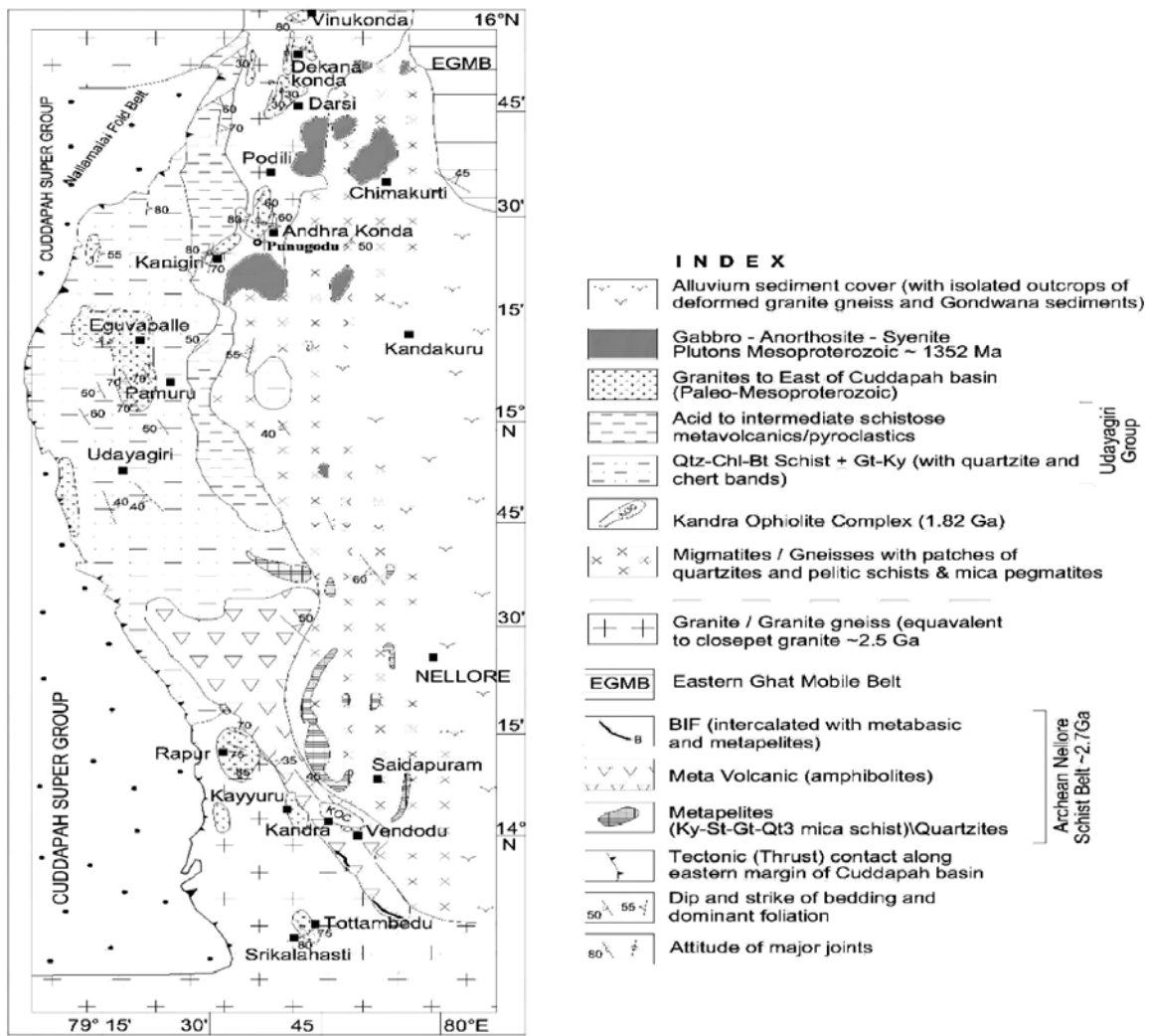


Figure 2. Geological Map of Nellore Schist Belt and adjoining areas, Andhra Pradesh, India showing the location of Proterozoic Granite Plutons.

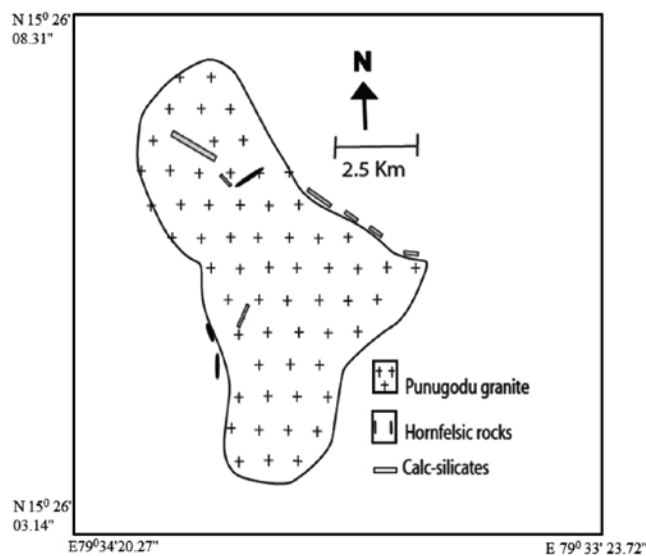


Figure 2a. Geological Map of the Punugodu Granite Pluton, Northern part of the Nellore schist belt, EDC, India.

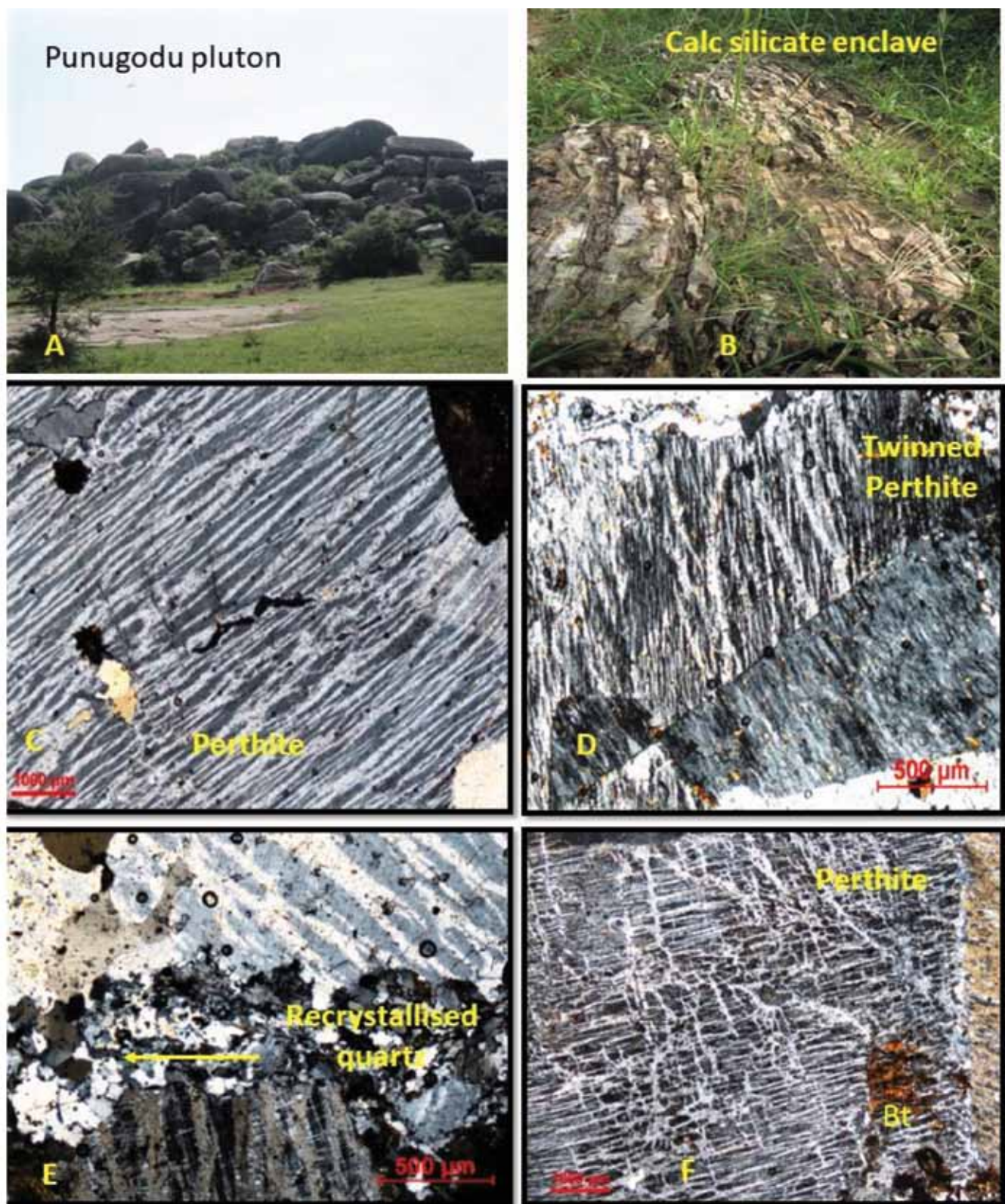


Figure 3. A. Field photograph showing the Punugodu pluton. B. Field photograph showing the calc silicate enclave in Punugodu pluton C. Photomicrograph in cross nicols showing the perthite intergrowth in Punugodu granite D. Photomicrograph in cross nicols showing the twinned perthite in Punugodu granite E. Photomicrograph in cross nicols showing recrystallized quartz within the perthitic K-feldspar F. Photomicrograph in cross nicols showing the string type micropertthite with inclusions of biotite

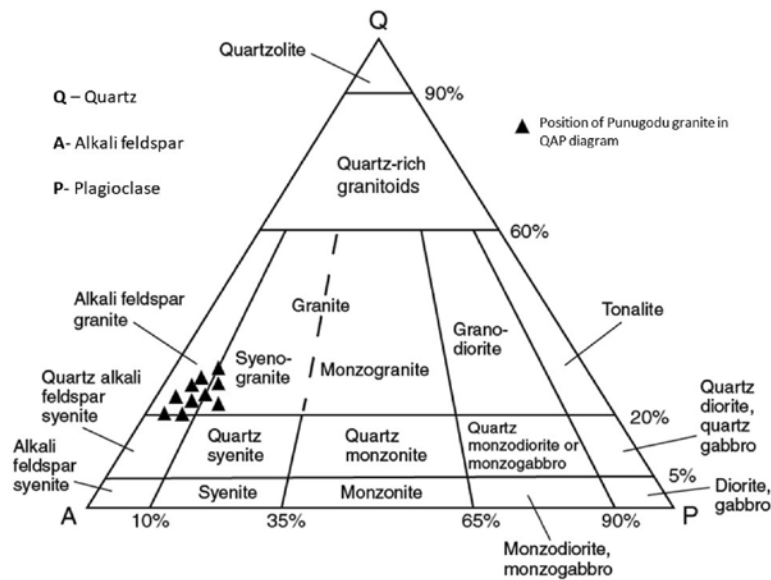


Figure 4. Position of Punugodu granite in QAP diagram (after Streckeisen, 1974).

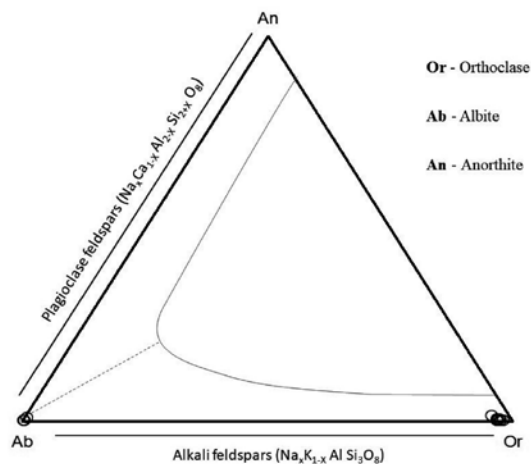


Figure 4a. Position of alkali feldspar host and plagioclase exsolved lamellae of Punugodu granite in the Or-Ab-An feldspar mineral chemistry diagram

Perthitic alkali feldspar (Figure 3c) is the dominant mineral phase in the rock followed by quartz, biotite and amphibole. Zircon, titanite, fluorite, apatite and opaques are the accessory minerals. Relict clinopyroxene is noticed at places. Quartz is anhedral and often shows wavy extinction and occurs amidst the larger perthite grains. Biotite is interstitial and pleochroic in shades of brown. Hornblende is pleochroic in shades of green to brown. At places clusters of biotite and amphibole are noticed in Punugodu granite. Alkali feldspar is mainly represented by microcline. Perthite intergrowth texture is prominently noticed in the rock. At places coarse grained perthite exhibits twinning (Figure 3d). Recrystallised quartz is noticed amidst large perthite grains. An admixture of relatively small size quartz grains along with minor amounts of biotite is noticed at places giving

rise to development of mortar texture indicating deformed state of the rock (Figure 3e). String type of perthite is dominant among the intergrowth alkali feldspar (Figure 3f). Inclusions of biotite are often noticed in the perthite grains (Figure 3f). Fluorite is interstitial in nature. Apatite is euhedral and occurs as both discrete grains as well as inclusion in mafic phases. Zircon and titanite are noticed as euhedral grains and are often associated with the mafic minerals. Zircon is also seen as minute euhedral inclusions in perthite grains. In the IUGS QAP diagram (Streckeisen, 1974), the Punugodu granite mainly falls in the field of alkali feldspar granite (Figure 4). However, a few samples also fall at the boundary of granite-alkali feldspar granite and at the boundary of alkali feldspar quartz syenite and alkali feldspar granite.

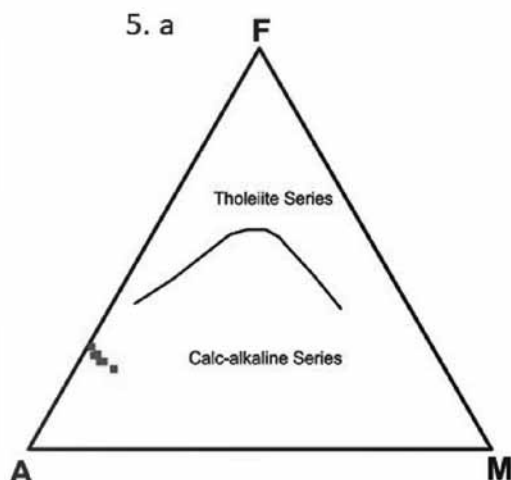


Figure 5a. Punugodu granite exhibition calc alkaline nature in AFM diagrams (Irvine and Barager, 1971).

Feldspar mineral chemistry

To ascertain the mineral chemistry of the perthitic feldspar from the Punugodu granite Electron Probe Micro Analyses (EPMA) was carried out. Analytical results indicate that the host alkali feldspar is close to the orthoclase end member composition with $Or_{95.10 \text{ to } 97.51}$ and the exsolved plagioclase in the perthite is near albite end member composition with $An_{98.78 \text{ to } 99.63}$ (Figure 4a). Exsolved lamellae of albite analysed $Na_2O - 11.40\%$ to 11.73% , $K_2O - 0.07\%$ to 0.12% , $CaO - 0.11\%$, $SiO_2 - 68.21\%$ to 68.31% , $Al_2O_3 - 19.52\%$ to 19.76% , while the host K-feldspar analyses $K_2O - 15.53\%$ to 16.14% , $Na_2O - 0.34\%$ to 0.39% , $SiO_2 - 63.49\%$ to 64.53% , $Al_2O_3 - 17.91\%$ to 18.93% . EPMA analyses were carried out at Southern Region Petrological Laboratory, GSI, and Hyderabad with the aid of CAMECASx100. Analyses conditions: Accelerating voltage: $15kV$, current: $12nA$ and Beam size: 1μ . All natural standards have been used except for Mn and Ti, for which synthetic standards have been used. Major oxide analyses were carried out by XRF method at the Geological Survey of India, Chemical Laboratory, Southern Region and Hyderabad.

Geochemistry

The Punugodu granite is characterised by high SiO_2 contents ranging from 69.62% to 72.7% , high $Na_2O + K_2O$, relatively low MgO contents ranging from 0.13% to 0.76% . The Al_2O_3 content ranges from 11.74% to 13.44% and the TiO_2 content ranges from 0.30% to 0.37% . The K_2O contents (5.65 to 6.44%) are more

5. b A/CNK-A/NK plot (Shand 1943)

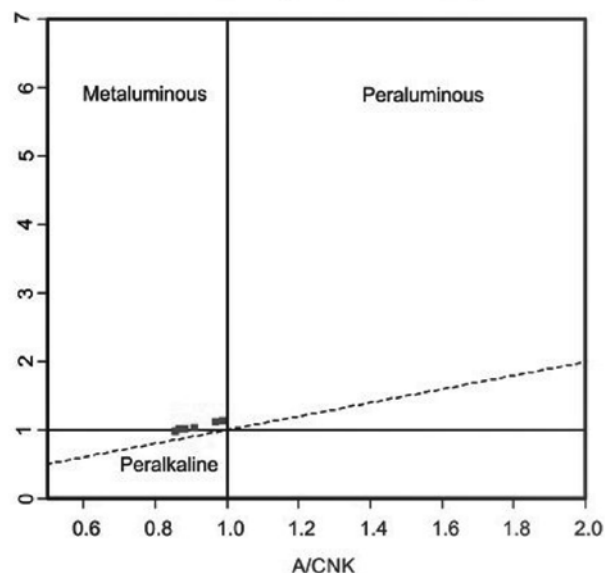


Figure 5b. Metaluminous nature of Punugodu granite on A/NK-A/CNK diagram (Shand, 1943).

than the Na_2O contents (3.31 to 3.73%) in the alkali feldspar dominated Punugodu granite. The CaO content is relatively low and ranges from 0.93% to 1.18% , characteristic in metaluminous syenites. The $CaO-Na_2O-K_2O$ contents range from 10.15% to 11.14% and less than the Al_2O_3 content in the Punugodu granite, indicating the metaluminous nature. In the A/NK – A/CNK diagram (Shand, 1943), some samples from the Punugodu granite fall close to the boundary of metaluminous – peralkaline field (Figure 5b). Geochemical studies indicate that the Punugodu granite is metaluminous in nature and exhibits calc alkaline trend (Figure 5a and Figure 5b).

Trace element geochemistry indicates incompatible element enrichment in the Punugodu granite. Relatively higher values of high field strength elements (HFSE) are analysed; Zr values range from 85.54 to 311.83 ppm, Y values range from 108.07 to 156.60 ppm and Nb values range from 131.59 to 216.61 ppm. Th values range from 36.38 to 51.62 ppm and Ta values range from 4.65 to 11.25 ppm. Among the Large ion lithophile elements (LILE), relatively higher values of rubidium range from 179.08 to 251.74 ppm in the Punugodu granite. In the Y+Nb vs Rb trace element tectonic discrimination diagram (Pearce et al., 1984), the Punugodu granite falls in the Within plate granite field (WPG). Chondrite normalised Rare Earth Element (REE) diagram shows relative enrichment of Rare Earth Element Elements (LREE) and negative europium (Eu) anomaly for the Punugodu granite and the Eu / Eu^* values range from 0.04 to 0.07 . The Σ REE contents in Punugodu granite range from 648.29 to 1829.45 ppm indicating an overall REE enriched nature of Punugodu pluton.

Petrological and Geochemical Characterisation of the Punugodu Granite Pluton Nellore Schist Belt; Implications for Proterozoic Anorogenic Granite Magmatism in the Eastern Dharwar Craton, Southern India

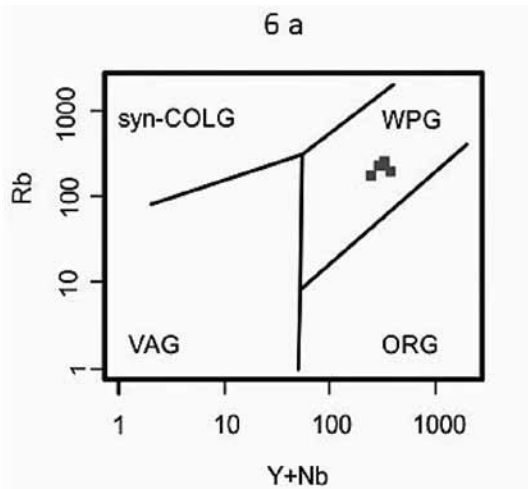


Figure 6a. Y+Nb vs Rb trace element tectonic discrimination diagram (Pearce et al., 1984), showing the WPG nature of Punugodu granite.

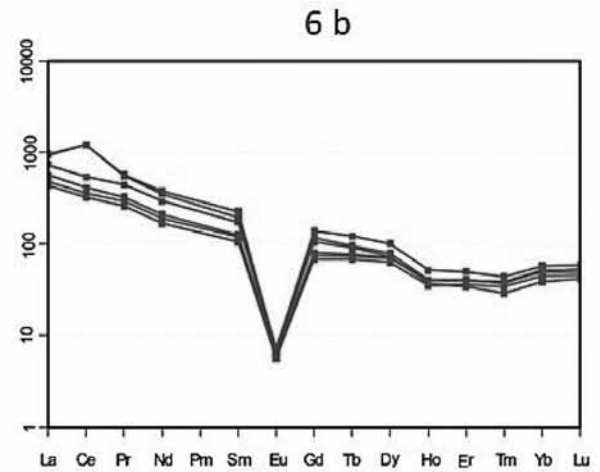


Figure 6b. Chondrite normalised REE diagram showing LREE enrichment and negative Eu anomaly for the Punugodu granite.

Table 1. Major oxide analyses of Punugodu granite, Nellore schist belt, EDC, India

Sample	PG-3	PG-5	PG-6	PG-8	PG-9	PG-10
SiO ₂	71.17	71.18	69.77	71.39	69.62	72.7
Al ₂ O ₃	13.3	12.45	13.23	13.44	13.34	11.74
Fe ₂ O ₃	3.6	2.93	3.58	3.2	3.36	3.02
MnO	0.07	0.06	0.07	0.05	0.06	0.05
MgO	0.13	1.1	0.45	0.32	0.76	0.58
CaO	0.99	1.18	1.15	0.96	0.93	0.97
Na ₂ O	3.31	3.54	3.73	3.39	3.67	3.55
K ₂ O	6.02	5.91	6.26	5.8	6.44	5.65
TiO ₂	0.37	0.3	0.35	0.3	0.3	0.27
P ₂ O ₅	0.02	0.05	0.03	0.02	0.03	0.03
LOI	0.64	0.68	0.82	0.54	0.68	0.52
SUM	99.62	99.38	99.44	99.41	99.19	99.08
CIPW Norm						
Q	26.87	25.00	22.07	27.07	21.35	28.82
C	0	0	0	0	0	0
Or	35.57	34.92	36.99	34.27	38.05	33.39
Ab	28.00	29.95	31.56	28.68	31.05	28.92
An	3.652	0.625	0.867	4.325	0.905	0
Ne	0	0	0	0	0	0
Ac	0	0	0	0	0	0.978
Di	0.089	3.186	2.418	0	2.104	3.014
Wo	0	0	0.247	0	0	0
Hy	0.283	1.263	0	0.797	0.918	0.048
Ol	0	0	0	0	0	0
Il	0.15	0.15	0.128	0.15	0.107	0.128
Hm	3.6	4.62	2.93	3.58	3.2	3.36
Tn	0.715	1.034	0.571	0.666	0.217	0.571
Pf	0	0	0	0	0	0
Ru	0	0	0	0	0.156	0
Ap	0.047	0.284	0.118	0.071	0.047	0.071
Sum	98.99	98.64	98.71	98.63	98.88	98.52

Table 2. Trace and rare earth element analyses of Punugodu granite, NSB, EDC, India

Sample	PG-3	PG-5	PG-6	PG-8	PG-9	PG-10
Sc	1.849	1.779	1.905	1.924	1.923	1.852
V	2.001	1.426	1.557	1.283	1.256	1.229
Cr	7.864	7.92	8.06	8.175	8.081	8.308
Co	0.401	0.373	0.406	0.541	0.481	0.57
Ni	1.513	1.407	1.276	1.196	1.169	1.358
Cu	0.481	0.497	0.496	0.471	0.472	0.444
Zn	42.31	37.552	48.865	45.125	52.406	38.759
Ga	37.556	37.025	38.915	36.924	40.41	35.427
Rb	197.34	179.08	224.74	241.15	251.47	225.28
Sr	9.589	10.82	10.401	11.414	9.872	8.391
Y	156.60	108.07	129.48	137.87	137.49	123.57
Zr	128.39	85.54	153.56	278.95	311.83	275.63
Nb	216.61	131.59	194.90	183.02	188.05	167.13
Cs	1.589	1.527	1.95	1.936	2.011	1.646
Ba	32.67	39.95	37.364	58.361	56.391	69.456
Hf	4.861	3.238	6.121	10.238	12.918	10.056
Ta	8.188	4.657	8.178	8.065	11.259	8.52
Pb	17.396	16.942	17.287	21.497	19.788	14.544
Th	51.627	36.388	47.13	42.974	45.006	39.198
U	5.953	3.755	5.182	6.428	6.423	8.369
La	312.75	242.53	320.03	187.86	161.25	144.13
Ce	1056.6	469.78	1047.8	359.97	314.77	280.37
Pr	64.947	49.94	62.215	36.84	32.94	29.15
Nd	238.74	184.5	224.23	133.2	119.4	105.7
Sm	46.258	35.48	39.358	25.72	24.04	21.57
Eu	0.542	0.487	0.572	0.475	0.468	0.431
Gd	38.263	29.15	32.084	22.14	20.69	18.84
Tb	5.72	4.258	4.562	3.644	3.488	3.193
Dy	34.824	25.22	27.388	24.42	23.86	21.70
Ho	3.629	2.585	2.849	2.787	2.757	2.472
Er	11.218	7.711	9.213	9.042	8.975	8.191
Tm	1.318	0.863	1.104	1.13	1.156	1.034
Yb	12.636	8.536	11.076	10.84	11.33	9.978
Lu	2.011	1.413	1.815	1.656	1.786	1.537
Eu/Eu*	0.04	0.05	0.05	0.06	0.06	0.07
ΣREE	1829.5	1062.	1784.3	819.8	726.9	648.4

DISCUSSION

Anorogenic granites are emplaced in extensional setting and are characterised by their distinct mineralogy and geochemistry (Loiselle and Wones, 1979; Whalen et al., 1987; Eby, 1990). Presence of fluorite and interstitial biotite, high SiO₂, Na₂O + K₂O contents, low CaO, Sr contents along with enriched Zr, Y, Rb, high REE contents in Punugodu hypersolvus granite and LREE enrichment indicate anorogenic character for the Punugodu granite. Thorium values range from 36.38 ppm to 51.62 ppm. Pronounced negative Eu anomaly coupled with significant

enrichment of the Light rare earth elements (LREE) ranging from 580.92 to 1719.29 ppm indicates an enriched crustal source. Hypersolvus anorogenic granites of Proterozoic age have been reported from the Labrador (eg Collerson, 1982). Punugodu pluton is located to the south of Podili pluton and falls within the Proterozoic granite magmatism zone, close to the eastern margin of the Cuddapah basin (Sessa Sai, 2013a) in EDC. Both the hypersolvus Podili alkali granite and the sub solvus Kanigiri biotite are fluorite bearing and are geochemically characterised by high SiO₂, Na₂O + K₂O contents, low CaO, Sr contents and enriched HFSE contents (Sessa Sai, 2013a).

Petrological and Geochemical Characterisation of the Punugodu Granite Pluton Nellore Schist Belt; Implications for Proterozoic Anorogenic Granite Magmatism in the Eastern Dharwar Craton, Southern India

Table 3. EPMA analyses of the feldspar from the Punugodu granite, NSB, EDC, India.

SiO ₂	63.48	68.30	64.89	69.30	64.39	64.63	64.56	68.21	64.53	68.35	63.79	63.72
Al ₂ O ₃	17.91	19.51	18.25	19.49	18.22	18.20	18.25	19.76	18.13	19.60	17.42	17.73
FeO	0.17	0.04	0.11	0.08	0.04	0.17	0.15	0.13	0.02	0.04	0.46	0.61
CaO	0.24	0.11	0.00	0.01	0.00	0.00	0.00	0.00	0.07	0.00	0.05	0.00
Na ₂ O	0.39	11.40	0.34	11.63	0.38	0.27	0.36	11.73	0.34	11.49	0.29	0.23
K ₂ O	15.53	0.12	15.97	0.10	16.01	15.96	15.69	0.07	16.14	0.09	16.37	16.48
MgO	0.02	0.01	0.00	0.00	0.01	0.01	0.00	0.00	0.00	0.00	0.00	0.08
Cations on the basis of 32 oxygen												
Si	12.00	11.98	12.03	12.02	12.01	12.02	12.02	11.94	12.02	11.98	12.04	11.98
Al	3.99	4.03	3.99	3.98	4.00	3.99	4.01	4.07	3.98	4.05	3.87	3.93
Fe(ii)	0.03	0.01	0.02	0.01	0.01	0.03	0.02	0.02	0.00	0.01	0.07	0.10
Ca	0.05	0.02	0.00	0.00	0.00	0.00	0.00	0.00	0.01	0.00	0.01	0.00
Na	0.14	3.88	0.12	3.91	0.14	0.10	0.13	3.98	0.12	3.90	0.11	0.08
K	3.74	0.03	3.77	0.02	3.81	3.79	3.73	0.01	3.83	0.02	3.94	3.95
Mg	0.01	0.00	0.00	0.00	0.00	0.00	0.00	0.00	0.00	0.00	0.00	0.02
TOTAL	19.95	19.95	19.93	19.95	19.96	19.92	19.91	20.02	19.97	19.96	20.05	20.07
End members												
An	1.23	0.54	0.00	0.05	0.00	0.00	0.02	0.00	0.33	0.00	0.26	0.00
Ab	3.67	98.78	3.09	99.41	3.45	2.49	3.39	99.63	3.05	99.52	2.61	2.09
Or	95.10	0.68	96.91	0.53	96.55	97.51	96.59	0.37	96.62	0.48	97.13	97.91

Anorogenic granites are characteristically emplaced in extension tectonic setting and are characterised by their distinct mineralogy, whole rock and trace element composition (Loiselle and Wones, 1979; Collins et al., 1982; Whalen et al., 1987; Eby, 1990).

In the Y+Nb vs Rb trace element tectonic discrimination diagram, the Punugodu granite falls in the within plate granite field (WPG).

CONCLUSION

The paper presents the field, petrographic and geochemistry of the Punugodu granite pluton of Nellore schist belt, Eastern Dharwar Craton, South India. The deformed nature along the margins and presence of enclaves of metavolcanics of the Nellore schist belt indicate the intrusive nature. The alkali feldspar enriched Punugodu granite falls to the south of the Podili alkali granite pluton. Presence of fluorite, apatite and interstitial biotite, high SiO₂ and Na₂O + K₂O, relatively low MgO and relatively enriched in HFSE contents along with the within plate character in the trace element tectonic discrimination plot indicates its anorogenic nature.

ACKNOWLEDGEMENTS

The first author expresses sincere gratitude to University Grant Commission, New Delhi for providing financial assistance under BSR-RFSMS Fellowship scheme. Sincere thanks are due to Head and faculty members of department of Applied Geochemistry, Osmania University, Hyderabad

for their encouragement and valuable suggestions. Dr. Vikash Tripathy of Geological Survey of India is thankfully acknowledged for critical review and helpful suggestions. Dr. P.R. Reddy, Chief Editor, JIGU is thanked for editorial handling.

Compliance with Ethical Standards

The authors declare that they have no conflict of interest and adhere to copyright norms.

REFERENCES

- Banerjee, D.C., Maithani, P.B., Ranganath, N., and Jayaram, K.M.V., 1983. Rare-metal mineralisation in granitic rocks of Kanigiri area in the Prakasam district, Andhra Pradesh, India. *Chemical Geology*, v.39, pp: 319-334.
- Chetty, T.R.K. and Murthy, D.S.N., 1994. Collision tectonics in Eastern Ghats Mobile Belt: Mesoscopic to Satellite scale structural observations. *Terra Nova*, v. 6, pp: 72-81.
- Chetty, T.R.K., 1999. Some observations on the tectonic framework of Southeastern Indian Shield. *Gondwana Res.*, v.2, pp: 651-653
- Chetty, T.R.K., 2017. Proterozoic Orogens in India; A critical Window to Gondwana. Elsevier publication. p:426
- Collerson, K.D., 1982. Geochemistry and Rb-Sr geochronology of associated Proterozoic peralkaline and sub alkaline anorogenic granites from Labrador. *Contributions to Mineralogy and Petrology*, v.81, no.2, pp: 126-147
- Collins, W.J., Beams, S.D., White, A.J.R., Chappell, B.W., 1982. Nature and origin of A-type granites with particular reference

- to southeastern Australia. *Contributions to Mineralogy and Petrology*, v.80, pp: 189–200.
- Dharma Rao, C.V. and Reddy, U.V.B., 2007. Petrology and geochemistry of Paleoproterozoic A-type granite at Kanigiri in the Nellore Khammam schist belt, Andhra Pradesh, India. *Journal of Asian Earth Sciences*, v.30, no.1, pp: 1-19.
- Eby, G.N., 1990. The A-type granitoids: a review of their occurrence and chemical characteristics and speculations on their petrogenesis. *Lithos*, v.26, pp: 115-134.
- GSI, 2013. Geological Survey of India, Southern Region, Briefing Book, March 2013. pp: 1-291
- Gupta, J.N., Pandey, B.K., Chabria, T., Banerjee, D.C., and Jayaram, K.M.V., 1984. Rb-Sr geochronological studies of the granites of Vinukonda and Kanigiri, Prakasam district, Andhra Pradesh, India. *Precambrian Research*, v.26 pp:105-109.
- Irvine, T.N., and Baragar, W.R.A., 1971. A guide to the chemical classification of the common volcanic rocks: *Canadian Journal of Earth Sciences*, v. 8, pp: 523-548.
- Litvinovsky B.A., Jahn B., Zanzvilevich A.N., Saunders A., Poulain S., Kuzmin D.V., Reichow M.K. and Titov A.V., 2002. Petrogenesis of syenite–granite suites from the Bryansky Complex (Transbaikalia, Russia): implications for the origin of A-type granitoid magmas. *Chem Geol*, v.189, pp: 105-133.
- Loiselle, M.C., Wones, D.R., 1979. Characteristics and origin of anorogenic granites. *Geological Society of America Abstracts with Programs*, v.11, no.7, p: 468.
- Moenen, S., 1998. P-T estimates from the Nellore schist belt (India) and evidence for superimposed metamorphic events. *Geological Journal*, v.33, no.1, pp: 1–15
- Nagaraja Rao, B.K., Ramalingaswamy, G., Rajurkar, S.T., 1987. Stratigraphy, structure and evolution of the Cuddapah basin. In: *Purana basins of Peninsular India*. Geological Society of India Memoir v.6, pp: 33-86.
- Narshimha, Ch., Subramanyam, K.S.V., and Reddy, U.V.B., 2016. Enclaves of diverse origin in Punugodu granite pluton, Prakasam District, Andhra Pradesh, India: Implications for source rock composition and crustal contamination. Abstract, 35th International Geological Congress, Cape Town., p: 3920.
- Pearce, J.A., Harris, N.B.W., Tindle, A.G., 1984. Trace element discrimination diagrams for the tectonic interpretation of granitic rocks. *Jour. of Petrology*. v.25, pp: 956-983.
- Poitrasson, E, Duthou, J.L. and Pin C., 1995. The relationship between petrology and Nd isotopes as evidence for contrasting anorogenic granite genesis: Example of the Corsican Province (SE France). *J. Petrol*, v.36, pp: 1251-1274
- Prasada Rao, A.D., Ahluwalia, A.D., 1974. Geology of parts of Podili and Darsi taluks, Prakasam district, Andhra Pradesh. *Geol. Surv. Ind. Prog. Rep.* pp: 1973-74 (Unpublished).
- Ravikant, V., 2010. Palaeoproterozoic (~1.9 Ga) extension and breakup along the eastern margin of the Eastern Dharwar Craton, SE India: new Sm–Nd isochron age constraints from anorogenic mafic magmatism in the Neoproterozoic Nellore greenstone belt. *Journal of Asian Earth Sciences*, v.37, pp: 67–81.
- Reddy, U.V.B., 1989. Proterozoic anorogenic magmatism along the eastern margin of the Cuddapah basin, Andhra Pradesh, India. In: *Workshop Vol., Proterozoic Rocks of India*, pp: 79-80.
- Reddy, U.V.B., Sessa Sai, V.V., 2003. Occurrence of rare Rhyodacite from the Kanigiri area, Prakasam District, Andhra Pradesh. *Ind. Acad. Geosci.*, v.46, pp: 25-27.
- Reddy, U.V.B., 1991. Granite magmatism east of Cuddapah basin. *Jour. Indian Acad. Geosci.*, v.34, pp: 1-6.
- Saha, D., Sain, A., Nandi, P., Mazumder, R., Kar, R., 2015. Tectonostratigraphic evolution of the Nellore schist belt, southern India, since the Neoproterozoic. In: *Mazumder, R., Eriksson, P.G., Edited Precambrian Basins of India: Stratigraphic and Tectonic Context*. Geological Society, London, v. 43, pp: 269-282.
- Sain, A., Saha, D., Joy, S., Jelsma, H., Armstrong, R., 2017. New SHRIMP Age and Microstructures from a Deformed A-Type Granite, Kanigiri, Southern India: Constraining the Hiatus between Orogenic Closure and Post orogenic Rifting. *Journal of Geology*. v.125, no.2, pp: 241-259
- Sessa Sai, V.V., 2004. Petrographic and Petrochemical characterisation of Proterozoic granites in Nellore schist belt and northeastern fringes of Cuddapah basin. *Rec. Geol. Surv. Ind.* v.137, no.5, pp: 184-188.
- Sessa Sai, V.V., 2006. Petrographic and Petrochemical characterisation of Proterozoic granites in Nellore schist belt and northeastern fringes of Cuddapah basin. *Unpub. Progress Report Geol. Surv. Ind.* FS 2001-2002 and 2002-2003. pp: 20.
- Sessa Sai, V.V., 2013 a. Proterozoic Granite Magmatism along the Terrane Boundary Tectonic Zone to the East of Cuddapah Basin, Andhra Pradesh – Petrotectonic Implications for Precambrian Crustal Growth in Nellore Schist Belt of Eastern Dharwar Craton. *Journal of Geological Society of India*, v.81, pp: 167-182
- Sessa Sai, V.V., 2013 b. Occurrence of rare titanium–niobium-rich astrophyllite in the Podili alkali granite pluton, Prakasam district, Andhra Pradesh, India. *Current Science*.v.104, no.10, pp: 1290-1293
- Sessa Sai, V.V., 2016. Proterozoic ferroan feldspathic magmatism in Eastern Dharwar Craton; Constraints from the petrogenesis of Mesoproterozoic granite magmatism to the East of the Nallamalai Fold Belt, SE India. 35th International Geological Congress, Cape Town, South Africa, 2016, Abstract # PB 105
- Shand, S. J., 1943. *The Eruptive Rocks*, 2nd edn. New York: John Wiley, p: 444.
- Srinivasan, K.N. and Roop Kumar, D., 1995. Geological mapping of Podili-Kanigiri section in northern part of Nellore schist belt, Prakasam district, AP. Unpublished progress report of G.S.I. FS 1992-93

Petrological and Geochemical Characterisation of the Punugodu Granite Pluton Nellore Schist Belt; Implications for Proterozoic Anorogenic Granite Magmatism in the Eastern Dharwar Craton, Southern India

- Srinivasan, K.N. and Roopkumar, D., 2007. Certain geological observations in Peddarikatla-Kanigiri area, Prakasam District, Andhra Pradesh. Proc. A.P. Akademi of Science, Hyderabad. v.11, no.1, pp: 89-93.
- Streckeisen, A.L., 1974. Classification and Nomenclature of Plutonic Rocks. Recommendations of the IUGS Subcommittee on the Systematics of Igneous Rocks. Geologische Rundschau. Internationale Zeitschrift für Geologie. Stuttgart. v.63, pp: 773-785.
- Tripathy, V., and Saha, D., 2015. Inversion of calcite twin data, paleostress reconstruction and multi-phase weak deformation in cratonic interior – Evidence from the Proterozoic Cuddapah Basin, India. Journal of Structural Geology, v.77, pp: 62-81.
- Vilalva F.C.J. and Vlach S.R.F., 2010. Geology, petrography and geochemistry of the A-type granites from the Morro Redondo Complex (PR-SC), southern Brazil, Graciosa Province. Anais da Academia Brasileira de Ciências (2014), v.86, no.1, pp: 85-116
- Whalen J.B., Curie K.L. and Chappel B.W., 1987. A-type granites: Geochemical characteristics, discrimination and petrogenesis. Contributions to Mineralogy and Petrology, v.95, pp: 407-419.

Received on: 2.12.2017, Revised on:25.12.2017, Accepted on:27.12.2017

Long range forecast and development of a weak southwest monsoon during 2017- Pt. I: Long range forecast

Onkari Prasad*, O. P. Singh¹ and K.Prasad²

¹43, Ritu Apartments, A-4 Paschim Vihar, New Delhi-110063

²B44, First Floor, Parshvath Paradise, Mohan Nagar, Ghaziabad (U.P.)-201007

³D-104, Seema Apartments, Sector 11, Dwarka, New Delhi-110085

*Corresponding Author: prasadonkari123@yahoo.in

ABSTRACT

India received below normal rainfall during 2017 southwest monsoon. Formulation of Long Range Forecast (LRF), based on South Indian Ocean Convergence Zone (SIOCZ) model and the results of verification of the forecasts at district and subdivision levels and for India as a whole have been discussed in this part of the study. For the sake of comparison, the forecast from the operational models have also been reproduced. The results of verification have shown that SIOCZ model's district level forecast was in 'Excellent' category in the states of Tamilnadu, Andhra Pradesh, Himachal Pradesh, Maharashtra and Goa and in 'Very Good' category in Telangana. At the subdivision level forecast was in 'Excellent' category in the months of June, July and August and in 'Very Good' category in September. The forecast for bi-monthly rainfall was in 'Excellent' category for all the three bi-monthly periods of Jun+ Jul, Jul+ Aug and Aug+ Sep and also for the season as a whole (Jun-Sep). For India as a whole, forecast was in 'Useful' category in August and September and during the bi-monthly periods of Jul+ Aug and Aug+ Sep. An Update had been issued in August for improvement of rainfall during the second half of the season. However, the improvement in rainfall did not take place over Central and Northwest India. Instead it remained confined to south Peninsula only.

Key words: Southwest monsoon, South Indian Ocean Convergence Zone model, Long range forecast, Update, Forecast verification.

INTRODUCTION

Long range forecasting of monsoon rainfall has continued to remain an important aspect of weather forecasting in India, ever since the first Long Range Forecast (LRF) of monsoon rainfall was issued by IMD in 1886 (Blanford,1884). With changes, from time to time, in number of parameters used for preparing the forecast, its format and content, issuing of operational LRF of monsoon rainfall using parametric models has continued till date. But, the operational models often fail to foreshadow the extreme seasons (Drought/ Excess monsoons), e.g., the deficiency in rainfall, for India as a whole, during four consecutive years, 1984 (-4%), 1985(-8%), 1986 (-13%) and 1987 (-18%) could not be forecast. Failure of the operational models in foreshadowing the deficiency, in any of these four years, became a cause of concern. An urgent need was felt to improve long range forecasting of monsoon rainfall. Department of Science and Technology (DST), IMD and the Indian Institute of Tropical Meteorology (IITM) jointly proposed Parametric and Power Regression Models (Gowariker et al., 1989) as an improvement to the existing models. Real time forecast from the models became available from 1989 onwards. After the failure of the improved models in foreshadowing the drought in 2002, efforts were made by IMD to further improve the Parametric and Power regression models in 2003. Issuing forecast for four geographical regions of India,

viz., Northwest India, Central India, East and Northeast India and south Peninsula, in addition to the forecast for India as a whole, also began from that year. However, the improved version of the model also could not foreshadow the drought in 2004. The efforts of Gupta and Onkari Prasad (1992), both from IMD, resulted in proposing Southern Hemispheric Equatorial Trough (SHET) model. Real time forecast from this model became available from 1990. The improved version of the model is now known as South Indian Ocean Convergence Zone (SIOCZ) model (Prasad, Singh and Prasad, 2014). The model has since produced reasonably good forecast of rainfall for India as a whole and its subdivisions (35 till 2002 and 36 thereafter) for the past 28 years including 2017. It may be mentioned here that SIOCZ model alone could foreshadow the deficiency in rainfall in drought years of 2002, 2004, 2009 and severe drought like conditions during the first half of the season in 1992 and 2012. Results of verification of the forecasts, in some of the years, have been reported by Onkari Prasad (1993, 2000, 2001). The verification of the forecasts for the year 2016 has been reported by Onkari Prasad et al., (2018).

SIOCZ model differs from other models because of its ability to identify the precursors, as features in the activity of SIOCZ, as seen in cloud/OLR data from the Indian Ocean region. The precursors are distinctly different for Excess, Normal and Deficient monsoons. Several

Table 1. Long range forecast of rainfall during 2017 southwest monsoon issued by IMD and realized rainfall

Region	Period	Forecast as % of Long Period Average (LPA)		Five category probability forecast			Realized rainfall (%) of LPA	
		18 April	6 June	Category	Rainfall range as % of LPA	Probability (%)		
						Forecast		Climate
All India	Jun-Sep	96 ± 5	98 ± 4	Deficient	≤ 90	7	16	95
Northwest India	Jun-Sep	96 ± 8		Below normal	90-96	28	17	90
Central India	Jun-Sep	100 ± 8						94
Northeast India	Jun-Sep	96 ± 8		Normal	96-104	50	33	96
South Peninsula	Jun-Sep	99 ± 8						100
All India	July	96 ± 9		Above normal	104-110	13	16	102
	8 August							
All India	August	99 ± 9		Excess	> 110	2	17	87
All India	Aug-Sep	100 ± 8						87
All India	Jun-Sep	100 ± 4		Excess	> 110	2	17	95

Source: Press releases on 18th April, 6th June and 8th August and 'End of season report' on 2017 southwest monsoon issued by IMD.

improvements have been made in the model (Prasad, Singh and Prasad, 2014), since the first forecast was prepared in 1990. The improved version of the model has enabled to prepare forecast of seasonal rainfall in the districts of Tamilnadu for the past 13 years (2005-2017) (Prasad, Singh and Subramanian, 2010), Himachal Pradesh for 10 years (2008-2017) (Prasad and Singh, 2007), Andhra Pradesh and Telangana for 4 years (Prasad, Singh and Prasad, 2016b,c) and Maharashtra and Goa for 2 Years (2016-17) (Prasad, Singh and Prasad, 2016d). Identification of precursors, formulation of LRF of rainfall during 2017 southwest monsoon and its verification is discussed in this part of the study.

LONG RANGE FORECAST

Long Range Forecast (LRF) of 2017 monsoon was available from the following models:

- i. Operational Statistical Ensemble Forecasting System (OSEFS)
- ii. Monsoon Mission Coupled Forecasting System (MMCFS)
- iii. South Indian Ocean Convergence Zone (SIOCZ) model

Forecast from OSEFS

The operational LRF of rainfall for 2017 monsoon had been issued by IMD in 3 stages, i.e., on 18th April, 6th June and 8th August. The 18th April forecast was for India as a whole and for the season as a whole. The 6th June forecast was an update on the forecast of 18th April. In addition to forecast for India as a whole, forecast for seasonal rainfall for four broad regions of India, namely, Northwest India

(NW India), East and Northeast India (E&NE India), Central India, South Peninsula and rainfall for the country as a whole for the months of July were also included. The forecast of 8th August consisted of the rainfall for the month of August and for the second half of the season, both for India as a whole. The forecast, probability forecast and the realized rainfall are reproduced in Table 1.

Forecast from MMCFS model

Atmospheric and oceanic initial conditions for the month of March 2017 had been used to generate the forecast. Forecast had been computed as an average of 44 ensemble members. The model had suggested that the rainfall averaged for the country as a whole and for the season (Jun-Sep) was likely to be 96% ±5% of LPA. The forecast had been upgraded to 100% ±5% on 6th June.

Forecast from SIOCZ model

It had been shown earlier by the authors that assigning SAI could be done by using either cloud or OLR data (Onkari Prasad, Singh and Prasad, 2014). This had been done by using both Cloud and OLR data for two excess monsoons (1988 & 1994), two normal monsoons (1993&1997) and two droughts (2002&2009). Beginning from 2017, SIOCZ model forecasts are being issued using OLR data from INSAT-3D as provided by IMD and OLR Total and OLR anomaly maps as made available by NOAA/ESRL/PSD on their website (<http://www.esrl.noaa.gov/psd/map/clim/sst.shtml>), on real time basis. OLR anomaly data were not available from INSAT satellites. NOAA OLR anomaly charts for the period February-July 2017 are reproduced

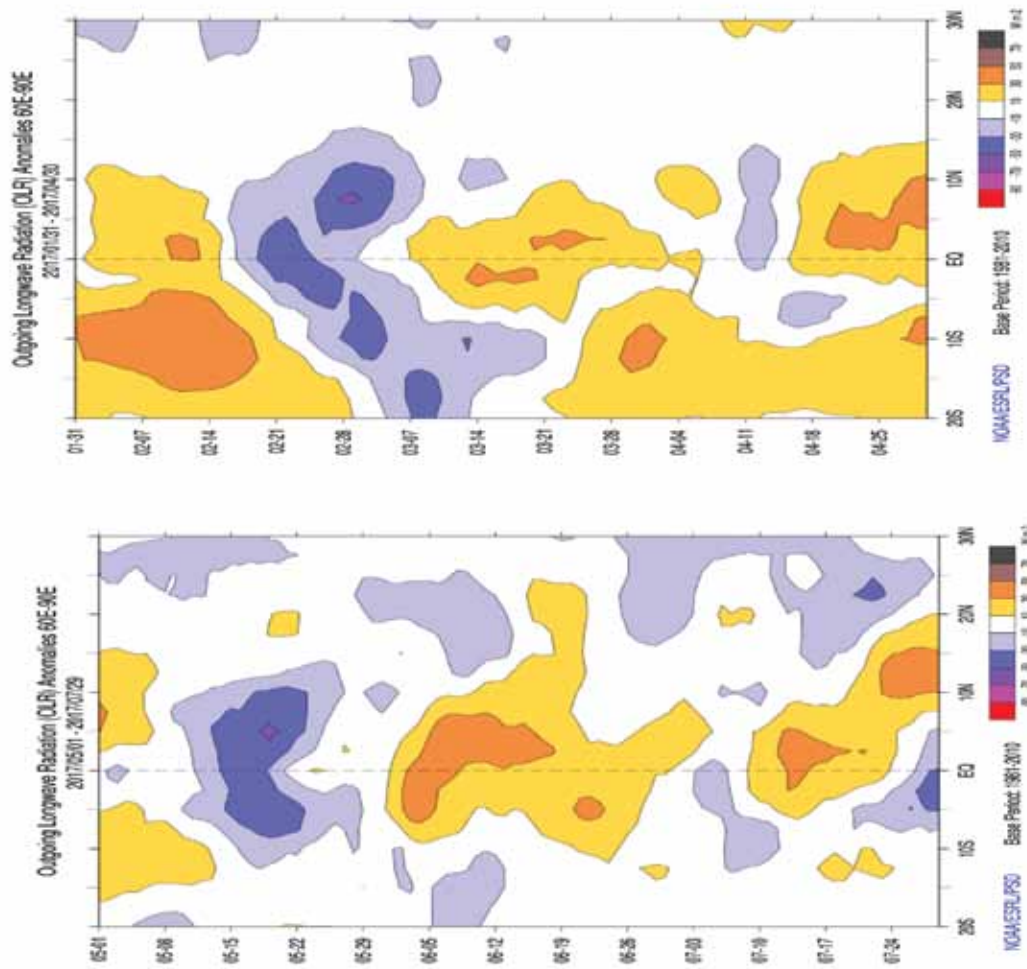


Figure 1. Upper panel: Weekly mean OLR anomaly over the region bounded by 30°N-20°S and 60°E-90°E during February-April 2017. **Lower panel:** Same as upper panel but for the period May-July 2017.

in Figure 1. SIOCZ model forecasts were issued in 3 stages: (i) on 30th March, (ii) 5th June and (iii) 10th August (Update) (Onkari Prasad, Singh and Prasad, 2017). The features in the activity of SIOCZ till the first half of February 2017 had indicated development of a 'Normal' monsoon. However, there was a change in the feature in the activity of SIOCZ during the second half of February-March, when weak convection (negative OLR anomaly, shaded in blue in Figure 1) developed over equatorial areas of Indian Ocean (IO). The convection moved northward as well as southward during the next 3 weeks and 4 weeks, respectively. While the convection moved north of equator up to 15°N, it moved to the south of equator up to 20°S. Convection persisting for 3-4 weeks, in continuation, to the south of equator during February-March and its movement as far south as 20°S, was an early signal for development of a 'Weak' monsoon. During March of 'Normal'/'Active' monsoon years, convection either moves northward or it remains confined to the areas close to the equator. Thus, an early signal indicating likely development of a 'Weak' monsoon appeared during Feb-Mar 2017. In order to

foreshadow 2017 summer monsoon as a 'Weak' monsoon, repeat of this feature during the pre-monsoons of April-May was awaited. Accordingly, the first stage forecast issued on 30th March was ***"2017 southwest monsoon is likely to develop as a 'Normal' monsoon with Indian summer Monsoon Rainfall on the lower side of its Normal (100%)."***

As two monsoons can never be exactly similar, the features in the activity of SIOCZ are also not the same in any two years. However, there were years in the past when the important feature in the activity of SIOCZ was comparable. Available cloud data show that the feature, as seen in the activity of SIOCZ during Mar-May 2017, i.e., development of SIOCZ for 3-4 weeks in continuation, had occurred in 1982, 2002, 2004 and 2009. ISMR in these years was deficient: 1982 (Jun: -17%, Jul:-23 %, Aug: 9 %, Sep:-32%, and Jun-Sep: -15%), 2002 (9%, -54%, -2%, -13%, and -19%), 2004 (-1%, -20%, -4%, -30% and -14%) and 2009 (-47%, -4%, -26%, -20% and -22%), respectively. However, two changes, suggesting likely improvement in rainfall scenario, were taking place at the time of issuing the forecast: (i) The spell of convection, which developed

Table 2. Forecast, Update, realized rainfall as % departure from normal (100%) and Model Error (ME).

Forecast, update and realized rainfall have been shown in bold italics in the subdivisions where CC between SAI and rainfall is significant at 95% level or more.

Subd. S. No.	Jun(10*)			Jul(20*)			Aug(12*)				Sep(16*)			
	FC	RR	ME	FC	RR	ME	FC	UD	RR	ME	FC	UD	RR	ME
1	-23D	-20D		-12N	-4N		-6N	-5N	3N		-16N	-9N	-14N	
2	-19N	-25D		6 N	-3N		-14N	0N	22E		22E	15N	-18N	
3	-15N	-18N		5N	-25D		-12N	-7N	6N		2N	2N	4N	
4	-26D	24E	3	-2N	22E		-11N	-8N	48E		5N	-1N	20E	
5	-17N	-18N		11N	-22D		-8N	-2N	56E		-3N	-2N	-7N	
6	-9N	-21D		12N	47E		2N	2N	-15N		-1N	9N	-34D	
7	-4N	-2N	7	-5N	4N		0N	6N	-17N		-13N	3N	-19N	5
8	-4N	-39D		-10N	47E	4	-11N	-9N	-22D		3N	14N	-49D	
9	-3N	-50D		13N	11N		-9N	-6N	18N		-9N	-6N	-42D	
10	-3N	-53D	9	-14N	10N	5	-24D	-14N	-37D	4	-2N	3N	-57D	
11	-6N	13N	11	-20D	-30D	6	-15N	-10N	-55D		-27D	-7N	-5N	8
12	-10N	5N		-13N	8N		-15N	-11N	-18N		-18N	-1N	3N	7
13	28E	162LE	15	-12N	-58D	12	-10N	4N	-58D		-41D	-13N	2N	12
14	39E	148LE		-11N	-49D	11	-11N	7N	-30D	7	-47D	-19N	-33D	10
15	3N	30E	7	-26D	-29D	5	-26D	-17N	-3N		-34D	-14N	-25D	7
16	23E	144LE		-12N	-6N	11	-9N	22E	-13N	11	-34D	-19N	-53D	
17	15N	174LE	19	-22D	114LE	9	-32D	0N	-53D	9	-27D	-4N	-49D	
18	-8N	42E	17	-16N	30E	9	-11N	-6N	-54D		-53D	17N	-53D	26
19	-14N	14N	9	-17N	1N		9N	7N	-44D		-43D	-20D	-11N	14
20	-22E	-12N	12	-27D	2N	4	-6N	6N	-52D		-13N	-4N	-28D	
21	4N	5N		-26D	9N	10	-3N	22E	-37D	8	-33D	3N	-58D	16
22	17N	-5N		-34D	16N	12	5N	12N	22E		-45D	7N	-45D	
23	2N	20E		-13N	-2N		6N	14N	-35D		-26D	11N	58E	13
24	14N	31E		-19N	16N	5	5N	14N	-20D		-9N	14N	24E	9
25	-6N	27E		-17N	-57D	7	-7N	19N	40E	11	-28D	5N	-11N	12
26	-1N	-12N		-21D	-19N	5	2N	7N	-8N		-41D	-9N	-21D	11
27	-9N	-1N		-19N	0N		-52D	-10N	66LE		-32D	-8N	-18N	9
28	-7N	44E		-19N	-6N	7	-4N	11N	82LE	6	-10N	1N	-12N	
29	-8N	49E		-16N	-41D	6	-6N	13N	-17N	7	-23D	-6N	-30D	6
30	15N	34E		-15N	-45D	8	-5N	26E	-10N	12	3N	6N	45E	
31	-11N	4N		-13N	-39D		-13N	1N	-14N	9	24E	11N	42E	
32	-3N	-4N		-12N	-29D		8N	18N	10N		-21D	11N	6N	12
33	17N	25E		-20D	-43D		-2N	12N	-5N	6	0N	3N	43E	
34	15N	-23D		-25D	-41D	6	-11N	11N	14N	5	21E	16N	81LE	
35	-8N	-11N		-16N	-48D		-7N	-2N	10N		-9N	10N	78LE	
36	6N	58E		-6N	-43D	6	0N	10N	-5N		-2N	7N	32E	
%*	80			85			83	66			75	81		
India	-6BN	4N	5	-13D	2N	5	-9BN	1N	-13D	5	-17D	0N	-12D	5

Name of subdivisions: 1. Bay Is. 2. Ar. Pradesh 3. Assam & Megha, 4. NMMT, 5. SHWB & Sikkim, 6. GWB 7. Orissa, 8. Jharkhand, 9. Bihar, 10. EUP, 11. WUP, 12. Uttarakhand, 13. Dlh, Har, Cha, 14. Punjab, 15. H.P., 16. J&K, 17. W. Raj, 18. E. Raj, 19. WMP, 20. EMP, 21. Guj Reg, 22. Sau. & Kutch, 23. Konkan Goa, 24. Madhya Maharashtra, 25. Marathwada, 26. Vidarbha, 27. Chhattisgarh, 28. CAP, 29. Talangana, 30. Rayala, 31. Tamilnadu & Puducherry, 32. Coastal karnataka, 33. North Interior Karnataka, 34. South Interior Karnataka, 35. Kerala and 36. Lakshadweep. (x*)- x is the No. of subdivisions where CC between SAI and rainfall was significant at 95% level or more, %*: % of sub- divisions (out of the number of subdivisions where CC is significant in the month or bimonthly period/season) where forecast was in 'Useful' category.

Categorization of rainfall (as followed in IMD) (i) for rainfall in districts and sub-divisions: Large Excess (LE):60% or more, Excess (E):59% to 20%, Normal (N):±19%, Deficient (D): -20% to -59% and Large Deficiency (LD): -60% or less.

(ii) for India as a whole: Excess(E): > 10%, Above Normal (AN): 10% to 5%, Normal (N): ±4%, Below Normal (BN): -5% to -10%, Deficient(D): < -10%.

Table 3. Same as Table 2 but for the season as a whole.

Jun- Sep (26*)														
Subd. S.No.	FC	UD	RR	ME	Subd. S.No.	FC	UD	RR	ME	Subd. S.No.	FC	UD	RR	ME
1	-15N	-8N	-9N		14	-14 N	9N	-22D	9	27	-20D	-9N	-10N	6
2	-3N	1N	-11N		15	-25 D	-13N	-13N	5	28	-11 N	5N	14N	6
3	-5 N	-2 N	-10N		16	-11N	9N	2N	8	29	-14N	2N	-13N	6
4	-10N	-8 N	25E		17	-31 D	11 N	39E	12	30	-1N	16N	27E	6
5	-3 N	-1 N	2N		18	-21 D	-2N	-8N	7	31	-21 D	9N	31E	10
6	4 N	10 N	-3N		19	-15N	-1 N	-16N	5	32	-6 N	4N	-16N	4
7	-5N	1N	-9N		20	-16 N	-4N	-10N	10	33	-6 N	5N	3N	3
8	-6 N	2N	-10N	3	21	-25N	11N	9N	10	34	-3 N	8 N	2N	
9	-2 N	2N	-9N		22	-17N	6N	35E	3	35	-9 N	-3N	-9N	3
10	-13 N	-2 N	-28D	4	23	-5N	3 N	10N	6	36	-1 N	6 N	11N	
11	-21D	-10N	-31D	5	24	-5N	9 N	17N	8	%*	96	80		
12	-15 N	-6N	-2N	3	25	-16N	2N	-6N	5	India	-12D	0 N	-5BN	5
13	-14N	9N	-26D	10	26	-17N	-3 N	-23D	3					

from the week ending on 15th May for the next 2 weeks was weak in the region south of equator and (ii) positive SST anomaly over the Equatorial Indo-Pacific region had started decreasing beginning from the first week of May. Considering that both the developments were in phase for likely improvement in rainfall, the assigned value of SAI had been moderated from 16 to 14. SAI=14 corresponds to 12% below normal ISMR with model error of ±5%. SIOCZ model had, therefore, foreshadowed 2017 southwest monsoon as a ‘Weak’ one with ISMR expected to be 12% below normal, i.e., in ‘Deficient’ category. The value assigned to SAI for the subdivision of Tamilnadu and Puducherry was 15. Monthly, bi-monthly and seasonal rainfall forecast as well as realized rainfall in the subdivisions and for India as a whole and forecast of seasonal rainfall in the districts of Tamilnadu, Andhra Pradesh, Telangana, Himachal Pradesh and Maharashtra & Goa and realized rainfall are included in Tables 2-4.

Update

In the past, Update/Updates had been issued in 2010 (Onkari Prasad and Singh, 2013b), in 2013 (Onkari Prasad, Singh and Prasad, 2016a) and 2016 (Onkari Prasad, Singh and Prasad, 2018). In 2017, an intra-seasonal change in the activity of SIOCZ, suggesting improvement in rainfall took place during July: As a recurrence of the main feature in the activity of SIOCZ, an active spell of SIOCZ developed during the week ending on 10th July. But it turned out to be very weak (**Lower panel** of Figure 1). Thereafter, another active spell of SIOCZ developed during the week ending on 24th July. These developments in the activity of

SIOCZ were a departure from the main feature, i.e., SIOCZ remaining active for 3-4 weeks in continuation. This was an indication of likely improvement in rainfall scenario and, therefore, it formed the basis for the issue of an Update. In addition, decrease in SST anomaly in Nino 3.4 region from 0.48°C in May to 0.35°C in July also favoured probable return of normal monsoon conditions over India during the second half of the season. A value of 9, which corresponds to normal rainfall over India, was assigned to SAI for computing rainfall during August & September and for the season as a whole in the subdivisions, India as a whole and in the districts of Andhra Pradesh, Telangana and Himachal Pradesh. The value assigned to SAI for Tamilnadu and Maharashtra and Goa was 11. The updated forecast rainfall figures are included in Tables 2-4.

Verification of Forecasts

For verification at district and subdivision level, forecast as well as realized rainfall figures have been considered in two broad categories only, i.e., ‘Large Excess (LE)/Excess(E)/Normal(N)’ and ‘Deficient(D)/Large Deficiency (LD)’. Verification of forecasts is discussed below, in brief, for those districts and subdivisions only where CC between SAI and rainfall is significant at 95% level or more. The district level forecast/Update has been categorized as ‘Average’, ‘Good’, ‘Very Good’ and ‘Excellent’, if the forecast/Update was in ‘Useful’ category between 50% and 59% districts of a state where CC was significant, 60% districts, 61-80% districts and 81-100% districts, respectively. This categorization has been used for differentiating subdivision-wise forecasts for monthly, bi-monthly and seasonal forecasts.

Table 4a. Same as Table 2 but for the districts in the states

Tamilnadu (30*/32)					Andhra Pradesh(12*/13)				
District	FC	UD	RR	ME	District	FC	UD	RR	ME
Ariyalur	-26D	-13N	40 E	8	Srikakulam	-2N	2 N	20E	
Chennai	-7 N	5N	2 N	9	Vizianagram	-10N	-4N	6N	2
Coimbatore	19 N	26E	169LE	18	Visakhapatnam	2 N	11N	8N	3
Cuddalore	-15N	-5N	22 E	8	East Godavary	-8 N	6N	14N	6
Dharmapuri	-12N	0N	2 N	8	West Godavary	-12N	2 N	3N	5
Dindigul	-10N	7N	39 E	6	Krishna	-13N	3N	-1N	6
Erode	16 N	30E	35 E	18	Guntur	-9N	8N	18N	7
Kanchipuram	-17N	-1	0 N	9	Prakasham	-7N	7N	18N	5
Kanyakumari	8N	5N	-16 N		Nellore	-1N	12N	50E	5
Karur	-19N	-1N	57 E	8	Kurnool	-11N	2N	13N	5
Krishnagiri	-12N	0N	32 E	8	Anantpur	-13N	5N	18N	7
Madurai	7N	12N	21 E	6	Cuddapah	-12N	5N	34E	7
Nagapattinam	-22D	-1N	5 N	8	Chittor	-1N	16N	47E	7
Namakkal	-11N	5N	12 N	8	% of districts where FC/Update was in 'Useful' category	100%	100%		
Nilgiri Hills	-17N	-11N	-4 N		Telangana(10*/10)				
					District	FC	UD	RR	ME
Perambalur	-46D	-26D	90LE	8	Adilabad	-6N	12N	-28D	9
Puddukotai	-24D	-9N	16 N	8	Nizamabad	-14N	-2N	-25D	9
Ramanathpurm	-32D	-10N	41 E	9	Karimnagar	-1N	12N	-25D	5
Salem	-16N	-6N	10 N	8	Medak	-14N	1N	-15N	7
Sivganga	-13N	-3N	75LE	6	Warangal	-8N	7N	3N	6
Thanjavur	-30D	-8N	51 E	8	Khammam	-6 N	5N	2N	6
Theni	17N	25E	131LE	6	Rangareddy	-20D	-1N	-15N	7
Thiruvallur	-12N	4N	10 N	9	Hyderabad	-6N	5N	9N	5
Thiruvarur	-26D	0N	32 E	18	Nalgonda	-20D	2N	-6N	6
Thoothukudi	-6 N	-4N	41 E	9	Mahbubnagr	-26 D	-9N	-9 N	6
Trichirapally	-22D	6N	14 N	8	% of districts where FC/Update was in 'Useful' category	70%	70%		
Tirunelveli	0N	4N	49 E	8					
Tirupur	-12N	-4N	100LE	8	Himachal Pradesh (6*/12)				
					District	FC	UD	RR	ME
Tiruvannamalai	-20D	-7N	33 E	9	Bilaspur	-7N	-1N	9 N	
Vellore	-17N	1N	23 E	8	Chamba	-33 D	-26D	-50 D	
Villupuram	-25D	-9N	8 N	8	Hamirpur	-3N	14N	0 N	7
Virudhunagar	-9 N	9N	49 E	6	Kangra	-15N	-5N	3 N	4
% of districts where F/C / Update were in useful category	90%	100%			Kinnaur	-29 D	-15N	-32 D	6
					Kullu	-1N	-9 N	14 N	4
					Mandi	-19 N	-11N	9 N	
					Simla	-21D	-10N	1 N	4
					Sirmur	-37 D	-29D	-8 N	
					Solon	-27D	-15N	-16 N	5
					Una	11N	23E	18 N	
					Lahol-Spiti	NA	NA	-70 D	
					% of districts where FC/Update was in 'Useful' category	83%		100%	

Table 4b. Same as Table 4a but for the districts in Maharashtra & Goa

Maharashtra & Goa (32*/36)									
District	FC	UD	RR	ME	District	FC	UD	RR	ME
Thane	-5N	3N	32 E	4	Jalna	-14N	7N	-2 N	7
Mumbai City	4N	4N	10 N	4	Beed	-13N	8N	12 N	8
Raigarh	-6 N	4N	17 N	4	Parbhani	-26D	8N	-21 D	8
Ratnagiri	-4N	3N	5 N	4	Hingoli	-20D	7N	-28 D	7
Sindhudurga	0N	4N	-4 N	3	Osmanabad	-21D	6N	24 E	6
North Goa	1N	3N	-13 N	3	Latur	-21D	8N	2 N	8
South Goa	-2N	3N	-14 N	3	Nanded	-18N	9N	-22 D	9
Nandurbar	-1N	7N	-11 N	7	Buldhana	-10N	5N	2 N	5
Dhule	-3N	5N	-2 N	5	Akola	-6N	5N	-22 D	5
Jalgaon	-10N	6N	-15 N	6	Wasim	-8N	5N	-28 D	5
Nasik	-1N	3N	31 E		Amraoti	-7N	4N	-30 D	4
Ahmednagar	-8N	7N	55 E	7	Yeotmal	-15N	7N	-34 D	7
Pune	-3N	3N	50 E		Wardha	-13N	4N	-14 N	4
Satara	25E	3N	17 N		Nagpur	-12N	5N	-4 N	5
Solapur	-9N	6N	25 E	6	Bhandara	-15N	4N	-27 D	4
Sangli	-4N	3N	-11 N		Gondia	-11N	4N	-37 D	4
Kolhapur	14N	3N	-14 N	3	Chandrapur	-16N	5N	-32 D	5
Aurangabad	-16N	6N	-7 N	6	Gadchiroli	-7	4N	-22 D	4
% of districts where FC/Update was in 'Useful' category						81%	62%		

In the districts

At district level, a forecast is considered 'Useful', if both the forecast as well as the realised rainfall were in the same broad departure category, as mentioned above, or they became so when model error was taken into account. The forecast, realised rainfall and Model Error (ME) in the districts of Tamilnadu, Andhra Pradesh, Telangana, Himachal Pradesh and Maharashtra & Goa are included in Table 4. In Tamilnadu, forecast was in 'Useful' category in 90% of districts and the Update in 100% of districts. In Andhra Pradesh, the % of 'Useful' forecast as well as for the Update was 100%. The updated forecast was closer to the realised one. However, the realised rainfall was, in general, higher than the updated values. In Telangana, the forecast as well as the Update was in 'Useful' category in 70% districts. In Himachal Pradesh, forecast was in 'Useful' category in 83% districts and the updated forecast in all the 6 districts, where CC is significant. In Maharashtra & Goa, forecast was in 'Useful' category in 91% of districts and the Update in all the 32 districts, where CC is significant. Thus the district level forecast was in 'Excellent' category in Tamilnadu, Andhra Pradesh, Himachal Pradesh and Maharashtra & Goa. The forecast as well as the Update was in 'Very Good' category in Telangana.

In subdivisions

At sub-divisional level also, a forecast is considered 'Useful', if both, the forecast as well as the realised rainfall, are in the same broad departure category or they become so after ME is taken into account. The ME is different for different subdivisions and the same is included in Tables 2&3. The forecast rainfall was in 'Useful' category in 80%, 85%, 83% and 75% subdivisions in the months of June, July, August and September, respectively. The Update was in 'Useful' category in 67% and 81% of subdivisions for the months of August and September, respectively. Thus the forecast was in 'Excellent' category in Jun, Jul and Aug and in 'Very Good' category in Sep. The Update was in 'Very Good' category in Sep and in 'Good' category in Aug. The table containing the data on forecast, Update and realized rainfall for the bi-monthly periods could not be included here due to lack of space. However, the same could be obtained as an average of monthly forecast/Update/realized rainfall for two consecutive months. The ME for bimonthly periods is available in one of the earlier publications by Onkari Prasad and Singh (2013a). The number of subdivisions, where CC between SAI and bi-monthly rainfall during Jun+ Jul, Jul+ Aug and Aug+ Sep, was 24, 24 and 20 respectively. The forecast was in 'Useful' category in 92%, 83%, and 95% of

subdivisions. The Update was in 'Useful' category in 71% of subdivisions during Jul+ Aug and 60% during Aug+ Sep, respectively. Thus the Update was in 'Very Good' category during the bi-monthly period of July+ Aug and in 'Good' category during Aug+ Sep.

For India as a whole

The forecast, Update and the realised rainfall for country as a whole are included at the bottom of Tables 2&3. For India as a whole, a forecast is categorized to be in 'Useful' category, if the forecast as well as the realized rainfall were in the same departure category, or the forecast came in the departure category of realized rainfall after the ME ($\pm 5\%$) was taken into account. Otherwise the forecast was considered as not in useful category. The monthly forecast was in useful category in June, August and September. The bi-monthly forecast was in useful category for the bi-monthly periods of Jul+ Aug and Aug+ Sep. The forecast for the seasonal rainfall, i.e., 12% below normal as compared to 5% below normal of realized rainfall, was slightly below the useful category mark. The Update issued in August was not in useful category for the bi-monthly period of Aug+ Sep and also for the season as a whole.

CONCLUSIONS

1) The main feature in the activity of SIOCZ, i.e., development of an active spell of SIOCZ for 3-4 weeks in continuation, first appeared during February-March and continued up to October. An intra-seasonal change got superimposed over the main feature in July and continued up to October.

2) Though 2017 southwest monsoon, with 5% below normal Indian Summer Monsoon Rainfall (ISMR), has been entered in the records as a 'Below normal' monsoon, monthly rainfall in the subdivisions during Jul-Sep was similar to that for a 'Deficient' monsoon.

3) SIOCZ model's forecasts for a normal monsoon with rainfall on the lower side of 'Normal' (100%) issued on 30th March, for a weak monsoon on 5th June and the Update issued on 10th August for likely improvement in rainfall during the second half of the season, were able to capture most of the features of rainfall distribution during 2017 southwest monsoon season. However, the improvement in rainfall during the second half of the season, as indicated in the Update, remained confined to southern Peninsula only.

4) The performance of SIOCZ model forecast was better in the districts of the states, compared to that in the subdivisions and for the country as a whole.

5) Intra-seasonal change in the activity of SIOCZ during the second half of 2017 southwest monsoon was

more closely related to the distribution of rainfall over India than the mid-season transition from El Nino to ENSO Neutral conditions in equatorial East Pacific.

ACKNOWLEDGMENTS

Zonal weekly mean OLR data was supplied by IMD. Monthly and seasonal rainfall data was made available by IMD through their 'Southwest monsoon-2017- End of season Report'. Rainfall data on daily and weekly progress of monsoon, used in the present study, was downloaded from IMD website. Real time SST, OLR total and OLR anomaly charts issued by NOAA/ESRL/PSD and SST anomaly forecast charts issued by IRI, JASMTEC, ECMWF were also consulted, while carrying out the present study. Development of a weak summer monsoon and intra-seasonal changes during 2017 is discussed in Pt. II of the study. Thanks are due to Dr.U.S.De for useful suggestions. Thanks are due to Dr.P.R.Reddy, Chief Editor for continued support and for final editing.

Compliance with Ethical Standards:

The authors declare that they have no conflict of interest and adhere to copyright norms.

REFERENCES

- Blanford, H.E., 1884. On the mechanism of the Himalayan snowfall and season of droughts in India, Proc. Royal. Soc., London, v.37, pp: 3-22.
- Gowariker, V., Thapaliyal, V., Sarker, R.P., Mandal, G.S., and Sikka, D.R., 1989. Parametric and power regression models: New approach to long range forecasting of monsoon rainfall in India, Mausam, v.40, pp: 115-122.
- Gupta, G.R., and Onkari Prasad, 1992. Role of southern hemisphere ic equatorial trough in long range forecasting, Jalvigyan Sameeksha- a publication of Indian National Committee on Hydrology, v.VII, pp: 83-97.
- Onkari Prasad, 1993. Performance of Southern hemispheric Equatorial Trough model of sub-division-wise long range forecast of rainfall during southwest and northeast monsoons, Proceedings of TROPMET Symposium-1993, held at New Delhi, 17-19 March 1993.
- Onkari Prasad, 2000. Subdivision-wise long range forecast of rainfall during southwest monsoon, Proceedings of TROPMET-2000, National Symposium on Tropical Meteorology, pp: 222-226.
- Onkari Prasad, 2001. Subdivision-wise long range forecast of bi-monthly rainfall during southwest monsoon season, Proceedings of TROPMET-2001, National Symposium on meteorology for sustainable development, pp: 252-257.

- Onkari Prasad and O.P, Singh, 2007. District level long range forecast of seasonal rainfall during southwest monsoon, *Vayu Mandal*, v. 34, no.1-4, pp: 51-56.
- Onkari Prasad, O.P, Singh and S.K.Subramanian, 2010. Seasonal forecast of southwest monsoon rainfall- District level, *J. Ind. Geophys. Union*, v.14, no.2, pp: 93-113.
- Onkari Prasad and O. P. Singh, 2013a. South Indian Ocean Convergence Zone model- A new approach to seasonal forecasting of summer monsoon rainfall in India Part III: Forecast for meteorological subdivisions, *J. Ind. Geophys. Union*, v.17, no.1, pp: 75-91.
- Onkari Prasad and O. P. Singh, 2013b. South Indian Ocean Convergence Zone model- A new approach to seasonal forecasting of summer monsoon rainfall in India Part IV: Intra-seasonal changes and long range forecast of rainfall during 2010 southwest monsoon season, *J. Ind. Geophys. Union*, v.17, no.3, pp: 289-305.
- Onkari Prasad, O. P. Singh and K. Prasad, 2014. South Indian Ocean Convergence Zone model- A new approach to long range forecasting of summer monsoon rainfall in India, Part-VI: Merits of the model and limitations in seasonal forecasting of rainfall in India, *J. Ind. Geophys. Union*, v.18, no.3, pp: 363-386.
- Onkari Prasad, O. P. Singh and K. Prasad, 2016a. Intra-seasonal changes and long range forecast of rainfall during 2013 southwest monsoon season based on South Indian Ocean Convergence Zone model, *J.Ind.Geophys.Union*,v.20, no.1, pp:89-100.
- Onkari Prasad, O. P. Singh and K. Prasad, 2016b. District level long range forecast of rainfall during southwest monsoon in Andhra Pradesh, *J. Ind.Geophys.Union*,v.20, no.2, pp: 254- 264.
- Onkari Prasad, O.P, Singh and K, Prasad, 2016c. District level long range forecast of rainfall during southwest monsoon in Telangana, *J. Ind.Geophys.Union*, v.20, no.4, pp: 432-439.
- Onkari Prasad, O.P, Singh and K. Prasad, 2016d. District level long range forecast of Rainfall during southwest monsoon in Maharashtra & Goa, *J. Ind.Geophys.Union*, v.20, no.6, pp: 586-595.
- Onkari Prasad, O.P, Singh and K. Prasad, 2017. Long range forecast of southwest monsoon rainfall issued on 30th March, 5th June and 10th August 2017.
- Onkari Prasad, O. P. Singh and K. Prasad, 2018. 2016 southwest monsoon and its long range forecast, *J.Ind.Geophys.Union*, v.22, no.1, pp: 90-100.

Received on: 4.12.2017, Revised on: 14.12.2017; Accepted on: 23.12.2017

Defluoridation of water using *Mentha longifolia* (Mint) as Bioadsorbent

V.Sunitha* and B.Muralidhara Reddy

*Department of Geology, Yogi Vemana University, Kadapa, A.P.

*Corresponding Author: vangala_sunitha@yahoo.com

ABSTRACT

Excessive fluoride concentrations have been reported in ground waters of 19 states of India. Acute fluorosis is noticed in many problem areas of these states. In spite of several existing physical and chemical defluoridation methods, there is an urgent need to develop cost effective and biodegradable methods to effectively treat high fluoride concentration in ground water. Experiments at room temperature were performed to evaluate the adsorption capacity of *Mentha longifolia* (Mint) from aqueous solutions. The effect of some major parameters like pH, contact time and amount and particle size of adsorbent and concentration of fluoride ions of the uptake on adsorbent materials is investigated from kinetic viewpoint. Adsorption studies are performed by batch technique to obtain the rate and equilibrium data. The Freundlich and Langmuir sorption isotherms were used to quantify sorption properties. Results show that *Mentha longifolia* (Mint) is effective in removing fluoride from groundwater samples.

Key words: Defluoridation; Biosorption; *Mentha longifolia*; pH; Adsorption kinetics.

INTRODUCTION

Free fluorine plays no part in toxicology because it reacts immediately to form fluoride compounds. The presence of dissolved fluorides in natural waters is possible only when favorable conditions facilitate long residence times of the F⁻ species in solution. Occurrence of fluorine in groundwater has drawn worldwide attention due to its considerable impact on human physiology. The permissible limit of F⁻ in drinking water is 1.5 mg/l (W.H.O 1984). It is generally accepted that fluoride stimulates bone formation (Richards et al., 1994) and optimum concentration of fluorides have beneficial effects on the teeth by hardening the enamel and reducing the incidence of dental caries (Fung et al., 1999). At lower levels (<2 ppm) soluble fluoride in the drinking water may cause mottled enamel during the formation of teeth, but at higher levels other toxic effects may be observed. Excessive intake of fluoride results in skeletal and dental fluorosis (Czarnowski et al., 1999). Fluorides in drinking water may be beneficial or detrimental depending on its concentration and total amount ingested. Fluoride is beneficial especially to young children below eight years of age when present within permissible limits of 1.0-1.5 mg/L for calcification of dental enamel. Excess fluorides in drinking water cause dental fluorosis and/or skeletal fluorosis (Sorg, 1978). The main source of fluoride in the groundwater is fluoride bearing rocks. Such host rocks due to weathering leach out fluoride and contaminate the ground water. Fluorides occur in three forms, namely fluorspar or calcium fluoride (CaF₂), apatite or rock phosphate (Ca₃F (PO₄)₃) and cryolite (Na₃AlF₆) (Sunitha et al., 2012). Defluoridation means the removal

of excess fluoride from water (Jamode et al., 2004; Saha S, 1993). The National Environment Engineering Research Institute (NEERI), Nagpur, India has evolved an economical and simple method of defluoridation, which is referred to as the Nalgonda technique. UNICEF has worked closely with the Government and other partners in defluoridation programmes in India, in the areas of excessive fluoride in groundwater. In the 1980s, UNICEF supported the Government's Technology Mission to identify and address the fluoride problem and the Government subsequently launched a massive programme, still under way, to provide fluoride-safe water in all the areas affected (Ranjeeta, 2015). Defluoridation of drinking water is the only practicable option to overcome the problem of excessive fluoride in drinking water, where alternate source is not available. After the discovery of fluoride as the cause of fluorosis, extensive research has been done on various methods for removal of fluoride from water and wastewater. These methods are based on the principle of adsorption (Raichur et al., 2001) ion-exchange (Singh et al., 1999), precipitation-coagulation (Saha et al., 1993; Reardon, 2000), membrane separation process (Amer et al., 2001; Dieye et al., 1998), electrolytic defluoridation (Mameri et al., 2001) and electro dialysis (Hichour et al., 1999; Hichour et al., 2000; Adhikari et al., 1989).

The various adsorbents that have been used for fluoride removal are alumina, alumina in combination with manganese dioxide, iron oxide, calcium minerals. Also, several clays and soils have been tried as an adsorbent medium for defluoridation. A technology for the granulation of Fe-Al-Ce nano-adsorbent (Fe-Al-Ce) in a fluidized bed has also been developed

(Lin Chen et al., 2009). Defluoridation studies based on membrane techniques and the use of reverse osmosis (RO) membranes for fluoride removal from contaminated water sources were reported earlier. However, this technique has not been successful due to low permeate fluxes. Moreover, the process also generates more concentrated waste as reject (Anand Babu et al., 2011). In addition, due to high cost or lower efficiency or non-applicability on mass scale, these techniques are not in use. This paper presents the findings of an investigation on the use of leaf powder of Mint leaves (Pudina) for the defluoridation of water.

MATERIALS AND METHODS

All the reagents used were of AR grade. Fluoride stock solution was prepared by dissolving 221 mg anhydrous sodium fluoride in 1000 mL distilled water and using this stock solution, fluoride standard solution is prepared by diluting 100 mL stock solution to 1000 mL distilled water in volumetric flask. This 1 mL solution has 0.1 mg of fluoride. The biomass powder is treated with acid and alkali treatment. Fluoride ion is determined by Orion ion meter as per standard methods. pH meter, and shaking machine for agitating the samples for the required period at a speed of 200 strokes/minute are used. The surface area of the adsorbent particle, porosity and density are measured by using surface area analyzer, mercury porosimeter and specific gravity bottles, respectively.

The most important electro analytic method for determination of fluoride ion in water solution is usage of ion selective electrode for fluorides. Fluoride selective electrode is very sensitive, and temperature range of electrode varies from 0 to 50°C. For potentiometric analysis of fluoride ion, electrodes with homogenic membrane made from fluoride lanthana (LaF₃), which was first suggested by Frant and Ross are mostly used commercially (Frant and Ross, 1966; Frant, 1994; Frant, 1999).

The great selectivity of electrode is important as only fluoride ions are included in the process of diffusion (Cammann, 1979). The potentiometric method is based upon measurements of the potential electromotive force of a galvanic element. Direct potentiometric determinations are almost always performed using ion selective electrodes (ISEs), which are capable of rapid and selective measurements of analyte concentration (Sunitha et al., 2014).

Material Development

Fresh leaves chosen from mint plant (Pudina) are sun-dried for 3-4 days, put in a cotton jute bag and crushed manually (This process can save the energy expended in hot air oven drying and mechanical crushing). The powder was sieved to get various particle sizes, viz. 600 m, 710 m, and 850

m, 1 mm, and 1.4 mm. Leaf powder biomass was further digested by chemical methods.

Sorption Studies

The effect of some major parameters like pH, contact time and amount and particle size of adsorbent and concentration of fluoride ions of the uptake on adsorbent materials is investigated from kinetic viewpoint. Adsorption studies are performed by batch technique to obtain the rate and equilibrium data. Experiments are carried out by shaking 10 g/L of adsorbent dose with 50 mL of aqueous solution containing known concentration of fluoride ions and by agitating the samples on shaking machine at a speed of 200 strokes/min. Samples containing fluoride ions are maintained at a desired pH (5-6) by adding 0.5N HNO₃/0.1M Na OH. All the experiments are conducted at room temperature (29 ± 0.5°C). Preliminary investigations on the uptake of fluoride ions on the adsorbent material at their optimum pH values indicate that the processes are quite rapid. Typically, 80% of the adsorption occurs within the first hour of the contact for fluoride ions with an initial concentration and adsorbent dose of 10 mg/L for treated bio-sorbents.

Sorption Mechanism

The sorption data for the removal of fluoride ions has been correlated with Freundlich and Langmuir models (Jamode et al., 2004).

I. Freundlich Equation:

It has the general form of

$$q_e = K_f C_e^{1/n}$$

The linearised Freundlich adsorption isotherm, which is of the form

$$\log(q_e) = \log K_f + 1/n \log C_e$$

where q_e is the amount of metal ions adsorbed per unit weight of adsorbents (mg/g), K_f and $1/n$ are the Freundlich constants, if $1/n < 1$, bond energies with surface density, if $1/n > 1$, bond energy decreases with surface density and if $1/n = 1$ all surface sites are equivalent. C_e is the equilibrium concentration (mg/L). Linear plots of $\log q_e(x/m)$ vs $\log C_e$ at different adsorbent doses are applied to confirm the applicability of Freundlich models as shown in Figure.1. The calculations for Freundlich model for the removal of fluoride ions are shown in Table 1.

II. Langmuir isotherm

Langmuir isotherm is based on the assumption that point of valence exists on the surface of the adsorbent and that each of these sites is fit for adsorbing one molecule. Thus, the absorbed layer will be one molecule thick. Moreover, it is expected that all the adsorption destinations have break

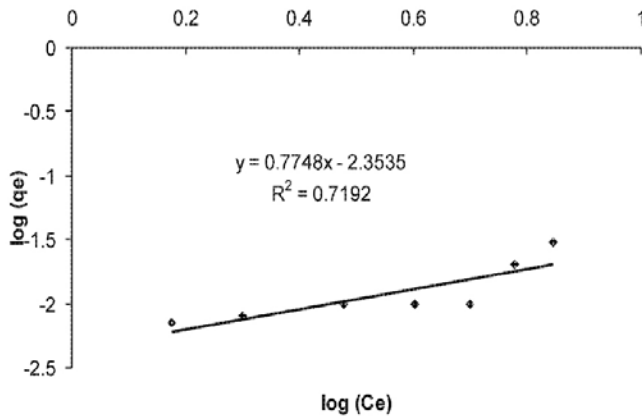


Figure 1. Linear model of Freundlich isotherm.

Table 1. Calculation of Freundlich isotherm.

Dose (mg/L)	C _e (mg/L)	Q _e (mg/g)	1/C _e	1/q _e
50	8	0.04	0.9031	1.4
100	7	0.03	0.8451	-1.6
200	6	0.02	0.7782	-1.7
500	5	0.01	0.699	-2
600	4	0.01	0.6021	-2
700	3	0.01	0.4771	-2
1000	2	0.008	0.301	-2.097
1200	1.5	0.0071	0.1761	-2.15

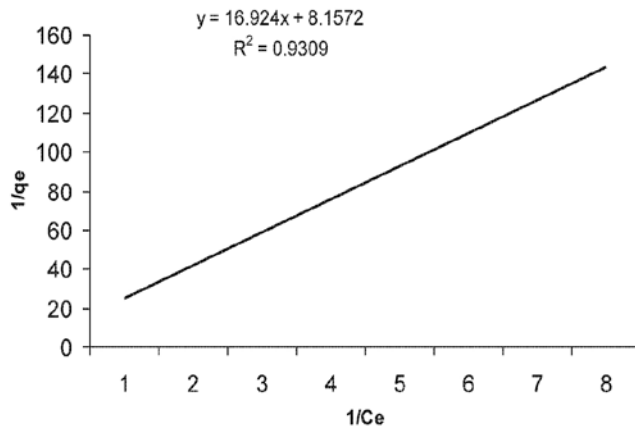


Figure 2. Linear model of Langmuir isotherm.

even with affinities for particles of the adsorbate and that the vicinity of adsorbed atoms at one site won't influence the adsorption of atoms at a nearby site. The Langmuir mathematical statement is normally composed as

$$q_e = Q_0 b C_e / (1 + b C_e)$$

where q_e is the amount adsorbed (mg/g) and C_e is the equilibrium concentration of adsorbate (mg/L), Q_0 and b are the Langmuir constants related to capacity and energy of adsorption, respectively.

The linear form of the Langmuir isotherm can be expressed as,

$$1/q_e = (1/Q_0) + (1/bQ_0 C_e)$$

Whenever $1/q_e$ is plotted against $1/C_e$, a straight line with incline $1/bQ_0$ is obtained. This demonstrates that the adsorption takes after the Langmuir isotherm, as shown in Figure 2. The Langmuir constants b and Q_0 are figured from the slant and catch with Y-pivot. The key attributes of a Langmuir isotherm can be communicated as far as

Table 2: Calculation of Langmuir isotherm.

Dose (mg/L)	C _e (mg/L)	Q _e (mg/g)	1/C _e	1/q _e
50	8	0.04	0.125	25
100	7	0.03	0.1429	33.3
200	6	0.02	0.1667	50
500	5	0.01	0.2	100
600	4	0.01	0.25	100
700	3	0.01	0.3333	100
1000	2	0.008	0.5	125
1200	1.5	0.0071	0.6667	141

dimensionless detachment consider and depict the sort of isotherm characterized by,

$$R = 1/(1 + bC_0)$$

where b and C_0 are terms appearing in Langmuir isotherm.

From figures 1 and 2, it is found that the R^2 value for Langmuir model is near to unity and hence the process of defluoridation using treated biosorbent follows well the Langmuir isotherm. Table 2 gives the calculations of Langmuir model for the removal of fluoride ions and the various constants of this model.

CONCLUSION

Results demonstrate that these minimal effort bioadsorbents could be productively utilized for the evacuation of fluoride over an extensive variety of fixations. Treated biosorbents are seen to be effective for the uptake of fluoride particles somewhere around 2.0 and 10.0 pH. Fluoride removal for a given bio-adsorbent size increased with time attaining equilibrium within 1.5 h. The rate of fluoride removal is observed to be a component of adsorbent dosage and time at a given introductory solute concentration. It expands with time and adsorbent dosage; however, higher initial solute fixation will diminish the time and adsorbent dosage. Biosorbents absorption method follows the Langmuir isotherm, which comprises statistical and empirical data estimated from Isotherm equation. The adsorption capacity of treated biosorbents is studied by varying the initial concentration of fluoride ions between 2 and 15 mg/L. With the largest particle size of 1.4 mm, the amount of fluoride ions adsorbed is found to be 95%. With smallest particle size of 600 μ for an initial fluoride ion concentration of 10 mg/L, 90% adsorption is observed. Small particle size provides more active surface area and hence such results. Treated biosorbents can be removed effortlessly. There is no compelling reason to recover the depleted biosorbents as they are accessible bounteously, effortlessly, economically and locally. This system is financially perceptive, environment friendly and straightforward and can be embraced in provincial and also urban foundation consistently. Water

filtration systems are frequently costly or inadmissible for the situations where they are generally required. The developed technique reported in this study has the advantages of high fluoride removal capacity, ease of operation, economic, environmental friendly and thus making this approach is most desirable to the people, especially in the rural areas with high ground water flouride contaminations.

ACKNOWLEDGEMENTS

The work was funded by the department of science and technology (DST), New Delhi under the Young Scientist Scheme. The financial support from DST for carrying out this study is gratefully acknowledged. Thanks are due to Dr.V.V.Sesha Sai for useful suggestions and objective evaluation. We are grateful for the continued support extended by Dr.P.R.Reddy, Chief Editor of JIGU, for finer refinement and for carrying out final editing.

Compliance with Ethical Standards

The authors declare that they have no conflict of interest and adhere to copyright norms.

REFERENCES

- Adhikari, S.K., Tipnis, U.K., Harkare, W.P., and Govindan, K.P., 1989. Defluoridation during desalination of brackish water by electrodialysis. *Desalination*, v.71, pp: 301-312.
- Amer, Z., Bariou, B., Mameri, N., Taky, M., Nicolas, S., and Elmidaoui, A., 2001. Fluoride removal from brackish water by electrodialysis. *Desalination*, v.133, pp: 215-223.
- Anand Babu, C., Sujish, D., Murugappa, M.S., Mohanakrishnan, G., Kalyanasundaram, P., and Baldev, Raj., 2011. A comprehensive treatment method for defluoridation of drinking water. *Indian Journal of Chemical Technology*, v.18, pp: 314-318.
- Camman, K., 1979. Working with Ion- Selective Electrodes. *Chemical Laboratory Practice*, Springer-Verlag, Berlin Heidelberg New York, p. 225.

- Czarnowski, W., Krechniaki, J., Urbanska, B., Stolarska, K., Taraszewski-Czunowska, and Murasko-Klaudiel, M., 1999. The impact of water-borne fluoride on bone density Fluoride, v.32, p: 91-95.
- Dieye, A., Larchet, C., Auclair, B., and Mar-Diop, C., 1998. Elimination des fluorures par la dialyse ionique croisee, J. Eur. Polym, v.34, pp: 67-75.
- Frant, M., and Ross, J., 1966. Electrode for sensing fluoride anion activity in solution, Science, v.154, no.3736, pp: 1553-1556.
- Frant, M.S., 1999. History of the Early Commercialization of Ion-Selective Electrodes, Analyst, v.199, pp: 2293-2301.
- Fung, K., Zahang, Z., Wong, J., and Wong, M., 1999. Fluoride content in tea and soil from tea plantations and release of fluoride into tea liquor during infusion.
- Hichour, M., Persin F, Sandeaux, J., Molenat, J., and Gavach, C., 1999. Water defluoridation by donann dialysis and electro dialysis. Rev. Sci. Eau, v.12, pp: 671-686.
- Hichour, M., Persin F, Sandeaux, J., and Gavach C., 2000. Fluoride removal from waters by Donann dialysis, Sep. Purif. Technol. v.18, pp: 1-11.
- Jamode, AV, Sapkal, VS., and Jamode, VS., 2004. Defluoridation of water using inexpensive adsorbents. J Indian Inst Sci, v.84, pp: 163-171.
- Lin Chen., Hai-Xia-Wu., Ting-Jie Wang., Yong Jin., Yu Z hang and Xiao- Min Dou., 2009. Powder Technol, v.193, no.1, pp: 59-64.
- Mameri, N., Lounici, H., Belhocine, D., Grib, H., Piron, D.L., and Yahiat, Y., 2001. Defluoridation of Sahara Water by small electrocoagulation using bipolar aluminium electrodes. Sep. Purif. Technol. v.24, pp: 113-119.
- Ranjeeta., 2015. Removal of Fluoride from Drinking Water Using Fly Ash after Pre Treatment. J Environ Anal Toxicol, S7: 004. doi:10.4172/2161-0525.S7- 005.
- Raichur, A.M., and Basu, M.J., 2001. Adsorption of fluoride onto mixed rare earth oxides. Sep. Purif. Technol, v.24, pp: 121-127.
- Reardon, E.J., and Wang, Y., 2000. A limestone reactor for fluoride removal from wastewaters. Environ. Sci. Technol, v.34, pp: 3247-3253.
- Richards, A., Moskilder, I., Sogaard, C.H., 1994. Normal age-related changes in fluoride content of vertebral trabecular bone-relation to bone quality, bone, v.6, pp: 15-21.
- Singh, G., Kumar, B., Sen, P.K., and Majumdar, J., 1999. Removal of fluoride from spent pot liner leachate using ion exchange, Water Environ, Res, v.71, pp: 36-42.
- Sunitha, V., Reddy B., Rajeswara, Reddy M., Ramakrishna 2012. Groundwater Quality Evaluation with Special reference to Fluoride and Nitrate Pollution in Uravakonda, Anantapur District, Andhra Pradesh- a case Study. Int. J. Res. Chem. Environ, v.2, no.1, pp: 88-96.
- Sunitha, V., and Reddy B Muralidhara, 2014. Determination of Fluoride Concentration in Ground Water by Ion Selective Electrode International Journal of Current Research and Academic Review, v.2, no.8, pp: 159-166.
- Saha, S., 1993. Treatment of aqueous effluent for fluoride removal. Water Res, v.27, pp: 1347-1350.
- WHO, 1984. Guidelines for drinking water quality, Health criteria and other supporting information. World Health Organization, Geneva, v.12.

Received on: 13.10.17; Revised on: 16.11.17, Accepted on: 20.11.17

Quotations on Fluoridation and de-fluoridation of water

“There is significant evidence to suggest that the risks from the use of fluoride for prevention of tooth decay exceed any questionable benefit that is achieved.

Clarence Brown (1890 -1987) was an American film director.

“The health risks associated with the use of fluoride in drinking water outweigh, to a significant degree, the slight benefits from that use.”

Phillip M. Allen (1939 -2012) was an American stage, film, and television actor.

Fluoride seems to fit in with lead, mercury and other poisons that cause chemical brain drain. The effect of each toxicant may seem small, but the combined damage on a population scale may be serious, especially because the brain power of the next generation is crucial to all of us.”

Philippe Grandjean (1950--) is a Danish scientist working in environmental medicine.

Feasible Mitigation Options for Air Pollution and Traffic Congestion in Metro Cities

Kopal Verma and Umesh Kulshrestha*

School of Environmental Sciences, Jawaharlal Nehru University, New Delhi 110067 INDIA

*Corresponding Author: umeshkulshrestha@gmail.com

ABSTRACT

Increasing needs of urban population and exploitation of natural resources are the major concerns for environmental degradation. Growing urbanization and unplanned expansion of large cities, especially in developing countries have led to high levels of air pollution. It has been realized that the megacities are the hot spots of air pollution. The Asian and African megacities such as Cairo, Beijing, Delhi, Mumbai, Bengaluru and Kolkata are some of the examples showing alarming levels of air pollutants. Hence, it is the high time for the policy makers to take urgent and apt initiatives that can mitigate urban traffic congestion and air pollution. This paper highlights the possible options such as introduction of bullet train, more intensive network of metro trains, Odd-Even scheme, work from home, flying cars, transit elevated bus, electric vehicles, bi-cycles, compulsory use of public transport along some highly congested roads and restriction in owning more than one car per family, for congestion reduction and air pollution prevention & control in metro cities.

Key words: Environmental degradation, Air pollution, Traffic congestion, Hydrocarbon emission, Greenbelt

INTRODUCTION

Increasing population and associated needs are the rising concerns of the present era. The extent of increase in number of industries and vehicles is much higher compared to the appropriate infrastructure. In urban areas, the number of vehicles is increasing at much faster rate than the road length, resulting in severe road congestion and air pollution. It leads to wastage of time and money and inconvenience while traveling, resulting in health problems. Sao Paulo faces world's worst daily traffic jams (Downie, 2008). According to the Time Magazine, Sao Paulo is known for record breaking 344 km long cumulative queues in the evening peak hours. In 2010, China experienced world's worst traffic jam ever, famously called as "Great Chinese Gridlock of 2010", which was 100 km long and lasted for 11 days. Indian cities such as Delhi, Bengaluru and Mumbai also have frequent traffic jams (Mishra and Chaturvedi, 2017). During the 19th Century, non-motorized modes of transport like walking, bullock carts and cycling were very common. Unfortunately, with the advent of modern technology based vehicles, commuters have variety of alternatives such as motorbikes, cars, trucks and other modes of fast moving vehicles in order to save time and to have enhanced safety over the non-motorized modes. The scenario of traffic congestion and air pollution was the worst in Delhi during 1990's. Later on, the construction of flyovers, introduction of Metro trains and CNG buses provided some relief to the citizens of the capital. The causes of congestion and the feasible options to reduce the congestion and air pollution in the metro cities, especially in India are detailed in this paper.

TRAFFIC CONGESTION AND AIR POLLUTION

According to Central Pollution Control Board (CPCB, 2006), approximately 70% of CO, 30-40% of NO_x and 50% of hydrocarbons are being contributed by the vehicles in metropolitan cities in India. Now, this percentage greatly varies with the type and engine of vehicle, fuel type, road geometry, time of the day (peak or off-peak hours), idling time, vehicle weight, number and duration of stops, flow speed, vehicle operating mode, etc. (Durbin et al., 1998; Beydoun and Guldmann, 2006; Faiz et al., 1996). On-road emissions from urban traffic during interrupted and congested flow conditions are too high as compared to free-flow condition and often influenced by accelerating and decelerating speed due to frequent stop-and-go. According to the Pollution reports, the higher emissions have been noticed at very specific times e.g.: (i) during acceleration stage, which depends on road quality and geometry (Shukla and Alam, 2010; Pandian et al., 2009; Gokhale, 2012), (ii) during the transitional phase, the flow of traffic changes from free to congested condition (Zhang et al., 2011) and (iii) when heavy duty diesel vehicles are moving with low speed and having frequent acceleration and deceleration cycles, especially that of CO and hydrocarbons (Chen et al., 2007). Hydrocarbon emissions can come not only from a vehicle's engine but also directly from the fuel tank and lines, making emission free environment a difficult proposition. In addition to these, vehicles with 2-stroke engines (autos or two-wheelers), which do not have catalytic convertor emit higher (approximately 20% more) CO and hydrocarbons than passenger cars having 4-stroke engines (Choudhary and Gokhale, 2016; Reynolds et al., 2011).

Table 1. Comparison of population and motor vehicles per 1000 people in various countries.

S.No.	Country	Population in 1996 (in millions)	Population in 2016 (in millions)	Motor Vehicles per 1000 people
1	San Marino	0.025	0.031	1263
2	Monaco	0.030	0.037	899
3	USA	269.4	324.5	797
4	Australia	18.31	24.36	736
5	Canada	26.97	36.28	662
6	Japan	125.8	126.28	591
7	UK	58.17	65.18	519
8	Russia	148.2	143.4	293
9	China	1218.0	1383.4	128
10	India	973.1	1329.5	18

(Source: Real time world index: www.worldometers.info/).

Although, the usage of cars and taxis is much higher than the two-wheelers, it outweighs the pollution caused by the later (Ramachandra, 2009; Singh, 2006).

CHALLENGES POSED

The urban transport also includes public and non-motorized transport with badly managed road facilities. On top of this, political decisions make the whole process lengthy and inefficient (Ahmad and Puppim de Oliveira, 2016). The concept of lane driving, footpaths, crossings, etc. which are very common in developed countries are almost non existing in India. Hence, there is mixed traffic on roads usually such as cars, trucks, pedestrians, animal-driven carts, two-wheelers, cycles, rickshaws and auto-rickshaws (in addition to cattle).The quixotic nature of these mixed traffic increases the chances of accidents, leading to further traffic jams.

According to the Eddington Transport Study, traffic congestion leads to a loss of £11 bn every year and for approximately 90% of businesses it is a significant problem (Eddington, 2006). On one hand, the number of vehicles per family in developed countries is increasing at an alarming rate—while on the other hand, developing countries are still struck in the problems of poor quality of roads, fuel adulteration, illegal parking, wrong-way driving, overloading, mixed traffic, lack of traffic lights, flooding of the roads due to improper drainage, ill-managed diversions during on-road constructions, narrow one-ways, weak implementing of pollution check, etc. The lack of coordination between PWD and/or R&B and various departments such as telephone and electricity (cable laying), water, gas lines, and sewerage (pipe lines) is leading to frequent excavation of roads, adding to more traffic problems.

STATISTICS OF TRANSPORTATION

Table 1 gives the number of motor vehicles per 1000 people in various countries. It is surprising to note that small countries such as San Marino and Monaco in Europe with land areas of 6100 hectare and 202 hectare respectively, are having very high number of motor vehicles per 1000 people, and yet hardly any significant incident of traffic congestion has occurred. On the other hand, countries like China and India, ranking first and second respectively in the world's population index, are having very low number of motor vehicles per 1000 people but frequently face extremely bad traffic congestion. Major cities ranked as per their congestion levels based on Tom Tom Traffic Index (www.tomtom.com/en_gb/trafficindex/list) have been shown in Table 2.

Various Methods to Estimate Traffic Congestion:

(i). Horn-OK Project: Under this project, speed of the moving vehicle is detected by capturing the horn blown by vehicles (by a pair of road-side microphones), as they will show Doppler shift and hence traffic congestion can be estimated.

(ii). GPS based sensing: This is the most popular and frequently used technique to get the updates about traffic density scenario and alternate routes. Because of telecommunication network failure especially during adverse weather, people get stuck up in the traffic, having taken the wrong route and unavailability of alternate route. If the whole city is provided with the facility of high speed Wi-Fi network, automatic traffic and alternate route updating can eventually become fast and reduce the traffic congestion.

(iii). Sensors on Roads: Roads with usual events of traffic congestion can be rebuilt with a layer of sensors,

Table 2. Comparison of congestion levels of major cities in the world.

World Rank	City	Country	Congestion Level (Extra Travel Time)	Morning Peak	Evening Peak
1	Mexico City	Mexico	59%	97%	94%
2	Bangkok	Thailand	57%	85%	114%
3	Istanbul	Turkey	50%	62%	94%
4	Rio De Janeiro	Brazil	47%	66%	79%
5	Moscow	Russia	44%	71%	91%
6	Bucharest	Romania	43%	83%	87%
7	Salvador	Brazil	43%	67%	74%
8	Recife	Brazil	43%	72%	75%
9	Chengdu	China	41%	73%	81%
10	Los Angeles	United States	41%	60%	81%
14	Beijing	China	38%	62%	78%
16	London	United Kingdom	38%	63%	66%
39	New York	United States	33%	49%	61%

(Source: www.tomtom.com/en_gb/trafficindex/list).

which will monitor the number of vehicles on it and when the number is tending to congestion then it will automatically block the road to avoid further use by other vehicles.

FEASIBLE MITIGATION OPTIONS FOR REDUCING TRAFFIC CONGESTION

In order to reduce the road traffic volume and air pollution in urban areas, a proper planning towards development of whole transportation system and land use management have to be opted, which will be governed and controlled by public authorities for its proper functioning (Tennoy, 2010). The various approaches and strategies to be adopted to reduce the problem of traffic congestion and air pollution would be specific to the region of the country. These should include: reducing Green House Gas (GHG) emissions from the vehicle per km, total travel length of the trip, frequency of the trips, shift from public and non motorized transport to private transport (Tennoy, 2010). Hence, the problem of traffic congestion has to be dealt extensively on priority basis. Examples of the feasible options are mentioned below.

Metro Rail Network

Metro rail network is an electricity based rapid transit train system for faster commuting inside the city. The successful examples of metro systems across the world are underground London metro, the oldest of all; Shanghai Metro system, the one with longest route length; Beijing metro system is known as subway and has the highest number of people in the world using this mode for

commuting. Metro rail system has also been introduced in Delhi, which has now stretched its limit to Gurugram, Noida and Ghaziabad. Various studies have been carried out, which have proved that Metro Rail network has brought down a significant amount of congestion, for example, west Bengaluru has witnessed 15% decrease in traffic congestion because of metro.

Electric Vehicles

Electric vehicles are basically totally clean and green mode of transportation because they run on rechargeable batteries that store chemical energy in it. With the modern technology, continuous efforts are in process to convert the fuel based modes of transport into electricity based vehicles. At present, bicycles, motorcycles, scooters, cars, buses, trucks and even trains run on rails and watercrafts have taken the form of electric vehicles. Among the all-electric car models, Nissan Leaf has topped the sales all over the world followed by Tesla Model S. According to NITI Aayog, the nation is estimated to see sales of 30.81 million electric vehicles by 2040. Arcimoto is an emerging electric vehicle, which runs on electricity, carries two passengers comfortably and safely. It can be driven at a maximum speed of 85 km/hr and acquires one-third of the parking space required usually by cars. Look and comfort wise it is a mixture of car and motorcycle, so if only one or two passengers have to travel, it is the best option as it is environmental friendly and also covers much less space as compared to the car. The Arcimoto can be looked upon as the future generation transportation for daily trips and it has already launched its eight generations.

Flying Car

The time is not far when flying cars of science fiction will come into reality. A flying car is a personal air vehicle, which can provide the transportation both by air and road as per the requirement. Many models like AeroMobil, Urban Aeronautics' XHawk, The Moller Skycar M400, The Xplorair, etc have already been built and tested but its production has not yet started for public use.

Solar Car

Solar vehicles are also an example of electric vehicle only just with the difference that they are powered by solar energy directly. The electrical energy used in solar vehicles is converted from solar energy by photovoltaic cells carried in solar panels. So far, demonstration models of solar cars, solar bike, solar train, solar watercraft, etc. are ready. However, finer adjustments need to be completed to bring these to the commercial front.

Odd-Even Rationing of Vehicles

Under the Odd-Even Rule, the four wheelers with odd number can travel on odd dates and vice versa. This practice was introduced in Delhi, the capital of India in two terms each of 15 days. This practice was expected to reduce the number of vehicles on road. Such a reduction was achieved to some extent but it has increased the chaos among the public also (Hindustan Times, 27 April 2016). If we talk in terms of pollution level during the Odd-Even Rule in Delhi, its critical assessment indicated hardly any improvement in pollutants level such as $PM_{2.5}$, PM_{10} and CO (Singh and Kulshrestha, 2016). Nevertheless, the scheme reduced the traffic congestion during both the Odd-Even trials.

Transit Elevated Bus

Transit Elevated Bus is a new concept to cope up from the problem of traffic congestion, with alternative names such as straddling bus and land airbus. This kind of bus is actually elevated, so that it can straddle above the road traffic. China is the pioneer in creating such kind of a bus and had its first trial in 2016. Vehicles with a height of 2m can pass from below this straddling bus, which is 4-4.5m high and a capacity to carry 300 passengers (Limer, 2016). It will function like the normal buses, just that the stops of these buses will be elevated. Though this concept has yet not been functionalized, because it is being criticized on the fact that whether the vehicles under this bus will be safe or not and usually lanes are not straight all along for its smooth functioning.

Work and Learn from Home

The concept of work from home is new and is being explored. It is linked with E-commerce. In the age of technologies and high speed network of internet, offices and colleges can be set up in home itself; one need not travel to carry out office work. With the help of Skype or other networking sites, online official conferences or college classes can be made possible. In order to legalize this approach of study, government can take actions and make plans as to how one can do all the requisite things like admission, attendance, examination, issuing degree with least possibilities of fake entries. Also, nowadays, migration of students from small places to metro cities is very common, in order to avail better opportunities and better studies. If the extent of communication technology can be expanded till the nook and corner of each city, town and village, one can avail such opportunity at their home itself and the reasons to migrate will subside.

Bullet Train

Bullet train is a high-speed rail transport system, which is much faster than the traditional trains and can easily maintain a speed of maximum 350km/hr. This mode of transportation took its birth in Japan and is now spreading all over the world as a quicker and comfortable way to commute. It is just launched on September 14, 2017 in India too. The first bullet train will run between Ahmedabad and Mumbai covering 508 km distance in 2.07 hours. There are many benefits of bullet trains. A large number of passengers can travel at a time; it saves time, energy and money by covering large distances with its fast speed; highways and runways for traveling in the city can be relieved and also congestion and delays are avoided even during rush hours.

Taxes for Toll Roads

The concept of toll roads is very old where road user is charged for distance driven in a particular area. Access fees and time based charges are applied for accessing a particular area for a given amount of time by the road user; infrastructure tolling for incurring the cost of building infrastructures like bridges, tunnel, mountain pass, flyovers, etc. However, many times road users have complaints of waiting in long queues, which further add to the traffic congestion. But the waiting and queue problem can be resolved by online payment facility of toll taxes and providing a separate lane for the free flow of the road users who have already paid the taxes. In general, toll booths have such provision but the facility can be provided at smaller booths too.

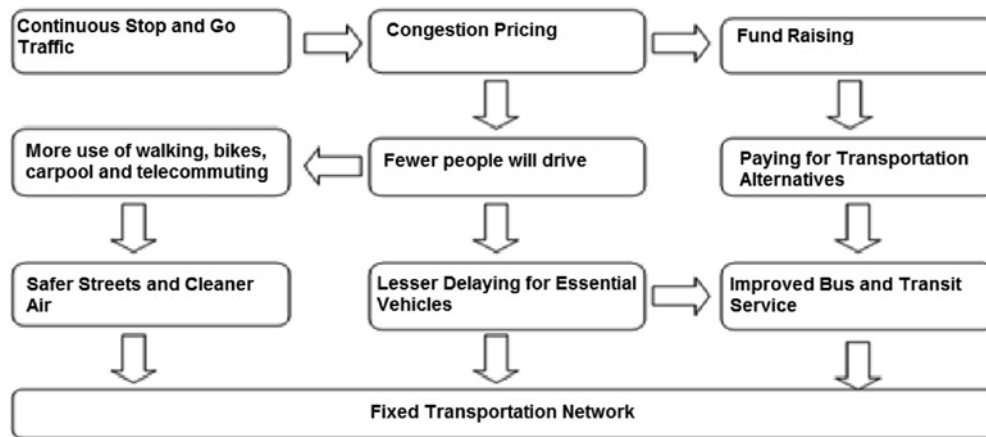


Figure 1. A flow chart to describe the strategy of congestion pricing. (Source: Congestion Pricing-Wikipedia).

Introduction of Congestion Price

In congestion pricing method, a fee is charged from the road users in rush hours, which is variable depending upon the time and day. Singapore has become the first city of the world to apply this scheme (Small et al., 2007). During rush hours or peak timings of the day, the congestion price is highest whereas in off-peak hours it is the lowest and sometimes there is no charge at all. This is a viable economic way of decongestion as this method ensures the minimum traffic on road (Sheldon et al., 1995). This method is worthy to implement as commuters become more cautious to avoid congestion, and would start thinking of the alternate ways to get to their destination in rush hours (Small et al., 1998). Figure 1 illustrates how congestion pricing works.

Limit the Number of Vehicles or Vehicles from other regions during peak hour

This can prove to be a very useful strategy towards reducing the traffic congestion and increase the usage of public transport. Already China has introduced such measures, where only 20,000 new passenger cars can be issued in a month (the registered residents of the city will be assigned new license plates by lottery system and 88% of the cars are reserved for private car users) and not allowing vehicles from outside regions in the main parts of the city during rush hours.

Systemized Urban Planning

There is yet another way to look at the solution for traffic congestion, which is to restructure the planning of the cities (Verma and Singh, 2017). If all or majority of these purposes are clubbed and offered at a single place, there will be no need to travel such large lengths, which will further reduce congestion. For example, for a particular section of people who are working for the same

profession, a society can be constructed, which is having the facilities of their common office, housing, garden and parks, fitness clubs, swimming pool, shopping mall, multiplexes, school, college and other basic facilities. In order to closely observe how traffic flow and density are related in urban areas, Macroscopic Fundamental Diagram (MFD) is a very useful tool. With the help of MFD, effective urban planning can be done, so that resource allocation can be done efficiently. The MFD thoroughly examines the congestion and evaluates its relation with density and hence can very well correlate the features of transportation network and land use pattern, which can further help in designing the city with optimum land use, well planned road network and traffic control. MFD can easily monitor and model congestion and can prove to be a useful aid in framing policies for smooth traffic flow and minimum possible environmental pollution in the city. Tsekeris and Geroliminis (2013) have proposed and studied in detail a model of the city, which is mono-centric in nature and has surrounding neighborhood in concentric pattern.

EFFORTS MADE BY INDIAN GOVERNMENT

According to the National Highways Authority of India, the average growth rate of number of vehicles is 10.16 percent per year in India. Major sufferers of traffic congestion are cities like Mumbai where every km of road is holding about 674 vehicles (Hindustan Times, 23 Mar 2012); Bangaluru with 3000km of road stretch is having around 5 million vehicles; Delhi alone has more vehicles than Kolkata, Chennai and Mumbai together (Economic Survey of Delhi, 1999-2000). Indian government is making explicit efforts to combat the problem of traffic congestion. It has recently sanctioned a \$50 billion highway project in order to enhance the 40,000kms of highways of India. The Urban Transport Working Group is designing a completely new framework, which will consist of major use of public

transport such as Bus Rapid Transit and Metro rail, traffic signals, development of more lanes and one-way streets.

In December 2005, a seven-year plan was launched, Jawaharlal Nehru National Urban Renewal Mission (JNURM) city-modernization scheme with a total investment of \$20 billion, which will work towards the upgrading of city structure, socially and economically, planning to minimize traffic congestion, broadening roads and construction of more flyovers and foot bridges. In order to cope up with the traffic problem, Government has developed a strategy called Delhi's Master Plan 2021, which promises to increase the use of public transport by around 80% of the commuters by 2020.

Some of the additional measures of air pollution and congestion prevention and control include- increased greenbelt, control of construction dust, development of flyovers and express by passes, enforcing stringent Pollution Under Control (PUC) check up, implementation of Bharat VI standards, projecting only one nodal agency as a top management body for effective implementation, spreading more public awareness, making rule for primary school not beyond 5 km circle and by emphasizing for quality controlled monitoring data for policy formulation.

CONCLUSION

Traffic congestion is a monster for a commuter. Reducing traffic congestion should be the priority for both the government and the public. In addition to the metro expansion, road widening, flyovers, bypasses reduction of sales of new vehicles and withdrawal of vehicles of 12 years age need to be enforced to reduce congestion. Our top recommendation for reducing congestion is to legally allow 'work from home' culture, which will not only reduce congestion but also solve or reduce the personal or family problems such as attending to the needs of kids, old parents and other family members.

ACKNOWLEDGEMENTS

We would specifically like to acknowledge the award of fellowships from UGC (University Grants Commission) and CSIR to the first author. We sincerely thank the constant support from DST-Purse Grants to make this study possible. We thank Dr.M.R.K.Prabhakara Rao for some useful suggestions. We place on record our thanks to Dr.P.R.Reddy, Chief Editor for restructuring of the manuscript, proper editing and continued support.

Compliance with Ethical Standards

The authors declare that they have no conflict of interest and adhere to copyright norms.

REFERENCES

- Ahmad, S., PuppimdeOliveira, J.A., 2016. Determinants of urban mobility in India: Lessons for promoting sustainable and inclusive urban transportation in developing countries. *Transport Policy* v.50, pp: 106–114.
- Downie, A., (2008-04-21). "The World's Worst Traffic Jams". Time. Retrieved on 2008-06-20.
- Beydoun, M., Guldmann, J.M., 2006. Vehicle characteristics and emissions: logit and regression analyses of I/M data from Massachusetts, Maryland, and Illinois. *Transport. Res. Part D*, v.11, pp: 59–76.
- CPCB, Central Pollution Control Board. Air Quality Trends and Action Plan for Control of Air Pollution from Seventeen Cities. Series: NAAQMS/29/2006-07, September 2006.
- Chen, C., Huang, C., Jing, Q., Wang, H., Pan, H., Li, L., Zhao, J., Dai, Y., Huang, H., Schipper, L., Streets, D.G., 2007. On-road emission characteristics of heavy-duty diesel vehicles in Shanghai. *Atmospheric Environment*, August 2007, v.41, no.26, pp: 5334-5344.
- Choudhary, A., and Gokhale, S., 2016. Urban real-world driving traffic emissions during interruption and congestion. *Transportation Research Part D*, v.43, pp: 59-70.
- Wikipedia, Congestion pricing: https://en.wikipedia.org/wiki/Congestion_pricing.
- Hindustan Times, Dharmendra Jore (2012-03-23) "Mumbai has 674 vehicles for every km of road".
- Durbin, T.D., Truex, T.J., Norbeck, J.M., 1998. Particulate Measurements and Emissions Characterization of Alternative Fuel Vehicle Exhaust. Center for Environmental Research and Technology, College of Engineering, University of California, Riverside.
- Economic Survey of Delhi, 1999-2000. Chapter 12. Transport.
- Eddington, R., 2006. The Eddington Transport Study, The case for action: Sir Rod Eddington's advice to Government. UK Department for Transport. Archived from the original on 2008-03-24.
- Faiz, A., Weaver, C.S., Walsh, M.P., 1996. Air Pollution from Motor Vehicles: Standards and Technologies for Controlling Emissions. World Bank Publications.
- Gokhale, S., 2012. Impacts of traffic-flows on vehicular-exhaust emissions at traffic junctions. *Transport. Res. Part D: Transp. Environ.* v.17, pp: 21–27.
- Limer, Eric., 2016. "Chinese Straddling bus can carry 300 people". Yahoo Tech. Retrieved 4 August 2016.
- Mishra, M., and Chaturvedi, M., 2017. Air pollution of megacities. In *Air Pollution & Climate Change in South Asia; Issues, Impact and Initiatives* (Editor: Umesh Kulshrestha), Athena, IK, pp: 119-127.
- Pandian, S., Gokhale, S., Ghoshal, A.K., 2009. Evaluating effects of traffic and vehicle characteristics on vehicular emissions near traffic intersections. *Transport. Res. Part D: Transp. Environ.* v.14, no.3, pp: 180–196.

- Ramachandra, T., 2009. Emissions from India's transport sector: state wise synthesis. *Atmos. Environ.* v.43, no.34, pp: 5510–5517.
- Reynolds, C.C., Kandlikar, M., Badami, M.G., 2011. Determinants of PM and GHG emissions from natural gas-fueled auto-rickshaws in Delhi. *Transport. Res. Part D: Transp. Environ.* v.16, no.2, pp: 160–165.
- Sheldon, G., Strickland, Wayne Ber., 1995. Congestion Control and Demand Management. *Public Roads Magazine. U.S. Federal Highway Administration.* v.58, no.3.
- Shukla, A., and Alam, M., 2010. Assessment of real world on-road vehicle emissions under dynamic urban traffic conditions in Delhi. *Int. J. Urban Sci.* v.14, no.2, pp: 207–220.
- Singh, S.K., 2006. Future mobility in India: implications for energy demand and CO2 emission. *Transp. Policy* v.13, no.5, pp: 398–412.
- Singh, Y., and Kulshrestha, U.C., 2016. Critical Assessment of Odd and Even in Delhi. *Journal of Energy Environment and Carbon Credits.* v.6, pp: 1-6.
- Small, Kenneth A., José A., Gomez-Ibañez., 1998. Road Pricing for Congestion Management: The Transition from Theory to Policy. The University of California Transportation Center, University of California at Berkeley. p: 213.
- Small, Kenneth A., Verhoef, Erik T., 2007. *The Economics of Urban Transportation.* Routledge, New York. ISBN 978-0-415-28515-5, p: 120.
- Tennoy, A., 2010. Why we fail to reduce urban road traffic volumes: Does it matter how planners frame the problem? *Transport Policy* v.17, pp: 216–223.
- Tsekeris, T., and Geroliminis, 2013. City size, network structure and traffic congestion. *Journal of Urban Economics* v.76, pp: 1–14.
- Verma, K., and Kulsreshtha, U.C., 2015. CO2 emissions and soft approaches of mitigation fro NCR-Delhi. *World Focus*, October, 2015.
- Verma, K., and Singh, Y., 2017. *Air Pollution & Climate Change in South Asia; Issues, Impact and Initiatives*, Editor: Umesh Kulshrestha. Chapter 13: Climate Change Mitigation.
- Zhang, K., Batterman, S., Dion, F., 2011. Vehicle emissions in congestion: comparison of work zone, rush hour and free-flow conditions. *Atmos. Environ.* v.45, no.11, pp: 1929–1939.

Received on: 21.9.17; Revised on: 5.11.17; Accepted on: 12.11.17

Quotations on Air Pollution and Traffic Congestion

“Water and air, the two essential fluids on which all life depends, have become global garbage cans.”

Jacques-Yves Cousteau (1910–1997) was a French naval officer, filmmaker, scientist, author and researcher.

“The environmental effects of the automobile are well known: motor vehicles cause, for example, as much as 75 percent of the noise and 80 percent of the air pollution in our cities, and the industry must face mounting pressure from environmentalists.”

Stewart Udall (1920–2010) was an American politician.

This isn't life in the fast lane, its life in the oncoming traffic.

Terry Pratchett (1948 -2015) was an English author of fantasy novels, especially comical works.

Traffic is only one of the side effects of growth.

Roy Barnes (1948--) is an American attorney and politician.

“The more we pollute the earth, the less we deserve to live on earth!”

Mehmet Murat ildan(1965--) Was a Turkish playwright and writer.

Relationships are like traffic lights. And I just have this theory that I can only exist in a relationship if it's a green light.

Taylor Swift (1989--) is an American singer-songwriter.

Probing Chemical Heterogeneity of the Mantle Using Open System Isotopic Models of the Silicate Earth

Seema Kumari* and Debajyoti Paul

*Department of Earth Sciences, Indian Institute of Technology Kanpur, Kanpur 208016, Uttar Pradesh, India

*Corresponding Author:091089seema@gmail.com

ABSTRACT

The layering and convection within the Earth's mantle plays a major role in the formation of continental crust as well as tectonic activities and the heat budget of the Earth. The mode of mantle convection (whole versus layered) is still debatable despite concerted geophysical and geochemical studies for the past several decades. This study is an exhaustive numerical approach to develop an open system geochemical model for the Earth comprising bulk continental crust (CC), depleted upper mantle (UM)–source of mid–ocean ridge basalts (MORB), a lower non-chondritic mantle (LM)–source of ocean island basalts (OIB), and an isolated reservoir (IR). The model is solved numerically using fourth-order Runge-Kutta method at 1 Ma time step over the age of the Earth, simulating the evolution of key radioactive isotope systems in terrestrial reservoirs. Coupled Rb–Sr, Sm–Nd, and U–Th–Pb isotope systematics will constrain various aspects related to the Earth's differentiation processes leading to chemical heterogeneity within the mantle. Various crustal growth scenarios (linear vs. non-linear, early vs. delayed, and continuous vs. episodic growth) and their effects on the evolution of isotope systematics in the silicate reservoirs have been evaluated. The most plausible model-derived solution is the one that produces the present–day concentrations as well as isotopic ratios in the terrestrial reservoirs, constrained from published data. Modeling results suggest that a whole mantle (compositionally similar to the present–day MORB) model fails to satisfy observational constraints. However, a layered mantle model, in which the present–day UM is ~ 60% of total mantle mass and the lower mantle is non–primitive produced the required isotopic ratios and abundances in the terrestrial reservoirs. Modeling also suggests that isotopic evolution in reservoirs is strongly affected by the mode of crustal growth. It is observed that Pb paradoxes result from open system evolution, which allows large-scale mass exchange between reservoirs.

Key words: Mantle convection, open system modeling, crustal growth pattern, Pb paradox.

INTRODUCTION

Several geochemical approaches have been adopted to study layering and convection in the mantle, which includes mass balance models (Jacobsen and Wasserburg, 1981; Turcotte et al., 2001), open system evolution models consisting both forward transport modeling and inverse approach (e.g., Kramers and Tolstikhin, 1997; Allègre et al., 1983; Paul et al., 2002; Kellogg et al., 2002 and 2007). This study presents a four–reservoir open system evolution model of the Earth comprising a bulk continental crust (CC), a depleted upper mantle (UM) that is source of mid– Ocean ridge basalts (MORB), an enriched lower mantle (LM) that is source of plume– derived ocean island basalts (OIB), and a highly–enriched isolated reservoir (IR) at the base of the mantle where majority of the subducted lithospheric material is stored. The term “depleted and enriched” are used with reference to highly incompatible trace elements. Incorporating Rb–Sr, Sm–Nd, Lu–Hf and U–Th–Pb isotope systematics, isotopic evolution in terrestrial reservoirs is numerically simulated with time (age of the Earth) from an initial to its final state ($t = 4.55$ Ga; age of the Earth) that is constrained by the present–day compositions.

Further, the secular growth of the continental crust may have been largely affected the distribution of chemical heterogeneities within the mantle to the extent of producing chemically distinct layers. In other words, continuous production of crust, episodic production at certain time intervals, higher growth initially followed by negligible growth etc. as well as recycling of this crustal material at different times will affect the timing of depletion of highly incompatible radioactive parents in the mantle and consequential enrichment in the crust. This, in turn would affect the evolution of daughter isotopic compositions in the respective reservoirs. Therefore, growth of continental crust with time should be an important constraint in open system models. One of the key goals of this study is to understand the means and to quantify the mass transfer processes between different portions of the Earth through the geologic time in an open system isotope evolution model.

METHODOLOGY

In our model (schematics shown in Figure 1), the continental crust grows at the expense of magmatic fluxes from both the upper and lower mantle. Also the mass of

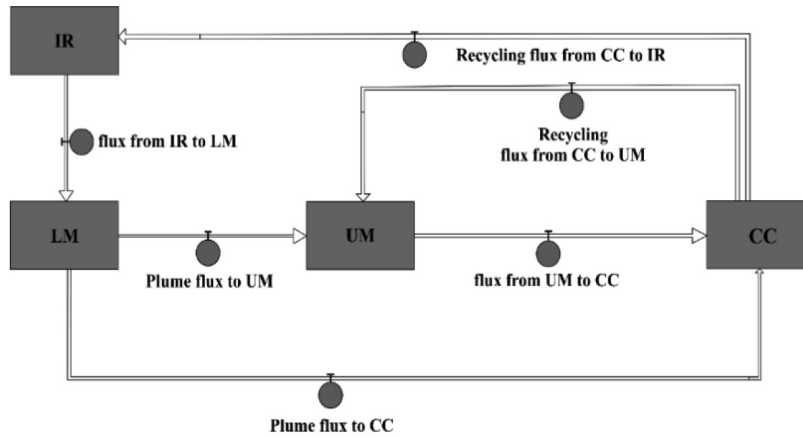


Figure 1. Open system mass transfer model considered in this study. Input and output flux to the reservoir is shown by arrows. UM– Depleted Upper Mantle; LM– Lower Mantle; CC–Bulk Continental Crust; IR–Isolated Reservoir.

UM is a function of input fluxes such as plume flux from LM, recycling flux from CC and the output flux from UM to the CC. Similarly, LM mass grows due to incoming flux from CC that is stored in the IR reservoir at first and then slowly mixed with the LM after a transit time of about one billion years. LM also contributes to the growth of UM and CC in the form of rising plume.

Mathematically, the rate of change of mass of the continental crust can be expressed as

$$\begin{aligned} \frac{dM_{CC}}{dt} &= F_{LM \rightarrow CC} + F_{UM \rightarrow CC} - F_{CC \rightarrow D \text{ layer}}^R - F_{CC \rightarrow UM}^R \\ &= c_1 e^{\lambda(b-t)} f_{LM} + c_1 e^{\lambda(b-t)} (1 - f_{LM}) \\ &\quad - c_2 M_C e^{\lambda(b-t)} f_C - c_2 M_C e^{\lambda(b-t)} (1 - f_C) \quad (\text{Eq. 1}) \end{aligned}$$

where b and λ are constants and M_{CC} refers to the mass of the continental crust. Initially, $t = 0$, and for the present-day $t = b$, where b represents the age of the Earth. The parameters c_2 are adjusted in different scenarios such that the model must yield present-day mass of the continental crust (M_{CO}); c_1 is a function of c_2 . The parameter λ is scaled according to the radiogenic heat generation in the mantle, which is directly proportional to the concentration of heat producing elements (HPE: U, Th and K) in the mantle. f_{LM} and f_C are fractional contributions of LM to the crust and crust to the LM (through IR), respectively. Hence, $1 - f_{LM}$ is the fractional contribution of UM to the crust and $1 - f_C$ is the fractional contribution of crust to UM. The first two terms on the R.H.S of equation (1) are additive as they are the growth terms (magmatic fluxes from LM and UM to the crust), whereas the other two terms are subtractive as it represents the recycling fluxes from crust to LM and UM. The rate of change of total amount i.e. moles of isotopic species in each reservoir can be specified in a very similar manner as that of the mass transfer. For a given species i (e.g. ^{87}Sr), the flux from reservoir a to reservoir b (F_{ab}), is a function of the mass flux $F_{a \rightarrow b}$, the concentration of i in reservoir a , and the mean enrichment factor for that

species/element during the transfer between the reservoirs. Note that the mean enrichment factor essentially controls the extent of enrichment of the incompatible trace element in the crust, and is a variable parameter in our model.

The initial state of the model is assumed to be of homogeneous chondritic composition, which further differentiated into crust and mantle reservoirs. A set of differential equations fully constraining the Rb–Sr, Sm–Nd, U–Th–Pb isotope systems are solved repeatedly using Runge–Kutta numerical algorithm over the age of the Earth at 1 Ma time steps.

DISCUSSION AND CONCLUSIONS

The geochemical modeling explores how different continental crust extraction models (continuous versus episodic and early versus late and concave upward versus concave downward growths) modify the geochemical evolution of the silicate reservoirs. The objective was to reproduce the present-day isotopic ratios in the UM and crust (shown in Figure 2 as vertical bars in the right-hand side Y-axis), which are well-constrained values from global data bases. Our modeling results strongly favor exponential crustal growth (Brown, 1979). The temporal evolution of $^{87}\text{Sr}/^{86}\text{Sr}$ and Nd isotopic ratios (ϵ_{Nd}), respectively are shown in Figure 2 for the exponential crustal growth case.

The failure of other crustal growth models (not shown here) in reproducing the present-day isotopic compositions in the CC and mantle reservoirs suggests that neither the production of the entire crust within the first 1 Ga nor the rapid growth in a single event where $\sim 80\%$ of crust formed by the end of Archean within 700 Ma period, are viable scenarios. Particularly, concave upward growth models in which $\sim 50\%$ of crust was formed in the past 1 Ga failed to satisfy isotopic constraints. The simulations show it is possible to resolve the Pb paradox in an evolutionary

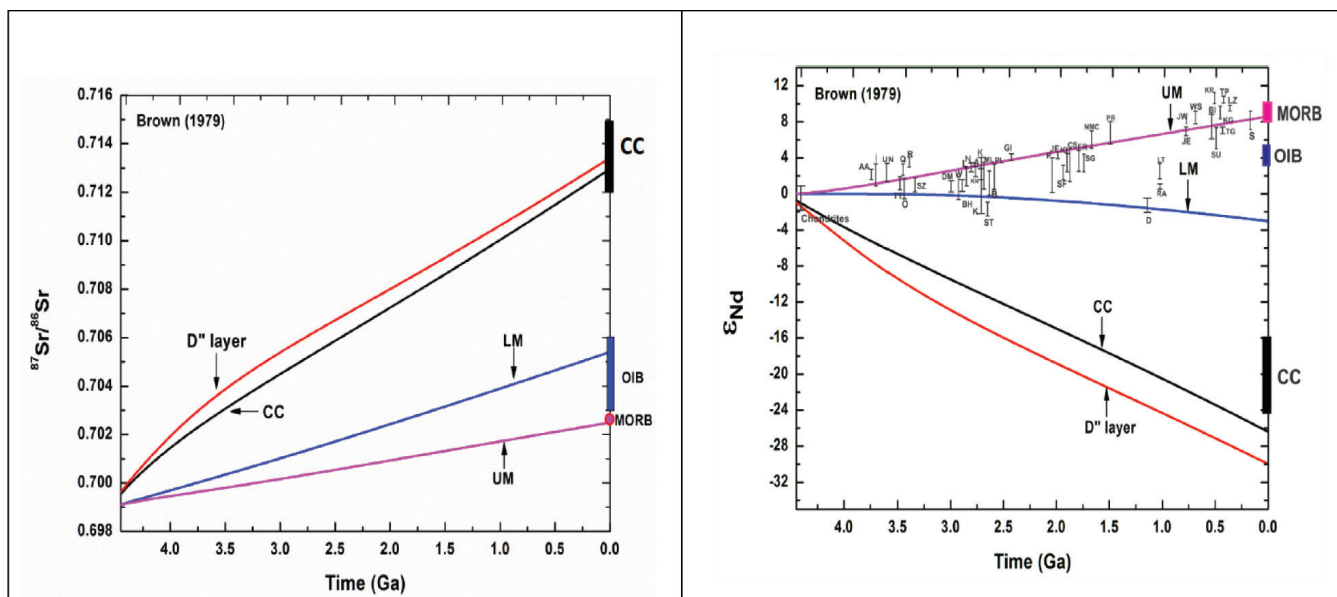


Figure 2. Evolution of Sr and Nd isotopic composition in terrestrial reservoirs in case of the exponential crustal growth model. The model-derived ϵ_{Nd} evolution pattern in UM is compared with the available initial ϵ_{Nd} values in mantle-derived products of known age, such as komatiites, other volcanics, granites and ophiolites, compiled by Galer et al., (1989).

model that also matches mass balance constraints. This study represents an important effort to better constrain the chemical and geodynamic evolution of the silicate Earth.

ACKNOWLEDGMENTS

This research was supported by Department of Science and Technology, India grant to D. Paul (SR/S4/ES-509/2010). We thank Dr. P.R. Reddy, Chief Editor of JIGU for reviewing and editing the manuscript.

Compliance with Ethical Standards

The authors declare that they have no conflict of interest and adhere to copyright norms.

REFERENCES

Allègre, C.J., Hart, S.R., Minster J.E., 1983. Chemical structure and evolution of the mantle and continents determined by inversion of Nd and Sr isotopic data, II. Numerical experiments and discussion, *Earth and Planetary Science Letters*, J.66, pp: 191-213.

Brown, G.C., 1979. The changing pattern of batholith emplacement during earth history, In: Atherton, M.P., Tarney, J., (Eds.),

Origin of Granite Batholiths. Shiva, Nantwich, UK, pp: 106-115.

- Galer, S.J.G., Goldstein, S.L., O’Nions, R.K., 1989. Limits on chemical convective isolation in the Earth’s interior, *Chemical Geology*, v.75, pp: 257-290.
- Jacobsen, S.B., Wasserburg, G.J., 1981. Transport models for crust and mantle evolution, *Tectonophysics*, v.75, pp: 163–179.
- Kellogg, J.B., Jacobsen, S.B., O’Connell, R.J., 2002. Modeling the distribution of isotopic ratios in geochemical reservoirs, *Earth and Planetary Science Letters*. v.204, pp: 183-202.
- Kellogg, J.B., Jacobsen, S.B., O’Connell, R.J., 2007. Modeling lead isotopic heterogeneity in mid-ocean ridge basalts, *Earth and Planetary science Letters*, v.262, pp: 328-342.
- Kramers, J.D., Tolstikhin, I.N., 1997. Two terrestrial lead isotope paradoxes, forward transport modelling, core formation and the history of the continental crust, *Chemical Geology*, v.139, pp: 75-110.
- Paul, D., White, W.M., Turcotte, D.L., 2002. Modelling the isotopic evolution of the Earth, *Phil. Trans. Royal Society London.*, v.360, pp: 2433-2474.
- Turcotte, D.L., Paul, D., White, W.M., 2001. Thorium–uranium systematics require layered mantle convection, *Journal of Geophysical Research*, v.106, no. B3, pp: 4265-4276.

Received on: 30.10.17; Reviewed on: 29.11.17; Revised & Accepted on: 10.1.18

Dynamics of drought and present status of drought prediction- an overview

P.R.Reddy

Scientist- G (Retd); CSIR-NGRI, Hyderabad-500007, Telangana State.
Email: parvatarreddy@gmail.com

PREAMBLE

We suffer due to almost all types of natural hazards. Yet, there is no permanent solution to these disaster related negative impacts. One can understand our limitations in addressing earthquakes, tsunamis, avalanches and unusual cloud bursts. Many wonder why do we continue to suffer year after year due to floods and droughts, when there is vast data available about location and magnitude of these two disasters. Even after significant technological developments in locating drought prone locations and area specific dynamics of droughts through remote sensing our efforts to lessen the impact due to droughts continue to persist due to various factors including lack of co-ordination between experts and suffering common man and farmers.

Occurrence of Droughts and floods in one part of the country or the other has become a regular feature, affecting almost entire population of our country directly or indirectly. 2017 Southwest monsoon has created havoc in the north eastern states, especially Assam. Even though experts predict good rains in 2017, the prolonged dry spells followed by good showers is hurting the farmer in ensuring proper sowing operations. Monsoon aberrations and absence of a set pattern of rains has enhanced percentage of occurrence of agriculture drought. As per standard definition a drought is a period of drier-than-normal conditions that results in water-related problems. Precipitation (rain or snow) falls in uneven patterns across the country leading to indecision regarding sowing operations. The resultant setbacks due to insufficient water availability make farming community socio-economically vulnerable and distraught. This set back reflects in escalation of food prices and over all despondency in the part of rural and urban labour and water crisis resultant setbacks to middle class and at places even upper middle and rich. Drought can have many devastating effects on communities and the surrounding environment. The amount of devastation depends on the strength of the drought and the length of time an area is considered to be in drought conditions. Drought has greater impacts on poorer communities than on more prosperous communities who have better opportunities to bring in resources from other areas. Drought, however, can be very harsh at times on any type of community, including the rich. Drought prediction at least couple of months before

can help agricultural operations significantly. In spite of noteworthy scientific studies involving remote sensing data and on land hydrological parameters we are yet to master the art of proper forecasting. However, in the recent past reasonable success has been achieved. All the details pertaining to basics and state of the art drought forecasting are detailed in this write up, hoping details at one place can help focused future research studies.

Key Words: Drought prediction, Dynamics of drought, meteorological drought, hydrological drought, agricultural drought, impacts of drought, Global Drought Forecasting, droughts in India.

DYNAMICS OF DROUGHT AND DROUGHT PREDICTION

There are different types of drought

Drought can call to mind images of dry, cracked earth; low reservoir levels; and barren fields, yet these are actually examples of different types of drought, each of which is measured differently.

We most often think about drought in relation to precipitation, assessing the degree of dryness (in comparison to a local or regional average) and the duration of the dry period. This is known as a *meteorological drought*, which is highly specific to a region as average precipitation may vary considerably both temporally and spatially. We can also think about *hydrological drought*, or how decreased precipitation affects streamflow, soil moisture, reservoir and lake levels, and groundwater recharge. Farmers are most concerned with *agricultural drought* when available water supplies are not able to meet crop water demands. Agricultural droughts can occur for a variety of reasons, including low precipitation, the timing of water availability, or decreased access to water supplies. For instance, earlier snowmelt may not change the total quantity of water available but can lead to earlier runoff that is out of phase with peak water demand in the summer. Thus, it is possible to suffer an agricultural drought in the absence of a meteorological drought. (Source: http://www.ucsusa.org/global_warming/science_and_impacts/impacts/causes-of-drought-climate-change-connection.html#.Wc4uCPmCyM8)

Main Contributors of Drought:

Generally speaking, there are three main contributors to drought: (1) land and sea surface temperatures, (2) atmospheric circulation patterns, and (3) soil moisture content. Each of these physical parameters is linked to the others intricately; changing any one of them significantly will typically set up a chain of events that causes the other parameters to change. Sometimes, this chain of events becomes a vicious cycle in which the changing parameters, feeding off one another, are amplified to produce extreme climate conditions-such as flood or drought. Researchers using global climate models find that as average surface temperatures rise there is an increase in water evaporation leading to more extreme weather events. In summer, land surface temperatures are linked directly to the availability of moisture. If the soils are wet, then much of the heat from incoming sunlight is used to evaporate water, so temperatures are kept cooler and there is generally more precipitation. But if the soil is dry, then there is little or no water available to evaporate. Consequently, the incoming sunlight can only continue to warm the surface, thereby making conditions hotter and drier, thus beginning the chain of events leading toward drought. Atmospheric circulation patterns can make or break a vicious drying cycle. As such, soil moisture plays an important role in preventing or prolonging summer droughts. When the ground is wet, water evaporates as the day warms up. The warm, moist air rises until it encounters colder air high above the Earth's surface, leading to afternoon rain showers. The water remains in the ground through the cool night, and the cycle repeats the next day. Dry soil has the opposite effect on rainfall. As the temperature rises during the day, the air near the Earth's surface heats up and rises, but does not contain enough moisture to form rainclouds. As each day passes more moisture is removed from the ground, enhancing the effect.

Scientists observe that atmospheric circulation is closely connected to the surface temperature of the sea. Heat released from the ocean creates temperature gradients in the atmosphere that cause air currents. And because warm water evaporates more readily than cold water, warmer sea surface temperatures contribute to more cloud formation and more rainfall downwind of the general flow of air currents. Using satellite remote sensing data, scientists have confirmed there is a direct relationship between sea surface temperature variations in the Atlantic and Pacific Oceans and large-scale atmospheric circulation patterns that bring rain or dry spells.

(Source: https://earthobservatory.nasa.gov/Features/NAmerDrought/NAmer_drought_2.php)

How Droughts hurt

Droughts are some of the most costly economic stressors.

Frequently, droughts are billion dollar weather events and are one of the top three threats to population in the world (along with famine and flooding). There are three main ways droughts impact lives and communities:

1. Farmers are often the first to feel the stresses from drought, and feel them hardest. The *economic impacts* of drought include losses in the timber, agricultural, and fisheries communities. Many of these losses are then passed on to consumers in the form of higher food prices. In less developed countries, once crops fail, famine can become a major problem.
2. *Social impacts* include increased chance of conflict over commodities, fertile land, and water resources. Other social impacts include abandonment of cultural traditions, loss of homelands, changes in lifestyle, and increased chance of health risks due to poverty and hygiene issues.
3. The *environmental impacts* of drought include loss in species biodiversity, migration changes, reduced air quality, and increased soil erosion.

(Source: <https://www.thoughtco.com/what-causes-droughts-3443828>)

Impact due to droughts:

Drought effects are incremental and happen over a long period of time, hence receive little attention in early phases. Due to this, any initiative taken at a later phase of drought yields none too useful results. Drought impact is felt by man, flora and fauna.

Water may become especially polluted during times of drought due to the lack of rain water to dilute industrial and agricultural chemicals. This toxic water can be harmful to plants and animals that use it and make it difficult to clean for drinking water. Crops are also receiving less water by volume. In some areas, farmers may be able to irrigate by pumping from groundwater or surface water like farm ponds. However, as a drought worsens, these options may disappear. In the worst droughts, farmers are unable to maintain their fields because of the drought conditions and the restrictions placed on water. Some farmers and communities will relocate to other less drought areas in order to sustain a living. The now untended land dries up from the lack of moisture and most plants will not be able to survive in these drought areas. Plants absorb the nutrients from the soil in order to survive. When these nutrients are used up, the plants will begin to wilt. Without water getting into the soil, the ground will dry out and become unstable.

Global Drought Monitoring and Forecasting

Lifeng Luo et al., (2008) carried out intensive study to monitor drought monitoring and forecasting and brought out a very interesting article. Some salient details of their study are detailed below to better plan drought monitoring and forecasting using comprehensive integrated models using satellite remote sensing data coupled with land hydrogological data inputs.

Over many parts of the world, droughts are among the most damaging of natural disasters in human, environmental and economic terms. The consequences of drought are perhaps nowhere more urgent than in Africa where IPCC projections of increase future drought frequency have perilous implications for the livelihood of residents who depend heavily upon ecosystem services. Unlike other natural disasters, droughts develop slowly over large areas and over an extended period of time, making it difficult to identify them until they have become severe and some damage has already occurred. Therefore, accurate quantitative assessment of drought conditions and the prediction of the on-set duration and recovery of droughts in real-time is critical for drought planning and preparedness.

Studies over the last two decades have demonstrated the feasibility of seasonal climate predictions with dynamical climate models. The skill of seasonal predictions is believed to come from the slow varying components of the climate system, mainly tropical Pacific sea surface temperature, although more recently surface soil moisture has also shown certain contributions over transition zones between dry and wet climatic regions (Koster et al., 2000 and 2004). At present, seasonal climate predictions are made routinely at several weather and climate prediction centers and research institutes, including the European Centre for Medium-range Weather Forecasting (ECMWF), and in the U.S. the National Centers for Environmental Prediction (NCEP). The predictions have shown significant skill over the tropics, while in the mid-latitudes their skill is improving, with some models showing skill comparable to the skill from statistical models. There is the expectation that these seasonal dynamical climate forecasts can contribute to the development of seasonal hydrologic prediction capabilities.

However, challenges must be overcome in utilizing seasonal climate forecasts from dynamical climate models in a seasonal hydrologic prediction system. One significant challenge is to correct the biases in climate model predictions, especially those related to precipitation and temperature. Another challenge is to resolve the disparity in spatial scales between the ones resolved in climate models and those needed for hydrologic applications. For instance, the current operational NCEP global coupled ocean-atmosphere model, called the Climate Forecast

System (CFS) runs at T62L64 resolution (~1.875 degree in longitude). The climate models in the European Union (EU) DEMETER project provide hind casts at a resolution of $2.5^{\circ} \times 2.5^{\circ}$. However, the hydrologic predictions need atmospheric forcing at a much finer resolution. As an example, the North America Land Data Assimilation System (NLDAS), which provides real-time hydrologic simulations across the continental U.S., has adopted a spatial scale of 1/8th degree. Such disparities require a seasonal hydrologic forecast system to spatially downscale the information provided by the climate models to the finer hydrologic scale where the information can be properly used. The third challenge is to create realistic daily atmospheric forcing for hydrologic modeling from the monthly information provided by the climate models. Climate model forecasts are generally only available as a monthly forecast while the hydrologic models are run at daily or sub-daily time steps. To make skilful seasonal hydrologic predictions, a good strategy is needed to overcome these challenges. Scientists have briefly described the methodology for the Drought Monitoring and Prediction System (DMAPS), and presented examples of its implementation for the US and its pilot extension to Africa. (Source: Lifeng Luo et al., 2008, Science and Technology Infusion Climate Bulletin, NOAA's National Weather Service, 33rd NOAA Annual Climate Diagnostics and Prediction Workshop, Lincoln, NE, 20-24 October 2008)

Prediction of floods and droughts is an effective measure for adapting to climate change

Operational water management based on accurate and reliable hydrological predictions can be an effective means of limiting the economic and social damage caused by an increasing frequency and intensity of summer rainstorms, droughts and wintry precipitation. This will require advanced hydrological modelling and prediction. This was put forward by Prof. Albrecht Weerts, special professor Hydrologic Predictability, during his inaugural address at Wageningen University & Research on 2 March, 2017. Prof. Albrecht Weerts explained why we need to improve our ability to predict water levels in rivers, creeks and other hydrological infrastructure. Accurate and reliable predictions that can help us improve the management of our waterways in times of drought, or when floods threat, will have an excellent return on investment, regardless of the extent of the climate change. He has proposed an accurate and reliable national *probabilistic now-casting & forecasting* system for water levels and discharge volumes based on short-term radar precipitation measurements (0-6 hours) combined with high resolution weather forecasting (0-48 hours) that enables smart water management. Such a system can provide a window of time to warn the public and take local measures. Refining hydrological models to be

able to predict smaller scales in space and time (e.g. from daily to hourly and from square kms to hectares) will not automatically lead to better hydrological predictions. "This is due to all sorts of uncertainties in the model structure, parameters and estimated initial conditions. Moreover, before we use the precipitation forecasts in our hydrological models, it may be useful to apply a correction to the precipitation forecasts first. We should also make better use the real-time available data on discharge or water levels to adjust the initial condition of the hydrological models to increase the accuracy of the predictions."

(Source:<http://www.wur.nl/en/newsarticle/Prediction-of-floods-and-droughts-is-an-effective-measure-for-adapting-to-climate-change.htm>)

Humans to Blame for Higher Drought Risk in Some Regions

The world's population relies on the global water cycle for food security and economic prosperity. However, human activities may be jeopardizing this critical resource; new research by *Douville and Plazzotta* confirms that human emissions of greenhouse gases have already begun to alter the water cycle, resulting in a drying trend and increased risk of drought in certain parts of the world. To many researchers, these new findings are not surprising. For more than a decade, observational and numerical modeling studies have predicted that anthropogenic emissions would cause warming that could change the water cycle and expand dry regions.

Nonetheless, other recent studies have cast serious doubts on these predictions. Two studies cautioned that simplified calculations used to process observational data could result in incorrect predictions of evaporation due to warming over land. Other researchers uncovered large uncertainties in climate predictions made by the fifth phase of the Coupled Model Intercomparison Project (CMIP5), a widely used, multimodel tool for climate analysis.

The authors of the new study set out to address these doubts. They performed a three-pronged analysis, investigating both recent observational data and long-term CMIP5 projections of drying trends over the midlatitudes of the northern continents in summertime. In addition, the researchers applied a previously developed algorithm to distinguish between anthropogenic and natural influences on observed variations in sea surface temperatures and sea ice concentration. Then, they performed multiple climate simulations to determine the causes of recent changes in soil moisture and other land-based variables. The results of the analysis suggest that a summertime drying trend has indeed emerged over the midlatitudes of the northern continents and that anthropogenic climate change is the main cause. This drying appears to be the beginning of a long-term drying trend. The findings also suggest that in

the absence of direct observations, most CMIP5 models previously underestimated long-term summertime drying. (Source: *Geophysical Research Letters*, <https://doi.org/10.1002/2017GL075353>, 2017)

Rising air pollution worsens drought, flooding, new study finds

Increases in air pollution and other particulate matter in the atmosphere can strongly affect cloud development in ways that reduce precipitation in dry regions or seasons, while increasing rain, snowfall and the intensity of severe storms in wet regions or seasons, says a new study by a University of Maryland-led team of researchers.

The research provides the first clear evidence of how aerosols -- soot, dust and other small particles in the atmosphere -- can affect weather and climate; and the findings have important implications for the availability, management and use of water resources in regions across the United States and around the world, say the researchers and other scientists.

Using a 10-year dataset of extensive atmosphere measurements from the U.S. Southern Great Plains research facility in Oklahoma researchers have uncovered, for the first time, the long-term, net impact of aerosols on cloud height and thickness, and the resultant changes in precipitation frequency and intensity. The study found that under very dirty conditions, the mean cloud height of deep convective clouds is more than twice the mean height under crystal clean air conditions. The probability of heavy rain is virtually doubled from clean to dirty conditions, while the chance of light rain is reduced by 50 percent. The scientists obtained additional support for these findings with matching results obtained using a cloud-resolving computer model.

These new findings of long-term impacts, using regional ground measurements, also are consistent with the findings researchers have obtained from an analysis of NASA's global satellite products in a separate study. Together, they attest to the needs of tackling both climate and environmental changes that matter so much to our daily life. These findings have significant policy implications for sustainable development and water resources, especially for those developing regions susceptible to extreme events such as drought and flood.

Some experts note the significance of the new findings. They pointed out that understanding interactions across clouds, aerosols, and precipitation is one of the grand challenges for climate research in the decade ahead. Findings of this study represent a significant advance in our understanding of such processes with significant implications for both climate science and sustainable development. Scientists have known for a long time that aerosols impact both the heating and phase changes

[condensing, freezing] of clouds and can either inhibit or intensify clouds and precipitation. What they have not been able to determine, until now, is the net effect. This study by Li and his colleagues from Maryland University shows that fine particulate matter, mostly from air pollution, impedes gentle rains while exacerbating severe storms. Scientists opine that it adds urgency to the need to control sulphur, nitrogen, and hydrocarbon emissions.

According to climate scientist Steve Ghan of the Pacific Northwest National Laboratory, "This work confirms what previous cloud modeling studies had suggested, that although clouds are influenced by many factors, increasing aerosols enhance the variability of precipitation, suppressing it when precipitation is light and intensifying it when it is strong. This complex influence is completely missing from climate models, casting doubt on their ability to simulate the response of precipitation to changes in aerosol pollution."

Greenhouse gases and aerosol particles are two major agents dictating climate change. The mechanisms of climate warming impacts of increased greenhouse gases are clear (they prevent solar energy that has been absorbed by the earth's surface from being radiated as heat back into space), but the climate effects of increased aerosols are much less certain due to many competing effects outlined above. Until now, studies of the long-term effects of aerosols on climate change have been largely lacking and inconclusive because their mechanisms are much more sophisticated, variable, and tangled with meteorology. While the mechanisms for some of these effects remain uncertain, the well-defined relationships discovered here clearly demonstrate the significance of the effects. Developing this understanding to represent the controlling processes in models remains a future challenge, but this study clearly points in important directions.

Source: Zhanqing Li et al., Long-term impacts of aerosols on the vertical development of clouds and precipitation. *Nature Geoscience*, 2011; DOI: 10.1038/ngeo1313)

Predicting the Future of Drought Prediction

As extreme weather events go, droughts—like the one that singed Russia's wheat crop in 2010 and the one that engulfed the United States in July, 2012—are about as tricky as it gets. Unlike hurricanes and tornadoes, drought does not have an obvious start or end. In fact, there isn't even a clear definition for it, making it hard to measure and monitor, let alone predict. But with better observations of the earth, oceans, and atmosphere and improvements in computer modeling, scientists think they'll be able to foresee the chances of drought up to a decade in advance, and better predict droughts that arise suddenly or last longer than a few months.

Today, scientists can forecast drought only about three months ahead for most parts of the world with any

significant certainty. "Forecasting drought is an inexact science," says Brian Fuchs, a climatologist. According to him drought is typically characterized by slow onset and slow recovery. To pick up signals of something that happens over weeks or months is hard for computer models."

Drought involves a seemingly inexhaustible list of factors—from local ones such as groundwater level, stream flow, soil moisture, and vegetation, to large-scale global weather patterns such as El Niño and La Niña. All of these change over different time periods, from days to decades, and many are tied to each other. Global warming tops off the chaotic mix.

Nevertheless, scientists in the United States have produced some of the most sophisticated tools to monitor and predict drought. Resource planners and policymakers rely mainly on the U.S. Drought Monitor, an online map of dryness that has been updated. The monitor combines several mathematical indices calculated by feeding computer models with temperature, precipitation, and soil moisture data. While monitoring has been done for decades, forecasting drought is still in its infancy. Today, it blends science and art, and the only place it's done on a national scale is at NOAA's Climate Prediction Center (CPC). Twice every month, meteorologists there subjectively produce the U.S. Seasonal Drought Outlook, which predicts conditions for the next three months. To create the Drought Outlook, scientists mix data from the Drought Monitor with soil moisture information and the CPC's three-month forecast of temperature and rainfall. They also incorporate current climate conditions along with past heat and precipitation. An expert stated that more-powerful computers would make it possible to include more-detailed physics and more climate system components. Greater computing prowess would also mean that each simulation step would cover a shorter time and distance—a few minutes and a few kms as opposed to the hours and tens of kms used now. This would improve the ability to capture smaller, more rapid changes in temperature and precipitation.

Other advances expected in the coming years include more extensive ground observation networks and NOAA's next-generation polar satellite, which is equipped with advanced visual and infrared imagers that produce data with a higher temporal and spatial resolution. These will give better temperature, precipitation, and soil moisture data, which will improve the accuracy of drought prediction.

Scientists anticipate that longer-term drought prediction could be possible by 2018. That's when NOAA scientists are expecting to next upgrade the climate model, to include decade-long climate fluctuations. They hope to do this by simulating known long-term ocean fluctuations such as the Atlantic multi-decadal oscillation. Scientists anticipate to see continuing drought monitoring and prediction.

(Source: prachipatel,2012,<http://spectrum.ieee.org/energy/environment/predicting-the-future-of-drought-prediction>)

Global integrated drought monitoring and prediction system

A 2007 ministerial summit with representatives from 70 nations, held in Cape Town, South Africa, recognized the growing problem of drought and its impact on food security and sustainability of water resources, and highlighted the need for a global drought early warning system¹. Drought effects are incremental and happen over a long period of time, hence receive little attention in early phases.

Each year droughts result in significant socioeconomic losses and ecological damage across the globe. Given the growing population and climate change, water and food security are major challenges facing humanity. Nearly 1 million people perished in East Africa in the mid-eighties because of a major drought that led to a widespread famine. More recently, in 2010-2011, two events in East Africa and Southeast Asia affected 9 million people, causing famine in East Africa and significant ecological impacts in Southeast Asia. Production of adequate food to avoid food crises requires advanced drought early warning and prediction systems. In particular, a global model is needed that can support regions where famine and food crisis are prevalent because of economic and social instability and climatic variability. In recent years, several research and operational drought monitoring models have been developed. However, drought warning and prediction systems are still the least developed systems among other natural disasters primarily because of the complex processes involved in drought onset and development. On a regional scale, there are a number of drought monitoring tools tailored for local to continental scale applications such as, the U.S. Agency for International Development (USAID) Famine Early Warning System Network (FEWS Net), United States Drought Monitor, African Drought Monitor, and the University of Washington Experimental Surface Water Monitor.

In an interconnected world where a drought in the United States, Russia or Australia could affect global food prices, a regional perspective to drought monitoring and prediction may not be sufficient. Currently, few global drought models are available, including the Global Information and Early Warning System on Food and Agriculture (GIEWS), Humanitarian Early Warning Service (HEWS) by the World Food Programme (WFP), Global Drought Monitor by the University College London (UCL), the Standardized Precipitation-Evapotranspiration Index Global Drought Monitor, and the Global Drought Portal (GDP) by the United States National Climatic Data Center. The aforementioned models, however, do not provide probabilistic forecasts of drought condition for risk assessment. While these outputs are valuable, probabilistic seasonal drought forecasts can substantially improve drought early warning capability.

United Nations Environment Programme (UNEP) report calls for a drought prediction system based on a comprehensive and *integrated* approach that would include multiple drought indicators. While droughts originate from a deficit in precipitation, an effective drought monitoring and prediction system should integrate multiple drought-related variables. The United Nations (UN) Strategy for Disaster Reduction (ISDR) argues that an early warning system should have the following features: (a) Monitoring and predicting components, (b) Risk knowledge, (c) Disseminating information, and (d) Response. Following the above recommendation, the Global Integrated Drought Monitoring and Prediction System (GIDMaPS) is developed to provide drought information based on multiple drought indicators and input data sets. GIDMaPS includes a seasonal probabilistic prediction component that supports *risk knowledge*. The probabilistic forecasts offer essential information for early warning, preventive measures, and mitigation strategies. GIDMaPS provides both monitoring and prediction components, as well as a data dissemination interface. (Source: Hao, Z et al., Global integrated drought monitoring and prediction system. *Sci. Data* 1:140001 doi: 10.1038/sdata.2014.1 (2014)).

A new tool for predicting drought: an application over India

This is the first attempt of application of atmospheric electricity for rainfall prediction. The atmospheric electrical columnar resistance based on the model calculations involving satellite data has been proposed as a new predictor. It is physically sound, simple to calculate and not probabilistic like the standardized precipitation index. After applying this new predictor over India, it has been found that the data solely over the Bay of Bengal (BB) are sufficient to predict a drought over the country as a whole. Finally, two independent new methods to predict drought conditions and a preliminary forecast of the same for India for year 2014 have been given. Unlike the existing drought prediction techniques, the identification of drought conditions in a pre-drought year during 1981–1990 and 2001–2013 over India has been achieved 100% successfully using the suggested new methods. The association between rainfall and this new predictor has also been found on the sub-regional scale. So, the present predictor is expected to get global application and application in climate models. From the analysis, generally, a long period rising trend in aerosol concentration over the BB causes weak monsoon over India but that for a short time i.e. in pre-monsoon period strengthens it. (Source: M.N.Kulkarni, *Sci Rep.* 2015; 5: 7680. Published online 2015 Jan 8. doi: 10.1038/srep07680)

Status of preparedness in meeting droughts in India

In India, around 68% of the country is prone to drought in varying degrees. 35% which receives rainfall between 750 mm and 1125 mm is considered drought prone while 33% receiving less than 750 mm is chronically drought prone.

The agriculture drought assessment and monitoring, under National Agriculture Drought Assessment and Monitoring System (NADAMS project), is carried out using multiple satellite data, rainfall, soil moisture index, potential sowing area, irrigation percentage and ground observations. A logical modeling approach is followed to classify the districts into Alert, Watch and Normal during June, July and August and Severe, Moderate and Mild drought conditions during September and October. The monthly Drought Assessment Reports are communicated to all concerned State and national level agencies and also kept on the MNCFC website (www.ncfc.gov.in).

IMD is the designated agency for providing drought early warning and forecasting. Agricultural Meteorology Division, Pune provides timely advice on the actual and expected weather and its likely impact on the various day-to-day farming operations. Drought Research Unit, Pune provides Crop Yield Forecasts. The National Centre for Medium Range Weather Forecasting, a constituent unit of the Department of Science & Technology provides, in consultation with IMD, ICAR and State Agricultural Universities, agro-meteorological advisory service at the scale of agro-climatic zones to the farming community, based on location specific medium range weather forecasts. The Central Research Institute for Dryland Agriculture (CRIDA), Hyderabad and the All India Coordinated Research Projects on Agri-Meteorology and Dryland Agriculture (AICRPAM and AICRPDA) each of them having 25 centres across the country, take part in drought studies pertaining to assessment, mitigation, risk transfer and development of decision support software for drought prone States. Central Arid Zone Research Institute, Jodhpur for assessing agricultural drought situation in 12 arid Districts of western Rajasthan and disseminates bi-weekly crop-weather agro-advisory bulletins to the farmers. Ministry of Earth Sciences in collaboration with ICAR has set up 89 centres for short and medium range monitoring and forecasting of weather. National Agricultural Drought Assessment and Monitoring System Developed by the Department of Space for the Department of Agriculture and Cooperation monitors vegetation cover through satellite data based helping in drought assessment by comparative evaluation of vegetation cover with those of previous years. It prepares State-wise monthly reports. There are institutional mechanisms for drought monitoring and early warning at national and state levels. However, these are considered to be inadequate

for meeting the demands of drought management and their capacity needs to be strengthened for the purpose of data collection, analysis and synthesis of information. Crop Weather Watch Group (CWWG), an inter-Ministerial mechanism of Central Govt. meets once a week during rainy season (June-September). The frequency of meetings increases during drought occurrence. (Source: <http://wrmin.nic.in/forms/list.aspx?lid=312> & <https://reliefweb.int/report/india/national-agriculture-drought-assessment-and-monitoring-system>)

When the Indian Ocean heats up, the intensity of the monsoon season reduces

A team from the Indian Institute of Meteorology (IITM) in Pune, has recently revealed in the journal *Nature Communications* that the warming of the Indian Ocean, by up to 1.2°C in some areas over the last century, is reducing the intensity of the Indian monsoon season by around 10 to 20% in the country's central, eastern and northern regions.

Scientists made this discovery using an ocean-atmosphere coupled climate model, specially developed by the IITM for making monsoon season forecasts. Thanks to this model, researchers were able to demonstrate that the reduction in rainfall observed over the subcontinent since the 1950s is due to the rapid warming of the ocean. The Intergovernmental Panel on Climate Change (IPCC) anticipates that ocean temperatures will rise further as a result of the greenhouse gas effect. The study goes on to explain the reason for the observed reduction in rainfall associated with the Indian monsoon season. The Indian subcontinent has warmed up by only a very small amount during the last few decades, reducing the summer temperature difference between the ocean and the land, which triggers the monsoon winds. This phenomenon is weakening the monsoon season dynamic and is drying up the subcontinent, bringing harmful consequences for agriculture along the Ganges-Brahmaputra-Meghna basins and the Himalayan spurs, an activity requiring extensive irrigation. Will India continue to dry up? Projections based on the majority of the climate models used in the IPCC's latest evaluation report do not see this trend replicated in future years. Some anticipate quite the opposite: increased rainfall due to increased water vapour in the atmosphere and a far more noticeable warming of the subcontinent in the future. This divergence between current observations and model-based trends underlines the uncertainties involved when it comes to future climate change in the region, particularly in terms of the water cycle and the monsoon regions. (Source: Mathew Koll Roxy et al., Drying of Indian subcontinent by rapid Indian Ocean warming and a weakening land-sea thermal gradient. *Nature Communications*, 2015; 6: 7423 DOI: 10.1038/ncomms8423)

Indian monsoon: Novel approach allows early forecasting

The Indian monsoon's yearly onset and withdrawal can now be forecasted significantly earlier than previously possible. A team of scientists developed a novel prediction method based on a network analysis of regional weather data. Future climate change will likely affect monsoon stability and hence makes accurate forecasting even more relevant.

"We can predict the beginning of the Indian monsoon two weeks earlier, and the end of it even six weeks earlier than before -- which is quite a breakthrough, given that for the farmers every day counts. We found that in North Pakistan and the Eastern Ghats, a mountain range close to the Indian Ocean, changes of temperatures and humidity mark a critical transition to monsoon," explains," says Veronika Stolbova from the Potsdam Institute for Climate Impact Research (PIK) and the University of Zurich. Conventionally, the focus has been on the Kerala region on the southern tip of India. Information about monsoon timing is key for Indian farmers to determine when to carry out the sowing. Crops like rice, soybean and cotton are normally grown during the June to September monsoon rainy season. Even a slight deviation of the monsoon can lead to droughts or floods, causing damages. Also, the length of the monsoon is relevant for planning hydro power generation since the rains are necessary to fill the dams and reservoirs.

The scientists tested their method with historical monsoon data. It gives correct predictions for onset in more than 70 percent and for withdrawal in more than 80 percent of the considered years. The main advantage of the proposed approach is that it allows improving the time horizon of the prediction compared to the methods currently used in India. In addition, the new scheme notably improves the forecasting of monsoon timing during years affected by the global weather phenomenon El Nino -- Southern Oscillation (ENSO), particularly in its La Nina phase. This phenomenon significantly alters monsoon timing and decreases the prediction accuracy in existing methods.

Using the network analysis of complex non-linear systems, an advanced mathematical approach, for monsoon forecasting is unprecedented -- yet the approach shows good results. The major innovation, the authors say, is to combine the network analysis with the subtle statistical analyses of the early warning signals for the monsoon onset and withdrawal. These precursor phenomena are often buried by huge piles of weather data and hence get overlooked. We discovered how to use precursors in a new way -- to find regions where critical conditions for an occurrence of the Indian monsoon originate. In the future, this method can also help to unravel mysteries of other climate phenomena.

Global warming due to mankind's greenhouse-gas emissions from burning fossil fuels already affects the Indian monsoon and -- if unabated -- is expected to do even more so in the future. The timing of Indian summer monsoon, on which the livelihoods of many million people depend, is likely becoming more erratic. In view of this early and accurate forecasting has become ever more crucial. Such a forecasting also helps in predicting probable onset of a drought and its duration. (**Source:** Veronika Stolbova et al., 2016. Tipping elements of the Indian monsoon: prediction of onset and withdrawal. *Geophysical Research Letters*, 2016; DOI: 10.1002/2016GL068392)

New method for monitoring Indian Summer Monsoon (ISM)

Researchers from Florida State University have created a tool for objectively defining the onset and demise of the Indian Summer Monsoon -- a colossal weather system that affects billions of people annually. The research scientists outline a methodology that uses rainfall rates to mark the span of the ISM at any given location throughout the affected region.

For generations, scientists have struggled to produce a model for reliably defining the duration of the monsoon. No existing system has allowed researchers to reliably define the parameters of the season at this fine a scale."Current weather forecasting and monitoring protocols focus attention on monsoon onset at one location -- specifically the state of Kerala in the southwest corner of the country -- and extrapolate for the rest of the region. We have gone down to specific locations, we've covered the whole country, and we've objectively defined the onset and demise dates for any given year." Said Prof.Misra.

The lack of a clear, granular and objective benchmark for ISM onset and demise for all areas of the country has been a longtime source of consternation for the Indian people. In some parts of the country, the torrents of rain that characterize monsoon season account for more than 90 percent of the total annual precipitation. Consequently, many rhythms of Indian political and agricultural life can be destabilized by dubious or false claims of monsoon onset. That leads to tremendous amounts of frustration and confusion for the general public and for the people who are trying to monitor the monsoon because nobody has really gotten down to do it at a granular scale. The new system, which ties the onset of the monsoon to location-specific rainfall thresholds, can work to allay that frustration.

Up until now, regional meteorological departments have relied on their own *ad hoc* criteria for determining ISM onset, which can often lead to contradicting claims. A more inclusive method will allow officials and researchers throughout the country to define the monsoon season using

a standardized system that, through rigorous testing, has been shown to capture ISM evolution comprehensively.

Anchoring the definition of onset and demise solely in local rain rates eliminates the need to rely on less accessible atmospheric variables. This streamlined approach makes it considerably easier to monitor monsoon evolution. "Our research enables quite easy real-time monitoring of the onset and demise of the Indian monsoon. We've tested this for 105 years of available data, and this criterion hasn't failed once for any location over India." Misra said. By orienting this novel framework around rates of rainfall in a given area the scientists have effectively removed the necessity for broad extrapolation. With this methodology, a question that has baffled meteorologists for decades finally has a simple, actionable answer.

"You don't need complicated definitions," Misra said. "Now we completely base the definition on rainfall, and it hasn't failed."

(Source: Vasubandhu Misra et al., 2017. Local onset and demise of the Indian summer monsoon. *Climate Dynamics*, 2017; DOI: 10.1007/s00382-017-3924-2)

Drought impact in 2017- South Indian Scenario

Southwest Monsoon 2017 has made timely onset over southern parts of Kerala on May 30. With this, we expected rains to pick up pace across Kerala and over parts of Karnataka and Tamil Nadu. One and all eagerly awaited good monsoon owing to the dwindling status of water reservoirs in southern parts of the country. According to the statistics, these reservoirs reported acute shortage of water i.e. below 10% even in June. Condition in many reservoirs even during third week of August is very depressing. This has cited major cause of concern for the agriculture sector for the region down south, which is also already battling worst drought of the decade. Moreover, lack of irrigation has further worsened the situation. Blame it all on the fluctuating Monsoon rains during the last three years. While 2014 and 2015 were the severe drought years, 2016 despite recording normal Monsoon rains left the southern region parched. Last year, Kerala was deficit by 34%, South Interior Karnataka-21%, Coastal Karnataka 21% and Tamil Nadu by 19%. However, this year, Skymet Weather has predicted Southwest Monsoon to be marginally below normal at 95% with an error margin of +/- 5%. In fact, weather models indicated correctly that June would likely to witness good Monsoon rains. Unfortunately, failure of monsoon in July and below normal rainfall in August and September considerably dampened the spirits of farmers in almost all the southern states, especially Telangana. Unexpected continuous good spell of rains in October, fortunately, improved the condition and helped in reasonable quantities of inflows in to many reservoirs in Telangana and parts of Andhra Pradesh. However, this delayed monsoon affected Kharif crops. Many are afraid

that even these belated good Monsoon rains from the fourth week of September will not be enough to improve the overall agriculture output. It is essential to closely examine the soil fertility levels and overall impact of weak monsoon from July till third week of September and take curative measures to ensure the negative impact on soil fertility will not adversely affect the long term nutrient capacity of soil mantle.

As per the data released by the Central Water Commission on May 25, 2017, the southern region has 31 reservoirs having total live storage capacity of 51.59 BCM. The Southern region includes states of Andhra Pradesh, Telangana, Karnataka, Kerala and Tamil Nadu. As per Reservoir Storage Bulletin, the total live storage available in these reservoirs is 3.92 BCM which is 8% of total live storage capacity of these reservoirs. The storage during corresponding period of last year was 11% and average storage of last ten years during corresponding period was 17% of live storage capacity of these reservoirs. Thus, storage during current year is less than the corresponding period of last year and is also less than the average storage of last ten years during the corresponding period. As per Press Information Bureau, Government of India, Ministry of Water Resources, dated 4th August in the Southern region that includes States of Andhra Pradesh, Telangana, AP&TG (Two combined projects in both states) Karnataka, Kerala and Tamil Nadu status of 31 reservoirs is as follows. There are 31 reservoirs under CWC monitoring having total live storage capacity of 51.59 BCM. The total live storage available in these reservoirs is 14.28 BCM which is 28 % of total live storage capacity of these reservoirs. The storage during corresponding period of last year was 30% and average storage of last ten years during corresponding period was 46% of live storage capacity of these reservoirs. Thus, storage during current year is less than the corresponding period of last year and is also less than the average storage of last ten years during the corresponding period.

Situation is very tough for southern states as reservoirs have reached to dead storage. There is no water left for agriculture. Now to assess the meteorological drought of southern states, Skymet Weather has calculated the Standardized Precipitation Index (SPI), a widely used index to characterize meteorological drought on a range of timescales. On long timescales, the SPI is closely related to groundwater and reservoir status. On short timescales, the SPI can be related to soil moisture or the agricultural drought. Generally, SPI varies between +3 to -3. Positive values suggest floods and negative drought.

SPI analysis is done over 3 scenarios. In first scenario, weather experts have assumed that the rainfall will be normal, whereas the second and third scenarios are generated for 5% and 10% extra rainfall till December 2017. Through the combined analysis, it can be said that under assumed scenario of forecasted precipitation, the

water availability issue in these sub divisions will remain severe in the season. From agricultural point of view, water backlog may not be filled in this region. So, we can see in both sub-divisions for 9-monthly and 12-monthly SPI that if normal or 5% more than normal or 10% more than normal rainfall occurred from June-2017 to Dec-2017, then also hydrological drought won't be made less effective(**Source:** <https://www.skymetweather.com> · Weather News and Analysis).

This prediction has been proved wrong with copious amount of monsoon rains in about a month starting from third week of September, exposing the limitations of our prediction capabilities. As per information released by Ministry of Water resources, Govt of India the total live storage available in these reservoirs as on 26th October, 2017 is 34.15 BCM which is 66% of total live storage capacity of these reservoirs. The storage during corresponding period of last year was 50% and average storage of last ten years during corresponding period was 69% of live storage capacity of these reservoirs. Thus, storage during current year is better than the corresponding period of last year but is less than the average storage of last ten years during the corresponding period.

(**Source:** <http://pib.nic.in/newsite/pmreleases.aspx?mincode=38>)

With the Nagarjunasagar dam reaching a comfortable storage level, and Srisailem dam already being filled, and with more inflows expected for at least another week, both Telangana state and Andhra Pradesh are readying to seek fresh indents of around 250 tmc ft of water for raising the Rabi crop. Allotment of additional water to these two states depends on various factors, including onset of North east monsoon and sustenance of water levels in these reservoirs(P.S: Unfortunately the north east monsoon has not added any additional amount of water, due to its failure in Telangana and many parts of Rayala Seema till end of November, 2017, making releasing of sufficient quantities of water difficult from big and medium reservoirs for Rabi season, further exposing our limitations in predicting intra seasonal precipitation). Effective implementation of various water dependent projects has become a guessing game, exposing our limitations of predicting drought situation in some vulnerable segments in the next 6 months.

Effective implementation of global models- impediments and apt strategy

While perturbed by the painful reality, as scientists it is our bounden duty to address this recurring problem. Let us look in to global initiatives (detailed in the earlier subsections) and try to implement recent advancements in drought prediction to lessen negative impact. Until such time we collect good quality dense data using different modes of data acquisition and without fear or favour implement global strategies(after setting aside area specific temporal

and spatial details) we will continue to make errors in our prediction, leading to below par preparedness.

Although some droughts last a single season and affect only small areas, the instrumental and paleo-climate records show that droughts have sometimes continued for decades and have impacted millions of square kms in North America, West Africa, East Asia and even India. To cross the spectrum of potential drivers and impacts, drought information systems have multiple sub-systems which include an integrated risk assessment, communication and decision support system of which early warning is a central component and output. An early warning system is much more than a forecast – it is a linked risk information (including people's perception of risk) and communication system that actively engages communities involved in preparedness. There are numerous drought warning systems being implemented at different scales of governance. Indian scientists can draw on the lessons of over 21 drought early warning systems around the world, in both developing and developed countries and at regional, national and community levels. The successes illustrate that effective early warning depends upon a multi-sectoral and interdisciplinary collaboration among all concerned actors at each stage in the warning process from monitoring to response and evaluation. However, the links between the community-based approach and the national and global EWSs are relatively weak, as evidenced from our response to El Nino impact during the last three to four years. These impacts can lead to drought in many parts of our country, unless close knit co-operation in data dissemination at regional and global level is achieved at the earliest opportunity. Using the rich experience of information systems across the globe, agro meteorologists and disaster management experts can identify pathways for knowledge management and action at the relevant scales for decision-making in response to a changing climate.

(**Source:** Weather and Climate Extremes, Volume 3, June 2014, Pages 14-21; <https://doi.org/10.1016/j.wace.2014.03.005>)

CONCLUSION

We have been facing droughts and floods regularly in one part of the country or the other, due to monsoon variability and intra monsoon fluctuations .Our scientific efforts have not yielded proper results, due to various factors, including the limitations of our research options and approaches. If not exactly, the accuracy in area specific monsoon onset and withdrawal predictions can significantly help us in knowing in advance to a considerable extent onset of drought, its intensity and duration. For the success of these predictions aerially and temporally we have to continuously upgrade our prediction models by using significant successes achieved by international research organisations. Scientists have found

that the frequency of heat waves accompanied by drought has increased not only in magnitude but in area too over the past three decades in Gujarat and central parts of our country, making this segment of the country vulnerable to become chronic drought prone region. Researchers believe intricate relationship of land surface processes, soil moisture, evapotranspiration and local climate could play vital role in making a region drought prone. As such researchers should increase agro-meteorological data collection stations in these parts to enhance success rate in drought prediction. The recent spurt in research focused on Indian Summer Monsoon clearly indicates that international weather experts are fully aware of the adverse impact on millions of South Asians due to even minor aberrations in the prediction models. Making use of the interest shown by international weather experts we can achieve much better

results in the near future, thereby helping one and all, including in particular the farming community, residing in vulnerable segments of our country.

ACKNOWLEDGEMENTS

This write up has been prepared extracting internet based relevant information from different studies. The extracted information was then screened and linked to develop this write up. Source of every sub topic is given in the text to help the interested readers.

Compliance with Ethical Standards:

The author declares that he has no conflict of interest and adheres to copyright norms.

Quotations on Drought

Nature, like a loving mother, is ever trying to keep land and sea, mountain and valley, each in its place, to hush the angry winds and waves, balance the extremes of heat and cold, of rain and drought, that peace, harmony and beauty may reign supreme.

Elizabeth Cady Stanton (1815-1902) was an American suffragist, social activist, and abolitionist.

God has cared for these trees, saved them from drought, disease, avalanches, and a thousand tempests and floods. But he cannot save them from fools.

John Muir (1838 -1914) was a Scottish-American naturalist, author, environmental philosopher.

Any party which takes credit for the rain must not be surprised if its opponents blame it for the drought.

Dwight Morrow (1873 -1931) was an American businessman, diplomat, and politician.

Friends are “annuals” that need seasonal nurturing to bear blossoms. Family is a “perennial” that comes up year after year, enduring the droughts of absence and neglect. There’s a place in the garden for both of them.

Erma Bombeck (1927-1996) was an American humorist.

For most of the history of our species we were helpless to understand how nature works. We took every storm, drought, illness and comet personally. We created myths and spirits in an attempt to explain the patterns of nature.

Ann Druyan (1949--) is an American writer and producer specializing in the communication of science.

I think we are bound to, and by, nature. We may want to deny this connection and try to believe we control the external world, but every time there’s a snowstorm or drought, we know our fate is tied to the world around us

Alice Hoffman (1952--) is an American novelist and young-adult and children’s writer.

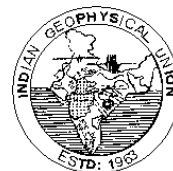
The world is a drought when out of love.

Brandon Boyd (1976--) is an American singer, songwriter, musician, author and artist.

“Not every dream grows on every land, so you got to watch out! “Sugar cane” dreams should find the environment where there is flooding of great ideas from great people. It will die off if it is planted at the place where the drought of discouragement is a well cherished culture!”

Israelmore Ayivor (1989--) is an inspirational writer, blogger and Life Skills Entrepreneur.

NEWS AT A GLANCE



FORTHCOMING EVENTS:

1. 10th INTERNATIONAL CONFERENCE AIR AND WATER COMPONENTS OF THE ENVIRONMENT

15 - 17 Mar 2018, Sovata, Romania.

Topics: Hydrology, Meteorology and climate change, Geography, Global Positioning System, Earth Observation, Oceanography, Ecosystems, Environment and Sustainable Development, Air and water environment monitoring, Climatic and hydrological hazards, Water resource management, Climatic changes and their impact, Pollution and protection of air and water environment, Weather and hydrological forecast

Event website: <http://aerapa.conference.ubbcluj.ro/Engleza/index.htm>

2. CONFERENCE "GEODESY, MINE SURVEY AND AERIAL TOPOGRAPHY"

05 -16 Feb 2018, Moscow, Russia.

Topics: Geodesy, Mine Survey and Aerial Photography, Digital Geo information technology,

Mining & Mineral Processing.

Event website: <http://www.con-fig.com/>

3. National Academy of Sciences

Topics: Economics, Environment, and Sustainable Development

17-18 Jan, 2018, NAS Building, Washington, DC.

Event Website: <http://www.nasonline.org/about-nas/events/?month=1&year=2018>

4. 3rd GoGREEN SUMMIT -18

23 -24 Mar 2018, St Giles Classic Hotel, Manila, Philippines.

Topics: Earth and planetary sciences, Ecology, Biodiversity, Agriculture, Environmental engineering, Environmental science and toxicology, Bioremediation and Pollution control

Event website: <https://bioleagues.com/conference/gogreensummit/about.php>

AWARDS AND RECOGNITION

** 54th Annual Convention of Indian Geophysical Union (IGU)

During the convention the following awards have been given for 2017 by Prof. Shailesh Nayak, President of IGU.

* **IGU-Dr. Hari Narain Lifetime Achievement Award**
Prof. D. Guptasarma

* **IGU-Decennial Award**
Dr. Anil Bhardwaj

* **IGU-Krishnan Medal**

1. Dr. Nimisha Vedanti
2. Dr. Devleena Mani

* **IGU-Anni Talwani Memorial Prize**

Dr. Shakeel Ahmed

* **IGU-Prof. D. Lal Best Paper Award**

Dr. C.D. Reddy and Dr. Mahesh N Shrivastava.

IGU-Prof. Jegdeo Singh and Dr. S. Balakrishna Memorial Grant for student toppers- 2017 have also been presented.

** **Ministry of Earth Sciences Annual Awards -2017**

- * In recognition of empowering many young Indian students to pursue world class research in Isotope Geoscience **Prof. K. Gopalan** has been awarded "**Life Time Excellence Award**" by MOES for the year 2017.
- * In recognition of his outstanding contributions in the field of Marine Geophysics, Ministry of Earth Sciences (MoES) honoured **Prof. Kolluru Sree Krishna** with the "**National Award** in the field of Geoscience and Technology" for the year 2017.
- * In recognition of his outstanding research contributions in the field of Earth System Science the MOES honoured **Dr. Vikram Vishal** with the "Young Researcher Award in the field of Earth System Science" for the year 2017.
- * **Mrs. Shyla Minhas** is awarded the Certificate of Merit by MOES for her outstanding contribution in the field of Atmospheric Science & Technology for the year 2017.
- * **Dr. R. R. Mali** is awarded the Certificate of Merit by MOES for his outstanding contributions in the field of Atmospheric Sciences and Technology for the year 2017.

SCIENCE NEWS

Pollution of land, ocean and atmosphere has affected not only environment but life on Earth. One of the pollutants is plastics. In spite of various measures, albeit a half hearted attempt, the pollution has reached unbelievable levels not only affecting land but also oceans. Some of the pertinent details are given below, to motivate one and all to take steps to eradicate this menace.

* **What is Plastic Pollution?**

As the world's population continues to grow, so does the amount of garbage that people produce. On-the-go lifestyles require easily disposable products, such as soda cans or bottles of water, but the accumulation of these products has led to increasing amounts of plastic pollution around the world. As plastic is composed of major toxic pollutants, it has the potential to cause great harm to the environment in the form of air, water and land pollution. Put simply, plastic pollution is when plastic has gathered in an area and has begun to negatively impact the natural environment and create problems for plants, wildlife and even human population. Often this includes killing plant life and posing dangers to local animals. Plastic is an incredibly useful material, but it is

also made from toxic compounds known to cause illness, and because it is meant for durability, it is not biodegradable.

Plastic pollution involves the accumulation of plastic products in the environment that adversely affects wildlife, wildlife habitat, or humans. Plastics that act as pollutants are categorized into micro-, meso-, or macro debris, based on size. The prominence of plastic pollution is correlated with plastics being inexpensive and durable, which lends to high levels of plastics used by humans.^[3] However, it is slow to degrade.^[4] Plastic pollution can unfavourably affect lands, waterways and oceans. Living organisms, particularly marine animals, can also be affected through entanglement, direct ingestion of plastic waste, or through exposure to chemicals within plastics that cause interruptions in biological functions. Humans are also affected by plastic pollution, such as through the disruption of the thyroid hormone axis or hormone levels. In the UK alone, more than 5 million tonnes of plastic are consumed each year, of which an estimated mere 24% makes it into recycling systems. That leaves a remaining 3.8 million tonnes of waste, destined for landfills. Plastic reduction efforts have occurred in some areas in attempts to reduce plastic consumption and pollution and promote plastic recycling.

* Effects of Plastic Pollution

It seems rather obvious that this amount of a material that isn't meant to break down can wreak havoc on natural environments, leading to long-term issues for plants, animals, and people. Some of the major long-term effects of plastic pollution are:

1. It Upsets the Food Chain: Because it comes in sizes large and small, polluting plastics even affect the world's tiniest organisms such as plankton. When these organisms become poisoned due to plastic ingestion, this causes problems for the larger animals that depend on them for food. This can cause a whole slew of problems, each step further along the food chain. Plus, it means that plastic are present in the fish that many people eat every day.

2. Groundwater Pollution: Water conservation is already a concern in places ranging from California to parts of India, but the world's water is in great danger because of leaking plastics and waste. If you've ever seen a garbage dump, imagine what happens every time it rains – then imagine that being in your drinking water. Groundwater and reservoirs are susceptible to leaking environmental toxins. Most of the litter and pollution affecting the world's oceans also derives from plastics. This has had terrible consequences on many marine species, which can lead to consequences for those that eat fish and marine life for nutrients – including people.

3. Land Pollution: Chlorinated plastic can release harmful chemicals into the surrounding soil, which can then seep into groundwater or other surrounding water sources and also the ecosystem. This can cause serious harm to the species that drink the water. Landfill areas contain many different types of plastics. In these landfills, there are many microorganisms which speed up the biodegradation of plastics. The microorganisms include bacteria such as *Pseudomonas*, nylon-eating bacteria, and Flavobacteria. These bacteria break down nylon through the activity of the nylonase enzyme. Breakdown of biodegradable plastics releases methane, is a very powerful greenhouse gas that contributes significantly to global warming.

4. Ocean Pollution: In 2012, it was estimated that there was approximately 165 million tons of plastic pollution in the world's oceans. One type of plastic that is of concern in terms of ocean plastic pollution is nurdles. Nurdles are manufactured plastic pellets (a type of microplastic) used in the creation of plastic products and are often shipped via cargo ship. Many billions of nurdles are spilled into oceans each year, and it has been estimated that globally, around 10% of beach

litter consists of nurdles. Plastics in oceans typically degrade within a year, but not entirely. In the process, toxic chemicals such as bisphenol A and polystyrene can leach into waters from some plastics. Polystyrene pieces and nurdles are the most common types of plastic pollution in oceans, and combined with plastic bags and food containers make up the majority of oceanic debris. One study estimated that there are more than 5 trillion plastic pieces (defined into the four classes of small microplastics, large microplastics, meso- and macroplastics) afloat at sea. The litter that is being delivered into the oceans is toxic to marine life, and humans. The toxins that are components of plastic include diethylhexyl phthalate, which is a toxic carcinogen, as well as lead, cadmium, and mercury. Plankton, fish, and ultimately the human race, through the food chain, ingest these highly toxic carcinogens and chemicals. Consuming the fish that contain these toxins can cause an increase in cancer, immune disorders, and birth defects. The majority of the litter near and in the ocean is made up of plastics. According to Dr. Marcus Eriksen of The 5 Gyres Institute, there are 5.25 trillion particles of plastic pollution that weigh as much as 270,000 tons (2016). This plastic is taken by the ocean currents and accumulates in large vortexes known as ocean gyres. The majority of the gyres become pollution dumps filled with plastic.

* Solutions to Plastic waste Pollution

The reality is that the only way this problem can be addressed is by individuals and companies around the world agreeing to implement practices that reduce waste on every level.

* The top tips for reducing plastic waste are:

Shop Friendly: Plastic bags were once a modern convenience but can be efficiently replaced by reusable bags, many of which fold up compactly in order to be portable. Just think about how many bags you typically carry out of a grocery store, and multiply that by the number of times you grocery shop. That's a lot of plastic! Carry a bag and always reuse plastic bags as much as possible if you have them. **Get Rid of Bottled Water:** People are meant to drink lots of water each day, and plastic water bottles have become a great way to stay hydrated throughout the day. However, most of these are only recommended for single use, and that means that every time someone finishes a bottle it goes into the trash. Many companies now sell reusable water bottles as a substitute, reducing plastic waste and exposure to leaking bottles. **Forget to-go Containers:** You would be surprised at how much plastic is involved in the making and packaging of food containers. Think the coffee shop's drink cup is paper? It's likely lined with plastic for insulation (pour a cup of coffee on some cardboard and see what happens). Plastic food containers, lids, and utensils are all easily replaced by reusable containers, which will cut down significantly on even a single meal's waste. **Educate Businesses:** Speak to local restaurants and businesses about options that they can switch to for packaging, storing, and bagging items. Many companies are starting to come up with excellent low-cost replacements, such as bamboo utensils in place of plastic ones. **Get Involved:** Speak to lawmakers and get involved with government on any level, and you'll see how many special interest groups have made it so that we are dependent on plastic without needing to be. Encourage development of items, and propose alternatives when applicable. **Recycle Everything:** Try and select items that come in non-plastic recycled and recyclable packaging, to do your best to properly handle items that can't be reused. Check everything before you put it in the trash, as more and more items are able to be recycled these days. Remember that because plastic doesn't break down easily (if ever), recycling plastic means that it is still plastic, just being used for a different purpose. Therefore, you're not actually reducing plastic amounts or exposure, even in the recycling process. (Sources: https://en.wikipedia.org/wiki/Plastic_pollution & <https://www.conserve-energy-future.com/causes-effects-solutions-of-plastic-pollution.php>)

Even though solutions are suggested it is going to be a mammoth task to eliminate/ reduce already created pollution. Significant success can be achieved only when every human being makes a concerted effort to arrest the plastic waste pollution. I am stating so after knowing that the plastic waste has literally encompassed every segment of our earth.

The following article elaborates it clearly.

'Extraordinary' levels of pollutants found in 10km deep Mariana trench Scientists have discovered "extraordinary" levels of toxic pollution in the most remote and inaccessible place on the planet – the 10km deep Mariana trench in the Pacific Ocean. Small crustaceans that live in the pitch-black waters of the trench, captured by a robotic submarine, were contaminated with 50 times more toxic chemicals than crabs that survive in heavily polluted rivers in China. "The fact that we found such extraordinary levels of these pollutants really brings home the long-term, devastating impact that mankind is having on the planet," Jamieson of UK said. Jamieson's team identified two key types of severely toxic industrial chemicals that were banned in the late 1970s, but do not break down in the environment, known as persistent organic pollutants (POPs). These chemicals have previously been found at high levels in Inuit people in the Canadian Arctic and in killer whales and dolphins in Western Europe. The research, published in the journal Nature Ecology and Evolution, suggests that the POPs infiltrate the deepest parts of the oceans as dead animals and particles of plastic fall downwards. POPs accumulate in fat and are therefore concentrated in creatures up the food chain. They are also water-repellent and so stick to plastic waste.

"The very bottom of the deep trenches like the Mariana are inhabited by incredibly efficient scavenging animals, like the 2cm-long amphipods we sampled, so any little bit of organic material that falls down, these guys turn up in huge numbers and devour it. It was not unexpected that some POPs would be found in the deepest parts of the oceans. When it gets down into the trenches, there is nowhere else for it to go. The surprise was just how high the levels were – the contamination in the animals was sky high." Jamieson pointed out. The level of one type of POP, called polychlorinated biphenyls (PCBs), was only equalled anywhere in the northwest Pacific in Suruga Bay in Japan, an infamous pollution blackspot. The researchers also found severe contamination in amphipods collected in the Kermadec trench, which is 7,000km from the Mariana trench. The pollution was ubiquitous, found "in all samples across all species at all depths in both trenches", the scientists said.

PCBs were manufactured from the 1930s to the 1970s, when their appalling impact on people and wildlife was realised. About a third of the 1.3m tonnes produced has already leaked into coastal sediments and the open oceans, with a steady stream still thought to be coming from poorly protected landfill sites. An expedition conducted by the US National Oceanic and Atmospheric Administration last year also found various manmade items on the slopes leading to the Sirena Deep, part of the Mariana trench, and the nearby Enigma Seamount. The results are both significant and disturbing, said the marine ecologist Katherine Dafforn at the University of New South Wales in Australia. The trenches are many miles away from any industrial source and suggests that the delivery of these pollutants occurs over long distances despite regulation since the 1970s. She said the new research showed that the deep ocean trenches are not as isolated as people imagine. Jamieson's team has provided clear evidence that the deep ocean, rather than being remote, is highly connected to surface waters. Their findings are crucial for future monitoring and management of these unique environments. POPs cause a wide range of damage to life, particularly harming reproductive success. Jamieson is now assessing the impact on the hardy trench creatures, which survive water pressures equivalent to balancing a tonne weight on a fingertip and temperatures of just 1C.

Plastic pollution, feared to be widespread in the oceans, which has been the focus of much recent attention, leading to bans on plastic microbeads

in cosmetics in the UK and US. Jamieson said it had been positive that the dangers of POPs had been identified and their use ended but that plastic pollution presented a new concern for contamination of the oceans.

(Source: <https://www.theguardian.com/environment/2017/feb/13/extraordinary-levels-of-toxic-pollution-found-in-10km-deep-mariana-trench>)

SIGNIFICANT CONTRIBUTION IN PROPAGATING THE IMPORTANCE OF GEOCHRONOLOGY

Kunchithapadam Gopalan



Kunchithapadam Gopalan (born 1938) is an Indian geochronologist of eminence and contributed significantly in propagating the importance of Geochronology, while working as a senior scientist and emeritus scientist at National Geophysical Research Institute. He is known for his studies on the chronologies of critical rock suites of the Indian subcontinent and is an elected fellow of the Indian Academy of Sciences, Indian National Science Academy, Indian Geophysical

Union and the National Academy of Sciences, India. The Council of Scientific and Industrial Research, the apex agency of the Government of India for scientific research, awarded him the Shanti Swarup Bhatnagar Prize for Science and Technology, one of the highest Indian science awards for his contributions to earth, atmosphere, ocean and planetary sciences in 1982.

K. Gopalan, born on 12 August 1938 in the south Indian state of Tamil Nadu, graduated in physics (Bsc hons) from the University of Madras in 1959 and completed his master's degree in nuclear physics from Andhra University in 1960, standing first in the university. As a graduate student in 1960 in the Physics Department of IISC, Bangalore, Gopalan switched from physics to earth sciences. His work was on quantitative dating of extraterrestrial (cosmochronology) and terrestrial rocks (geochronology) based on the time dependent transformation of naturally- occurring radioactive (parent) isotopes of some elements into isotopes (daughter) of other elements Enrolling at the Indian Institute of Science for his doctoral studies, he secured a PhD in 1966, working under the guidance of V. S. Venkatasubramanian and moved to the University of California, Los Angeles where he did his postdoctoral studies at the laboratory of George Wetherill on meteorites and lunar samples. As a postdoctoral associate of Prof. G.W. Wetherill in UCLA, Los Angeles, Gopalan determined Rb-Sr ages of close to 4,600 million years for individual groups of meteorites, thereby validating a few previous model dependent ages. He was selected for his expertise on meteorites to the team of scientists to analyze the first batch moon rocks from the Apollo II mission in July 1969. Although moon samples were harder than meteorites to date, Gopalan succeeded in dating them to give the first indication that the moon was volcanically active in its infancy. The US government invited him, as a Fulbright scholar, to talk on his work on lunar rocks in major Indian cities during the exhibition of a moon rock there in early 1970. On his return to India he joined the research group of Prof. D. Lal in the TIFR, Mumbai to initiate geochronological research in India. For this he designed and built a mass spectrometer, as commercial instruments were too expensive. He could, however, try out this instrument only after he moved to the Physical Research Laboratory (PRL) in Ahmedabad in 1974 following the appointment of Dr. D. Lal as its director. Interacting with GSI scientists in the collection of key rocks from Rajasthan, Gopalan discovered very old (Archean) crustal remnants to the east of the Aravalli Mountains and possible ancient tectonic plate margin to the west.

The prevailing view then was that volcanic rocks extruded on oceanic and continental crusts were derived from isotopically distinct mantle

segments. Gopalan saw an opportunity to test this dichotomy from strontium and neodymium isotopic ratios in different layers of the volcanic edifice, known as the Deccan basalts, in central India. Measuring these ratios precisely in collaboration with Prof. Macdougall of the Scripps Institution of Oceanography, Dr. Gopalan showed convincingly that the apparent difference between sub-continental and sub-oceanic mantles was an interact of crustal assimilation by the primary melt in the former case. Another important outcome of this work was the distinctness of the mantle sources of the older Raj Mahal basalts in eastern India and the younger Deccan basalts.

The Deccan volcanic eruption about 65 million years ago attracted global scientific interest, as it was believed to have been triggered by a large meteorite impact and caused the global mass extinction and deposition of iridium rich clay layer at that time. Dr. Gopalan developed ^{40}Ar - ^{39}Ar dating facility involving neutron irradiation of samples to precisely date the basal layers of the Deccan sequence. His results delinked Deccan eruption from a bolide impact. K/T mass extinction and clay layer are now believed to be due to a meteorite impact in the Atlantic ocean close to the US-Mexico eastern border and slightly later than the Deccan initiation.

Realizing that commercial mass spectrometers with much higher precision and sensitivity than possible with home-made instruments were indispensable for sophisticated studies, Gopalan accepted prof. V.K.Gaur's invitation in 1984 to organize a world class isotope laboratory around a commercial mass spectrometer in the National Geophysical Research Institute, Hyderabad. Before leaving PRL, he helped in establishing sophisticated mass spectrometric facilities for his colleagues to pursue other types of research. Dr. Gopalan built a clean chemical lab in NGRI for contamination-free chemical processing of samples to preserve their isotopic integrity, and introduced Sm-Nd analyses to complement Rb-Sr analyses.

Dr. Gopalan focused on mantle-derived rocks like kimberlites and carbonites in his new lab. He showed that diamond-bearing kimberlites in Andhra Pradesh (Vajrakarur) and Madhya Pradesh (Panna) were episodically emplaced just at one time-1100 million years ago. He discovered two spatially very close carbonatite bodies in Tamil Nadu (Sevatur and Hognekal) but which were emplaced at two incredibly-different times- 2400 and 700 million years ago. Their initial Sr and Nd ratios imply that both were derived from the same mantle source that evolved in isolation for as long as 2000 million years. Dr. Gopalan reported a precise Sm-Nd age of 4.570 ± 0.023 by for a recently fallen meteorite (Piplia Kalan) in the international conference in Ahmedabad in 1997. Prof. Wasserburg, a giant in the subject, commented from the audience that if the age result was correct, meteorite should contain evidence of the earliest solar system events. Dr. Gopalan's PRL colleagues indeed found that long elusive evidence later, validating the very old age of Piplia Kalan.

After his early studies on meteorites and lunar samples, Gopalan's focus shifted during his PRL days to geochronology. His work has been primarily in the field of geochronology and he is known to have conducted extensive studies on the chronologies of several critical rock suites of the Indian subcontinent for which he developed custom-built equipment. He worked on the precambrian Rajasthan and Madhya Pradesh using Rb-Sr dating techniques with mass spectrometer as well as the volcanic rocks of the Deccan plateau and his researches have assisted in a wider understanding of the ages of solid bodies in the solar system and basaltic volcanism in Mare Tranquillitatis. He is credited with the setting up of a mass spectrometer, a facility for Argon-argon dating of rocks, and an isotope facility at Physical Research Laboratory, a geochronology laboratory at National geophysical Research Institute and an Accelerator Mass Spectrometer for radiocarbon dating at the Institute of Physics, Bhubaneswar, the first such facility in India. His studies have been detailed in several peer reviewed articles; a number of them have been listed by online article repositories such as Research

Gate and Google Scholar. He has been associated with many science journals including the *Academy Proceedings in Earth and Planetary Sciences* as a member of their editorial boards and has delivered several invited or plenary lectures. His work has been cited by many authors and he has also mentored 8 doctoral scholars in their studies.

He is credited with the setting up of a mass spectrometer, a facility for Argon-argon dating of rocks, and an isotope facility at Physical Research Laboratory, a geochronology laboratory at National geophysical Research Institute and an Accelerator Mass spectrometer for radiocarbon dating at the Institute of Physics, Bhubaneswar, the first such facility in India. His studies have been detailed in several peer reviewed articles; a number of them have been listed by online article repositories such as Research Gate and Google Scholar. He has been associated with many science journals including the *Academy Proceedings in Earth and Planetary Sciences* as a member of their editorial boards and has delivered several invited or plenary lectures. His work has been cited by many authors and he has also mentored 8 doctoral scholars in their studies.

Dr. Gopalan's enduring satisfaction was to have empowered many young Indian students to pursue world-class research in isotope geosciences. He hopes that his concise book on radiometric dating (Cambridge University Press, 2017) will stimulate many young Indian students to take up a serious study of isotope geology.

AWARDS AND HONOURS

Gopalan, a Fulbright scholar during his doctoral studies, received the Krishnan Medal of the Indian Geophysical Union in 1982. The Council of Scientific and Industrial Research awarded him the Shanti Swarup Bhatnagar Prize, one of the highest Indian science awards, the same year. He was awarded the Eminent Mass Spectrometrists Award of the Indian Society for Mass Spectrometry in 1991. The Indian Academy of Sciences elected him as a fellow in 1986, followed by Indian National Science Academy in 1986, Indian Geophysical Union in 1988 and the National Academy of Sciences, India in 1992. He received " Prof.K.R.Ramanathan Memorial lecture Award " from Indian Geophysical Union. In 2017 Prof. Gopalan received "**Lifetime Achievement Award**" from Ministry of Earth Sciences (MOES) .

His significant research publications include:

Gopalan, K., Trivedi, J.R., M.N., Balasubrahmanyam, Ray, S.K., and Anjaneya Sastry, C., (September 1979). "Rb-Sr Chronology of the Khetri Copper Belt, Rajasthan". *Geological Society of India*. v.20, no.9.

Murari, R., Krishnamurthy, P., Tikhonenko, P. I., and Gopalan, K., (December 1993). "Magnesian Ilmenites in Picrite Basalts from Siberian and Deccan Traps—Additional Mineralogical Evidence for Primary Melt Compositions (?)". *Mineralogical Magazine*, v.57, no.389, pp: 733–735. doi:10.1180/minmag.1993.057.389.18.

Gopalan, K., Douglas Macdougall, J., and Christopher Macisaac, (September 2007). "High Precision Determination of $^{48}\text{Ca}/^{42}\text{Ca}$ Ratio by TIMS for Ca Isotope Fractionation Studies". *Geostandards and Geoanalytical Research*, v.31, no.3, pp: 227–236. doi:10.1111/j.1751-908X.2007.00847.x.

Gopalan, K., (April 2013). "A Simple Chemical Resistant Hotplate for Geochemical Applications". *Geological Society of India*, v.81, no.4.

Gopalan, K., Kumar, A., Kumar, S., and Vijayagopal, B., (August 2013). "Depositional history of the Upper Vindhyan succession, central India: Time constraints from Pb–Pb isochron ages of its carbonate components". *Precambrian Research*, v.233, pp: 108–117. doi:10.1016/j.precamres.2013.04.014.

P.R.Reddy

Proterozoic Orogens of India: A critical window to Gondwana by T.R.K.Chetty,
CSIR-NGRI, Hyderabad- 500 007, pp- 1 to 405, Elsevier publication, ISBN; 978-0-12-804441-4:
Book Review by P.R.Reddy.

Conflicting theories and opinions do exist in any science. They are more in earth science, as it is not an exact science like Physics and Chemistry. Because of such controversies many a time researchers spend considerable time in projecting their theories overlooking good content of other studies. To avoid such an attitude it is essential to integrate various inputs and come out with a theory or model that is in general nearer to reality. Presence of mineral grains of particular texture in a rock strata and absence of such a texture in the adjacent rocks of similar composition and structure excites an experienced field geologist and encourages him to explicitly study the two types of rock assemblages starting from the field and extending in to a well equipped lab to build structural and evolutionary models that can provide meaningful answers to some of the interpretational ambiguities existing for decades. Dr.T.R.K.Chetty is one such field geologist who has succeeded in opening new avenues and thereby provided a unique opportunity to understand the cross section of the well exposed and thoroughly studied part of the Earth's crust and the varied processes of continental collision, using a wealth of data and information from other branches of earth science in better deciphering the data generated by him through concerted efforts in the field. In his seminal and authoritative overview of the latest information on the Proterozoic Orogens of India he has succeeded to a significant extent in explaining vividly the pulses of reworking processes and their impact on magmatism, metamorphism, and deformational history of Proterozoic orogens, specifically regarding supercontinental formation. In presenting the varied types of interpretations and hypotheses by well known geologists on structural architecture, crustal blocks, shear zone systems, magmatism, metamorphism, geochemical and isotopic signatures, mineralization, and temporally and spatially varying tectonic models that exhibit unique variations not only laterally but also vertically of all the Proterozoic orogens of India, Dr.Chetty to a significant extent succeeded in narrowing down the ambiguities. While discussing various reworking processes he has utilised useful inputs, with an open mind, from geophysics, geochemistry and geochronology there by enhanced the quality of his presentations through valuable illustrations reflecting not only the field based rich data sets but also very useful multi structural integrated data sets. It is good to find in the Preface Dr.Chetty giving due importance to recent, especially the refinements of many geological, geochemical, geochronological, and geophysical studies role in uncovering many new facets of the geology of the Proterozoic orogens of India along with some proposed new lines of thinking of traditional concepts, which were previously developed but were lacking a substantial amount of information that we now have today. Dr.Chetty in a way by stating so has encouraged close co-ordination of scientists belonging to different branches of earth science. According to me it is an apt approach to arrive at a better understanding of the Proterozoic orogens evolution. In the present synthesis Dr.Chetty correctly laid much stress on the large volume of the recently obtained field based

multiscale data analysed properly through laboratory studies to clarify and address some of the earlier concepts to resolve many unknown controversies. In a way this approach has stressed the necessity to get proper data from the field, by planning in advance in selecting the main objective of acquiring such data instead of aimlessly collecting broad range of data sets that have no specific importance to a select study. When such randomly acquired data sets are processed using commercial software and routine lab studies one could succeed only in producing graphically colourful evolutionary models that can only add to the confusion instead of providing solutions to existing controversies. Publication of such models projecting them as cutting edge scientific research output negates growth of well articulated scientific research. From the details given in his book Dr.Chetty, while covering various aspects of an important segment of Proterozoic orogens of India, without hesitation brought out limitations of some of his studies in providing unequivocally apt solutions to some of the still existing controversies. In his own words Dr.Chetty mentioned that the wisdom gained through three decades of field based experience, in conjunction with the enormous wealth of literature he has made an attempt to present an unprejudiced view with an open mind without fear or compulsion. In this context the statement made by Ian Fitzsimons in the "Foreword" is interesting and supports the significant initiatives made by Dr.Chetty. He has mentioned "While it had long been recognized that Precambrian basement rocks of India comprised a series of orogenic belts that wrap around granite-dominated cratons, a paucity of robust isotopic data meant that many of these rocks were still attributed an Archean age simply on account of their crystalline nature, making it difficult to integrate their histories with any certainty to those established for other continents. This situation has improved markedly in recent years as modern geochronological techniques have been applied to Indian outcrops at a ever-accelerating rate, and India's basement orogens are now known to preserve Proterozoic tectonic events that correlate closely with the assembly of supercontinents." Dr.Chetty, aptly coupled geochronological data with structural, petrological, geochemical and geophysical data to produce exciting new models for the evolution of Proterozoic India and its tectonic and palaeographic relationships.

To properly exhibit uniqueness of different Proterozoic orogens, Dr.Chetty aptly sub divided his book into 6 chapters covering details on 1) Orogens, 2) The Southern Granulite Terrane, 3) The Eastern Ghats Mobile Belt, 4) The Central Indian Tectonic Zone, 5) The Aravalli-Delhi Orogenic Belt and 6) The Gondwana Correlations. Even though I carried out useful long range seismic refraction and deep reflection profiling studies and learnt many aspects of integrated geophysical and geological studies and published useful articles I have found it really difficult to objectively review Dr.Chetty's excellent presentation that contains number of subsections in each chapter covering almost all the facets of Proterozoic orogens of India. I do hope that my effort to bring out some important details through this review will motivate young

researchers in following the footsteps of Dr.Chetty in making their research initiatives meaningful and lasting for decades.

In the **first chapter** Dr.Chetty covered various facets of Orogens and highlighted their importance in deciphering the origin and evolution of specific crustal segments. The Proterozoic Orogens of India (POI) are defined by curvilinear, high-grade granulite-gneiss belts encompassing the entire Indian continent from Kanyakumari in the south to New Delhi in the north. The POI comprise a sinuous chain of four major orogens from south to north in a counter clockwise direction that include: the Southern Granulite Terrane (SGT), the Eastern Ghats Mobile Belt (EGMB), the Central Indian Tectonic Zone (CITZ), and the Aravalli-Delhi Orogenic Belt (ADOB). The SGT occurs at the southern margin of the Dharwar craton and the EGMB is situated along the east coast wrapping around Dharwar and Bastar cratons. The CITZ in central India is sandwiched between Bundelkhand craton to the north and the Bastar and Singhbhum cratons to the south, while the ADOB occurs to the west of Bundelkhand craton and extends up to the Himalayan orogenic belt in the north. These orogens are also described as fold-thrust belts. Details given in this chapter aptly introduce the focal theme of the book and explain in detail definition of Orogen and its classification. The orogens can broadly be grouped into collisional and accretional types. Accretionary orogenic systems (also described as "Pacific-type" or "Cordillera-type") are formed through on-going plate convergence during the period of supercontinent breakup and continental dispersal. Collisional orogenic systems (Himalayan-type) are generated when the ocean is closed during continental assembly and the formation of supercontinents. Collisional orogenic systems may be superimposed on accretionary systems, which can be described as subduction-to-collision orogenesis. Under General Characteristics subsection Dr.Chetty exposed the reader to various characteristics. Orogeny includes a collage of processes, such as: (1) magmatism, which generates continental crust; (2) rejuvenation and recrystallization by metamorphism where in the metamorphic belts occupy the orogenic core; (3) deformation to produce major structures of orogenic belts; and (4) sedimentation where the mountain-building activity takes place through the transportation of large volumes of sedimentary material. He has also detailed the importance of Plate Tectonics. It has been well established that the development of orogens involves plate tectonics through a variety of associated processes like subduction zones after the consumption of oceanic crust producing volcanoes and build island arcs magmatism. The other important associated processes include magmatism, metamorphism, crustal melting, and crustal thickening. However, these are dependent on the strength and rheology of the continental lithosphere and their change in their properties during orogenesis. Under the subsection Proterozoic orogens of India(POI) Dr.Chetty focused on the importance of POI. The Precambrian Indian shield is a mosaic of Archean cratons and Proterozoic orogens. There are four major cratons, which are characterized by Archean low grade granite greenstone sequences. The cratons are surrounded and separated by the Proterozoic orogens. The interface between cratons and orogens is marked by crustal-scale ductile shear zones. The Proterozoic period spans nearly 2 billion years, which can be divided into three eras: Palaeoproterozoic (2500 to 1600 Ma); Mesoproterozoic (1600 to 1000 Ma); and Neoproterozoic (1000 to 540 Ma). The Proterozoic is considered to be important because

of great crustal stabilization marked by the development of global scale orogens. He has covered under the subsection "Terminology of Important Geologic Units" suture zones, shear zones, sheath folds, duplex structures etc.

In the **second chapter** SGT is covered. The SGT has been one of the most intensely studied orogens in the last two decades by several national and international groups encompassing all aspects of geology and geophysics. Innumerable publications have brought out large volumes of data with several modern concepts and innovative ideas but with variable and contradicting interpretations. However, many of the controversial topics remain debatable even today, despite the accumulation of significant amount of geological, geochemical, geochronological, and geophysical data. The plethora of contrasting interpretations and the evolution and subdivision of crustal blocks within the SGT are a direct consequence of limited field observations, lack of field and structurally constrained geochronological data, and limitations of accessibility due to high elevation and dense vegetation. The east-west trending tectonic features and associated structural fabrics broadly characterize the SGT. However, there are distinct variations in different segments as well as within the shear zones, as succinctly presented by active and passive seismic investigations. Composite long range seismic refraction and deep reflection profiling studies have brought out varied structures in different crustal blocks divided by number of regionally extending shear zones, such as Mettur shearzone, Palghat-Cauvery shear zone and Achankovil shearzone. The seismic investigations have also brought out divergent reflectivity pattern, which Dr.Chetty and Dr.Bhaskar Rao named as a flower structure from their detailed investigations. Presence of a low velocity layer in middle and lower crust has been interpreted by well known geologists as a zone containing fluids. According to Dr.Chetty, based on the recent developments and significant advances, the SGT can be divided into five distinct crustal/tectonic units based on lithological assemblages, structural styles, geochronological characteristics, and geophysical signatures. From north to south, they are: (1) Northern Granulite Block (NGB), (2) Cauvery suture/shear zone (CSZ), (3) Madurai Granulite Block (MGB), (4) Achankovil suture/shear zone (AKSZ), and (5) Trivandrum Granulite Block (TGB). A comprehensive foliation trajectory map of the SGT is presented in the book. Apart from the crustal-scale shear zones, the map shows well defined foliation trajectories defining broad fold forms, variable trends and geometries at different places pointing to the existence of a mosaic of different tectonic blocks within the SGT. A composite schematic tectonic model envisages an early rifting stage with the development of the Mozambique Ocean, followed by the southward subduction of the oceanic plate. The tectonic history of the SGT reveals a progressive sequence from Pacific-type to collision-type orogeny, which finally gave rise to a Himalayan-type Cambrian orogeny with characteristic magmatic, metasomatic, and metamorphic factories operating in subduction and collision setting. Dr.Chetty quoting some significant studies by internationally reputed geologists stated that the evolution of the SGT involves accretion processes of island arc magmatic suites, thrust stacking with duplex structures, and deformed sheath fold geometries, granitic emplacements, and obduction of ophiolite complexes: a complete range of processes like transpression associated with extrusion and exhumation, typical of modern

orogenic belts. According to Dr.Chetty the SGT could be a classic representative of ancient subduction factory that witnessed large-scale collision related to Gondwana amalgamation.

In the **third chapter** EGMB is covered. Dr.Chetty covered this Proterozoic orogenic belt extensively and gathered a huge wealth of data and addressed various important aspects with an amount of authority. He has done a great service by covering in detail the significant studies carried out by luminaries like Narayan Swamy, Leelanandam, Ramakrishnan, Raith and many others. The Eastern Ghats Mobile Belt (EGMB), a Mesoproterozoic collisional orogen, occurs along the east coast of India with a strike length of over 900 km and a width varying from 50 km in the south to a maximum of 300 km in the north. The margins of the EGMB are characterized by lithospheric shear zones at the contact with the Archean cratons of Dharwar and Bastar in the west and the Singhbhum craton in the north. Tectonic Synthesis of EGMB must have witnessed several deformational and metamorphic events (as detailed by many researchers), but three events are considered as the most significant. The earliest deformational event that could be recognized is the development of the compositional fabric or the gneissic banding, which can be related to a 2.8 Ga deformational event during the Neoproterozoic. This event must have been associated with northwest directed thrusting generating NE-SW trending fabrics with gentle to moderate dips at the western margin juxtaposing the Bastar craton and ENE-WSW fabrics at the northern margin juxtaposing the Singhbhum craton. The event is also marked by northwest-verging thrusts, giving rise to large-scale recumbent fold structures and other flat lying fabrics associated with crustal thickening and granulite facies metamorphism during 3000 to 2600 Ma. This is consistent with the existence of several thrust zones that were demarcated all over the EGMB. The other most significant thermal event recognized in the evolution of the EGMB is the Grenvillian orogenic event (1100 to 800 Ma), which was marked by the development of shear zones and associated metamorphism and migmatization. Dextral transpressional kinematics and intense strain partitioning during Grenvillian orogenic event period seem to be the dominant tectonic scenario continued until the end of the Neoproterozoic up to 500 Ma. This deformational event was related to the Mesoproterozoic oblique convergence between the Indian shield and the East Antarctica, broadly coinciding with the formation of the Rodinia supercontinent. The other major event was the thrusting between 540 and 500 Ma, which was post tectonic to folding and granulite metamorphism of the cover rocks. However, according to Dr.Chetty, the ages and the nature of deformational history with respect to the events is still a matter of debate, for instance, the time of thrusting and whether it is synchronous or post tectonic with the granulite facies metamorphism. Dr.Chetty believes that future research can resolve these critical and controversial issues in complex terranes like the EGMB. The Pan-African event, recorded around 500 Ma, could possibly represent a third deformation event, most probably restricted to shear zones.

In the **Fourth chapter** the Central Indian Tectonic Zone (CITZ) is covered. It is a conspicuous zone of deformation in central India that extends from the west coast up to Meghalaya plateau in the east. The CITZ, also regarded as Satpura Mobile Belt, merges with the Aravalli-Delhi orogen in the west, while it swerves around the nucleus of Singhbhum craton (SC) and joins the Eastern Ghats Mobile belt in the east. It extends for about

1500 km with a width of about 180 km and divides the Indian subcontinent into two distinct crustal provinces: the Bundelkhand craton (BKC) surrounded by Vindhyan sediments to the north, and the Deccan province constituting Bastar, Singhbhum, and Dharwar cratons to the south. The entire tectonic zone has been studied by number of geologists, geochemists and geophysicists. The structural architecture of the CITZ, compiled from the available literature together with the newly interpreted shear zone systems, shows a set of crustal-scale ENE-WSW trending shear zones throughout the entire stretch. The NSL constitutes two bounding shear zones namely, the Son-Narmada-North Shear Zone (SNNSZ) and the SNSSZ. All the shear zones divide the CITZ into distinct geological terranes with contrasting geologic histories. The western extensions seem to be extending westward up to the Arabian Sea, where it merges with NE-SW trending Aravalli-Delhi orogenic belt. It is speculated that both of them may coincide with the East African orogen. Several contrasting tectonic models were proposed with wide variation on many critical issues like the polarity of subduction, timing of collision, and location of suture zone, etc., but the basic commonality was the recognition of an ancient plate tectonic regime involved in the tectonic evolution of the CITZ. Coincident seismic refraction and deep reflection results have clearly demarcated location of CIS and presence of two distinct crustal blocks on either side of CIS, with opposite dipping reflection horizons. These inputs and wealth of geological data resolved reasonably some of the controversies. According to Dr.Chetty the geological characteristics and lithological sequences within the CITZ are typical of ancient subduction-accretion - collision tectonic models. Since CITZ bifurcates Indian continent in to two distinct blocks studies and significantly different theories have surfaced from time to time, as suggested by many earth scientists including Dr.Chetty, concerted efforts need to be continued to resolve many controversies.

In the **Fifth chapter** Aravalli-Delhi Orogenic Belt is detailed. The Aravalli-Delhi Orogenic Belt (ADOB) is a prominent physiographic unit, located in the northwestern part of the Indian shield. The ADOB trends NNE-SSW and is a collage of two variably metamorphosed volcano-sedimentary belts, which are described as the Paleoproterozoic Aravalli Fold Belt (AFB) and the Mesoproterozoic Delhi Fold Belt (DFB). The basement of these fold belts is considered to be the Banded Gneissic Complex (BGC), a heterogeneous Archean terrain. The current status of our knowledge on the crustal evolution of the ADOB originated from numerous structural, petrological, geochemical, and geochronological investigations by scores of workers. Understood from a modern perspective, the ADOB can be described as a mosaic of juxtaposed geological terranes within a reworked Archean basement complex based on the lithological assemblages and structural architecture. For the sake of brevity and clarity, the ADOB can be divided and described in terms of major terranes separated by crustal scale shear zones. A multidisciplinary approach involving all geological and geophysical studies along a NW-SE trending geotranssect was attempted across the ADOB, under Deep Continental studies project of DST, covering the adjacent terranes. Geophysical data, in particular deep seismic reflection data, provide useful information in evaluating crustal architecture and mantle dynamics and have been recently employed in many studies in conjunction with the surface geological features to understand subduction-accretion-collision history in the Precambrian terranes. The reflectivity

pattern along the seismic profile from Nagaur to Jhalawar varies all along the N-J transect. The seismic reflection data was interpreted and modeled in terms of geological associations and plate tectonic controlled interactions in a broader framework of westward subduction. In contrast to the westward subduction described above, eastward subduction of the oceanic lithosphere under the continental margin of Mewar craton with the trench being located at the western boundary of SDT was also proposed recently by active seismic experts, utilising seismic reflection based crustal model. The model also successfully resolves the ambiguity by correlating the Marwar Terrane with the Rodinia assembly rather than later Pan-African orogeny located further west. The seismic images reveal possible subduction-collisional event in the form of SE-dipping reflection fabric throughout the Marwar terrane over which the 750 Ma Malani Igneous Suite (MIS) is emplaced. Recent studies of geology, geophysics and geochronology led the researchers to understand the evolution of the ADOB by involving the plate tectonic processes. It is now almost established that the ADOB was subjected to subduction-accretion-collisional processes like any other orogenic belt all over the globe. However, within the plate tectonic scenarios, conflicting opinions exist about the polarity of subduction. In summary, geological and geophysical studies established that the Plate tectonic processes were responsible for the evolution of Paleoproterozoic ADOB through an accretionary process of island arcs during subduction and/or by collision involving the Bundelkhand craton in the east and the Marwar terrane in the west. Individual terranes are recognized by differences in their seismic reflectivity characteristics and some of the crustal-scale shear zones may represent sutures that are characterized by various mineralized zones. The lithologic association and their nature of distribution are in accordance with a Paleoproterozoic Pacific-type orogeny in the Aravalli region with a westward subduction of the Archean cratonic margin and development of a wide accretionary belt, imbricated ocean plate stratigraphy including ophiolites and the extrusion of a high-grade regional metamorphic belt at the orogenic core following the final collision. The available geochronological data reinforces the suggestion that the tectonic history of the Banded Gneissic Complex (BGC-II) is distinct from that of BGC-I; the former is dominated by the Paleoproterozoic and Neoproterozoic intrusive and metamorphic events, and the latter appears to be entirely Archean. This needs to be further resolved. Dr.Chetty explicitly brought into focus the importance of this orogenic belt, by extensively quoting the significant studies carried out not only by eminent geologists but also by a highly talented team of geophysicists.

In the **last chapter** Gondwana Correlations have been discussed. This chapter deals with the brief description of the supercontinents with reference to their assembly- breakup history cycles and orogens of Gondwana supercontinent. Emphasis has been laid on the correlations and extensions of the shear zone network and suture zones associated with the Proterozoic orogens of India (POI) among different fragments of the Gondwana supercontinent. This is further substantiated with the help of the recent geochronological data that helped in understanding the assembly and breakup through different stages of Rodinia and Gondwana. The POI, representing a critical part of Gondwana

orogenic systems, delineate and juxtapose different Archean cratons of India (Dharwar, Bastar, Sighbhum, and Bundelkhand). These orogens, being in the central part of the Gondwana supercontinent, play a crucial role in the enhanced understanding of the reconstruction models of supercontinents such as Columbia, Rodinia, and Gondwana. The POI have attracted global attention in recent years for the reconstruction models related to timing and tectonics of the breakup and amalgamation of constituent fragments of Rodinia and Gondwana. The structural and metamorphic characteristics of POI, in general, are highly varied and they exhibit a wide range of styles, magnitudes, and peak temperatures. There is no unique set of characteristics that defines these orogens, and their first-order structural framework and development appears to be comparable to those of orogens formed in the Phanerozoic. The episodic character of orogenies since late-Archean times has led to speculations that Phanerozoic-style plate tectonics can be applied to the Proterozoic, and that continental land masses have periodically assembled and dispersed since the Paleoproterozoic as a result of plate convergence and separation. These speculations have provided a major stimulus to the reconstruction of ancient supercontinents, including Meso-, to Neoproterozoic Rodinia, Neoproterozoic Pannotia/ Gondwana, and Paleozoic Pangea that led to the emergence of global-scale collisional orogenies. The available geological and geophysical information from the Paleoproterozoic orogens of India, described in previous chapters, provide important clues on the broad architecture of these orogens and the subduction polarity. The POI are characterized by subduction-accretion and collision. Structurally, the orogens are generally composed of imbricated crustal terranes or nappes translated along low, to moderately dipping shear zones, and include the flow of middle or lower crust within nappe-or crustal-scale channels through melting. The crustal-scale shear zone structures associated with the POI can be extended to other adjacent continents, now-dispersed segments of the Gondwana landmass. Their linkage will provide a fresh basis for reconstructing the processes of supercontinent assemblage and breakup. It is well established that Mesoproterozoic rifting at the cratonic margins and subsequent crustal evolution along the Proterozoic orogens in the Indian shield can be correlated to plate tectonic processes linked to the assembly and breakup of supercontinents of Columbia, Rodinia, and Gondwana.

After going through this excellent book by Dr.Chetty I felt happy that earth science research would continue to flourish due to the concerted efforts made by learned scientists like Dr.T.R.K.Chetty, a good friend of mine. This book will be useful both as a text book and as a reference book for students, young researchers. It can also motivate senior researchers to continue their research activities, inspite of age related limitations, as earth science research alone can bail us out from the present chaotic and deteriorating nature of our environment. I conclude my review by congratulating Dr.T.R.K.Chetty for bringing out such an important publication by toiling night and day during the last three years. Since the quality of the book is exceptionally high a few minor typographic errors, present in the later part of the book may be corrected. Also, where ever possible the details given in figure captions are made more legible and formatted uniformly.

P.R.Reddy

Scientist-G (Retd) of CSIR-NGRI &
Former Emeritus Scientist of CSIR-NGRI

Short-Term Advanced Warning from Some Large Earthquakes

Indra N. Gupta, B.K. Rastogi* and Robert A. Wagner

Array Information Technology, Greenbelt, Maryland

*Former Director General, Institute of Seismological Research, Gandhinagar, India

*Corresponding Author: bkrastogi12@gmail.com

ABSTRACT

Several recent studies have identified short-term precursory activity before large earthquakes. Ambient seismic noise with spectral peaks at about 0.07 Hz and 0.2 Hz, due to primary and secondary microseisms, respectively, is observed everywhere at stations on hard basement rock. We examined pre-earthquake ambient seismic noise from four large earthquakes recorded at several three-component stations. Spectral characteristics of seismic noise within a narrow frequency range, which includes the larger-amplitude secondary spectral peak frequency, are found to be significantly altered by pre-earthquake activity when monitored by stations near the earthquake epicenter. For the M6 Nevada earthquake of 21 February 2008, spectral ratios of transverse/radial component or T/R observed at two recording stations along nearly orthogonal directions with respect to the epicenter suggest that the pre-seismic energy consists of the lowest frequencies up to about 0.2 Hz and increases in strength as it approaches the earthquake origin time. Moreover, the differences in T/R at the two stations are found to be in agreement with regional tectonics, therefore suggesting a mechanism of accelerating movement on pre-existing faults in the region. Analysis of several hours of observed pre-earthquake noise from four large earthquakes, obtained by converting observed data to particle displacement, show the low frequency amplitudes to increase in strength as the earthquake origin time approaches. Moreover, the advanced warning time appears to depend on earthquake magnitude; larger warning times for larger events. Our study appears to provide a method for obtaining advanced warning of a few hours or more before at least some impending large earthquakes.

Key Words: Advanced Warning, Short-term precursory activity, Ambient seismic noise, particle displacement.

INTRODUCTION

Several large earthquakes from all over the world have shown short duration precursory activity. A few examples are the 2011 M 9 Tohoku-oki earthquake (Sato et al., 2013; Uchida et al., 2016), the 2014 Iquique, Chile, Mw 8.2 Earthquake (Kato et al., 2016), and the 2004 Parkfield earthquake (Shelly, 2009). Similarly, in their study of the 1999 Mw 7.6 Izmit earthquake (Bouchon et al., 2011), the event was "preceded for 44 minutes by a phase of slow slip" but also "increased low frequency seismic noise". Although all these are after-the-fact indications, they do provide hope that short-term advanced warning should be possible.

The main feature of ambient noise spectra commonly observed at recording stations on hard rock are two peaks, the main peak is usually at about 0.2 Hz and the smaller peak at about 0.07 Hz and both peaks are due to ocean waves (Aki and Richards, 2009). Recently, Tian and Ritzwoller (2015) found that physical mechanisms and source locations of these primary and secondary microseisms are different. Gupta (1965) demonstrated that a significant fraction of the ambient short-period seismic noise at a given site may be attributed to stationary P waves with spectral characteristics strongly dependent on the geological structure underlying the recording station. In this study, we examine how the spectral characteristics

of ambient noise, especially its dominant peak at about 0.2 Hz, are impacted by pre-earthquake activity.

We analyzed pre-earthquake good-quality three-component continuous data from four large earthquakes, for several segments of time, including those starting several hours prior to the earthquake origin time and ending just before the first P from the event. These four earthquakes are (1) Nevada earthquake, 21 February 2008, epicenter at 41.15°N, 14.87°W, magnitude 6, depth 6.7 km.; (2) Southern California earthquake, 12 June 2005, epicenter at 33.53°N, 116.58°W, magnitude 5.2, depth 14.2 km.; (3) Craig, Alaska earthquake, 5 January 2013, epicenter 55.4°N, 134.7°W, magnitude 7.5, depth 10 km; and (4) Hindu Kush Earthquake, 26 October 2015, epicenter 36.5°N, 70.4°E, magnitude 7.5, depth 213 km.

ANALYSIS OF PRE-EARTHQUAKE SEISMIC NOISE FOR AN EARTHQUAKE IN NEVADA

We first analyzed pre-earthquake seismic noise from the Nevada 2008 event (Figure 1) by retrieving continuous ambient noise data recorded at several stations. Several hours' long samples of noise at three different times spanning a year, including a segment ending just a few seconds before the first P from the earthquake, were selected. For each segment, the horizontal components were

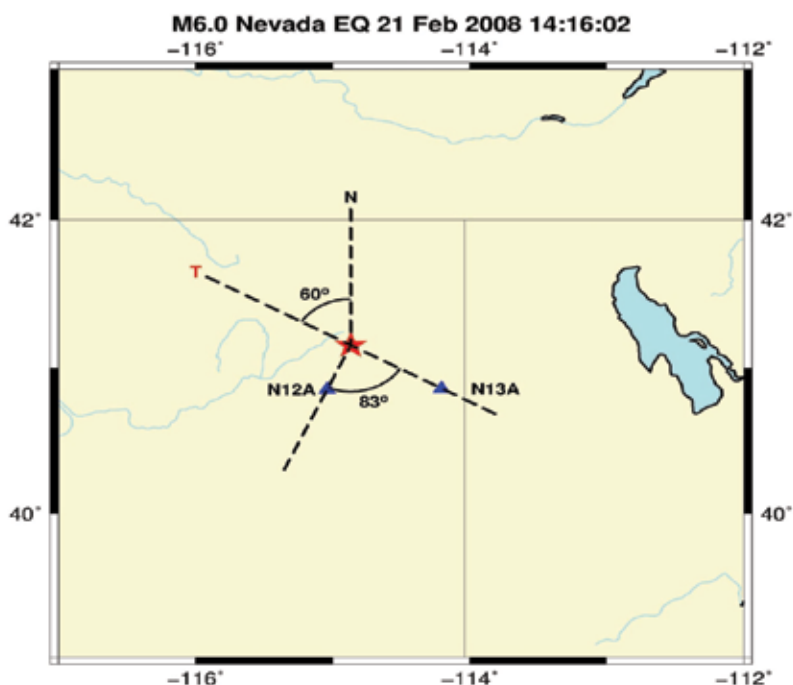


Figure 1. Epicentral location of Magnitude 6 earthquake in Nevada with its epicenter (red star) and two stations N12A and N13A at epicentral distances of 36 and 65 km, respectively. The two stations are nearly along orthogonal directions with respect to the epicenter and the known direction of T axis (N 60° W) coincides with the azimuthal direction of N13A.

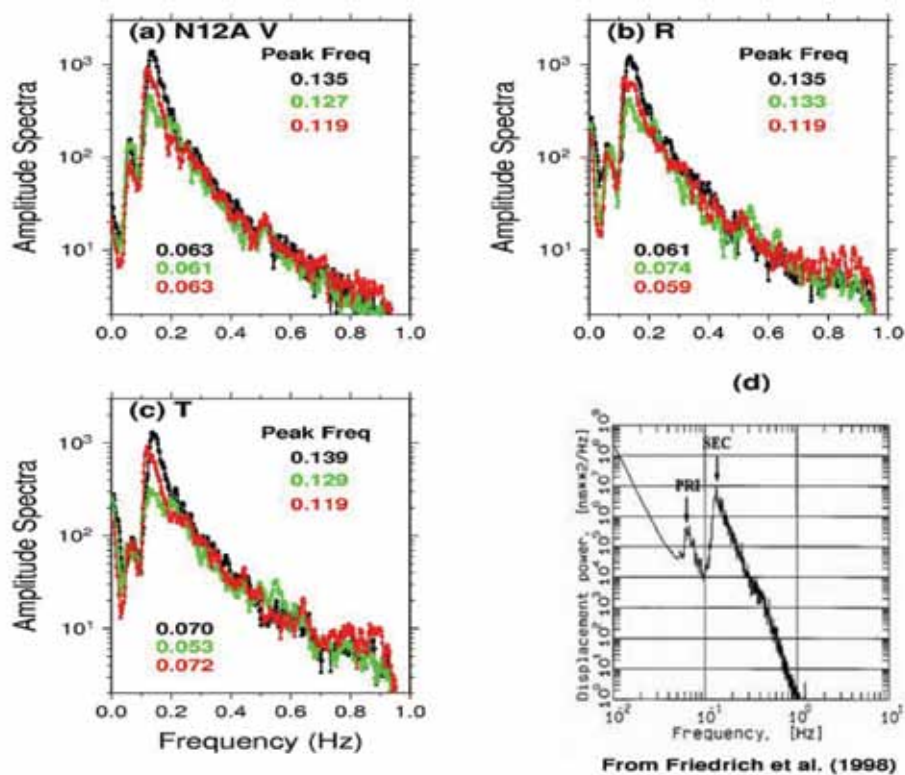


Figure 2. Spectra of (a) vertical (V), (b) radial (R) and (c) transverse (T) components of seismic noise at three different times preceding the earthquake: one-year before (black), one-month-before (green) and just-before (red). Each of the three sets of spectra shows two low-frequency peaks similar to those in (d) for V component at the Grafenberg array. The higher frequency peak values show a shift to lower values as the earthquake origin time approaches.

rotated into T and R components, based on the known epicenter. For the nearest station, N12A, spectra of vertical (V), radial (R) and transverse (T) components of 2048 sec long samples of noise at three different times preceding the earthquake: one-year-before (black), one-month-before (green) and just-before (red) are shown in Figure 2 (a), (b) and (c). These three figures used 2048 sec segments with sample rate of 2 samples per sec (decimated by 20) so that the Nyquist frequency is 1.0 Hz. An average of four spectral windows, each 512 seconds long, was used in order to show more detail at the lower frequencies. The three sets of spectra appear to be fairly similar with two prominent low frequency peaks for each component. It is interesting to note that two similar low-frequency peaks, considered to be due to primary and secondary microseisms, were observed in a study of ocean-generated seismic noise (vertical component) recorded at the Gräfenberg array by Friedrich et al., (1998), reproduced in Figure 2(d). The agreement between the spectral peak values in their study with ours for one-year before (black) is indeed remarkable. Apparent lack of agreement at the lowest frequencies is because of the fact that Figure 2(d) is in displacement whereas station N12A is a particle velocity instrument. For the three sets of spectra in Figures 2(a), (b) and (c), the larger amplitude spectral peaks within 0.1-0.2 Hz show a small systematic decrease in their frequency values for just-before (red) and one-month-before (green) segments of noise as compared to those for one-year-before (black).

Using data from both N12A and N13A, four spectral ratios, T/R, each based on averaging 5 windows, each 102.4 sec long for a total segment length of 512 seconds are shown in Figure 3(a). For recordings at the station N12A, T/R for the segment just-before the first P is shown in red whereas that for the one-year before segment is shown in black. Similar spectral ratios from N13A are shown in blue for the just-before segment and in dashed black for the one-year before segment. A comparison of the two just-before segments for N12A (red) and for N13A (blue) shows significant differences, including opposite trends for the lowest frequencies of up to at least about 0.2 Hz. The most likely reason for this is the large difference of 83 degrees in their epicenter-to-station azimuthal directions, which makes the transverse direction for one recording station nearly the same as the radial direction for the other station. Similar results, obtained by averaging 20 windows, each 102.4 sec long, for a total segment length of 2048 seconds, are shown in Figure 3(b). Results regarding opposite trends for the lowest frequencies at the two stations are similar but T/R amplitudes are smaller than those for the shorter noise segments, suggesting acceleration with amplitudes increasing with time up to the earthquake origin time.

Nevada is known to be a region of active tectonic processes with the direction of minimum principal stress to be about N 60° W (e.g. VanWormer and Ryall, 1980).

This happens to be the same as the azimuthal direction of N13A with respect to the epicenter. This means that the significant differences in the spectral ratios at the two stations (Figure 3) are fully consistent with regional tectonics and therefore indicate that pre-existing faults in the epicentral region start accelerating, accompanied by radiation of low frequency seismic waves, prior to the earthquake occurrence.

ADVANCED WARNING BASED ON BROADBAND DISPLACEMENT LOW FREQUENCY SPECTRA

We next analyze low frequency displacement spectra of pre-seismic noise by converting the observed spectral amplitudes from particle velocity to displacement. For this, we first analyzed pre-event noise from the Nevada earthquake recorded at two stations N12A and N13A and the results are shown in Figures 4 and 5. For each figure, we start with obtaining spectra of consecutive 256 sec windows, convert the observed spectral amplitudes to displacement and compute mean log amplitude within a narrow frequency range, such as 0.1 to 0.2 Hz, which includes the secondary peak frequency in ambient seismic noise. These mean values are plotted versus 120 time windows, covering a period of 8.4 hours of continuous pre-earthquake noise ending just before the event origin time, for (a) V, (b) R and (c) T components. The first half of these 120 windows is shown in green color and the other half in red. Mean values for the entire duration, after dividing it into 8 segments S1, S2, S3,.....S8, each consisting of 15 windows, are shown by superimposed black straight lines. For each component, the difference between the mean amplitude values of the last segment S8 and the first segment S1, $S8 - S1$ is indicated along with its value as a percentage increase. Both Figures 4 and 5 indicate almost systematic and significant pre-earthquake increase in amplitudes on all three components and the increase during the last four hours (red) appears to be larger than that during the first 4 hours (green).

Similar analysis of data for the Southern California earthquake of 12 June 2005 recorded at SND led to results shown in Figure 6. Note that the mean values, shown by superimposed black straight lines, again show systematic general increase with time but the increase is much smaller than in Figures 4 and 5. Most likely reason is the much smaller magnitude (M 5.2) of this earthquake as compared to the Nevada event (M 6).

Figure 7 shows results for the Craig, Alaska earthquake of 5 January 2013 recorded at CRAG at an epicentral distance of 97 km. Here the mean values show a large and almost steady increase over the entire duration of 120 windows, suggesting an advanced warning time of much longer duration.

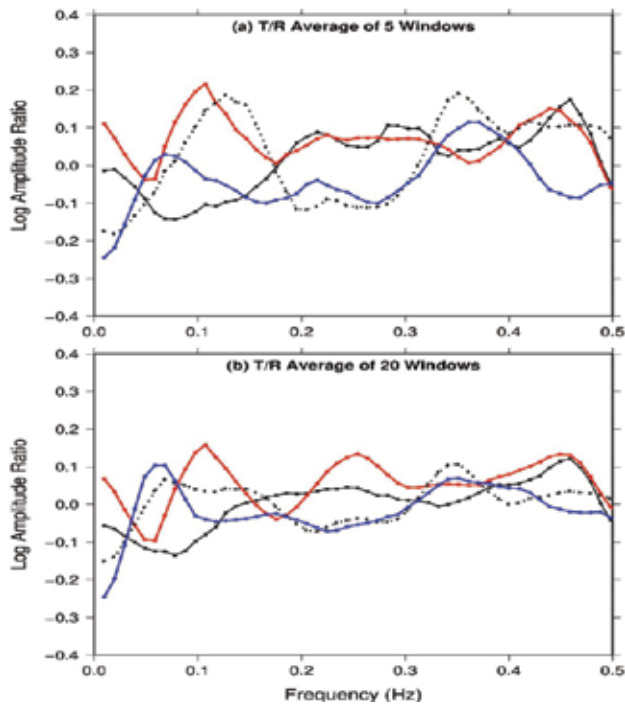


Figure 3. (a) Spectral ratios T/R for stations N12A and N13A for noise time segments of 512 sec each. For N12A, T/R for the segment just-before the first P is shown in red whereas that for the one-year before is shown in black. Similar spectral ratios from N13A are shown in blue and dashed black. A comparison of the two T/R for just-before segments for N12A (red) and for N13A (blue) shows opposite trends for the lowest frequencies of up to about 0.2 Hz. (b) Similar results for segment lengths of 2048 seconds also show opposite trends for the lowest frequencies at the two stations but T/R amplitudes are smaller than those in Figure 3 (a), suggesting acceleration with amplitudes increasing with time up to the earthquake origin time.

Results from the Hindu Kush earthquake of 26 October 2015 recorded at KBL are shown in Figure 8. Similar to the results for Craig, Alaska earthquake, there is steady increase in amplitude over the entire duration of over 12 hours. It seems therefore that for both these two M7.5 earthquakes, the increase in Mean Amplitude may have started earlier than 8 hours before the earthquake. Note that the pre-earthquake low frequency signals from these two large magnitude earthquakes are strong enough to be easily observed at large distances of 97 and even 250 km. Observation of strong precursory signals at an epicentral distance of 250 km for the Hindu Kush earthquake does seem hard to believe until one considers its large 213 km hypocentral depth. At this depth in the mantle, the S wave velocity is about 5 km/sec so that for a frequency of 0.1 Hz the wavelength is about 50 km and an epicentral distance of 250 km implies a distance of only 5 wavelengths.

The above results from four large earthquakes demonstrate that the pre-earthquake source consists of a

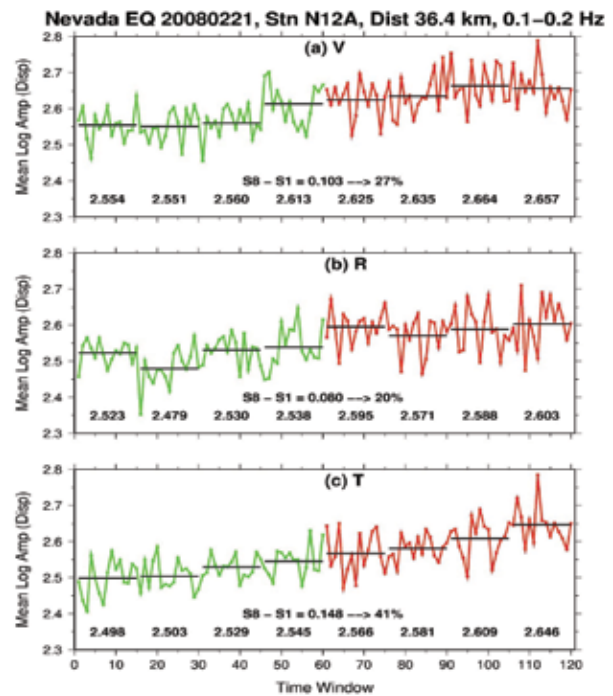


Figure 4. Mean log amplitude (displacement) for Nevada earthquake recorded at N12A vs 120 time windows, covering a period of 8.4 hours of continuous pre-earthquake noise ending just before the origin time, for (a) V (b) R and (c) T components, with the first half shown in green color and the other half in red. Mean values for the entire duration, after dividing into 8 segments S1, S2, S3,.....S8, each consisting of 15 windows, are shown by superimposed black straight lines. For each component, the difference between the last segment, S8 and the first segment S1, $S8 - S1$ is indicated along with its value as a percentage increase. As indicated by the mean values for the eight segments, this precursory signal progressively gains strength as the earthquake origin time approaches.

broadband displacement low frequency spectrum increasing in strength as the earthquake origin time approaches. Our observations indicate that such a signal, emanating from the pre-earthquake, gets superimposed on the ambient seismic noise spectra at recording stations. Moreover, a comparison of results for the four earthquakes suggests dependence of advanced warning time on magnitude of the earthquake, with larger warning time for larger events.

BACKGROUND AND DISCUSSION OF RESULTS

A short description of relevant studies of short-term pre-seismic phenomena follows. Dieterich (1978) proposed that “pre-seismic fault slip takes place in two stages. The first stage consists of the long-term stable propagation of slip along the fault. The second stage is the shorter interval of accelerated slip that culminates in seismic instability.” A review article by Chelidze and Matcharashvili (2007) contends that whereas long term prediction may never be

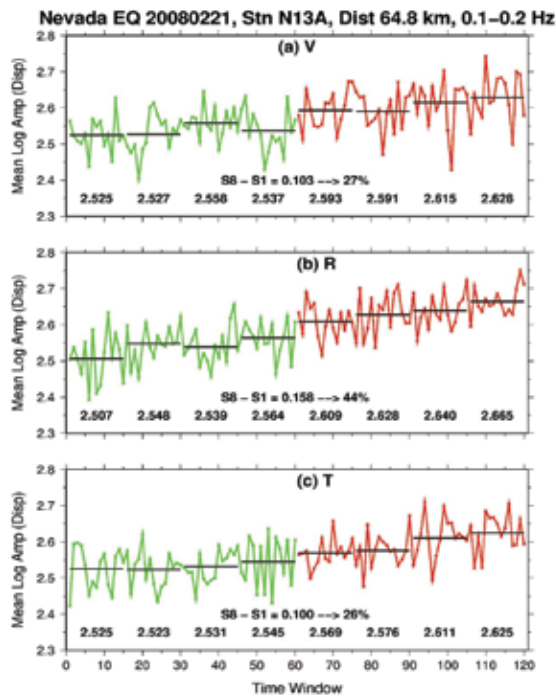


Figure 5. Similar to Figure 4 but for N13A. Again, the mean values, shown by superimposed black straight lines, indicate significant premonitory increase with time, more so during the last half (red).

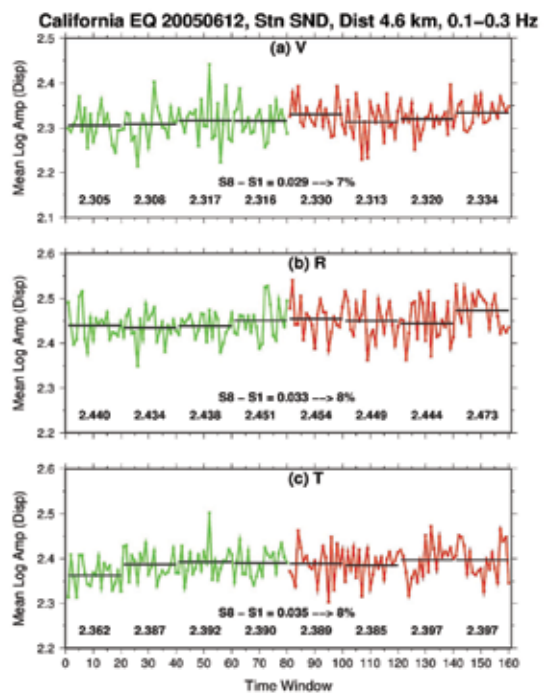


Figure 6. Similar to Figure 4 but for the Southern California earthquake recorded at SND. The mean values, shown by superimposed black straight lines, do indicate overall increase with time but much smaller than in Figures 4 and 5. The most likely reason is much smaller magnitude ($M 5.2$) of this earthquake as compared to the Nevada event ($M 6.0$).

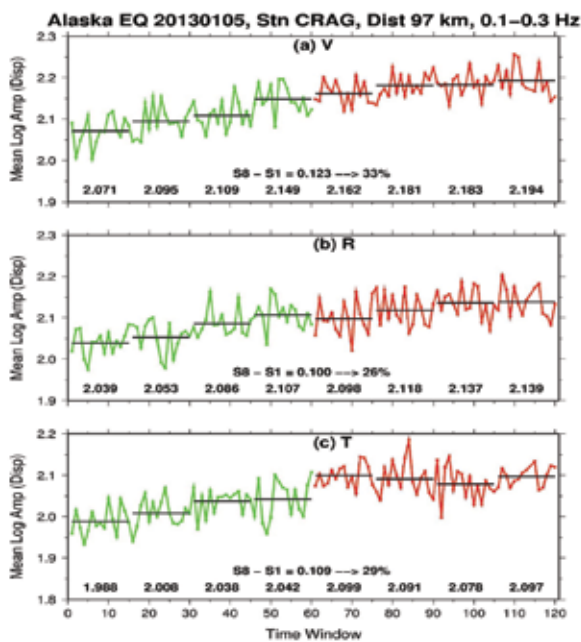


Figure 7. Similar to Figure 4 but for the Alaska earthquake recorded at CRAG. The mean values not only indicate strong increase with time but also the increase in Mean Amplitude may have started earlier than 8 hours before the earthquake.

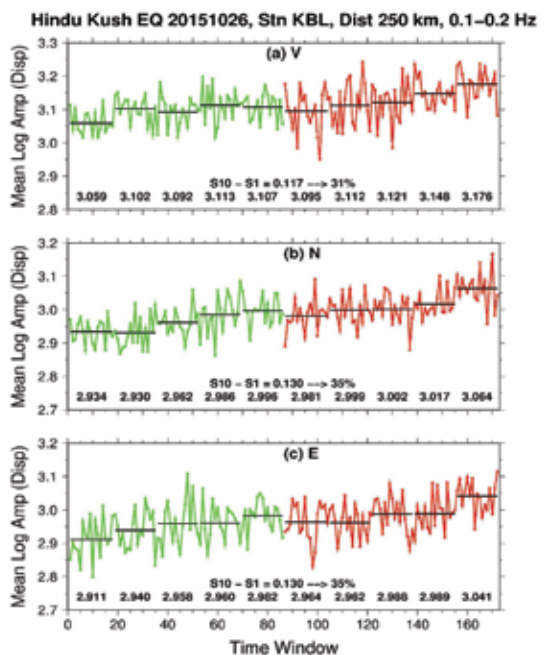


Figure 8. Similar to Figure 4 but for the Hindu Kush earthquake recorded at KBL based on over 18 hours of data. As for the Alaska earthquake (Figure 7), the mean values not only indicate strong increase with time but also the increase in Mean Amplitude may have started earlier than 8 hours before the earthquake.

possible, a limited time interval before a large earthquake should be predictable." Laboratory and theoretical studies suggest that earthquakes may be preceded by a phase of developing slip stability in which the fault begins to slip slowly before accelerating to dynamic rupture (Bouchon et al., 2011). A recent study by Uchida et al., (2016) found slow slip acceleration to precede the 2011 M 9 Tohoku-oki earthquake for which the slow slip began accelerating a few days before the main shock.

According to Marsan et al., (2015), "Researchers now understand that faults do not just remain totally locked between earthquakes (rapid slip events that efficiently radiate seismic waves) or creep steadily and slowly (without radiating). Instead, faults may be better described as patchworks of slip behaviors spanning a complete spectrum between these end members". Our results, suggesting that pre-existing faults in the epicentral region start accelerating accompanied by radiation of low frequency seismic waves prior to the earthquake occurrence, are therefore fully consistent with all these authors.

Analysis of low frequency data from four large earthquakes (Figures 4, 5, 6, 7 and 8) indicate that a broadband displacement low frequency signal emanates from the pre-earthquake source and gets superimposed on the existing ambient seismic noise and this signal becomes progressively stronger as the origin time approaches. These results may therefore be used to obtain advanced warning of a few hours or more before a large earthquake.

CONCLUSION

Our results suggest that the pre-earthquake fault slip before a large earthquake is associated with a broadband displacement low frequency signal, starting rather gradually a few hours before the earthquake and increasing in strength with time. This mechanism seems to be in agreement with several recent studies of pre-earthquake phenomena. Monitoring these temporal variations in mean amplitude over a narrow frequency band (which included the secondary spectral peak in ambient seismic noise) displayed an almost continuous temporal increase lasting up to the earthquake origin time. Our analysis of data from four large earthquakes provides remarkably consistent results leading to a relative simple methodology for obtaining warning of four hours or better before at least some large earthquakes.

ACKNOWLEDGMENTS

We sincerely appreciate numerous helpful suggestions from Professor Paul Richards and Dr. David Schaff, both at Columbia University. We are also most grateful to

Dr. Robert Blandford for his encouragement and numerous suggestions. We also thank Dr. H.M. Iyer for his review. Thanks are due to Shri D.N. Avasthi and Dr. P.R.Reddy for the efforts to publish this article in JIGU.

Compliance with Ethical Standards

The authors declare that they have no conflict of interest and adhere to copyright norms.

REFERENCES

- Aki, K., and P.G., Richards, 2009. Ambient seismic noise, in *Quantitative Seismology*, pp: 616-617.
- Bouchon, M., Karabulut, H., Aktar, M., Ozalaybey, S., Schmittbuhl J., and Bouin, M., 2011. Extended nucleation of the 1999 Mw 7.6 Izmit earthquake, *Science*, v. 331, pp: 877-880.
- Chelidze, T., and Matcharashvili, T., 2007. Complexity of seismic process; measuring and applications - A review, *Tectonophysics*, v.431, pp: 49-60.
- Dieterich, J. H., 1978. Preseismic Fault Slip and Earthquake Prediction, *Jour. Geophys. Res.*, v.83, pp: 3940-3947.
- Friedrich, A., Krüger, F., and Klinge, K., 1998. Ocean-generated microseismic noise located with the Gräfenberg array, *Journal of Seismology*, v.2, no.1, pp: 47-64.
- Gupta, I. N., 1965. Standing-wave phenomena in short-period seismic noise, *Geophysics*, v.30, pp: 1179-1186.
- Kato, A J., Fukuda, T., and Nakagawa, S., 2016. Accelerated nucleation of the 2014 Iquique, Chile, Mw 8.2 earthquake. *Sci. Rep.* v.6, pp: 24792.
- Marsan, D., Gomberg, J., and Bouchon, M., 2015. Exploring earthquakes, slow slip, and triggering, *Eos*, 96, 20 March 2015.
- Sato, T., Hiratsuka, S., and Mori, J., 2013. Precursory seismic activity surrounding the high-slip patches of the 2011 Mw 9.0 Tohoku-Oki earthquake, *Bull. Seism. Soc. Am.* v.103, pp: 3104-3114.
- Shelly, D. R., 2009. Possible deep fault slip preceding the 2004 Parkfield earthquake, inferred from detailed observations of tectonic tremor, *Geophysical Res. Lett.* v.36, pp: L17318.
- Tian, Y., and Ritzwoller, M. H., 2015. Directionality of ambient noise on the Juan de Fuca plate: implications for source locations of the primary and secondary microseisms, *Geophysical Journal International*, v.201, pp: 429-443.
- Uchida, N., Linuma, T., Nadeau, M.H., Burgmann, R., and Hino, R., 2016. Periodic slow slip triggers megathrust zone earthquakes in northeastern Japan, *Science*, pp: 488-492.
- VanWormer, J. D., and Ryall, A., 1980. Sierra Nevada-Great Basin boundary zone: earthquake hazard related to structure, active tectonic processes, and anomalous patterns of earthquake occurrence.

Received on: 13.1.18; Accepted on: 19.1.18.

54th Annual Convention of Indian Geophysical Union (IGU): A Report

The 54th Annual convention of IGU was jointly organized by CSIR-NGRI and IGU at CSIR-NGRI, Hyderabad during December 3-7 2017 on the main theme entitled "Recent Advances in Geophysics with Special Reference to Earthquake Seismology".

The convention was inaugurated by Dr. Girish Sahni, Director General of CSIR, and Secretary, DSIR, New Delhi. Prof. Shailesh Nayak, President of IGU presided over the function and presented the IGU awards to both the young and senior geo-scientists for their excellent contribution to Indian Earth Sciences. The Technical Program was meticulously designed under the supervision of Prof. Shailesh Nayak. Proper guidance was also provided by Prof. Harsh K. Gupta, Former President of IGU. Various activities were executed by a group of CSIR-NGRI Scientists with the needed support and guidance by Dr. V.M. Tiwari, Director, CSIR-NGRI. The Exhibition was inaugurated by Prof. V.L.S. Bhimasankaram, a renowned Professor of Geophysics. Prof. Mrinal K Sen, former Director of CSIR-NGRI inaugurated the poster session. Reputed scientists from different research institutes, universities and industries chaired the sessions covering several disciplines of Solid Earth & Marine Geo-sciences and Planetary & Atmospheric Sciences. Concerted efforts were made by Drs. D. Sri Nagesh, Ajai Manglik, Kirti Srivastava, E.V.S.S.K. Babu, Sandeep Gupta, Devender Kumar, Kusumita Arora, N. Satyavani and many others for making the five-day convention successful in all aspects. Dr. V.P. Dimri, Past President of IGU, Dr. D. Atchuta Rao and Dr. P.R. Reddy both Past Hon. Secretaries of IGU extended unequivocal supports in many ways.

After having welcomed the delegates, Dr. V.M. Tiwari highlighted the importance of Earth Sciences and its influence on the Society. Dr. Kalachand Sain presented the secretary's report and briefed about the convention. Prof. Shailesh Nayak emphasised the need of integrating the Geosphere, Biosphere and Atmosphere in understanding the important issues related to Earth's dynamics and climate change.

He also stressed upon the importance of Borehole Geophysics and Earthquake monitoring studies at Karad. Dr. Girish Sahni remarked that Earth Sciences, particularly Geophysics, is a very important branch of Science having direct relevance to society in terms of Energy, Minerals, Ground water, Geo-hazards etc, and it can provide solution to industry-challenges. He advised young researchers to achieve excellence through hard work and come out with innovations to meet the societal requirement.

There were about 250 delegates from different parts of the country as well as from abroad. Besides 3 Plenary and 16 invited talks, the convention had 80 oral and 118 poster presentations, apart from Prof. K. R. Ramanathan Memorial lecture and talks by the Decennial awardee and Krishnan medal awardees. Two special sessions were conducted on commemorating the 50 years of 'Seismological Observatory' and 'Airborne Geophysics' and Reservoir Triggered Seismicity. A Special lecture was also delivered in memory of Dr. J.G. Negi. Additionally, an over view session on Extreme Physics & Chemistry-Reservoirs & Fluxes and Deep Energy and Deep Life was conducted on 7th December.

Young researchers and students showed lot of enthusiasm in presenting their scientific results through posters and gained insights by interacting with experienced geoscientists. A special feature of the convention is the Young Researcher Programme organized for the benefit of young researchers those who submitted or about to submit their theses. To encourage the young brains in pursuing Earth sciences, young researchers were selected with the 'best oral presentation award'. To motivate the project assistants and post graduate students from different universities and institutes to come into the realm of Earth sciences, they were also selected for the 'best poster presentation awards'. The delegates thoroughly enjoyed the scientific proceedings and excellent hospitality provided by CSIR-NGRI. In this regard, Dr. Srinagesh, Dr. Kirti Srivastava and other team members deserve the compliments. Chair persons of various technical sessions are thanked

for conducting the proceedings as scheduled. Special thanks are due to Mr. Rafique Mohammad Attar, Treasurer of IGU for executing various works related to this Convention.

The closing session was presided over by Dr. Satheesh C. Sheno, Vice-President of IGU & Director, INCOIS. He advised the students and researchers to achieve excellence in whatever field they pursue their research. He handed over the Cash Prizes and Certificates to the Students and Research Scholars for their best performance in the 54th Annual Convention of IGU. Dr. VM Tiwari, Director, CSIR-NGRI handed over the Certificates to the Students who participated in the quiz competition earlier organized by the IGU-NGRI student Chapter.

Details of the main awards presented during the convention have been covered in the News at a glance of this issue of JIGU. Details of other awards are given below.

A) IGU-Prof. Jegdeo Singh & Dr. S. Balakrishna Memorial Grant to student toppers 2017

i. Dept. of Geophysics, Osmania University, Hyderabad

1. Ms. N. Mounika
2. Mr. Tabish Khan

ii. Dept. of Geophysics, Andhra University, Visakhapatnam

1. Mr. Chakka. Sathya Datta
2. Ms. Bangaru. Sushma

iii. Dept. of Marine Geophysics, Andhra University, Visakhapatnam

1. Mr. Vankara Pradyumnu
2. Ms. Bulusu Venkata Radha Santhoshi

iv. Dept. of Geophysics, Banaras Hindu University, Varanasi

1. Mr. Deepanshu Goyal
2. Mr. Ratnesh Pandey

v. Dept. of Earth Sciences, Indian Institute of Technology Roorkee, Roorkee

1. Nikhil Singh
2. Mulchandani Vishal Haresh &
3. Shubham Singh

vi. Dept. of Geophysics, Manonmaniam Sundarnar University, Tirunelveli

1. Ms. Anagha TJ
2. Ms. Sree Lakshmi A.S.

vii. Dept. of Geophysics, Swami Ramanand Teerth Marathwada University, Nanded

1. Mr. Lutte Sudhakar Balaji
2. Mr. Mohmad Salah Ahmad

viii. Dept. of Geophysics, Kurukshetra University, Kurukshetra

1. Ms. Neha
2. Mr. Hardeep

ix. Dept. of Geosciences, Dr. B.R. Ambedkar University, Srikakulam

1. Ms. A. Amani &
2. B. Maneesha
3. Mr. K. Venugopal

x. Dept. of Earth Sciences, Indian Institute of Technology Bombay, Mumbai

1. Tumul Rai
2. Madhuri Chauhan

xi. Dept. of Applied Geophysics, Indian Institute of Technology (ISM), Dhanbad

1. Sayan Mallick, 3 Yr. M.Sc. Tech
2. Avanie Jain, 5 Yr. Int. M.Sc. Tech

7. IGU-Anni Talwani Memorial Grant to Women Researchers

1. Ms. Indu Chowdhary, ISR, Gandhinagar
2. Ms. Laxmi Pandey, CSIR- NGRI, Hyderabad
3. Ms. Saranya Jayachandran, CSIR-NIO, Goa
4. Ms. Seema Kumari, IIT, Kanpur

The convention was co-sponsored by ESSO-Indian National Centre for Ocean Information Services (INCOIS), ESSO-National Centre for Antarctic and Ocean Research (NCAOR), ESSO-National Centre for Earth Science Studies (NCESS), Indian Institute of Geomagnetism (IIG), CSIR-National Institute of Oceanography (NIO), National Remote Sensing Centre (NRSC), Ministry of Earth Sciences (MoES), SERB-Department of Science & Technology (DST), Council of Scientific and Industrial Research (CSIR), Himalayan Heli Services Pvt. Limited, New Delhi, and SBI, Hyderabad.

The convention was concluded by rendering National Anthem.



Inauguration function: Lighting of traditional lamp and releasing of abstract volume by Dr. Girish Sahni, Chief Guest, Director General of CSIR & Secretary, DSIR. Prof. Shailesh Nayak, President of IGU & Distinguished Scientist, Dr. VM Tiwari, LOC Chairman & Director, CSIR-NGRI, Dr. Kalachand Sain, Hon. Secretary of IGU and Dr. Srinagesh, LOC Convener & Chief Scientist, CSIR-NGRI are also seen on the dais.



Prof. V.L.S. Bhimashankaram is inaugurating the Exhibition in presence of Prof. Harsh K Gupta, Member, Atomic Energy Regulatory Board (AERB) & Past President of IGU, Prof. Shailesh Nayak, President of IGU, Dr. VM Tiwari, Director, CSIR-NGRI, Dr. Anil Bhardwaj, Director, Physical Research Laboratory, Dr. ASSRS Prasad, Organizing Secretary of IGU. Group Photo of Delegates.



Prof. Mrinal K Sen, Jackson Chair in Applied Seismology at the University of Texas at Austin, USA is inaugurating the poster session in presence of Prof. Shailesh Nayak, President of IGU. Prof. Sen is interacting with the delegates



Concluding Session: Dr. Sateesh C Sheno, Vice- President of IGU & Director along with Dr. VM Tiwari, Director, CSIR-NGRI, Dr. Kalachand Sain, Hon. Secretary of IGU and Dr. O.P. Mishra, Joint Secretary of IGU. Dr. Tiwari is giving certificates to winners of Quiz Competitions organized by IGU Student Chapter of CSIR-NGRI.

Dr. K. Sain & Dr. A.S.S.R.S. Prasad

GUIDE LINES TO AUTHORS

The Journal of Indian Geophysical Union (J-IGU), published quarterly by the Indian Geophysical Union (IGU), is an interdisciplinary journal from India that publishes high-quality research in earth sciences with special emphasis on the topics pertaining to the Indian subcontinent and the surrounding Indian Ocean region. The journal covers several disciplines of earth sciences such as the Geosphere, its watery and gaseous envelopes (the Hydrosphere, the Cryosphere and the Atmosphere), and life (the Biosphere). It also publishes articles on Space and Planetary sciences. J-IGU welcomes contributions under the following categories:

- Research papers reporting new findings, results, etc.
- Review articles providing comprehensive overview of a significant research field related to earth sciences

In addition, J-IGU also welcomes short communications on opinion and report on scientific activity, personal information, book reviews, news and views, etc.

The manuscript should be submitted electronically as a single word format (.doc file) including the main text, figures, tables, and any other supplementary information along with the signed "Declaration Letter". The manuscript should be submitted by email (jigu1963@gmail.com) to the Editor.

After acceptance of the manuscript the corresponding author would be required to submit all source files (text and Tables in word format) and figures in high resolution standard (*.jpg, *.tiff, *.bmp) format. These files may be submitted to the Editor as a single *.zip file along with the "Copyright Transfer Statement".

IMPORTANT INFORMATION

Ethics in publishing

J-IGU is committed to ensuring ethics in publication and takes a serious view of plagiarism including self-plagiarism in manuscripts submitted to the journal. Authors are advised to ensure ethical values by submitting only their original work and due acknowledgement to the work of others in case used the manuscript. Authors must also refrain from submitting the same manuscript to more than one journal concurrently or publish the same piece of research work in more than one journal which is unethical and unacceptable. Editor of J-IGU is committed to make every reasonable effort to investigate any allegations of plagiarism brought to his attention, as well as instances that come up during the peer review process and has full authority to retract any plagiarized publication from the journal and take appropriate action against such authors if it is proven that such a misconduct was intentional.

Similarly, Editor and Reviewers are also expected to follow ethical norms of publishing by ensuring that they don't use any unpublished information, communicated to them for editorial or review purpose, in their own research without the explicit written consent of the author. They are also expected to keep manuscript/ data/ observations/ any other information related to the peer review confidential to protect the interest of the authors. Reviewers should refrain from reviewing the manuscripts in which they have conflicts of interest resulting from competitive, collaborative, or other relationships or connections with any of the authors, companies, or institutions connected to the manuscript.

Conflict of interest

All authors are requested to disclose any actual or potential conflict of interest including any financial, personal or other relationships with other people or organizations within three years of beginning the submitted work that could inappropriately influence, or be perceived to influence, their work.

Submission declaration

Submission of a manuscript implies that the work has not been published previously and it is not under consideration for publication elsewhere, and that if accepted it will not be published elsewhere in the same or any other form, in English or in any other language, without the written consent of the publisher. It also implies that the authors have taken necessary approval from the competent authority of the institute/organization where the work was carried out.

Copyright

After acceptance of the manuscript the corresponding author would be required to sign and submit the "Copyright Transfer Statement".

MANUSCRIPT PREPARATION

The corresponding author should be identified (include E-mail address, Phone/Mobile number). Full affiliation and postal address must be given for all co-authors.

Abstract:

An abstract of not more than 300 words must be included.

Text:

The manuscript should be structured to include a front page containing the title, Author(s) name, affiliation and address of the institute where the work was carried out, a short title, and 5-to-6 index terms/Key words. Author(s) present address, if different from the above mentioned address, may be given in the footnote. The corresponding author should be identified with an asterisk and his/her email ID should be provided. This page should be followed by the main text consisting of Abstract, Introduction, Methods/ Techniques/ Area description, Results, Discussion, Conclusions, Acknowledgements, and References. Tables and Figures with captions should be inserted in the main text of the manuscript at appropriate places.

Figures/ Illustrations:

All figures should be provided in camera-ready form, suitable for reproduction (which may include reduction) without retouching. Figures in high-resolution (at least 300 dpi) standard formats (*.jpg, *.tiff, *.bmp) are acceptable. Figures should be numbered according to their sequence in the text. References should be made in the text to each figure. Each figure should have a suitable caption.

Tables:

Authors should take note of the limitations set by the size and layout of the journal. Table should not exceed the printed area of the page. They should be typed on separate sheets and details about the tables should be given in the text. Heading should be brief. Large tables should be avoided and may be provided as supplementary information, if required.

Equations:

Equations should be numbered sequentially with Arabic numerals and cited in the text. Subscripts and Superscripts should be set off clearly. Equation writing software that presents each equation as an object in MS Word will be accepted. Style and convention adopted for the equations should be uniform throughout the paper.

References:

All references to publications cited in the main text should be presented as a list of references following the text and all references in the list must be cited in the text. References should be arranged chronologically, in the text. The list of references should be arranged alphabetically at the end of the paper.

References should be given in the following form:

Kaila, K.L., Reddy P.R., Mall D.M., Venkateswarlu, N., Krishna V.G. and Prasad, A.S.S.R.S., 1992. Crustal structure of the west Bengal Basin from deep seismic sounding investigations, *Geophys. J. Int.*, v.111, no., pp:45-66.

REVIEW PROCESS:

All manuscripts submitted to the journal are peer-reviewed. It is advisable to send the contact details of **4 potential reviewers** along with the manuscript to expedite the review process. Editor has the option to select reviewers from the list or choose different reviewers. The review process usually takes about 3 months. All enquiries regarding the manuscript may be addressed to the Editor.

GALLEY PROOF:

Technical editing of manuscripts is performed by the editorial board. The author is asked to check the galley proof for typographical errors and to answer queries from the editor. Authors are requested to return the corrected proof **within two days** of its receipt to ensure uninterrupted processing. The editor will not accept new material in proof unless permission from the editorial board has been obtained for the addition of a "note added in proof". Authors are liable for the cost of excessive alterations to galley proof.

PUBLICATION CHARGES:

There are no page charges for publication and printing charges for b/w figures. However, in view of substantial cost involved in printing of color figures, author will be charged for printing of pages containing color figures @ Rs. 2,500/- per page. The charges may be revised at any time based on cost of printing and production. Author will receive an estimate/ invoice of the color figures reproduction cost along with the galley proof. It is the responsibility of the author to remit the color figures reproduction cost **within one month** of the receipt of the estimate/invoice.

The corresponding author will receive a soft copy (pdf format) of his/her published article. Should the author desire to purchase reprints of his/her publication, he/she must send the duly signed Reprint Order Form (accompanies the galley proof and contains price details) along with the corrected galley proof to the Editor. The reprint charges must be paid **within one month** of sending the Reprint Order Form.

Any payment related to printing of color figures and/or purchase of reprints should be made in the form of a Demand Draft in the name of **Treasurer, Indian Geophysical Union**, payable at **Hyderabad**.

You may download the pdf file here: [Guide for Authors](#)